



The
University
Of
Sheffield.

Studies on bacterial detoxification systems for

NO and CO

Israa Al Hawani

A thesis submitted for the degree of:

Doctoral of Philosophy

September 2017

Department of Molecular Biology and Biotechnology

The University of Sheffield

Summary

Nitric oxide (NO), which is produced by nitric oxide synthases (NOS) from L-arginine in mammals and certain bacteria, has important physiological functions in the host. Among these is the generation of NO in macrophages by inducible NOS; the NO generated in bursts contributes, with reactive oxygen species to the arsenal of antimicrobial small molecules that destroy invading bacteria. However, bacteria have developed several strategies to detoxify NO both aerobically and anaerobically. The most efficient mechanism involves the flavohaemoglobin Hmp that catalyses the oxygenation (or denitrosylation) of NO by molecular oxygen to generate non-toxic nitrate. However, at very low or zero oxygen concentrations, an alternative mechanism is induced. Flavorubredoxin (NorV) and its reductase partner flavorubredoxin oxidoreductase (NorW) reduce NO to nitrous oxide (N₂O). NorV reduces NO to N₂O and usually contains two major domains with an additional C-terminal domain in *E. coli* that resembles rubredoxin (~6 kDa) and possesses an iron-sulfur center. NorW is the reductase for NorV and is crucial in NO detoxification, its role being to reduce NorV by transfer of an electron from NADH via FAD and then to the iron in the rubredoxin-like domain of NorV. This electron moves through the flavin-like domain of NorV to the diiron center in its β -lactamase-like domain, where ultimately it will reduce NO to N₂O. In this study, the genes encoding NorV and NorW were cloned from *E. coli* and expressed, the proteins purified and analyzed, including structure determination. The crystal structure of NorV was determined, and shows important details of the diiron center in the N-terminal β -lactamase-like domain and a flavin mononucleotide (FMN) in the second domain. However, the final rubredoxin domain was not observed in the structure. Physiological assays carried out *in vivo* and *in vitro* confirmed that NorV and NorW are work together to detoxify NO but suggested a possible additional role for NorW in direct NO conversion. The activity of NorW function *in vitro* was assessed by

measuring NO consumption using an NO electrode and PROLI-NONOate as an NO releasing molecule. These *in vitro* data showed that NorW consumes NO rapidly independent of NorV but in the presence of NADH, under aerobic, microaerophilic and anaerobic conditions.

Although, the *in vitro* results were very clear and suggested that NorW can consume NO, *in vivo* results, which used different *E. coli* mutants, didn't agree with the *in vitro* results. Measurement of NO susceptibility, NO consumption in intact cell suspension, growth curves and FTIR spectra did not show a clear effect of NorW on NO toxicity.

As part of the mammalian immune defense response to bacteria, macrophages produce carbon monoxide (CO) but mycobacteria are resistant to this normally toxic molecule. The identification of a *Mycobacterium tuberculosis* (Mtb) carbon monoxide resistance protein (Cor) that detoxifies CO has been proposed and was also included in this study. It was also published that transformation of *E. coli* cells with a *cor* gene expression system could confer CO resistance upon them.

However, the mechanism of Cor is unknown and a range of assays and biophysical analyses were performed in order to explore the function of Cor. Mtb Cor was successfully expressed in *Escherichia coli* by using an IPTG-inducible expression vector complemented with *rv1829* gene encoding the Cor protein.

A carbon monoxide dehydrogenase activity assay was carried out using methyl viologen as an electron acceptor, to check the ability of Cor to oxidize CO to CO₂, but no clear evidence was obtained to confirm that Cor can catalyse CO oxidation.

The ability of Cor to protect *E. coli* cells from CO toxicity was also tested by using CORM-2 as a CO releasing molecule. The result showed no clear evidence that Cor can protect *E. coli* against CO toxicity.

Amongst the analyses carried out, the purified His-tagged protein was tested for crystallization but no X-ray diffraction was obtained from the crystals tested. Further biophysical analysis was carried out by measuring an FTIR spectrum, to look for the final product of Cor activity, but no signal was seen for CO consumption or CO₂ production.

Another test was performed by NMR, in order to confirm if Cor can interact with CO, spectra of Cor with and without bubbled with CO were taken over 4 h. No changes were noticed between Cor with and without CO spectra over time, which suggests that Cor did not interact with CO. An NMR was performed to look for direct Cor interaction with CO but no changes were noticed in the spectrum for Cor after prolonged exposure to CO.

A pull-down assay was also performed to determine if Cor needs a protein partner for activity. The assay was carried out using *Mycobacterium smegmatis* and *Escherichia coli* cell free extract (CFE). No clear evidence was seen to suggest that Cor interacted with any other *M. smegmatis* or *E. coli* proteins.

DEDICATION

I dedicate this work to all who have stood by me and guided me all throughout and assisted me in the completion of this project.

First and foremost, would be to Allah, the reason for my existence and to Messenger Mohammed and his family who are the candlelight in my life.

I would also dedicate this work to my parents who have brought me up and provided for me and whose spirits still do watch over me. Also, I would remember and make note of all my fellow nationals who have shed their blood for the cause in my country of Iraq.

Finally, I would dedicate this work to my Loving Husband Hussein and my sweet heart child Ali.

ACKNOWLEDGEMENT

I would start my acknowledgement by thanking my supervisors, Dr. John Rafferty, who had been a great support for me in both my scientific and social life without whose advises and support I wouldn't have been able to achieve my goals and Professor Robert Poole to suggest this project and his valuable scientific advices.

I would also express my gratitude and thanks to Dr. Mariana Tinajero-Trejo for her effort to train me on the lab equipment and to support me in my lab work, Dr. Svetlana E Sedelnikova for her effort in protein purification and her valuable advises, and Thomas Smith (Chemistry department, University of Sheffield) for his help in FTIR experiments.

My great appreciation to Professor Jeff Cole, School of Bioscience, University of Birmingham for his generous gift of JCB5253 strain, and Dr. Michael U. Shiloh Department of Internal Medicine, University of Texas Southwestern Medical School, Dallas, Texas, USA for his generous gift of *cor* Mtb expression vector (pJ401). I express my appreciation also to the head of Molecular Biology and Biotechnology department, Dr. Alistar Goldman and his secretary, Mrs. Linda Harris for all the support offered during my PhD course.

This does stand to say that this wouldn't have been possible without my Sponsor, The Higher Committee for Education Development in Iraq (HCED). A sincere thanks to this organization for all the support they have provided financially. I

would also thank my patrons Dr. Hayder Abdhusein, Mr. Qais Al Hawani, and Mr. Mohammed Gazi.

I would thank Mrs Fiona HF Rodgers for ordering and helping me with the lab training, and both lab groups (crystallography and Poolism) for their help and support, especially Naer AlKaabawi, Sami Melebari, Hannah Southam, and Helen Jesse. And a very big thanks to my friends Olga and Sony for all the support and encouragement that they offer me in both personal and scientific fields.

Finally, I would conclude my acknowledgement by thanking my family who trust me and believed that I can do it, and kept pushing me forward, especially my brothers and their families. I couldn't have endured this venture without the supportive hands of my husband of which his love and patience were the best support I received during this long journey.

Thank you all for being so supportive and approachable both in my social life and for the completion of this work.

Abbreviation

Specific abbreviation

BLAST	Basic Local Alignment Search Tool
Cco	Cytochrome <i>c</i> oxidase
CFE	Cell free extract
CODH	Carbon monoxide dehydrogenase
Cor	Carbon monoxide resistance protein
<i>E. coli</i>	<i>Escherichia coli</i>
FDP	Flavodiiron proteins
Fe-S	Iron-sulfur cluster
FprA	A- type flavoproteins
fr	Fraction
Hcp	hybrid cluster protein
Hmp, flavoHb	Flavo-hemoglobin
Hrb	High molecular weight rubredoxin
iNOS	inducible nitric oxide synthase
LB	Lysogeny broth
<i>M. smegmatis</i>	<i>Mycobacterium smegmatis</i>
Mtb	<i>Mycobacterium tuberculosis</i>
Mwt	Molecular weight
NCBI	National Centre for Biotechnology Information
NOD	Nitric oxide dioxygenase
NOR	Nitric oxide reductase
NorV, F1Rd	Flavorubredoxin
NorW	NADH-Flavorubredoxin oxidoreductase
NOS2	Nitric oxide synthase type 2
NrfA	Cytochrome <i>c</i> nitrite reductase

NRO	NADH- rubredoxin oxidoreductase
OD ₆₀₀	Optical density at 600 nm
PDB	Protein data bank
PMN	Polymorphonuclear leukocytes
Rd	Rubredoxin
RdxR	Rubredoxin reductase
RNS	Reactive nitrogen species
ROO	Rubredoxin: Oxygen Oxidoreductase
ROS	Reactive oxygen species
δ ALA	δ-Aminolevulinic acid hydrochloride, 5-Amino-4-oxopentanoic acid hydrochloride
n	Number of biological repeats

Chemical abbreviation

APS	Ammonium per sulfate
C	Cysteine
cGMP	Cyclic guanosine monophosphate
CO	Carbon monoxide
CO ₂	Carbon dioxide
CORM-2	Tricarbonyldichlororuthenium (II) dimer
DETA-NONOate	(Z)-1-[2-(2-Aminoethyl)-N-(2-ammonioethyl) amino] diazen-1-ium-1,2-diolate,3,3-Bis(aminoethyl)-1-hydroxy-2-oxo-1-triazene,2,2'-(Hydroxynitrosohydrazino)bis-ethanamine
Eu ³⁺	Europium
F	Phneylalanine
FAD	Flavin adenine dinucleotide
Fe	Iron
FeCl ₃	Iron(III) chloride

FMN	Flavin mononucleotide
H ₂ SO ₄	Sulfuric acid
HCl	Hydrochloric acid
I	Isoleucine
IPTG	Isopropyl-1-thio-β-d-galactopyranoside
KI	Potassium iodide
MPD	2-Methyl-2,4-pentanediol
MV	Methyl viologen
N ₂	Nitrogen
N ₂ O	Nitrous oxide
NADP	Nicotine adenine dinucleotide phosphate
NaI	Sodium iodide
NaNO ₂	Sodium nitrite
NO	Nitric oxide
NO ₂	Nitrogen dioxide
NO ₂ ⁻	Nitrite
NO ₃ ⁻	Nitrate
O ₂	Oxygen
O ₂ ⁻	Superoxide anion
PEG	Polyethylene glycol
PI	Isoelectric point
PROLI-NONOate	1-(hydroxy-NNO-azoxy)-L-proline, disodium salt
Q	Glutamine
R	Arginine
S	Serine
SDS	Sodium dodecyl sulfate
TAE	Tris Acetate-EDTA buffer
tsp	Trimethylsilylpropanoic acid

W	Tryptophan
Y	Tyrosine
Zn	Zinc ion

Technique abbreviation

EPR	Electron paramagnetic resonance
FTIR	Fourier Transform Infrared spectroscopy
ICP-MS	Inductively coupled plasma mass spectrometry
MS	Mass spectrometry
NMR	Nuclear magnetic resonance
PAGE	Polyacrylamide gel electrophoresis
PCR	Polymerase chain reaction
SAXS	Small-angle-X-ray scattering

Crystallography abbreviation

ρ	The electron density
a,b,c	Real space unit cell dimensions
AU	Asymmetric unit
B-factor	Crystallographic temperature factor
CCD	Charge coupled device
CCP4	Collaborative Computational Project, Number 4
C α	Alpha carbon of amino acid
F	Structure factors
F(<i>hkl</i>)	Structure factor for reflection <i>h k l</i>
F _{cal}	Calculated structure factor
FFT	Fast Fourier Transform
<i>h k l</i>	Reciprocal lattice points
IP	Image plate detector
JCSG	Joint Centre for Structural Genomics
LLG	Log- Likelihood gain

MAD	Multi-wavelength anomalous dispersion
SAD	Single-wavelength anomalous dispersion
MIR	Multiple isomorphs replacement
SIR	Single isomorphs replacement
MR	Molecular replacement
$P(uvw)$	Patterson function
$P(xyz)$	Electron density at position xyz
PAK	Number of packing clashes
r.m.s.d	root-mean-square deviation of atomic positions
RF	The Rotation function
R_{free}	R-factor for free set of reflection
RFZ	Rotation function Z-score
R_{meas}	Measurement of uncertainty before merging the data
R_{merge}	The difference between two data set
R_{pim}	Multiplicity weighted merging R-factor
TF	The Translation function
TFZ	Translation function Z-score
u, v, w	Patterson space coordinates
x, y, z	Real space coordinates
α, β, γ	Real space unit cell angles
$ F(hkl) $	Structure factor amplitude for reflection $h k l$
$ F_{\text{calc}} $	Calculated structure factor amplitude
$ F_{\text{obs}} $	Observed structural factor amplitude
Units	
°	Degree
°C	Degree Celcius
Å	Ångstrom

Da	Dalton
g	gram
h	Hour
kDa	Kilo Dalton
min	Minute
m	Milli
M	Molar
ml	Millilitre
rpm	Rotation per minute
s	Second
w/v	Weight / volume
μ	Micro

Table of Content

Summary.....	II
DEDICATION.....	V
ACKNOWLEDGEMENT.....	VI
Abbreviation.....	VIII
Table of Content.....	XIV
Table of Figures.....	XIX
List of tables.....	XXII
Chapter 1 : Introduction.....	1
1. Introduction.....	2
1.1 Immune defense.....	2
1.2 Innate immunity.....	2
1.3 Nitric Oxide (NO).....	4
1.4 The role of NO in the biological systems.....	5
1.5 NO detoxification by bacteria.....	7
1.6 Nitrous oxide (N ₂ O).....	8
1.7 The production and consumption of N ₂ O.....	9
1.7.1 Heme and copper Nitric oxide reductase (NOR).....	10
1.7.1.1 cNOR (cytochrome <i>bc</i> type complex).....	10
1.7.1.2 qNOR.....	11
1.7.1.3 qCu _A NOR.....	12
1.7.2 Flavodiiron reductase or Flavodiiron proteins (FDPs).....	13
1.7.2.1 Flavohemoglobin (Hmp).....	15
1.8 <i>nor</i> operon.....	16
1.8.1 NorR.....	17
1.8.2 NorV (Flavorubredoxin FIRd).....	18
1.8.3. NorW (NADH: flavorubredoxin oxidoreductase).....	23
Scope of study.....	27
Chapter 2 : Theory of X-ray crystallography.....	28
2. Theory of crystallography.....	29
2.1 Introduction.....	29
2.2 Protein crystals.....	29
2.3 Protein sample preparation.....	31
2.4 Crystallization techniques.....	32
2.4.1 Vapor diffusion method.....	32
2.4.1.1 Sitting drop method.....	32
2.4.1.2 Hanging drop method.....	33
.....	34
2.5 Cryoprotectant and crystal mounting.....	34
2.6 X-ray & generators.....	36
2.6.1 Stationary anode X-ray tube.....	36
2.6.2 Rotating Anode X-ray tube.....	37
2.6.3 Synchrotrons.....	38
2.7 X-ray reflection and detectors.....	39
2.7.1 Image plate detectors (IP).....	39
2.7.2 Charge coupled device (CCD).....	40
2.8 X-ray diffraction and Bragg's law.....	41

2.9 Atomic scattering factors.....	43
2.10 Structure factors	44
2.11 Molecule scattering.....	45
2.12 Crystal scattering.....	45
2.13 Data processing.....	46
2.13.1 Auto-indexing.....	46
2.13.2 Integration	46
2.13.3 Scaling and merging.....	46
2.14 Phase determination	47
2.14.1 Molecular replacement.....	48
2.14.1.1 Rotation function search.....	49
2.14.1.2 The Translation function search.....	49
2.15 Electron density	49
2.16 Structure refinement	50
2.16.1 The B- factor.....	50
2.16.2 Judging the refinement by R-factor.....	51
2.17 Model validation	51
2.17.1 Ramachandran plot.....	51
Chapter 3 : Materials and methods.....	53
3. Materials and methods	54
3.1 Materials	54
3.1.1 Chemicals	54
3.1.2 Bacteria and plasmids	54
3.1.3 Oligos and restriction enzymes	56
3.1.4 Restriction enzymes.....	58
3.2.2 Genomic DNA isolation	59
3.2.3 Transformation trial.....	59
3.2.4 Plasmid DNA isolation.....	59
3.2.5 Agarose gel electrophoresis.....	60
3.2.6 Amplification of target genes by Polymerase Chain Reaction (PCR)	60
3.2.7 PCR clean up	61
3.2.8 Restriction digestion.....	61
3.2.9 Ligation	62
3.2.10 Transformation.....	62
3.2.10.1 Preparation of chemically competent <i>E. coli</i> Top 10	62
3.2.10.2 Preparation of electrocompetent <i>E. coli</i> Top 10	62
3.2.10.3 Heat shock transformation	63
3.2.10.4 Electroporation transformation	63
3.2.11 Ligation results analysis	63
3.2.11.1 Restriction digestion of the constructs.....	63
3.2.11.2 Colony PCR for pET21a	63
3.2.11.3 Sequencing	64
3.2.12 Site direction mutagenesis experiment	64
3.2.13 Protein overexpression.....	64
3.2.14 Checking the expression	65
3.2.15 Protein solubility.....	65
3.2.16 Small scale protein purification.....	65
3.2.17 Large scale protein production.....	66
3.2.18 Large scale protein purification	66
3.2.18.1 Ni and Ion exchange column purification.....	66
3.2.18.2 Gel filtration (GF) purification.....	67
3.2.19 Mass spectrometry (MS).....	67
3.2.20 Nuclear Magnetic Resonance (NMR) spectroscopy.....	67
3.2.21 Crystallization trial.....	67
3.2.22 Optimization trial.....	68

3.2.23 Data collection.....	69
3.2.24 Data processing	69
3.2.25 Structure determination.....	70
3.2.25.1 Phase determination.....	70
3.2.25.2 Structure refinement.....	70
3.2.25.3 Testing for the presence of the rubredoxin domain	71
3.2.26 Biochemical studies	71
3.2.26.1 NO consumption <i>in vitro</i> assay.....	71
3.2.26.1.1 NO and O ₂ electrode calibration.....	71
3.2.26.1.2 Preparation of PROLI-NONOate.....	72
3.2.26.1.3 Aerobic NO consumption	72
3.2.26.1.4 NO consumption with gradual change in O ₂ level.....	73
3.2.26.1.5 NO consumption with constant O ₂ level.....	74
3.2.26.2 <i>in vivo</i> assays	74
3.2.26.2.1 NO consumption in intact <i>E. coli</i> cell suspension (anaerobic assay)	74
3.2.26.2.2 NO susceptibility of <i>E. coli</i> strains	75
3.2.26.3 Growth curve of <i>E. coli</i> mutant strains.....	76
3.2.26.4 Fourier transform infrared spectroscopy (FTIR) assay	76
3.2.26.5 ICP-MS.....	77
3.2.26.6 Carbon monoxide dehydrogenase (CODH) assay	78
3.2.26.7 Assay of Cor protection of <i>E. coli</i> from CORM-2 toxicity.....	78
3.2.26.8 Hematin assay.....	79
3.2.26.9 Pull down assay using Cor with <i>E. coli</i> or <i>M. smegmatis</i> CFE	80
3.2.26.10 Fourier transform infrared spectroscopy (FTIR) of Cor with CO.....	81
3.2.26.11 Nuclear Magnetic Resonance spectroscopy (¹ H NMR) of Cor with CO	82
3.2.26.12 ICP-MS of Cor.....	82

Chapter 4 : Functional and structural studies of flavorubredoxin oxidoreductase (NorW) 83

4. Introduction: NorW can consume NO without NorV 84

4.1 <i>norW</i> cloning.....	84
4.2 Restriction digestion.....	85
4.3 Ligation.....	86
4.4 Transformation	86
4.5 Ligation analysis by restriction digest for pBAD/ <i>norW</i> constructs.....	87
4.6 Sequence analysis.....	91
4.6.1 pBAD/ <i>norW</i> constructs	91
4.6.2 pET21a/ <i>norW</i> constructs sequence results.....	96
4.7 Site directed mutagenesis.....	96
4.8 NorW expression	96
4.9 Protein solubility.....	100
4.10 Large scale expression.....	101
4.11 Protein purification.....	102
4.12 Crystallization results.....	110
4.13.1 NO consumption.....	111
4.13.1.1 NO (<i>in vitro</i>) consumption aerobic assay	111
A- Assay in the presence of NorV/NorW complex.....	111
B- Assay in the presence of NorV alone	114
C- Assay in the presence of NorW alone	114
4.13.1.2 NO anaerobic consumption by NorW (<i>in vitro</i>) assay.....	118
A- Assay on the effect of O ₂ level.....	118
B- Assay under constant O ₂ level	119
4.13.2 NO consumption by NorW <i>in vivo</i> assays	122
4.13.2.1 Susceptibility test.....	122
4.13.2.2 Growth curve for <i>E. coli</i> mutants under different concentrations of NONOate.....	124
4.13.2.3 NO anaerobic consumption in intact cell suspension	126

4.13.3 NO reduction to N ₂ O	128
4.14 Chemical characterization	129
4.14.1 Mass spectrometry	129
4.14.2. Inductivity Coupled Plasma- Mass Spectrometry (ICP-MS)	131
4.15 Discussion	131
4.15.1 Can NorW reduce NO to N ₂ O without NorV?	131
4.15.2 Protein purification.....	132
4.15.3 NorW crystallization	132
4.15.4 NorW consumes NO without NorV	134
A- <i>in vitro</i> assays	134
B- <i>in vivo</i> assays	135
4.15.5 Checking the final product of NO removal by NorW	137
4.15.6 Metal content of NorW	138
Chapter 5 : Flavorubredoxin (NorV) structure in <i>E. coli</i>	140
5. Introduction.....	141
5.1 Amplification of <i>norV</i> by polymerase chain reaction (PCR)	141
5.2 PCR clean up	142
5.3 Restriction digestion.....	143
5.4 Ligation	143
5.5 Transformation	143
5.6 Ligation results analysis.....	143
5.6.1 Restriction digestion of <i>norV</i> constructs.....	143
5.6.2 Sequence analysis of <i>norV</i> constructs.....	144
5.7 Site directed mutagenesis.....	146
5.8 Small scale protein expression.....	146
5.9 NorV solubility test.....	147
5.10 Large-scale expression.....	147
5.12 NorV purification.....	148
5.13 NorV Mass spectrometry (MS)	151
5.14 Crystallization trial	152
5.15 Optimization trial	154
5.16 Structure determination.....	155
5.16.1 Data collection.....	155
5.16.2 Structure determination and model building.....	160
5.16.2.1 Matthews probability calculation	160
5.16.2.2. Molecular replacement.....	162
5.16.2.3 Model refinement.....	163
5.16.2.4 Final refined structure.....	165
5.16.3 Comparison of <i>E. coli</i> NorV structures.....	169
5.17 Discussion	176
5.17.1 NorV production.....	177
5.17.2 NorV purification	177
5.17.3 NorV structure refinement and final structure.....	178
5.17.4 Comparison between <i>E. coli</i> NorV models and homologues.....	178
Chapter 6 : Does Cor protect <i>E. coli</i> from CO toxicity?	180
6. Introduction.....	181
6.1 Carbon monoxide (CO)	181
6.2 Bacterial heme oxygenase	182
6.3 Effects of CO on humans and bacteria.....	183
6.4 Carbon monoxide resistant protein (Cor)	185
Results	187
6.5 Cor Mtb expression.....	187
6.6 Solubility test	188

6.7 Large scale protein expression.....	189
6.8 Protein purification.....	190
6.9 Chemical characterization of Cor.....	194
6.9.1 Mass spectrometry.....	194
6.9.2 Nuclear magnetic resonance NMR.....	195
6.9.3 ICP-MS.....	195
6.10 Initial crystallization and optimization trials.....	196
6.11 X-ray Data collection.....	200
6.12 Studies to reveal Cor mechanism of action.....	200
6.12.1 Carbon monoxide dehydrogenase (CODH) assay.....	201
6.12.2 The ability of Cor to protect <i>E. coli</i> from CORM-2.....	201
6.12.3 Hematin assay.....	202
6.12.4 Pull down assay.....	204
6.12.5 FTIR (Fourier transform infrared spectroscopy).....	206
6.12.6 NMR for Cor with and without CO gas.....	207
6.13 Discussion.....	209
Carbon Monoxide Resistance protein (Cor).....	209
6.13.1 Cor purification.....	209
6.13.2 Chemical characterization of Cor.....	210
6.13.3 Crystallization and data collection.....	210
6.13.4 Biochemical studies for Cor.....	212
Chapter 7 : Conclusion and future plan.....	216
Conclusion.....	217
Ideas for future experiments.....	219
References.....	221
Appendices.....	256
Appendix 1: Genomic DNA isolation protocol.....	257
Appendix 2: Media.....	257
Appendix 3: Transformation protocol (Chemotransformation).....	258
Appendix 4: Buffers and solutions that were used in this study.....	258
Appendix 5: Hannah method for chemocompetent cell preparation.....	259
Appendix 6: electrocompetent cell preparation and electroporation.....	260
Appendix 7 Site directed mutagenesis.....	262
Appendix 8: protein expression.....	263
Appendix 9 Batch method for protein purification.....	264

Table of Figures

Figure 1-1 Polymorphonuclear leukocytes.....	3
Figure 1-2 Macrophags.....	3
Figure 1-3 NO generation within the macrophage.....	5
Figure 1-4 NO reduction in the non-denitrifiers	9
Figure 1-5 The membrane-bound and soluble NOR complexes	10
Figure 1-6 cNOR and qNOR trans-membrane helices	12
Figure 1-7 The electron transfer scheme in NO detoxification enzymes	14
Figure 1-8 <i>norRVW</i> operon	17
Figure 1-9 NorR domain structure	18
Figure 1-10 NorV protein sequence	19
Figure 1-11 NorV structure	21
Figure 1-12 NorV tunnel	22
Figure 1-13 NMR structure of the <i>E. coli</i> Rubredoxin	23
Figure 1-14 <i>E. coli</i> NorW protein sequence	24
Figure 1-15 Crystal structure of <i>Pseudomonas aeruginosa</i> rubredoxin reductase (RdxR) (NorW homologue)	25
Figure 1-16 Protein sequence alignment of the <i>E. coli</i> NorW with the homologue rubredoxin reductase (RdxR) from <i>Pseudomonas aeruginosa</i>	26
Figure 2-1 Phase diagram of protein crystallization.....	31
Figure 2-2 Sitting drop crystallization method.....	33
Figure 2-3 Scheme of hanging drop crystallization method.....	34
Figure 2-4 Crystal mounting loop.....	35
Figure 2-5 X-ray tube. The figure shows the X-ray tube components.....	37
Figure 2.6 Rotating anode X-ray tube.....	38
Figure 2.7 Synchrotron components.....	39
Figure 2.8 Image plate detector.....	40
Figure 2.9 Charge coupled device (CCD).....	41
Figure 2.10 The constructive and destructive interference of X-ray.....	42
Figure 2.11 Bragg's law.....	43
Figure 2.12 The atomic scattering factor curve for different atoms.....	44
Figure 2.13 A representation of the Rotation and Translation steps in the Molecular Replacement method.....	48
Figure 2.14 Example of a Ramachandran plot.....	52
Figure 3.1. CORM-2.....	79
Figure 4.1: DNA gel electrophoresis of <i>norW</i> PCR products.....	85
Figure 4.2: The DNA extracted from pBAD/ <i>norW</i> colonies.....	87
Figure 4.3: Restriction digestion results of the DNA of pBAD/ <i>norW</i> constructs.....	88
Figure 4.4: The DNA extracted from pBAD/ <i>norW</i> constructs.....	89
Figure 4.5: restriction digestion analysis of pBAD/ <i>norW</i> constructs.....	90
Figure 4.6: Colony PCR for pET21a/ <i>norW</i> constructs.....	91
Figure 4.7 A, B and C: DNA sequence alignment of pBAD/ <i>norW</i> constructs with and without His-tag with <i>E. coli</i> MG1655 <i>norW</i> by using NCBI blast.....	93-95
Figure 4.8: SDS-PAGE of His-tagged NorW expression from construct 9.....	97

Figure 4.9: SDS-PAGE of His-tagged NorW expression in construct 4.....	98
Figure 4.10: SDS-PAGE of His-tagged NorW expression in construct 4.....	99
Figure 4.11: SDS-PAGE of untagged NorW (construct 2) expression.....	100
Figure 4.12: SDS-PAGE of His- tagged and untagged NorW solubility.....	101
Figure 4.13: SDS-PAGE of a His-tagged NorW large scale culture expression.....	102
Figure 4.14: SDS-PAGE of Batch purification.....	103
Figure 4.15: His-tagged NorW purification by Ni-NTA column.....	104
Figure 4.16: NorW purification by gel filtration.....	105
Figure 4.17: NorW purified protein.....	106
Figure 4.18: Untagged NorW purification.....	107
Figure 4.19: SDS-PAGE of DEAE and GF purification of untagged NorW.....	108
Figure 4.20: Purification of untagged NorW by Resource Q column.....	109
Figure 4.21: Crystals observed during crystallization screening of NorW. After testing for X-ray diffraction, all of the crystals proved to be inorganic salts.....	110
Figure 4.22: <i>In vitro</i> NO consumption (Control).....	112
Figure 4.23: NO (<i>in vitro</i>) consumption using NorVW complex.....	113
Figure 4.24: NO consumption by NorV alone.....	114
Figure 4.25: NO consumption by NorW alone.....	115
Figure 4.26: Addition of PROLI-NONOate to check NO consumption by NorW....	115
Figure 4.27 A: NO uptake by NorW without NADH.....	116
Figure 4.27 B: NO uptake by NADH without NorW.....	116
Figure 4.28: NO uptake by varying concentration of NorW.....	117
Figure 4.29: The effect of FAD on NO consumption.....	117
Figure 4.30: NO consumption in aerobic, microaerophilic, and anaerobic condition	119
Figure 4.31: NO consumption with open O ₂ electrode.....	120
Figure 4.32: NO consumption with an open O ₂ electrode under higher concentrations of the oxygen depletion system and higher stir rate.....	121
Figure 4.33: NO consumption with an open O ₂ electrode.....	122
Figure 4.34: NO susceptibility test.....	123
Figure 4.35: NO susceptibility test using an <i>E. coli norVW</i> mutant strain.....	124
Figure 4.36: Growth curve of <i>E. coli norR hmp</i> mutant.....	125
Figure 4.37: Growth curves of <i>E. coli</i> multiple mutants by plate reader.....	126
Figure 4.38: NO consumption in cell suspension.....	127
Figure 4.39: NO consumption in intact cell suspension.....	128
Figure 4.40: FTIR spectra of different <i>E. coli</i> cultures with and without pBAD expression vector and treated with DETA-NONOate.....	129
Figure 4.41: Mass spectra of NorW His-tagged protein.....	130
Figure 5.1: The PCR product of <i>norV</i> before cleaning up.....	142
Figure 5.2: <i>norV</i> PCR product after clean up.....	142
Figure 5.3: <i>norV</i> / pBAD constructs.....	144
Figure 5.4: Sequence alignment of <i>norV</i> construct 11.....	145
Figure 5.5: SDS-PAGE of NorV small-scale culture to test expression in Top10 cells.....	146
Figure 5.6: The SDS-PAGE of NorV solubility test results.....	147

Figure 5.7: SDS-PAGE of NorV large-scale expression.....	148
Figure 5.8: NorV purification by using DEAE column.....	149
Figure 5.9: Gel Filtration purification.....	150
Figure 5.10: NorV purified protein.....	151
Figure 5.11 Mass spectrum for NorV.....	152
Figure 5.12: NorV crystals in the initial screens.....	153
Figure 5.13: NorV crystal grown in 0.2 M sodium sulfate and 20 % (w/v) PEG 3350.....	153
Figure 5.14 NorV crystal grown in the JCSG screen from protein purified with a protease inhibitor.....	154
Figure 5.15: NorV optimized crystals.....	154
Figure 5.16 NorV C2 crystal in the mounting loop.....	155
Figure 5.17: The initial density map produced from Phaser program.....	162
Figure 5.18: Steps of NorV structure refinement using REFMAC5.....	164
Figure 5.19: The final structure of NorV.....	166
Figure 5.20: NorV crystal lattice.....	167
Figure 5.21: SDS-PAGE of NorV crystal solution.....	168
Figure 5.22: MS for NorV protein diagnosis.....	169
Figure 5.23: Superposition of C2 model chain A with chain A of PDB entry 5LMC	172
Figure 5.24: Superposition of NorV C2 crystal structure with <i>Moorella thermoacetica</i> flavoprotein A (FprA 2).....	173
Figure 5.25: NorV (C2 and 5LMC) models superimpose.....	174
Figure 5.26: NorV P1 and 5LMC models superimpose.....	174
Figure 5.27: NorV 5LMC and P4 models superimpose.....	175
Figure 5.28: NorV 5LMC and P6 models superimpose.....	176
Figure 6.1: Alignment of cor gene in pathogenic <i>Mycobacteria</i> , <i>Rhodococcus facians</i> and <i>Thermotoga maritima</i>	186
Figure 6.2 The crystal structure of a Cor homologue from <i>Thermotoga maritima</i> (PDB entry 1VJL).....	187
Figure 6.3: 12% SDS-PAGE of Cor small-scale expression.....	188
Figure 6.4: 12 % SDS-PAGE of Cor solubility test.....	189
Figure 6.5: 12 % SDS-PAGE of <i>cor</i> large-scale expression.....	190
Figure 6.6: Cor purification by Ni column.....	191
Figure 6.7: Cor purification by Heparin and gel filtration columns.....	193
Figure 6.8: Mass spectrometry of Cor.....	194
Figure 6.9: ¹ H NMR one dimension spectrum of Cor.....	195
Figure 6.10: Result from the initial crystal screening of Cor.....	196
Figure 6.11: Crystal of Cor grown at 17 °C in higher Cor concentration.....	197
Figure 6.12: Cor crystal screen results.....	197
Figure 6.13: Cor crystals grown at 7 °C.....	198
Figure 6.14: CODH assay.....	201
Figure 6.15: Cor protein protection of <i>E. coli</i> cells from the toxic effects of CO.....	202
Figure 6.16: Hematin assay.....	203
Figure 6.17: Pull down assay.....	205
Figure 6.18: FTIR spectrum of Cor solution circulated with CO gas.....	206
Figure 6.19: Cor ¹ HNMR spectra with and without bubbling with CO gas.....	208

List of tables

Table 1-1 The role of NO in the immune system.....	7
Table 3-2 The table of strains and plasmids used in this work.....	59-60
Table 3.2 primers used for cloning.....	60-61
Table 3.3 The NO susceptibility cultures.....	81
Table 4.1 ICP-MS result. The table shows metals in mg/L found in NorW sample....	138
Table 4.2 Calculated number of atoms of selected elements per molecule of NorW.....	146
Table 5.1. The processing statics of NorV crystals	157-159
Table 5.2. Matthews coefficient.....	160-161
Table 5.3 the results of final refinement of NorV crystal forms judging from the R factor	163-164
Table 5.4 Statistics of NorV structures superposed.....	170-171
Table 6.1. Cor ICP-MS results.....	196
Table 6.2. Cor crystals optimization.....	199-200
Table 6.3. ICP-MS results for Cor.....	210

Chapter 1 : Introduction

1. Introduction

1.1 Immune defense

In vertebrates, two main immune responses can confront assault by microorganisms or their products: the innate and acquired immune responses. Each system has its components that might be cells or organs classified as physical barriers or highly developed systems.

1.2 Innate immunity

Innate immunity occurs from birth and is the first body defense and produces nonspecific (humoral) immune factors, which can attack a broad spectrum of substances that enter the body. Many organs, such as skin and mucosal membranes (a physical barrier that trap any material trying to enter the body), participate in this rapid process. The lungs, liver and many connective tissues have phagocytic cells that can attack, ingest and destroy infectious agents; bacteria and protozoa produce substances to attract the phagocytic cells, which also release a chemical material, cytokines that alert the immune system to invasion. There are many classes of phagocytic cells:

1- Polymorphonuclear leukocytes (PMN), or so-called granulocytes, play a very important role during infection, since they contain hydrolytic enzymes within the lysosome. PMNs also have bactericidal proteins such as lactoferrin in some of their granules and can produce toxic superoxide radicals and peroxide, but have relatively short lives (Figure 1.1).

2- Mononuclear phagocytic cells such as macrophages are the main component of the mononuclear phagocytic system, contain many lysosomes and have longer lives than granulocytes (Figure 1.2). Macrophages can be found in different tissue such as spleen, lymph nodes, liver, lung, connective tissue and blood and lymph sinuses. They trap and capture the attacking microorganism in the blood stream and expose it to T-lymphocytes, and work as cleaning cells, which destroy any aged or disordered host

cells, such as erythrocytes and cancer cells (Benjamini, 1991; Benjamini and Leskowitz, 1991).

Natural immunity depends on different rapidly activated mechanisms: phagocytosis, by macrophage or neutrophil ingestion of infectious agents; release of reactive hydrolytic enzymes or reactive oxygen intermediate radicals (oxidative burst); activation of

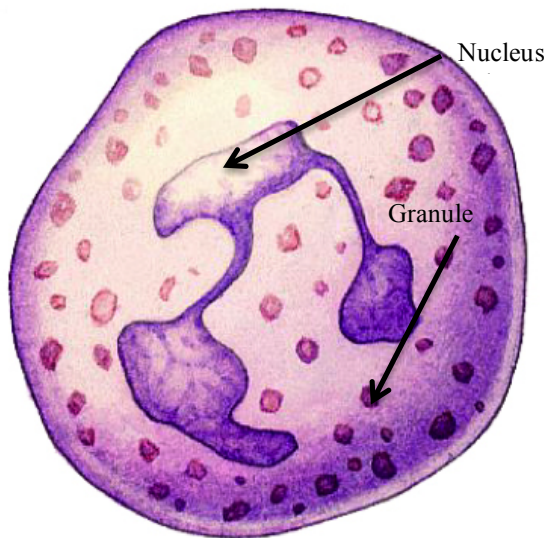


Figure 1-1 Polymorphonuclear leukocytes. The figure shows that the nucleus has 3-4 lobes with neutral granules in the cytoplasm.

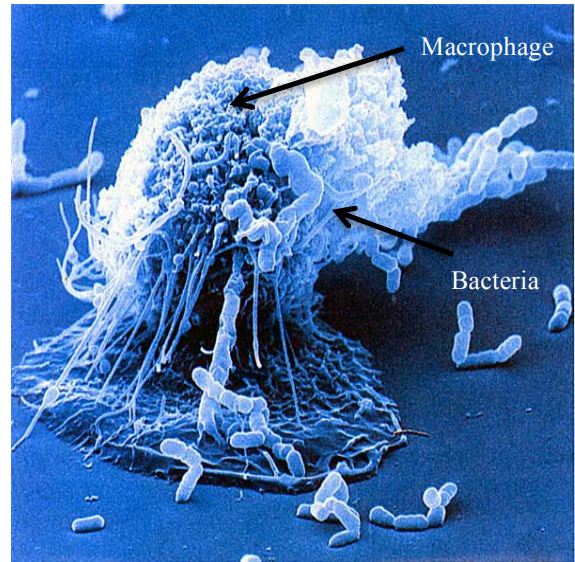


Figure 1-2 Macrophages

Macrophages have a single big nucleus and work to engulf cells. They ingest any foreign substances that attack the body. The figure shows the amoebae-like shape of the macrophage during the engulfment process.

natural killer cells (Fearon and Locksley, 1996); and NO production by (type 2 or inducible) nitric oxide synthase (Nathan, 1992, 1997). The reactive oxygen species (ROS) and the reactive nitrogen species (RNS), oxidative and nitrosative stress respectively, are produced endogenously, by bacteria that live in the same environment, or by the immune system during infection; where ROS can be produced when O_2 reduces to water, and NO is produced during the reduction of nitrite (NO_2^-)/nitrate (NO_3^-) to N_2 (Frey et al., 2002; Ji and Hollocher, 1988; Morita et al., 1997; Poock et al.,

2002). CO can also be produced by macrophages and neutrophils as a part of innate immunity (Wegiel et al., 2014).

Great attention is now on the denitrification process, because the effect of NO as a poison in many environmental issues. NO is known as a ground and a surface water pollutant.

1.3 Nitric Oxide (NO)

NO is a lipophilic (hydrophobic) small molecule, with the ability to diffuse through biological membranes (Pacher et al., 2007) and has an unpaired electron, which can interact with O_2 or O_2^- (Hughes, 1999). Its biological half-life is relatively short (30 min), then it is oxidized to NO_2 (Poole and Hughes, 2000).

Between 1985 and 1990, NO was introduced to the immunological world. NO was identified firstly as a vasodilatory messenger in 1987 (Ignarro et al., 1987b). NO is released by the endothelial cells as a response to different stimuli, and immediately after release, it activates the guanylate cyclase in the smooth muscle cells and platelets, which increases the intracellular messenger cGMP levels and this is followed by muscle relaxation and inhibition of platelet aggregation (Moncada and Higgs, 1993; Poole and Hughes, 2000).

NO is mainly produced from L-arginine by inducible nitric oxide synthase (iNOS) or nitric oxide synthase 2 (NOS2) (Figure 1.3) (Bogdan, 2001; Cutruzzolà, 1999; Vallance and Charles, 1998), in various parts of the human body, but mainly in immune system cells such as dendritic cells, natural killers, mast, and phagocytic cells, which include monocytes, macrophages, microglia, Kupffer cells, eosinophils, and neutrophils (Bogdan, 2001). NO has many roles in biological systems, as detailed in the next section.

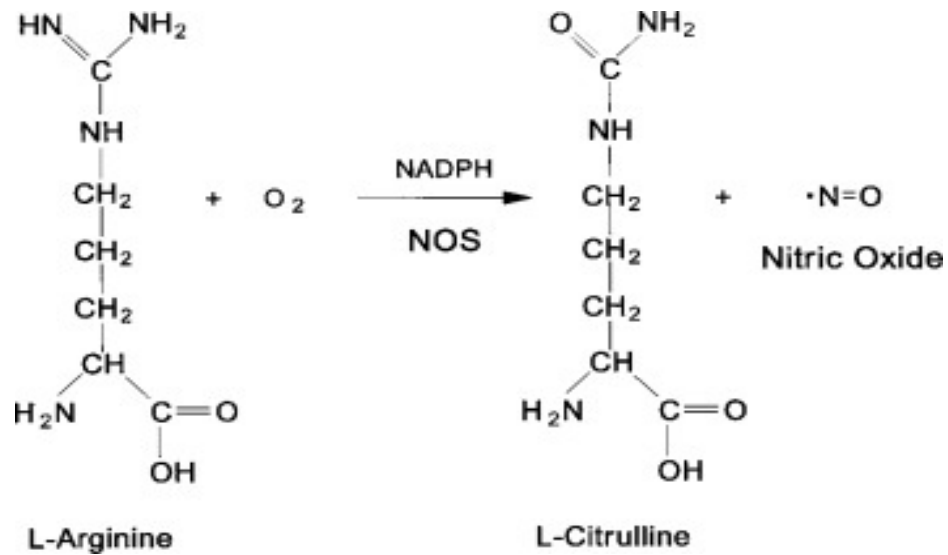


Figure 1-3 NO generation within the macrophage. The figure shows that L-Arginine is converted to citrulline and NO by isoform nitric oxide synthase (iNOS). (Hart , 1999)

1.4 The role of NO in the biological systems

In the environment NO is a part of the natural gases (Payne et al., 1997; Watmough et al., 1999; Zumft, 1997). In humans, NO synthases produce NO sufficiently, which poison pathogens, opportunistic organisms and neoplastic tissue (Fang, 1997). Ultimately, the cytotoxic and cytostatic effects of NO can also affect the host cells, and this depends mainly on the concentration of NO. In nanomolar concentration generated by NO synthase, NO works as a cell signaling molecule where it interacts with different soluble enzymes such as guanylyl cyclase and cytochrome *c* oxidase (Gomes et al., 2002a; Vallance and Charles, 1998; Zumft, 2002). At higher concentration, NO also inhibits the terminal oxidases and aerobic respiration (Gardner et al., 2001). Aconitase, a citric acid cycle enzyme, can be affected with low concentration of NO by destroying its distinct [4Fe-4S] centre (Gardner et al., 1997; Gardner et al., 2001). At higher concentration guanylyl cyclase, cytochrome *c* oxidase and other enzymes can be targeted by NO. This includes heme containing enzymes, enzymes with Fe-S clusters (aconitase, NADH dehydrogenase and succinate

dehydrogenase), non-heme metalloenzymes and ribonucleotide reductase. Other molecules such as DNA can also be disrupted by NO (Poole and Hughes, 2000; Vallance and Charles, 1998). NO plays a crucial role in different biological systems once it is released. Table 1.1 summarizes the role of NO in the immune system.

Table 1-1: The role of NO in the immune system. The table summarizes the main roles of NO in the immune system, the cells that produce it, and its effect.

Category	Producers of NO	Phenotypic effect of NO
Antimicrobial activity	Macrophages, microglia, neutrophils, eosinophils, fibroblasts, endothelial cells, epithelial cells, astroglia	Killing or reduced replication of infectious agents (viruses, bacteria, protozoa, fungi, helminths)
Anti-tumor activity	Macrophages, eosinophils	Killing or growth inhibition of tumor cells
Tissue-damaging effect	Macrophages, microglia, astroglia, keratinocytes, mesangial cells	Necrosis or fibrosis of the parenchyma
Anti-inflammatory– immunosuppressive effect	Macrophages ('suppressor phenotype')	Inhibition of : •T cell proliferation •B cell proliferation •Antibody production by CD5+ B cell Autoreactive T and B cell diversification Inhibition of leukocyte recruitment (adhesion, extravasation, chemotaxis)
Modulation of the production and function of cytokines, chemokines, and growth factors (pro- or anti-inflammatory effects)	Macrophages T cells endothelial cells fibroblasts	Up- and downregulation, <i>e.g.</i> , of: •IL-1, IL-6, IL-8, IL-10, IL-12, IL-18, IFN- γ , TNF •TGF- β , G-CSF, M-CSF, VEGF, •MIP-1 α , MIP-2, MCP-
T helper cell deviation	<i>e.g.</i> , macrophages	*Induction and differentiation of T _H 1 cells *Suppression of T _H 1 (and of T _H 2) cell responses * Suppression of tolerogenic T cell responses

Modified from (Bogdan, 2001).

Despite advantages of NO for eukaryotes, NO has many drawbacks in prokaryotes; a large literature describes the importance of NO as an antimicrobial agent, as part of the immune system to combat many invader microorganisms (Bogdan, 2001; Flatley et al., 2005; Gardner et al., 2001; Justino et al., 2005; Laver et al., 2010; McLean et al., 2010; McMullin et al., 2005; Vallance and Charles, 1998).

Shank and coworkers in 1962 proved that NO can prevent meat spoilage, and NO has antimicrobial property (Shank et al., 1962).

It has been also demonstrated that NO can defend cells against tumors, through many events including invasion, cell cycle, angiogenesis, apoptosis, and metastasis (Ying and Hofseth, 2007).

Blood pressure and cardiovascular health can be maintained by NO. It has been known that nitroglycerine which produces NO by mitochondrial aldehyde dehydrogenase, causes blood vessels to dilate, and increases blood flow (Chen et al., 2005).

During the infection, blood cells (especially macrophages) produce NO to kill the invader (Bogdan, 2001; Poole and Hughes, 2000). It has been found that NO can be very effective on the causative agent of pneumonia, especially in the intensive care patients (Ying and Hofseth, 2007). It has been proven that gaseous NO acts as a bactericidal at 200 ppm (McMullin et al., 2005). In the nervous system, NO stimulates brain and modulates many functions from behavior to gastrointestinal activity (Poole and Hughes, 2000).

It has been mentioned that NO lifetime in the aerobic condition of growth is shorter than in anaerobic. Therefore, the cytotoxic effect of NO in the anaerobic condition is much greater than in aerobic (Justino et al., 2005).

1.5 NO detoxification by bacteria

For pathogenic bacteria, the denitrification process occurs during the infection, since the macrophages produce NO as an antimicrobial agent.

To detoxify NO, bacteria use many systems under the aerobic and anaerobic conditions. The most important way under aerobic conditions is via flavohemoglobin (Hmp), a protein encoded by the *hmp* gene which oxidases NO to NO₃⁻ under aerobic conditions and reduces NO to N₂O under anaerobic conditions (Cramm et al., 1994; Favey et al., 1995; Gardner and Gardner, 2002).

Under anaerobic conditions there are many proteins that have been listed as participants in NO reduction: Hmp; cytochrome *c* or *c'* (Stamler et al., 1992); multi-heme nitrite reductase (Bueno et al., 1985; Watmough et al., 1999); bacterioferritin (Gardner, 2002); terminal respiratory oxidase (Gardner et al., 2002); copper-nitrite reductase (Plamann and Stauffer, 1983); ribonucleotide reductase (Haskin et al., 1995) and Cu, Zn-superoxide dismutase (McCord and Fridovic, 1969). Recently it has been reported that another NO reductase in *E. coli* known as hybrid cluster protein (Hcp) reduces NO to N₂O (van den Berg et al., 2000; Wang et al., 2016). Hmp and NOR play the most important role in NO detoxification (Baptista et al., 2012; Gardner and Gardner, 2002).

The N₂O product of NO reduction contributes in the greenhouse gas manifestation. N₂O has much concern related to the Ozone chemistry of the atmosphere.

1.6 Nitrous oxide (N₂O)

Nitrous oxide is water soluble, inert and produced as an intermediate gas in the denitrification process which makes a great contribution to the greenhouse gases effect (Richardson et al., 2009). N₂O is a non-toxic gas, because of its low affinity for binding to the metallic center of proteins such as hemoglobin. Microorganisms can tolerate a high concentration of N₂O reaches to millimolar unlike NO that is highly toxic in such concentration. N₂O can be used as a terminal electron acceptor and be reduced to N₂ in some bacteria (Smith, 1983). N₂O is produced indirectly during NO₃⁻ and NO₂⁻ reduction in the NO₃⁻ respiring, non-denitrifiers (such as enteric bacteria) (Smith, 1983) (Figure 1.4).

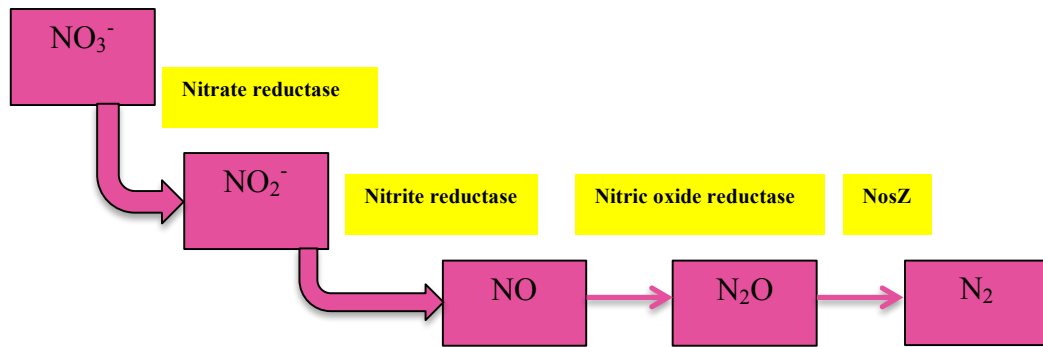


Figure 1-4 NO reduction in the non-denitrifiers. The figure shows that nitrate (NO_3^-) is reduced to nitrite (NO_2^-), which then is reduced to nitric oxide (NO), the nitric oxide ultimately is reduced to nitrous oxide (N_2O), and nitrous oxide eventually reduces to nitrogen (N_2).

1.7 The production and consumption of N_2O

Production and consumption of nitrous oxide is an intensively discussed topic (Spiro, 2012). Nitric oxide reductases (NORs) are the main enzymes that produce N_2O . NORs have two main classes: the heme and copper containing reductases, and the flavin containing reductases. Heme and copper containing reductases are subdivided to three main types: cNOR; qNOR and qCu_A NOR, as shown in Figure 1.5.

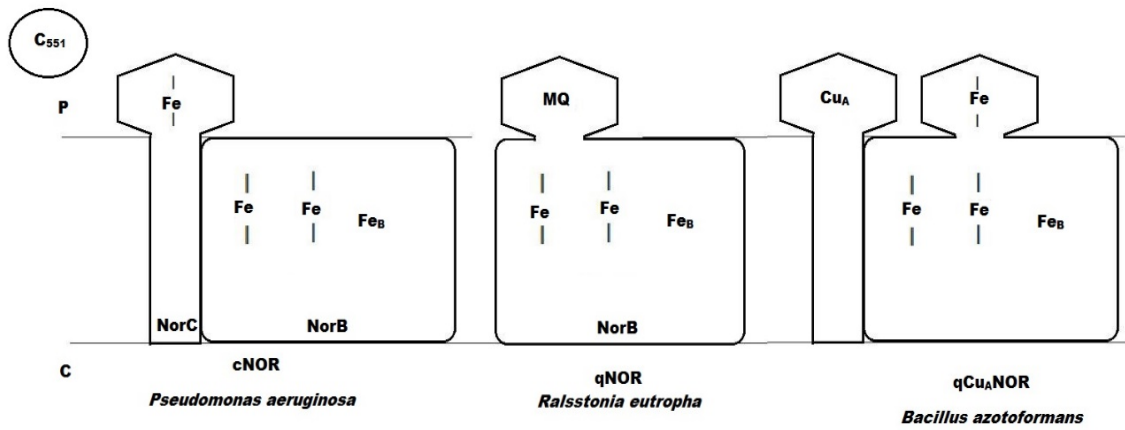


Figure 1-5 The membrane-bound and soluble NOR complexes. The cNOR has two membrane subunits and accepts electrons from a small soluble *c*-type cytochrome or pseudoazurin. The qNOR is a monomer that accepts electrons from the quinone pool. The qCu_ANOR accepts electrons either from a membrane-associated cytochrome *c* or from menaquinol. P and C indicate periplasmic and cytoplasmic compartments, respectively.

There is only one enzyme, which can convert N₂O to dinitrogen (N₂) named NosZ (Figure 1.5). NosZ is a homodimer which contains two copper centers: CuA and CuZ in each monomer (Brown et al., 2000).

1.7.1 Heme and copper Nitric oxide reductase (NOR)

Nitric oxide reductases catalyse detoxification of NO in microorganisms (Watmough et al., 1999; Zumft, 1997) and human (Gardner et al., 2001). They metabolize NO to N₂O under anaerobic conditions in bacteria and fungi.

1.7.1.1 cNOR (cytochrome *bc* type complex)

cNOR is unstable, membrane-bound protein and interacts with many cell components, it was isolated from *Pseudomonas stutzeri* (Heiss et al., 1989) and *Paracoccus denitrificans* (Dermastia et al., 1991). The purified cNOR is a heterodimer with molecular weight 70 kDa, consisting of two main subunits: a 17 kDa heme *c* and 53 kDa heme *b* subunit (Moenne-Loccoz et al., 2000).

Literature reports the structural homology between cNOR and cytochrome *c* oxidase (Cco) (Collman et al., 2008). Both have membrane-spanning helices and six conserved histidine residues. The differences between them were: in cytochrome *c* oxidase three histidine residues act as ligands to the high and low spin heme centre and three were coordinated to Cu_B, whereas in cNOR both high and low spin heme (heme *b* and heme *b*₃), and a non-heme iron (Fe_B) are present, with no Cu. Cu in Cco is replaced mainly by non-heme Fe in NOR (Wasser et al., 2002; Zumft, 1997). Spectroscopic studies confirmed the binuclear iron active site of NOR (Hendriks et al., 1998).

cNor contains two subunits: NorC and NorB (Figure 1.6). NorC is located in the periplasmic side of the cytoplasmic membrane, and carries heme *c*, which accepts electron from cytochrome *c*.

NorB is the second subunit, and is incorporated into the membrane by 12 spanning segments that contain six conserved histidine residues. NorB is the catalytic subunit, where the histidine residues coordinate the non-heme iron and two *b*-type heme metal centers. (Cheesman et al., 1998; Hendriks et al., 2000; Hendriks et al., 1998; Sakurai et al., 1998). The NorB subunit resembles the largest subunit of heme-copper cytochrome oxidase (Hendriks et al., 1998; Hino et al., 2010; Sakurai et al., 1998; Saraste and Castresana, 1994). In the catalytic centers of Cco and cNOR, the oxygen is reduced to water, and the nitric oxide to nitrous oxide respectively. (Babcock and Wikstrom, 1992; Moenne-Loccoz et al., 2000).

1.7.1.2 qNOR

The first menaquinol dependent NOR (qNOR) was discovered in *Ralstonia eutropha* (Cramm et al., 1999; Cramm et al., 1997). qNOR is a monomer and accepts electrons from menaquinols (Cramm et al., 1999). The comparison between qNOR and cNOR showed that there was no NorC in qNOR, and qNOR contains two additional N-terminal trans-membrane helices (250 residues) relative to NorB (Hendriks et al., 2000).

The sequence suggests an integral membrane protein but larger than NorB (by 1 helix) which is joined to a bit that looks like NorC (Figure 1.6). Therefore it has been suggested that qNOR is the fusion of NorB and C, and lost heme *c* during development. (Cramm et al., 1999)

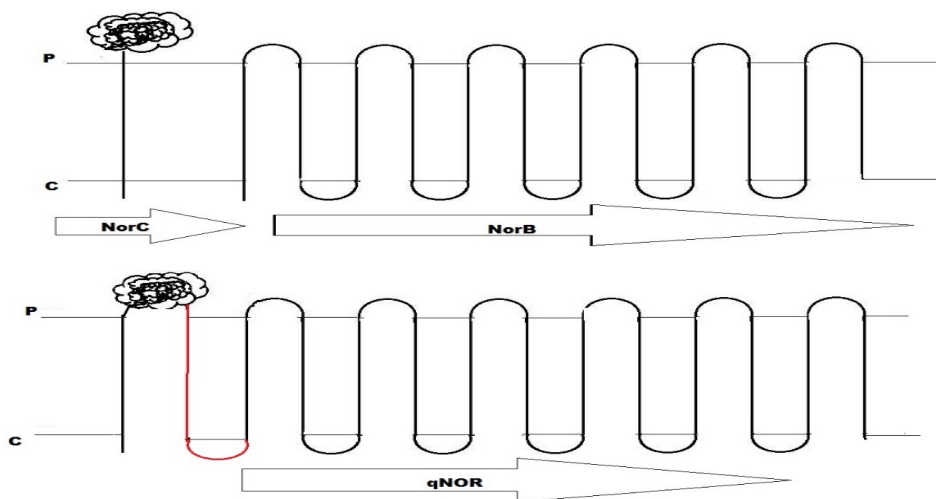


Figure 1-6 cNOR and qNOR trans-membrane helices. The figure shows that qNOR has the same structure as NorB from cNOR with an additional N- terminal part (labeled in red), which links it to a region of sequence that is similar to NorC from cNOR.

qNOR is found also in the hyperthermophilic archaeon *Pyrobaculum aerophilum*, but the qNOR of archaea has modification of the heme groups. It has been reported that qNOR has no accessory proteins necessary for the assembly or function, whereas the accessory proteins are essential for cNOR assembly and/or activity (de Vries et al., 2003). In *Ralstonia eutropha* qNOR encoded by *norB* gene, is co-transcribed with *norA* gene encoded NorA protein. NorA protein is involved in repairing iron-sulfur cluster damage and NO detoxification (Justino et al., 2007; Strube et al., 2007).

1.7.1.3 qCu_A NOR

Gram positive denitrifying bacteria such as *Bacillus azoformas*, contains a novel NOR enzyme (qCu_ANOR) (Suharti et al., 2001). qCu_ANOR is a hybrid of NOR and cytochrome oxidase. It contains copper in the form of Cu_A, which is unique in NOR, and heme *b* and non- heme iron, but not heme *c*. qCU_A NOR receives an electron from

menaquinol (Suharti et al., 2001). It has been proved that qCu_ANOR in *Bacillus azoformas* can also accept electron from ascorbate and an endogenous type of cytochrome *c* oxidase (*c551*) (Suharti et al., 2004).

1.7.2 Flavodiiron reductase or Flavodiiron proteins (FDPs)

FDPs are a very large sub family of flavoproteins that are distributed widely in both prokaryotes (facultative anaerobic bacteria and archaea) and unicellular eukaryotes (particularly protozoa) (Di Matteo et al., 2008; Vicente et al., 2012). FDPs are found also in strict anaerobes such as *Desulfovibrio vulgaris* (Gomes et al., 1997; Silaghi-Dumitrescu et al., 2003; Wasserfallen et al., 1998).

FDPs, previously called A- type flavoproteins (FprA), were known as nitric oxide and/or oxygen reductases (Saraiva et al., 2004). The core shared feature in all FDP members is that they are structurally composed of two main domains: a metallo- β - lactamase like domain with a non-heme diiron center; and a flavodoxin- like domain with a flavin mononucleotide (FMN) moiety (Frazao et al., 2000; Gomes et al., 2000). The flavin (either FMN or FAD) is a versatile coenzyme and enables them to perform a variety of chemical reactions involving one or two electron transfers (Massey, 1995; Massey and Hemmerich, 1980; Wasserfallen et al., 1998). Some members for example Flavorubredoxin (NorV) in *Escherichia coli* possess an extra C- terminal domain with a redox center, such as a rubredoxin (Rd) domain with an iron-sulfur cluster (Gomes et al., 1997; Silaghi-Dumitrescu et al., 2005a; Silaghi-Dumitrescu et al., 2005b).

The first FDP crystal structure solved was the Rubredoxin: Oxygen Oxidoreductase (ROO) from *Desulfovibrio gigas* (Frazao et al., 2000). More structures were solved subsequently from a range of different organisms (Di Matteo et al., 2008; Frazao et al., 2000; Silaghi-Dumitrescu et al., 2005a).

The ROO showed the classic features of FDP, with an 86 kDa homodimer, containing one flavin mononucleotide (FMN) and two non-heme Fe in each monomer. ROO consists of two main domains: a 400 amino acid β -lactamase like domain with a diiron centre and an FMN like domain with FMN (Silaghi-Dumitrescu et al., 2005a).

ROO is the terminal oxidase in a soluble coupled NADH oxygen reduction, which performs four-electrons reduction of oxygen to water, with no partially reduced oxygen species. ROO accepts electron from the reduced rubredoxin (Rd), which in turn accepts the electron from NADH- rubredoxin oxidoreductase (NRO) (Chen et al., 1993a, b; Chen et al., 1994) (Figure 1.7).

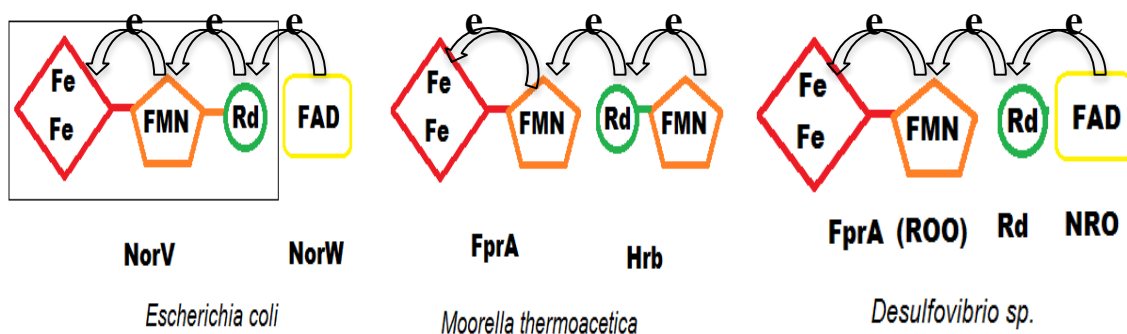


Figure 1-7 The electron transfer scheme in NO detoxification enzymes. NorV, FprA or ROO are NO reductases, which accept electrons from an NADH-dependent flavo-enzyme: NorW, a high molecular weight rubredoxin (Hrb) or an NADH: rubredoxin oxidoreductase (NRO), respectively. The rubredoxin protein is separate from the ROO protein in *Desulfovibrio sp.*, whereas in *E. coli* NorV, the rubredoxin domain is fused into the FMN domain.

Although the main function of ROO is as an oxidoreductase, many chemical and functional studies revealed that FDPs function as a terminal component in the nitric oxide reduction process (Busch et al., 2004; Gardner et al., 2002; Mukhopadhyay et al., 2004; Silaghi-Dumitrescu et al., 2003; Silaghi-Dumitrescu et al., 2005b). It has been

proven that FDPs protect organisms from nitrosative stress (Corker and Poole, 2003; Haveman et al., 2004; Poock et al., 2002).

1.7.2.1 Flavohemoglobin (Hmp)

Hmp belongs to the nitric oxide dioxygenases (NODs) family, and utilizes O₂ to convert NO to NO₃⁻.



It consists of a globin domain combined with a ferredoxin reductase-like FAD-NAD binding module. Hmp acts as an oxido-reductase in most bacteria and yeasts (Gardner et al., 2000a; Gardner et al., 2000b; Gardner et al., 1998c; Hausladen et al., 1998). The flavohemoglobin proteins are widely spread among prokaryotes and eukaryotes, although only one flavoHb gene was found per genus of enterobacteriaceae, whereas in actiniobacteriaceae and *Streptomyces* more than one flavoHb gene was found, and the unicellular eukaryote *Candida albicans* has up to five flavoHb genes (Bonamore and Boffi, 2008). The highly conserved residues in the heme and flavin-binding sites of the flavohemoglobin family, suggest the important role of the binding pockets in gas diffusion and electron transfer. (Bonamore and Boffi, 2008). Gardner and colleagues in 1998 verified that the nitric oxide dioxygenase activity was the enzymatic function of flavohemoglobin (Gardner et al., 1998a). It has been reported that the flavoHb activity in NO detoxification depends on O₂ (Gardner and Gardner, 2002). FlavoHb eliminates NO in an oxygen and NADH dependent reaction (Poole and Hughes, 2000). The NO detoxification by flavoHb was also shown under anaerobic conditions, but the activity was only to a negligible extent (Gardner and Gardner, 2002; Gardner et al., 1998a; Kim et al., 1999).

1.8 *nor* operon

E. coli possess five genes able to detoxify NO under anaerobic condition: *nrfA* encoding a periplasmic cytochrome *c* nitrite reductase (Poock et al., 2002); *hcp* encoding Hcp (hybrid cluster protein) (Wang et al., 2016), and the most important genes are *norV* or *ygaK* (b2710) encoding a flavorubredoxin (NorV) with an NO-binding non-heme diiron centre; and *norW* or *ygbD* (b2711) encoding an NADH (flavo) rubredoxin reductase (NorW). Both genes in *E. coli* have been studied intensively and together they metabolize NO under anaerobic growth conditions to N₂O (Gardner and Gardner, 2002; Gardner et al., 2002). The *norV* and *norW* genes are part of the same transcription unit (Gardner et al., 2002). *norR* or *ygaA* (b2709) is the transcriptional regulator, so a *norRVW* operon (Figure 1.8) is the main key component of NO reduction and detoxification under anaerobic conditions (Gardner et al., 2002; Gomes et al., 2000; Hutchings et al., 2002a; Pohlmann et al., 2000).

NorW plays an essential role in the flavorubredoxin catalysed NO reduction, through the transfer of an electron from the electron donor (NADH) to NorV which uses this electron to reduce NO to N₂O (Hutchings et al., 2002a).

Although, many studies have focused on mechanisms of the NO reduction reaction, understanding of the catalytic cycle has been weakened by a lack of structural information (Collman et al., 2008).

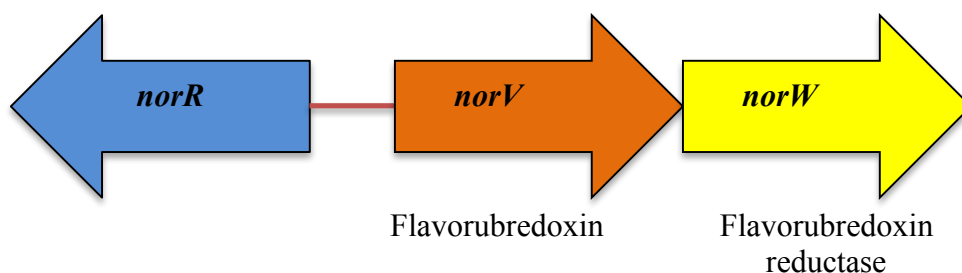


Figure 1-8 *norRVW* operon. The figure shows the main three parts of the *nor* operon: *norR* gene shown in blue is the regulatory gene, *norV* shown in orange encodes a flavorubredoxin (NorV) protein, which reduces NO to N₂O, and *norW* shown in yellow encodes a flavorubredoxin reductase NorW protein, which reduces NorV.

1.8.1 NorR

Many studies have been done to investigate NorR function as an activator protein. It activates nitric oxide reductase activity, in response to NO and other reactive forms of nitrogen generated from sodium nitroprusside (Gardner et al., 2002; Pohlmann et al., 2000). NorR has three domains: an N-terminal GAF domain, the site of small ligand interaction (Ho et al., 2000), GAF contains iron center which is essential to activate *norVW* expression, by using the EPR technique, D'Autreaux et al. was able to show a model of NO signalling in NO receptors containing non haem iron (D'Autreaux et al., 2005); AAA is the central domain, which hydrolyzes ATP and interacts with σ^{54} -containing RNA polymerase; and a final C-terminal domain (HTH) which binds the DNA (Pohlmann et al., 2000; Shingler, 1996) (Figure 1.9). Combining the sequence of the *norR* gene and phenotype similarity between *norR* and *norV* mutants, it has been proposed that *norR* (*ygaA*) regulates the expression of *norV* (Gardner et al., 2002).

It was proved that NorR protein is required for *norV* transcription and the structural gene expression is activated in aerobic and anaerobic growth conditions (Hutchings et al., 2002b).

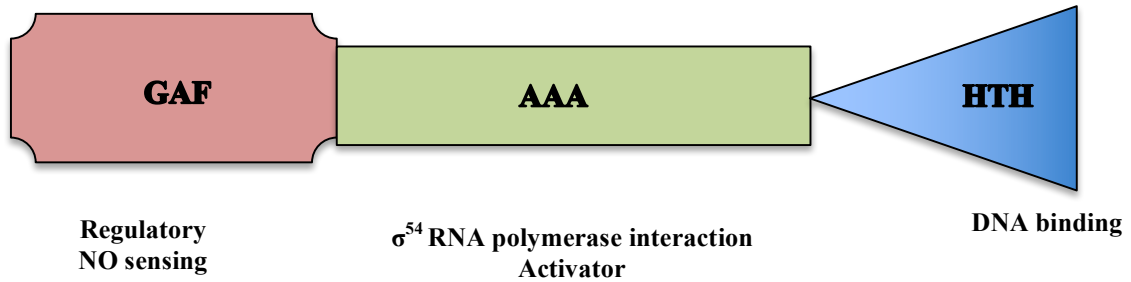


Figure 1-9 NorR domain structure. The NorR protein is composed of three parts: GAF (labeled in red) as NO sensing regulator; AAA domain (labeled in green) is bound to σ^{54} RNA polymerase, and HTH domain (labeled in blue) is the DNA binding site.

1.8.2 NorV (Flavorubredoxin FIRd)

The Flavorubredoxin (NorV) is a member of the flavoprotein type A family, a large family distributed widely among strict and facultative anaerobic bacteria and archaea (Gomes et al., 2002). NorV consists of two main domains: N-terminal metallo- β -lactamase-like domain, with a non-heme di-iron site and a flavodoxin-like domain harboring one FMN moiety. In *Escherichia coli*, there is an additional C-terminal module containing a rubredoxin-like domain, with an Fe-S cluster fused to the FMN-like domain (Gomes et al., 2000; Gomes et al., 2002). The rubredoxin domain in the *E. coli* flavoprotein adds a new sub-division to flavoproteins, a flavoprotein type B (Petoukhov et al., 2008).

Rubredoxin (Rd) is a small (~ 6 kDa) protein. The role of this protein remains elusive except for the well-documented alkane hydroxylation system in *Pseudomonas* (Ruettinger et al., 1977) and the oxygen-utilizing pathway in *Desulfovibrio gigas* (Chen et al., 1993a; Gomes et al., 1997). The first Rd has been isolated from eukaryotes (Wastl et al., 2000b), attached to photosystem II (Wastl et al., 2000a).

It has been reported that when *E. coli* grows anaerobically in the presence of NO, it develops NO reductase activity, whereas knocking out the gene encoding for NorR (*norR* or *ygaA*) or NorV (*norV* or *ygaK*) impairs this activity. In contrast, knocking out

the *norW* (*ygbD*) gene reduces this activity. Thus the *in vitro* and *in vivo* NO reduction by NorV have been demonstrated (Gardner et al., 2002; Gomes et al., 2002b).

E. coli norV is a 1440 base pair gene (synonyms are *b2710*, *ygaI*, *ygaJ*), encoding a NorV protein of 479 amino acids. The amino acid sequence of NorV is shown in Figure 1.10.

MSIVVKNNIHWVGGQRDWEVRDFHGTQYKTLRGSSYNSYLIREEKVLDITVDHKFSRE
FVQNLRNEIDLADIDYIVINHAEEDHAGALTELMAQIPDTPIYCTANAIDSINGHHHHPE
WNFNVVKTGDTLDIGNGKQLIFVETPMLHWPDSMMTYLTGDAVLFSNDAFGQHYCDE
HLFNDEVDQTELFEQCQRYANILTPFSRLVTPKITEILGFNLPVDMIATSHGVVWRDNP
TQIVELYLKWAAADYQEDRITIFYDTMSNNTRMMADAIAQGIAETDPRVAVKIFNVAR
DKNEILTNVFRSKGVLVGTSTMNNVMMPKIAGLVEEMTGLRFRNKRASAFGSHGWSG
GAVDRLSTRLQDAGFEMSLSLKAKWRPDQDALKLCREHGREIARQWALAPLPQSTVN
TVVKEETSATTTADLGPRMQCSVCQWIYDPAKGEMQDVAPGTPWSEVPDNFLCPECS
LGKDVFEELASEAK

Figure 1-10 NorV protein sequence. The figure shows the amino acid sequence of NorV from *E. coli* MG1655. The red-labeled region is the β -lactamase-like domain (1-250) residues. The blue region is the flavin-like domain (256-389) residues. The green region shows the rubredoxin-like domain (423-479) residues, and the black region shows the residue linkers.

Studies of the redox and spectroscopic properties of *E. coli* NorV and NorW, by using electron paramagnetic resonance (EPR), provided the first direct evidence for the non-heme diiron site in the FDPs family, which had never been observed before, because of the iron nuclei property of anti-ferromagnetic coupling (Vicente and Teixeira, 2005). The redox property of NorW was also observed by comparing the reduction potentials of two reductants (NADH and sodium dithionite). The reduction potential of NADH was approximately 30 mV lower than the dithionite, suggesting the reduction potential

of an FAD cofactor might be modulated slightly because of NAD binding (Vicente and Teixeira, 2005).

The kinetics of the electron transfer between NorW and NorV has been studied by stopped-flow absorption spectroscopy to investigate the electron transfer pathway. It has been found that NADH (not NADPH) reduces NorW quickly, which in turn reduces a rubredoxin domain (as part of NorV or as independent domain). Both reactions were pH and ionic strength dependent (Vicente et al., 2007).

The quaternary structure of *E. coli* NorV was first proposed by using a small-angle-X-ray scattering (SAXS) approach. A tetrameric structure of NorV in solution was observed, and a flexible contact between the Rd and FMN domains was modelled. The results of SAXS revealed the molecular envelopes for the full length NorV (residues 1-479 with a molecular weight of approximately 55 kDa), a truncated version FDP (residues 1-412 containing the β -lactamase like domain and FMN like domain only with a molecular weight of ~47 kDa) and the Rd domain alone (residues 401-479 including a 33 residues flexible linker with total molecular weight of ~8.6 kDa) (Petoukhov et al., 2008). These findings suggested that the Rd behaves as an independent domain and participates in the redox reaction freely.

More recently, the crystal structure of *E. coli* NorV has been solved, both in the oxidized (PDB entry 5LMC), and the reduced (PDB entry 5LLD) forms. The crystal structure of NorV showed a tetrameric head to tail arrangement in which the distance between the diiron center and FMN within one monomer is 40.7 Å, whereas in the tetrameric structure the a diiron center and FMN from different monomer subunits were separated by 10.3 Å only (Figure 1.11).

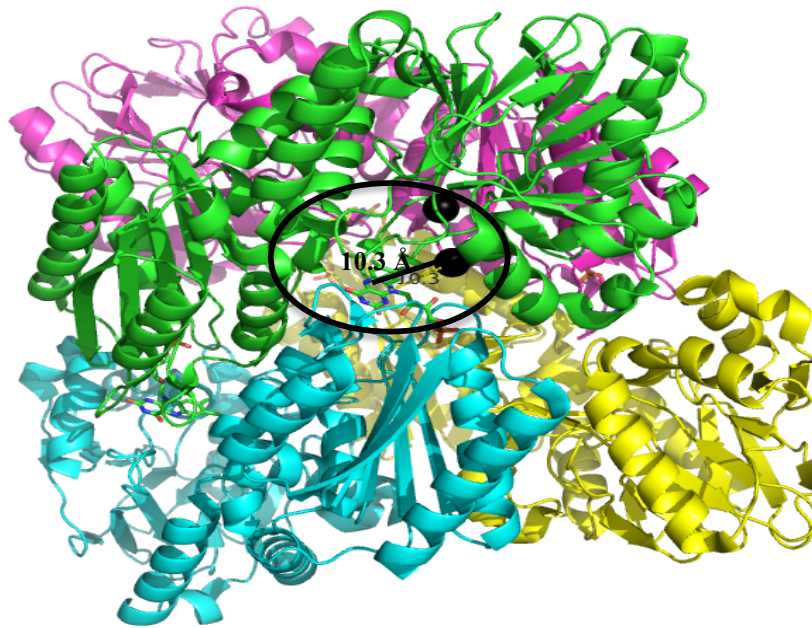
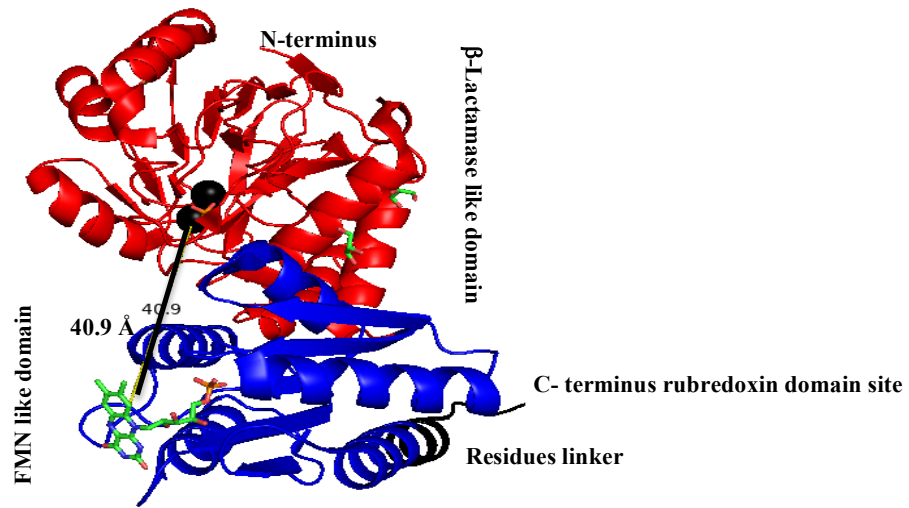


Figure 1-11 NorV structure. A- A NorV monomer, starting from the β -lactamase like domain (colored in red), to the FMN-like domain (colored in blue), and the amino acids linker (colored in black). The Fe is presented as a black sphere and FMN as sticks. The distance between the active centers (diiron and FMN) is 40.9 Å. B- The tetrameric structure of NorV. Each monomer is shown in a different color (green, magenta, yellow and cyan). The distance between the Fe from one monomer and FMN from an adjacent monomer is around 10.3 Å.

In the oxidized form the diiron center is bridged by a μ -hydroxo bridge, whereas this was not observed in the reduced form. An access route for the substrate to the active center is formed by a tunnel shown in (Figure 1.12).

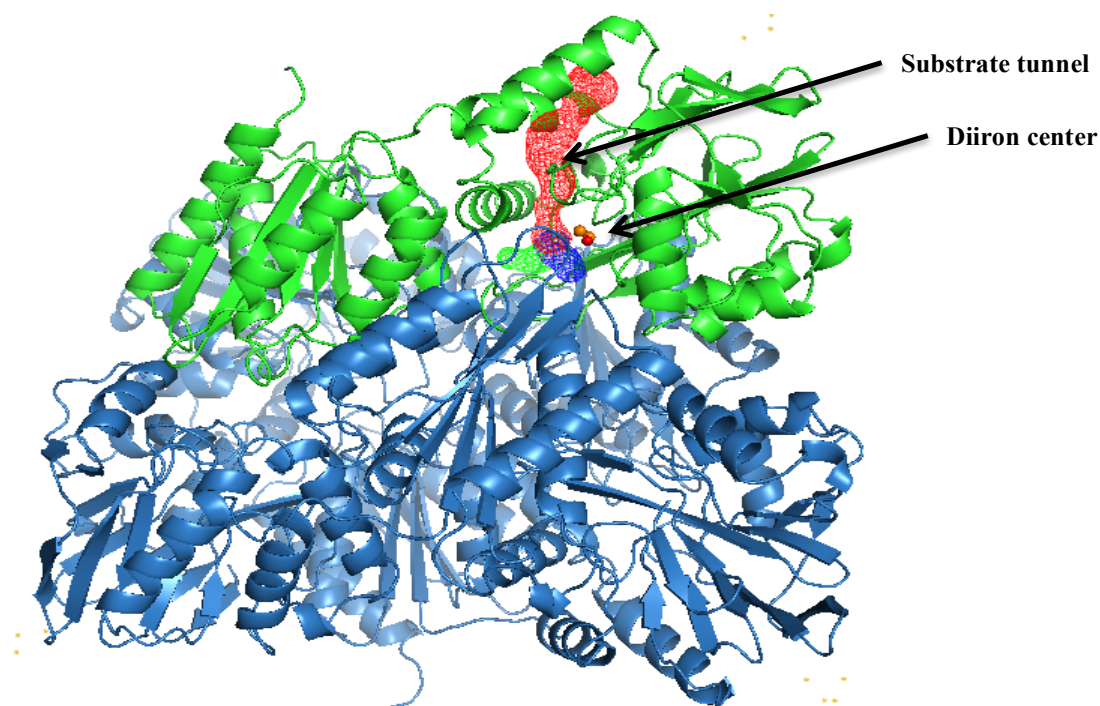


Figure 1-12 NorV tunnel. The figure shows two possible access routes for the substrate to the active site via tunnels, which reach the solvent surface. The long tunnel path represented in red is approximately 21.4 Å and the short tunnel path in blue is approximately 12.2 Å. And the active redox center (diiron) presented in orange spheres with red sphere as oxygen.

The Rd domain was missing in the structure and therefore the structure of the Rd domain was determined by NMR (Romao et al., 2016). It shows a Zn ion surrounded by conserved cysteine residues C428, C431, C461 and C464, and adjacent conserved aromatic residues W433, Y435, W452, F459 and F471 (Figure 1.13).

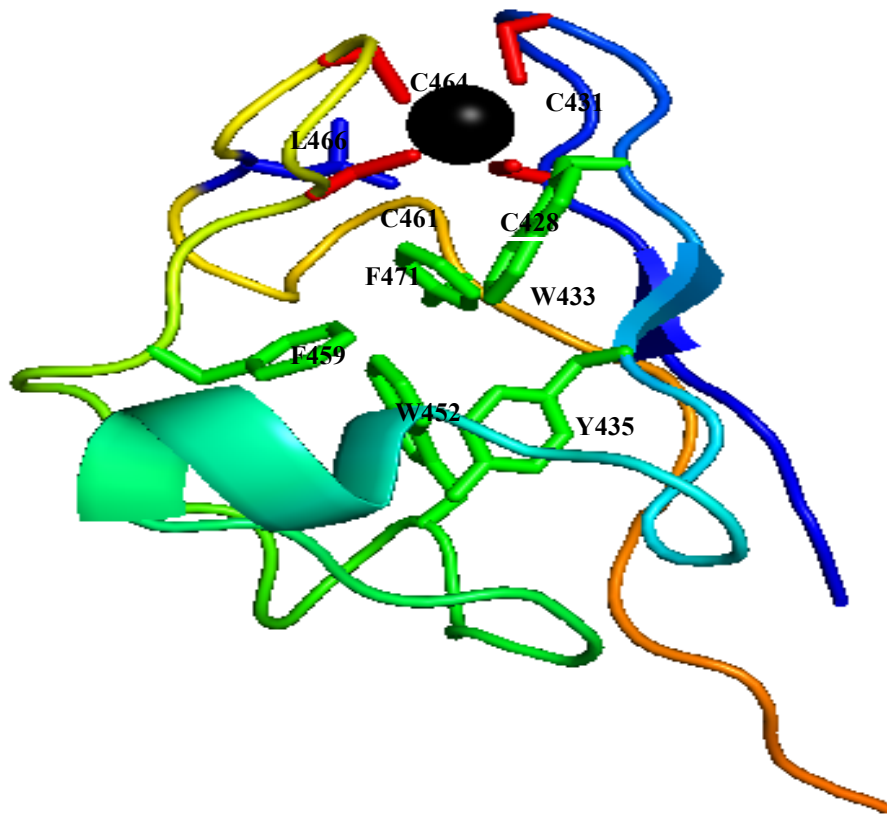


Figure 1-13 NMR structure of the *E. coli* Rubredoxin. The figure shows the overall structure of the rubredoxin domain from FIRd (NorV). The zinc ion (shown in black) lined by cysteine residues (shown in red). The aromatic conserved residues are shown in green, and the Leucine residue shown in blue. The figure was created by using Pymol and PDB ID 2MS.

1.8.3. NorW (NADH: flavorubredoxin oxidoreductase)

It has been demonstrated that NorW is the reductase partner of NorV (Gardner et al., 2003; Gardner et al., 2002; Gomes et al., 2002a; Gomes et al., 2000; Helmick and Gardner, 2002). NorW utilizes NADH to catalyse the electron transfer to the flavorubredoxin. NorW cofactor is flavin adenine dinucleotide (FAD) (Gomes et al., 2000).

NorW has a molecular weight of 41403.5 Da, and an isoelectric point (pI) on 6.03.

MSNGIVIIGSGFAARQLVKNIRKQDATIPLTLIAADSMDEYNKPDLSHVISQGQR
ADDLTRQTAGEFAEQFNHLFPQTWVTDIDAEARVVKSQNNQWQYDKLVLAT
GASAFVPPVPGRELMLTLNSQQEYRA^CETQLRDARRVLIVGGGLIGSELAMDF^C
RAGKAVTLIDNAASILASLMPPEVSSRLQHRLTEMGVHLLLKSQLQGLEKTDSG
IQATLDRQRNIEVDAVIAATGLRPETALARRAGLTINRGV^CVDSYLQTSNTDIY
ALGD^CAEINGQVLPFLQPIQLSAMVLAKNLLGNNTPLKLPAMLVKIKTPELPLH
LAGETQRQDLRWQINTERQGMVARGVDDADQLRAFVVSSEDRMKEAFGLLKT
LPM

Figure 1-14 *E. coli* NorW protein sequence. It shows that NorW consist of 377 residues, with 4 conservative cysteine residues highlighted in yellow, which is a possible binding site for a heavy atom.

Many studies have been accomplished on the rubredoxin reductase (RdxR) in *Pseudomonas* (Lee et al., 1998), *Clostridia* (Petitdemange et al., 1981) and *Pyrococcus furiosus* (Ma and Adams, 1999, 2001). The electron transition between the rubredoxin reductase and Fe in the rubredoxin has been studied by stop-flow spectroscopy, the thermodynamic analysis and transient kinetics of the electron transition from NADH to the flavin in FAD and then to the Fe in the rubredoxin has been characterized

The structure of a NorW homologue (Rubredoxin reductase (RdxR) from *Pseudomonas aeruginosa*, PDB ID: 2V3A) has been solved (Hagelueken et al., 2007b) (Figure 1.15). The structure revealed that the enzyme has three functional binding sites: one for flavin adenine dinucleotide (FAD) in the N-terminal domain FAD binding domain; the S one for nicotine adenine dinucleotide (NAD) in the NAD binding domain, and the last one is a rubredoxin binding site in the C- terminal rubredoxin binding domain (Hagelueken et al., 2007a).

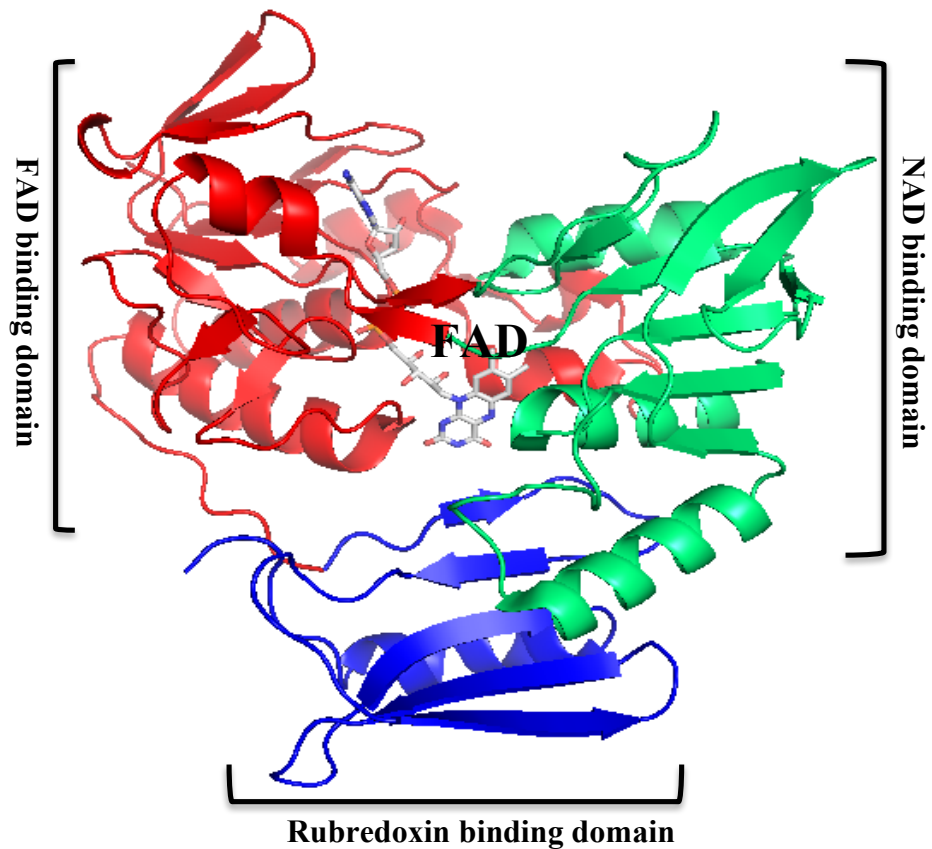


Figure 1-15 Crystal structure of *Pseudomonas aeruginosa* rubredoxin reductase (RdxR) (NorW homologue) (PDB ID: 2V3A). The N-terminal FAD binding domain is shown in red with FAD as stick form, the middle (NAD binding domain) is shown in green, and the C-terminal rubredoxin binding domain is shown in blue.

The protein sequence alignment of *E. coli* NorW with *Pseudomonas aeruginosa* rubredoxin reductase (RdxR) showed 34% sequence identity, which might suggest the same folding for both proteins. The identical residues were distributed along the sequence (Figure 1.16).

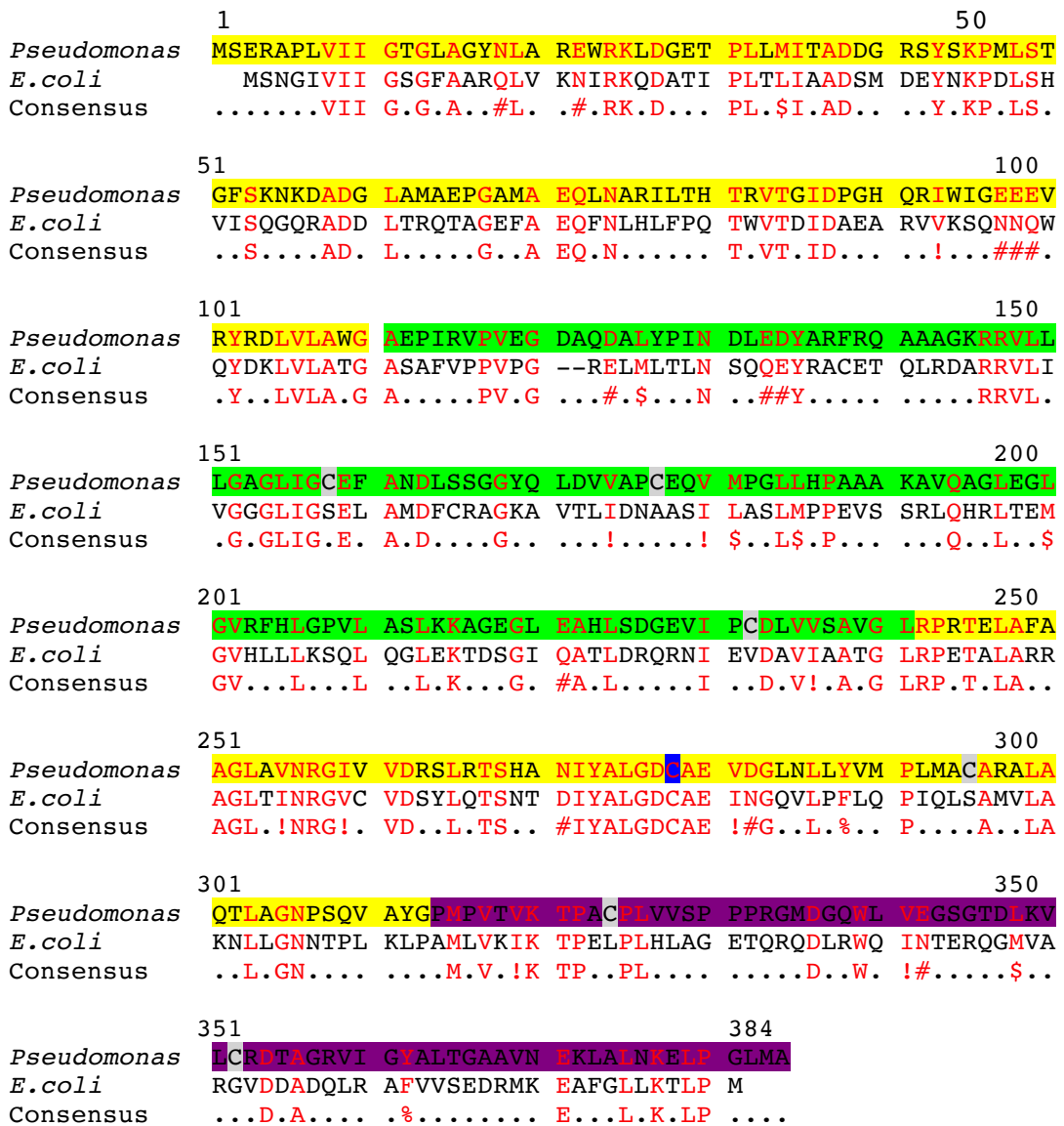


Figure 1-16 Protein sequence alignment of the *E. coli* NorW with the homologue rubredoxin reductase (RdxR) from *Pseudomonas aeruginosa*. The sequence is shown the similarity between both proteins. The identity was 34%, which might suggest that NorW has the same folding as RdxR. The figure shows the sequence of FAD, NAD and rubredoxin domains highlighted in yellow, green and purple respectively. The cysteine residues are highlighted in gray, and the cysteine identical to NorW cysteine is highlighted in blue.

Only one cysteine was identical in both proteins (NorW and RdxR), as shown in Figure 1.16.

Although, the structure and the electron transfer of the rubredoxin oxidoreductase have been studied in many organisms, the *E. coli* NADH: flavorubredoxin oxidoreductase (NorW) structure still not solved, and the mechanism of action still unrevealed.

Scope of study

Since increased microbial resistance to antibiotics is a real threat, an understanding of the mechanisms behind the microbial resistance to gases may offer opportunities to overcome it. The innate immune system produces different factors that attack the microorganisms invading the body, NO and CO are part of those factors, which are produced by macrophages to toxify and kill the invader microorganisms. As a result, the microorganisms develop different resistance factors to detoxify those gases. Flavorubredoxin (NorV) and flavorubredoxin reductase (NorW) can scavenge NO under anaerobic conditions, and carbon monoxide resistance protein detoxifies CO.

This study aimed to understand the mechanisms behind NorV, NorW and Cor activity, in this study assays *in vivo* and *in vitro* have been performed. Structural studies were carried out on NorV, NorW and Cor by using X-ray crystallography.

This thesis studies the impact of NO on laboratory bacteria (*E. coli* mutant cells) under anaerobic conditions, and the effect of purified NorV and/or NorW proteins on NO reduction under different oxygen levels. The final products of NO detoxification by NorW were studied by using FTIR spectrometry.

The potential CO detoxification activity by Cor was also studied in this thesis, by carrying different biochemical and biophysical assays. The protection of *E. coli* against CO toxicity was also investigated by using *Mycobacterium tuberculosis cor* expression vector transformed into *E. coli* BL21 cells.

Chapter 2 : Theory of X-ray crystallography

2. Theory of crystallography

2.1 Introduction

X-ray crystallography is a common technique used to determine the molecular structure of small and macromolecules, in arrays. The first evidence that X-ray can be diffracted from crystalline material came from Max von Laue in 1912 (Eckert, 2012; Helliwell et al., 2012). In the same year in England, William Henry and Lawrence Bragg, father and son, developed a new ideas about X-ray crystallography and X-ray spectroscopy, through solving the structure of small molecules (Bragg, 1913). After around 50 years of Bragg's structure, the first protein structure was solved (myoglobin) (Kendrew et al., 1958). Since that time, the crystallography field has grown and thousands of structures have been deposited in the protein data bank (PDB), the biggest database of macromolecules models (experimental models). There were around 25000 protein and nucleic acid models in the PDB in 2005, solved by X-ray, in addition to 4500 models of proteins containing less than 200 residues, solved by NMR (Rhodes, 2006). In May 2017, there were 130,599 structures in the PDB, of which 116,902 structures were solved by X-ray crystallography.

This Chapter will elucidate methods for obtaining and growing crystals, X-ray diffraction from crystals, and finally collection and processing of the data from X-ray diffraction.

2.2 Protein crystals

A crystal is an aggregation of molecules, atoms or ions, in a three-dimension array, and interact together by noncovalent interactions (Rhodes, 2006). Depending on the orientation and arrangement of the molecules within the crystal lattice, the crystal might have a specific shape and size. Protein crystallization is not a simple process, many requirements are needed for successful crystallization: the protein concentration and

homogeneity are critical factors in protein crystallization; high purity is generally needed for successful crystallization. The optimal protein concentration depends on the nature of the protein itself (Bergfors, 1999; McPherson, 1999). A range of concentrations (2-50 mg/ml) should be tried in the crystallization trials. The physical and chemical factors such as temperature, pH, precipitant and type of buffer are also factors effecting protein crystallization. The form of the protein (full length, truncated, chemically modified) can affect the crystallization process also (Benvenuti and Mangani, 2007).

In order for the protein to be crystallized, the physical phase of the protein should be changed from soluble to solid. The protein crystallization is a time and hard consuming process and not easy. There is no method that could be prescribed for successful crystallization, but generally the crystallization process depends on two stages: nucleation and crystal growth. Nucleation is the first step of the crystal formation, where the protein molecules aggregated together to form a small nucleus, to which layers of protein will be added, to initiate a protein crystal (Dessau and Modis, 2011).

In the crystallization process the protein is mixed with the precipitant in a drop, the equilibrium between the concentrations of protein and precipitant in the crystallization drop may prompt the crystal forming. A phase diagram can be constructed to illustrate this. The curve shows the behavior of protein versus precipitant depending on concentration, and it can be divided in four states: undersaturation, supersaturation, metastable and precipitation. The drop remains clear if the protein and precipitant concentrations are low (undersaturation), whereas a nucleation starts and a tiny crystal appears when the protein and precipitant concentration increases (supersaturation). As the crystal uses the protein, the protein concentration becomes lower and no more crystals form but the existing crystals continue growing (metastable phase). The

precipitation occurs when the protein and precipitant concentration is too high (Dessau and Modis, 2011) (Figure 2.1).

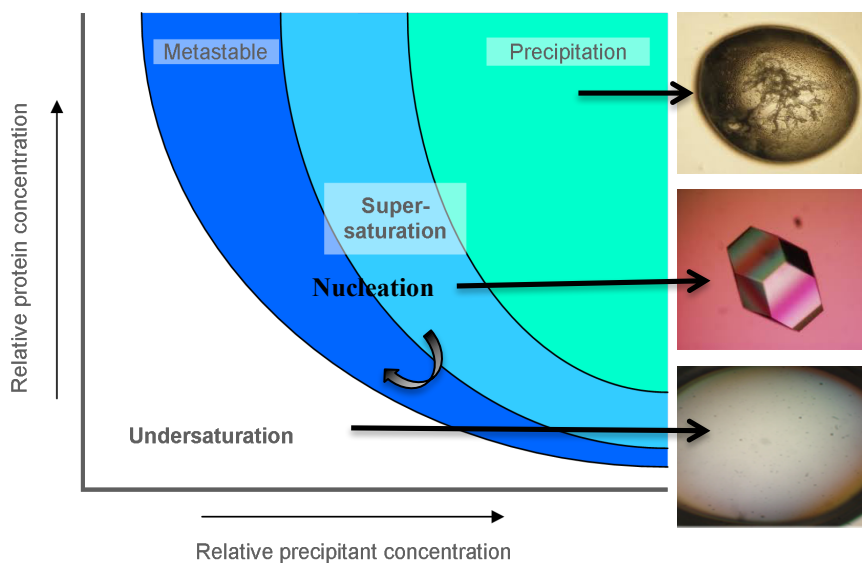


Figure 2-1 Phase diagram of protein crystallization. The scheme shows the protein versus precipitant concentration, and four different states of protein crystallization depending on protein/precipitant ratio. Modified from <https://crystal.csiro.au/en/User-Guide/Crystallisation.asp>

2.3 Protein sample preparation

Sample preparation is a critical step in the protein crystallization process; the protein sample used in the crystallization needs to be of in high purity and homogeneity, which depends mainly on the protein purification method. In order for a maximum opportunity to get a well diffracting crystal, no less than 90 % purity is desired (Giege et al., 1986). The protein concentration should usually be no less than 2 mg/ml (Dessau and Modis, 2011). The protein also needs to be soluble, stable and folded to use for crystallization. During sample preparation, the environment should be controlled, the humidity and temperature should be kept stable during crystallization experiments (Benvenuti and Mangani, 2007; Dessau and Modis, 2011; Gilliland and Ladner, 1996; Rhodes, 2006)

2.4 Crystallization techniques

There are several methods to obtain macromolecule crystals that have been reviewed in the literatures (Benvenuti and Mangani, 2007; Dessau and Modis, 2011; Gilliland, 1988). In the current study only a vapor diffusion method (sitting and hanging drop methods) were used.

2.4.1 Vapor diffusion method

Vapor diffusion is the most abundant and common method used for macromolecule crystallization. The two main techniques (sitting and hanging drop) share the same principle. The principle of this method is mixing the protein and precipitant in different ratios in a sealed chamber containing a reservoir of crystallization solution (precipitant, buffer and salt). The vapor pressure in the chamber will make the concentration of the precipitant equal in the drop and the reservoir, but initially mixing the precipitant with the protein reduces the precipitant concentration in the drop. This causes water to diffuse from the drop to the reservoir to equilibrate the precipitant concentration in both drop and reservoir. The conditions are therefore changed gradually and may affect the factors behind protein solubility; with the result that in favorable circumstances the crystal could form.

2.4.1.1 Sitting drop method

In this method, different types of plastic plates can be used (Figure 2.2), 96 or 24 wells tray might be used, and the setting might be done automatically by robots, or the trays might be set manually. It uses the principle of the vapor diffusion method. Commercial screens can be used in this method, which have different sets of crystallization solutions (salt, buffer and precipitant). The most common precipitant is polyethylene glycol (PEG) with different molecular masses; the second precipitant commonly used in crystallization is ammonium sulfate; both reagents together account for 60 % of

recorded crystallization precipitants (Dessau and Modis, 2011; Gilliland et al., 1994; McPherson and Gavira, 2014).

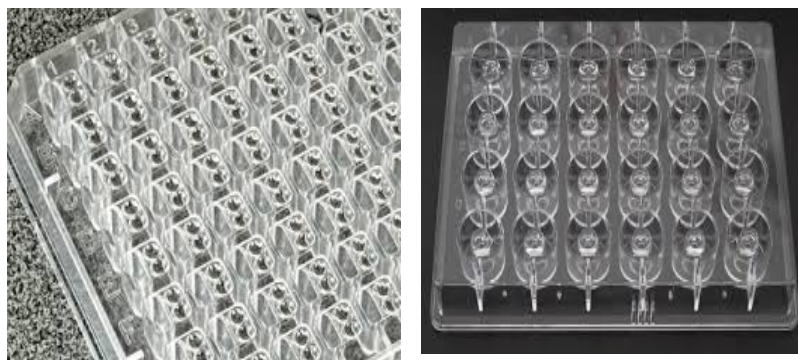


Figure 2-2 Sitting drop crystallization method. The figure shows sitting drop method trays, where on the left is a 96 well tray, and on the right is a 24 well tray. (Dessau and Modis, 2011).

2.4.1.2 Hanging drop method

Hanging drop method is the second type of vapor diffusion method for macromolecule crystallization. In this method, a drop of protein and crystallization solution sets on a pre-siliconised coverslip (to maintain the surface tension), the coverslip is then inverted and closes a well (pre-oiled to prevent air leaking and water evaporation) often in a 24 well plate. The wells contain a reservoir of crystallization solution with different chemical composition. The drops might contain equal or different ratios of protein to crystallization solution, and the reservoir typically contains 500-1000 μl of the crystallization solution (Figure 2.3). This method was used in crystals optimization in this study.

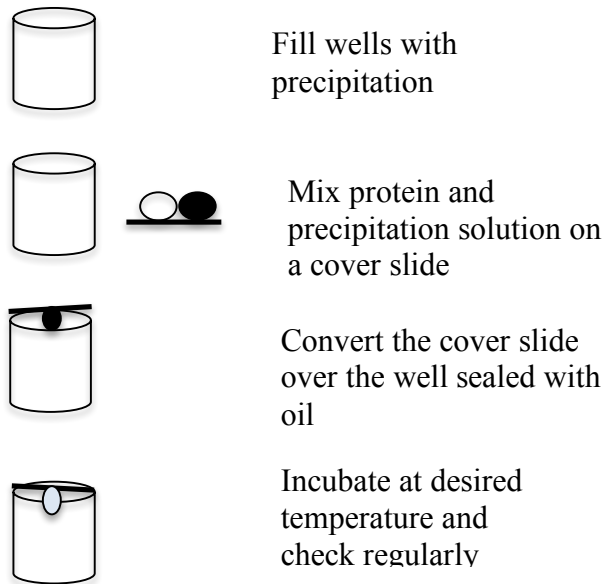


Figure 2-3 Scheme of hanging drop crystallization method.

2.5 Cryoprotectant and crystal mounting

The protein crystal can be rapidly destroyed by X-ray radiation at room temperature and thus during data collection, the crystal needs to be cooled to 100 K in nitrogen gas, to circumvent the problem of crystal damage by radiation. The protein crystal usually grows in a high water content solution, and to prevent ice crystal formation that damages the order of the crystal molecules, a cryoprotectant solution is needed. An effective cryoprotectant usually leads to the formation of an amorphous glass state in the aqueous liquid surrounding the protein crystal and protects it from damage. Different compositions of cryoprotectant can be used, depending on the mother liquor that the crystal grew from. The solution usually contains the same condition where the crystal grew, with cryoprotectant or anti-freeze agents such as glucose, sucrose, MPD, PEG, ethylene glycol or glycerol, in appropriate percentages. The mixture of cryoprotectant and crystallization solution should not show evidence of ice ring diffraction when exposing it to X-ray beam. This can be checked and the best cryoprotectant can be used for crystal mounting (Akihito Yamano, 2012)

In order to test the crystal for X-ray diffraction, the crystal should be mounted and is often saved in liquid nitrogen. The mounting devices are different and for all there are

many factors that need attention: the mounting device should not break the crystal; it should be small and transparent to the X-ray beam; it should be stable enough to hold the crystal for a long time during X-ray data collection; and it should be made of material that would not interact with the crystal and change its nature (Akihito Yamano, 2012). Small loops (0.05-1.0 mm) in diameter are typically used for crystal mounting (Figure 2.4), and these loops are generally composed of either a polymer attached to a pin, which is in turn attached to a magnetic base.

During crystal mounting, the loop is immersed in the mother liquor (where the crystal is found) viewed under a microscope, and the cryoprotectant solution is placed on the cover slip or a well next to the crystal well. The crystal attaches to the loop by surface tension, and is immediately placed in the cryoprotectant solution. The loop with the crystal is then placed on the X-ray goniometer under nitrogen gas, or dipped and stored in liquid nitrogen to send it for X-ray diffraction testing and data collection.

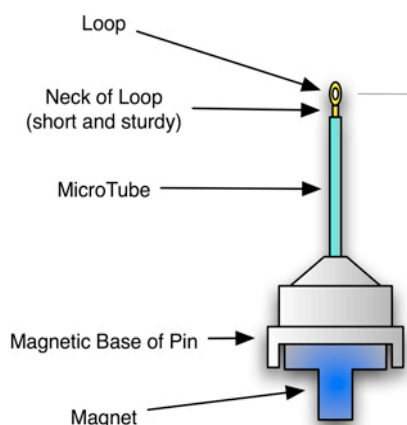


Figure 2-4 Crystal mounting loop. The figure shows that the loop consists of four main parts: the loop where the crystal attaches; the neck which connects the loop with the micro-tube; the micro-tube which attaches to the magnetic base; and the base which interacts with a magnet for easy the attachment of the loop to the X-ray apparatus.

The figure modified from

http://kiemlicz.med.virginia.edu/mcsg/pages/technology_determination

2.6 X-ray & generators

Although, the X-ray had been discovered by Wilhelm Conrad Röntgen in 1895, and used for imaging, the nature of X-ray was not understood well until Paul Peter Ewald a PhD student in Arnold Sommerfeld's group in the Physics Department, University of Munich, made his finding about light wave behavior, and X-ray interference within crystals (Hauptman, 1990). Max von Laue in 1912 examined X-ray diffraction on crystalline material (Eckert, 2012; Helliwell et al., 2012). von Laue's finding opened the door for a new era in X-ray utilization in crystallography. X-rays are a form of electromagnetic radiation, with wavelength between 0.1-1000 Å (shorter than UV and longer than gamma ray). The X-ray energy can be described in terms of photons. The energy is able to ionize atoms, and destroy molecular bonds. To determine the position of atoms within a crystal, hard X-rays have been used (wavelength 0.6-1.6 Å), whereas the longer wavelength (more than 2 Å) X-ray called soft X-rays are absorbed by water and air (Attwood, 2002; Rhodes, 2006). X-rays are produced by using three main sources: X-ray tubes; rotating anode generators or synchrotrons.

2.6.1 Stationary anode X-ray tube

In the X-ray tube, X-rays are generated by an electrically charged plate, where electrons are accelerated from a cathode (heated filament) to the metal target in a water-cooled anode. The X-rays leave the tube through a beryllium window. Some of the heat can be removed with the flow of cooling water. As a result, the strength of X-rays generated is limited (Figure 2.5).

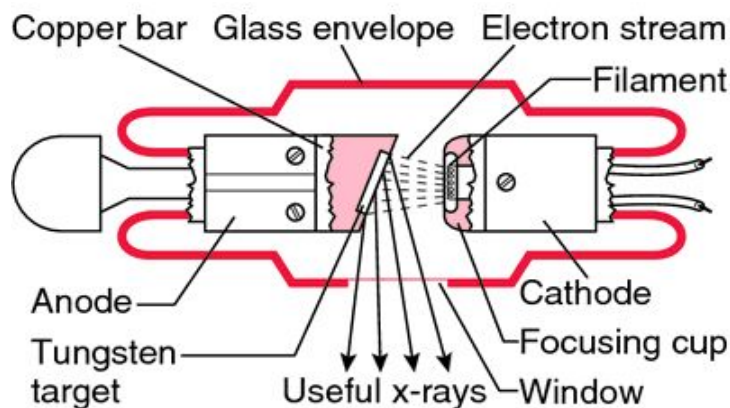


Figure 2-5 X-ray tube. The figure shows the X-ray tube components: the anode made from a copper stem and a central tungsten target; the cathode made of tungsten usually; and the whole tube which is covered by a glass envelope.

<https://www.pinterest.com/pin/375346950167663509/>

2.6.2 Rotating Anode X-ray tube

In this source, there is an X-ray vacuum tube with a cathode at one end and a rotating metal target anode (usually copper, molybdenum or chromium) at the other end (Figure 2.6). The metal located in the cathode is heated by an electric current, and emits an electron that moves at highly speed toward the anode. A large potential field created between the anode and cathode (30-50 kV), accelerates the electrons. The electron collision with the metal anode produces energy transfers to electrons in the lower orbital of the metal. The electron in the low orbital then moves from the K-shell and is replaced by a higher orbital electron from the L-shell, which results in X-ray being emitted as photons. In crystallography laboratories, using copper as the metal in the anode is popular, because electron transfer from the L shell of copper to replace by electron from the K shell, produces X-ray with wavelength 1.54 \AA called as $\text{CuK}\alpha$. The next metal desirable in crystallography is molybdenum, which can provide a shorter wavelength (0.71 \AA). A monochromatic source with a single wavelength is preferable for crystallography purposes, use two wavelengths (eg. $\text{CuK}\alpha$ and $\text{CuK}\beta$) causes difficulties in indexing due to reflections overlapping (Rhodes, 2006).

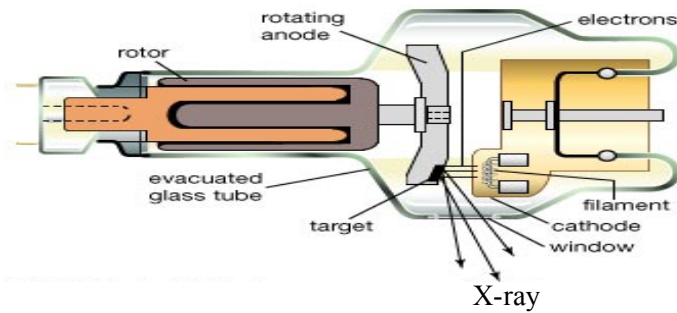


Figure 2.6. Rotating anode X-ray tube. The figure shows the main components of the rotating anode X-ray tube <http://www.wikiradiography.net/page/Physics+of+the+X-ray+Tube>

2.6.3 Synchrotrons

A synchrotron is the most powerful source for intense X-ray (Figure 2.7). The synchrotron consists of a number of parts: a particle accelerator; which accelerates electrons to a velocity approximate to the speed of light in a circulation vacuum; a storage ring, in which the electrons are stored to re-circulated for many times; bending magnets spread around junctions on straight sections of the storage ring; and other magnets found in the straight sections called insertion devices such as wigglers and undulators, used to increase X-ray intensity. Wigglers are used to create additional bending of the beam to provide a wide fan of X-rays for use by many experimental stations. The undulators are widely utilized in synchrotrons, as accessory devices to cause fluctuation in the electrons direction of flight and generate a high intensity X-ray beam. The resulting electromagnetic radiation is often called synchrotron radiation. The ability to produce different wavelengths is one of the advantages of using the synchrotron in determining phase angles and solving protein structures by using a monochromator, the unwanted wavelengths can be filtered out and the desired wavelength can be obtained. The wavelength can be selected to detect a heavy metal in a protein structure (Rhodes, 2006)

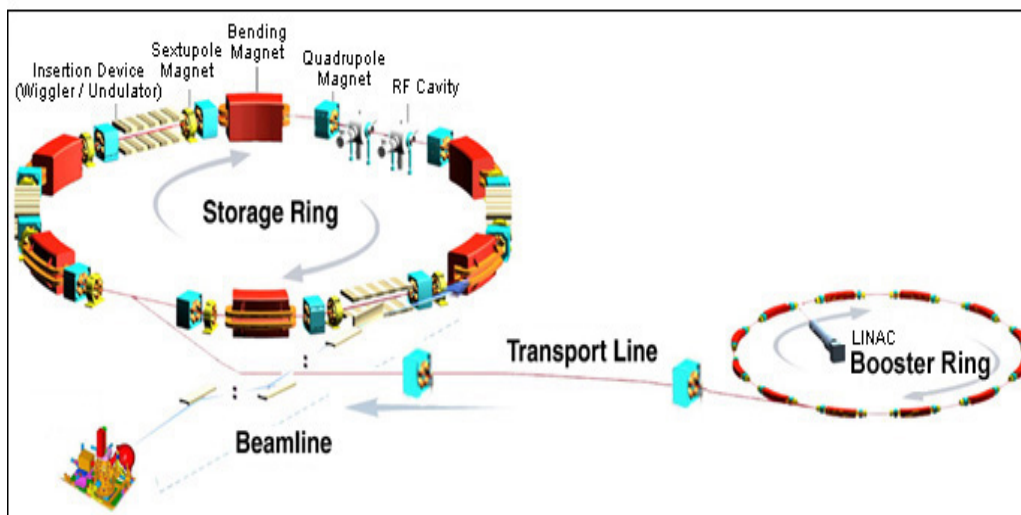


Figure 2.7. Synchrotron components. The figure shows the main components of an X-ray synchrotron. <http://www.nsrcc.org.tw/english/lightsource.aspx>

2.7 X-ray reflection and detectors

As the X-ray hits the crystal, it is diffracted, scattered by protein atoms and the signal of the diffraction is amplified by the ordered array of molecules in the crystal. Scintillation counters contain a phosphorescence material that can measure the reflection intensities by absorbing the X-ray photons. The phosphorescence material produces a flash, counted by photocells, when it absorbs X-ray photons. This technique was used in small molecule crystallography, because the number of reflections per data set is limited. With macromolecules, more reflection points are needed, so the scintillation counter was replaced by X-ray area detectors, such as a simple film detector, which was then replaced by more sensitive detectors such as image plates (IPs) and charge-coupled devices (CCDs) (Rhodes, 2006).

2.7.1 Image plate detectors (IP)

This detector has a reusable plastic sheet, coated with barium halides crystals (BaFBr), and covered by europium (Eu^{2+}) (Figure 2.8). When the crystals are stimulated by X-ray radiation, the halogen ion traps the electron and the europium is excited into a metastable state (Eu^{3+}). A red light (HeNe laser) of 632 nm is used to generate a

luminescence and as the Eu^{3+} relaxes back to Eu^{2+} , a signal at 400 nm proportional to the absorbed X-ray is emitted. The sheet then can be reused again after erasing it by visible light.

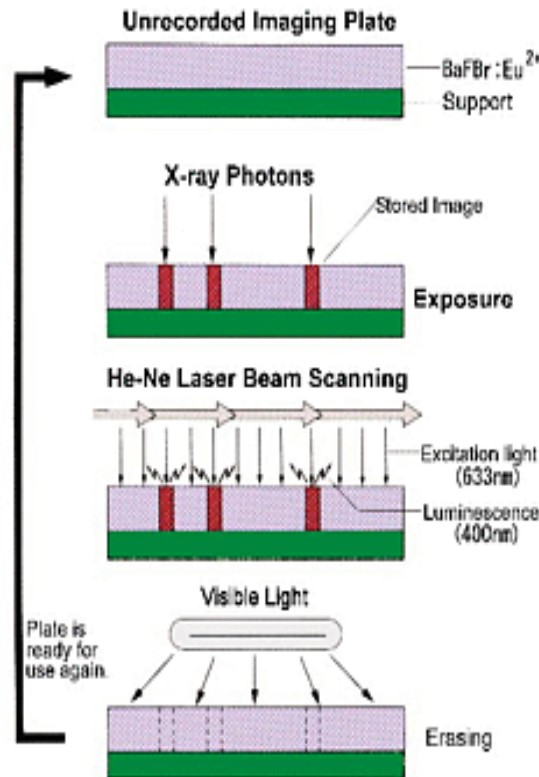


Figure 2.8. Image plate detector. The figure shows the main components of an image plate detector. A plastic sheet is coated with phosphorus crystals of barium halide and covered by a thin layer of europium. During exposure to X-ray, the photons trapped by the halogen cause the europium to be excited and an HeNe laser then relaxes the europium back to the lower energy state and creates an image.

2.7.2 Charge coupled device (CCD)

The CCD overcome the low speed of the IP (readout 1-2 min), by high speed (30-90 s exposure). They have a small active surface comparing with the large active surface of the IP. In addition, when the signal collects slowly, the CCD suffers from time-dependent noise; in modern synchrotron, the time-dependent noise is relatively small, due to very quick signal collection.

The CCD is coated by a phosphor face (Figure 2.9), which convert the X-ray photons bombarding to it into a visible light. The visible light is then changed to an electric charge image, which is converted to a numerical readout that can be read by a computer. Recently, the Pilatus 6M-F replace a CCD in many synchrotrons, in this detector the phosphor detector is replaced by a silicon pixel detector, it shares the same principle of any detector that the photoelectric effect is converted the X-rays to an electrical signal and substantially to a voltage, which is counted by cells bounded to a silicon detector.

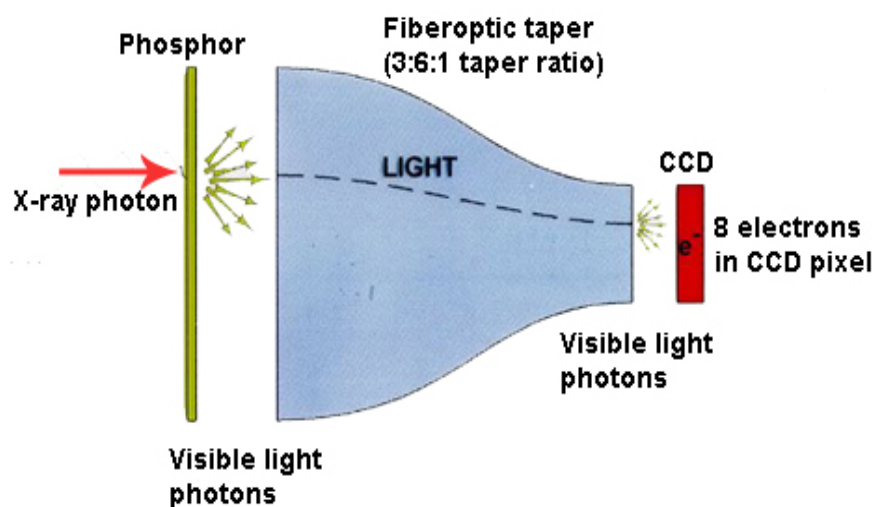


Figure 2.9. Charge coupled device (CCD). The figure shows the CCD components, the phosphor face converts the X-ray photons to a visible light, which then moves through the taper to compress the light image to size for a CCD chip. The electronic charge image is then digitalized by the CCD chip to pixels. The figure adopted from <http://www.xtal.iqfr.csic.es/Cristalografia/index-en.html>

2.8 X-ray diffraction and Bragg's law

The crystal is an ordered arrangement of molecules where each molecule contains atoms and each atom carries electrons in ordered energy shells. When the X-ray strikes the atom in the molecule in the crystal, it scatters in a distinct pattern, and this scatter produces an image on the detector of the X-ray apparatus. The diffraction reveals the

way that electrons are distributed around the atoms, known as the electron density of the molecule.

The unit cell is the building block of the crystal, in which one or more molecules can be found. The smallest portion in the unit cell that can be rotated and translated by system operators is called the asymmetric unit. When the electromagnetic radiation (X-ray) strikes a macromolecule crystal, the photons in this ray will interact with the electronic cloud surrounding each atom in the crystal, and at certain angles the X-ray scatter results in a well-ordered pattern (diffraction). From the scattering pattern results, an image of the crystal contents can be calculated. The crystal's atoms can interact with X-ray via constructive (in phase) and destructive (out of phase) interference. Constructive interference results when two or more crests and troughs of diffracted X-ray waves happened in the same time, in other words the amplitude of the resultant wave is the sum of two waves, whereas the destructive interference results when two waves have opposite crests and troughs, and the resultant amplitude is the subtraction of both waves (Figure 2.10).

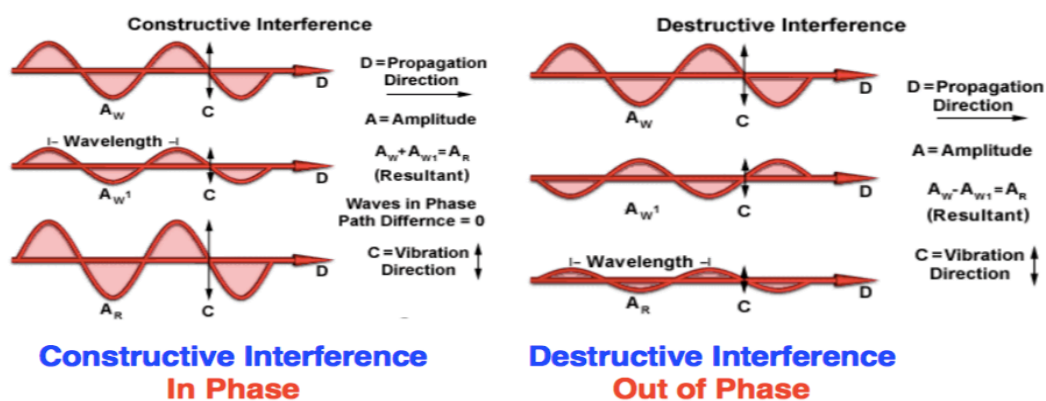


Figure 2.10. The constructive and destructive interference of X-ray. The figure shows how the waves of X-ray interfere with each other.

<http://web.pdx.edu/~pmoeck/phy381/Topic5a-XRD.pdf>

To explain the fact that crystal faces reflect an incident X-ray at certain angles, Sir William Henry Bragg and his son William Lawrence Bragg derived a simple law in 1913 (Figure 2.11). Bragg's law applies only to constructive interference that can be observed only at discrete angles.

Bragg's Law:

$$n \lambda = 2 d \sin (\theta)$$

where

λ is the wavelength of the rays

θ is the angle between the incident rays and the surface of the crystal

d is the spacing between layers of atoms

and constructive interference occurs when n is an integer (whole number)

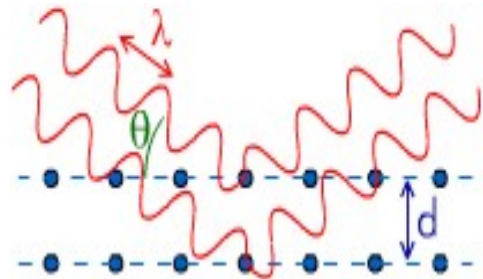


Figure 2.11. Bragg's law. The figure shows the three elements of Bragg law, $n\lambda = 2d \sin \theta$. $n =$ integer, $\lambda =$ wavelength of the X-ray beam, $d =$ distance between atomic layer in crystal and θ is the incident angle

http://www.outreach.phy.cam.ac.uk/camphy/xraydiffraction/xraydiffraction7_1.htm

2.9 Atomic scattering factors

The atomic scattering factor is the measurement of the scattering power for each electron in the atom of a crystal, in the other words how strong the interaction of the X-ray with each individual atom in the structure. Thus it depends on two factors: numbers of electrons in the atom, and the electrons positions in the electron cloud. The atomic scattering factors can be represented by atomic form factors (f), and are not affected by the X-ray wavelength, but depends on the electron density of the atom and the scattering angle as given in the equation:

$$f = \int \rho(r) \exp(2\pi i r \cdot S) dv$$

Where ρ =electron density, r = distance of the electron from the center of the atom, S = scattering vector. For atom in the same direction as the incident X-ray ($\theta=0$), the atomic scattering factor is equal to the atomic number. The atomic factor decreases with higher scattering angle (Figure 2.12).

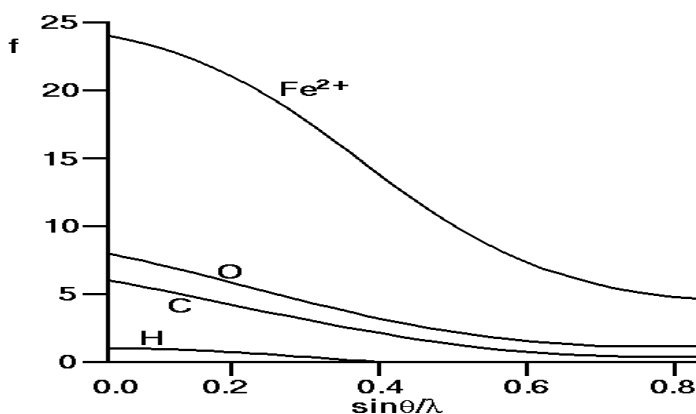


Figure 2.12. The atomic scattering factor curve for different atoms. The figure shows that with $\sin \theta / \lambda = 0$, the scattering factor (f) is equal to the total atomic number of the atom, for example the scattering factor of oxygen is equal to 8 (which mean all the electrons in the oxygen atom scatter), once the scattering angle becomes higher, the number of the contributing electrons in the scatter decreases and thus the atomic factor reduces. <http://pd.chem.ucl.ac.uk/pdnn/diff1/scaten.htm>

2.10 Structure factors

The direction, amplitude and phase of the diffracted X-ray reflections are the three main factors affecting the three-dimension structure of the crystal obtained from X-ray scattering. The atomic scattering factor (the X-ray scatter from atoms) can give an idea about the amplitude of the ray that was diffracted but no information about phase. This is described in a mathematical function called a structure factor which gives information about phase and amplitude of any X-ray reflection from each atom in the crystal. The structure factor is the information that is used to model the content of the crystal.

The structure factor of crystal is the sum of the X-ray diffraction of each single atom in a given direction. The sum of all the diffracted reflections provides information on

every atom in the crystal and a consequence is also that every atom contributes to every X-ray reflection.

The structure factor of single atom can be represented by the equation:

$$F = f \exp(2\pi i r \cdot S)$$

F = structure factor, f = atomic scattering factor, r = position relative to a fixed origin, $2\pi i r \cdot S$ = the phase differences between the scattering of the wave in position r and the origin position, and S = the scattering factor.

2.11 Molecule scattering

The molecule contains many atoms, each individual atom scatters the X-ray independently, and the sum of the scatter from each atom in the molecule will give the molecule scattering as in the equation below:

$$G(S) = \sum_{j=1}^{atoms} \exp(2\pi i r_j \cdot S)$$

where $(2\pi i r_j \cdot S)$ = phase difference generated from the two waves scattered from a molecule at the origin and other at r_j distance.

2.12 Crystal scattering

If the unit cell scatters the X-ray in phase in a given direction, the X-ray can be amplified, $(2\pi a \cdot S)$ is the phase difference between unit cells, in one dimensional scattering. If $a \cdot S = h$, where h is an integer, the adjacent unit cell scatters in phase also. In each crystal, a repeated unit cells are found, and the distance between those unit cells is represented by a translation vectors a, b, c . For each reflection in the diffraction, the translation vectors are represented by h, k and l respectively, and they are the called Miller indices.

h, k and l are integers. The structure factor for the unit cell can be calculated by combining the scattering from all the atoms with a term which relates to their repetition in the unit cells of the crystal.

$$F(hkl) = \sum_{j=1}^N \exp [(2\pi i)(hx_j + ky_j + lz_j)]$$

The x_j , y_j and z_j are the fractional coordinates of the unit cell, h, k and l are the crystal lattice planes that give rise to the measured reflections.

2.13 Data processing

To calculate the electron density map of the macromolecule, the diffraction data of the crystal should be converted to lists of Bragg reflections.

2.13.1 Auto-indexing

The auto-indexing for the data collected from the crystal diffraction can help determine the orientation, lattice type, and unit cell parameters and sometimes suggests a space group for the crystal. Each spot in the image is given a set of three integer values corresponding to the Miller indices (h, k and l). This information about cell dimension and orientation when combined with the known parameters such as X-ray wavelength and the crystal to detector distance can be used to predict diffraction on the images.

2.13.2 Integration

Integration is the process where the intensities of the reflections (seen as spots) in each image are determined. Even in the best data, the background noise can interact with the spot reflection, and to overcome this problem, the background is subtracted from the spot intensity. The next step in the integration is the profile fitting, in this step the strong spots are used to generate a profile (calculated profile) that will fit with the real profile and create a better estimate of the actual value of the spot intensity. The final product of this process is the mtz file that provides a list of intensities with an index for all the reflections in the data set that would be used in further processing.

2.13.3 Scaling and merging

Scaling and merging are the last steps in the data processing, and the statistics from these steps can diagnose and provide evidence about data quality and evaluate the data

collection process. The main role of those processes is to reduce the data set to a unique set of averaged reflection intensities. There are many factors that can influence the data quality such as inherent order in the crystal lattice; the effect of the cryoprotectant and presence of ice rings; the completeness of the multiplicity of the data collection; radiation damage; beam intensity and detector type.

2.14 Phase determination

During data collection, the detector can only record the intensity of the electromagnetic wave, but each reflection contains an amplitude (proportional to the reflection intensity) and a phase. The phase is lost during data collection; however, it is essential to have information from the phase to obtain the electron density map. There are different ways to find an initial phase estimate, which can then be refined: Direct Methods; Molecular replacement (MR); Multi/single-wavelength anomalous dispersion (MAD, SAD); and Multiple/single isomorphs replacement (MIR, SIR). In this study, MR was used for phase determination.

When all the phases are set as zero, a Patterson map can be initiated. Patterson functions $P(u\ v\ w)$ can be used to determine the structural information with all phase angles set to zero, by using the intensities as coefficient as in the equation below:

$$P(u\ v\ w) = \frac{1}{V} \sum_{hkl} |F(hkl)|^2 \cos [2\pi(hu + kv + lw)]$$

Where u , v and w are Patterson unit cell co-ordinates, the real unit cell coordinates, where the real unit cell coordinates are x , y and z . Patterson functions are very important in phase determination, and can be used to locate the position of the heavy atoms in MAD and MIR methods. They are also important as simplified descriptions of the molecule in the rotation and translation steps during MR.

2.14.1 Molecular replacement

MR is a very common method used to obtain phase information. The molecular replacement depends on using a known model structure that is a structure (homologue) with the unknown structure to obtain an initial phases information. Approximately 30% sequence identity is usually needed between the homologue protein used in MR and the target protein (Rossmann, 2001), based on the fact that similar protein folding would give similar X-ray diffraction. In this method, the calculated Patterson map (from the measured intensities) is compared with the Patterson map calculated from the structure of the homologue protein, and the location of the molecule then can be known by rotating and translating the Patterson maps in relation to each other (Figure 2.13).

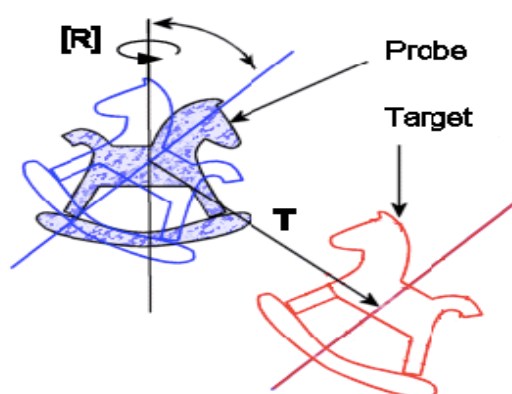


Figure 2.13. A representation of the Rotation and Translation steps in the Molecular Replacement method. The probe (blue horse) represents the known structure of a protein rotated (shown by [R]) and translated (shown by [T]) to fit the target protein (red horse) to which it is structurally similar. Simplified description (the horses) of the probe and target proteins can be made using Patterson functions that do not require any phase information.

It is often crucial during the MR to prepare the search model (homologue) by taking off all the non-conserved parts, such as loops and insertion regions and orient (rotate in 3D) the model to match the orientation of the target.

2.14.1.1 Rotation function search

The Rotation function (RF) search finds the best orientation to fits the Patterson functions of the model (known structure) with that of the protein of unknown structure. In the Patterson function, there are two main vectors: inter and intra- molecular vectors. The inter-molecular vector depends on the position of the molecule in the unit cell, whereas the intra-molecular vector is the orientation of the molecule within the unit cell. In the rotation function search, the intra-molecular vector is the most important parameter. The success of the rotation function depends on the resolution, usually between 3-6 Å, and thus low-resolution data can provide information about the overall shape of the molecule.

2.14.1.2 The Translation function search

The rotation function should give the correct orientation of the model amongst a set of possibilities, and therefore the next step is to search for the right position of the model within the unit cell. This can be achieved by a translation function (TF) search. In modern crystallography, Fast Fourier Transform (FFT) methods are used for the translation function to search for a correct position for the molecule within the unit cell that does not clash with the location and packing of other molecules. Generally, a cutoff value is applied in the programs such as PHASER to select the top hits from the RF which are then used in a set of translation function searches.

2.15 Electron density

After the molecular replacement, an initial set of phases are determined from the positioned model. Following this step, a first electron density map of the protein can be determined, and used to build the atomic model of the target protein. The electron density (ρ) in position (r) can be calculated by the equation below.

$$\rho(x, y, z) = \frac{1}{V} \sum_h^x \sum_k^x \sum_l^x F(hkl) \cdot \exp[-2 \pi i (hx + ky + lz)]$$

2.16 Structure refinement

The structure refinement is the last step in the structure solving process. Structure factors (F_{cal}) can be calculated from the model. The model built to fit the electron density is refined against the experimentally determined data. The F values calculated from the intensities of the spots are the reference and the model provides calculated F values that can be adjusted by altering the model to fit the maps better. Then new phases are generated. The refinement is a computational process in which the agreement between $|F_{\text{obs}}|$ from the data collection and $|F_{\text{calc}}|$ from the study model being built is improved by making small changes in the structure. There are many factors that can be monitored during the refinement process, such as the B- factor and the occupancy of the atoms in the model.

2.16.1 The B- factor

The B-factor (temperature or Debye-Waller factor) indicates how the electron density is spread out, or in another term, it is a measure of the mobility of the atom within the crystal (atom oscillation). Thus, it gives an indication of the uncertainty in the precise location of any atom within the model of the protein. The range of B-factors in protein structure is approximately 2-100 Å (Wlodawer et al., 2008), and it depends on the resolution of the data set. A B-factor less than 30 Å signifies a high confidence in atom position, whereas more than 60 Å indicates a high uncertainty in atom position or a disorder. In crystallography, the dynamic motion of atoms can be used as a parameter to judge the refinement process. The side chain atoms move more freely than the other atoms, and this movement can affect the diffraction pattern and contributes the B-factor of each atom in the structure refinement parameters.

2.16.2 Judging the refinement by R-factor

The model will have errors, and the aim of the refinement is to minimize these errors, which can affect the refinement process, thus the quality of the refinement process should be judged. The R-factor (the agreement between the observed and calculated.

$$R = \frac{\sum ||F_{\text{obs}}| - |F_{\text{calc}}||}{\sum |F_{\text{obs}}|}$$

structural factor amplitude) divided by the observed structural factor amplitude can be used for refinement monitoring.

The R-factor indicates how well is the refinement is going. If the R-factor value is low, it means a good agreement between the observed data and the search model being refined. A set of calculated structure factors comprising ~5 % of randomly selected reflections of the experimental (observed) data, which are never used in the refinement process, are compared with the same set of structure factor calculated from the new model being built to give another R-factor and this called the free R-factor (R_{free}) (Kleywegt, 2007). The R_{free} is used to validate the refinement process.

2.17 Model validation

To evaluate how well the calculated model fits the observed data before depositing the data into PDB, the refinement process should be validated. There are different parameters by which the refinement can be judged and a very important one of them is the Ramachandran plot.

2.17.1 Ramachandran plot

The Ramachandran plot refers to the distribution of the torsion angles ϕ and ψ of the polypeptide (Ramachandran et al., 1963). The ϕ angle between N-C α and the ψ angle between C α -C are rotated around C α , and the rotation of ϕ and ψ angles in each residue in the polypeptide is evaluated by Ramachandran diagram. The Ramachandran plot contains three regions: preferred, allowed; and outlier regions (Figure 2.14). Based on

the collision between atoms, the Ramachandran plot provides information about any disallowed rotation, and thus the ϕ and ψ angles provide information about correct protein folding, since they show the flexibility of the amino acid backbone to fit in certain places.

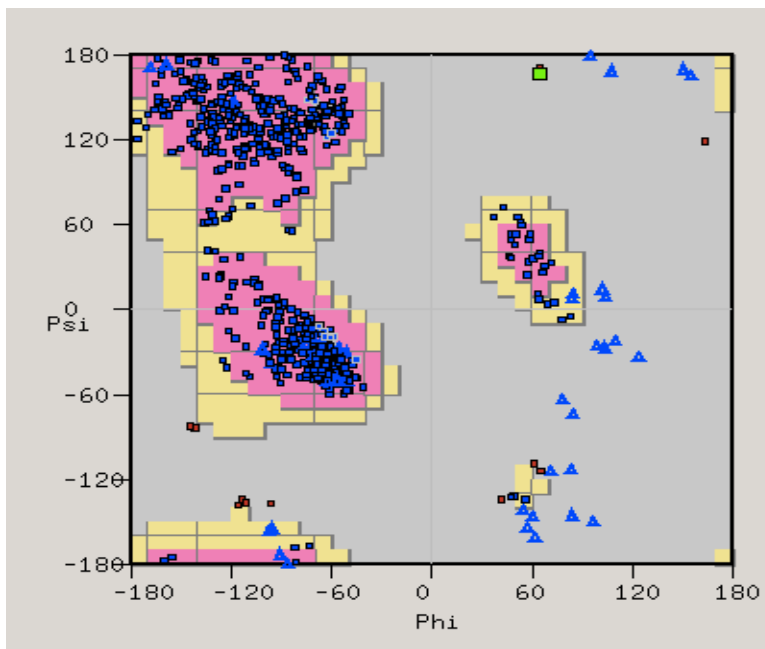


Figure 2.14. Example of a Ramachandran plot. The figure shows the torsion angles ϕ and ψ and the distribution of the residues in the preferred region (blue squares), the allowed region (blue triangles) and the outliers (red squares).

Chapter 3 : Materials and methods

3. Materials and methods

In this Chapter, all the methodology and the materials that were used in my project are detailed with their manufacturer. The protocols that were used to produce proteins, purify them, and crystallization protocols are stated. Procedures that were used in functional studies are also discussed in this Chapter

3.1 Materials

3.1.1 Chemicals

All the chemicals that were used in this study were provided by Sigma-Aldrich, Fisher or BDH unless another source is mentioned. All the concentrations mentioned in this Chapter are the final concentrations.

3.1.2 Bacteria and plasmids

All the plasmids and bacterial strains that were used in this study and their sources are listed in Table 3.1

Escherichia coli strain K12 *substrain* MG1655 was used to provide the genomic DNA.

Table 3-1 The table of strains and plasmids used in this work. The table provides the identities genetic composition and sources of the strains and plasmids used in the study.

Organisms	Genomic type	Source
<i>Escherichia coli</i> K12 sub. MG1655	F- lambda- <i>ilvG- rfb-50 rph -1</i>	<i>E. coli</i> Genetic stock culture Collection, Yale university
Top10	<i>F- mcrA Δ(mrr-hsdRMSmcrBC)</i> <i>φ80 lacZAM 15</i> <i>ΔlacX74 nupG recA1 araD139</i> <i>Δ(ara-leu)7697 galE15 galK16</i> <i>rpsL(Str^R) endA1 λ</i>	Invitrogen
DH5α competent cell	<i>F endA1 glnV44 thi-1 recA1</i> <i>relA1 gyrA96 deoR nupG</i> <i>Φ80dlacZAM15</i> <i>Δ(lacZYAargF)U169,</i> <i>hsdR17(r_K⁻ m_K⁺), λ-</i>	Fisher cat # VX18265017
Silver Efficiency competent cell		SLS Bioline cells cat # BIO85026
<i>E. coli</i> RKP5873	<i>hmp⁻ norR⁻</i> Transductant 26	Generously gifted from Prof. Jeff Cole lab
<i>E. coli</i> RKP5885	RKP5873 with pBAD/HisA	Generously gifted from Prof. Jeff Cole lab
<i>E. coli</i> RKP5884	RKP5873 with pPL3	Generously gifted from Prof. Jeff Cole lab
<i>E. coli</i> RKP163	<i>norVW</i>	Generously gifted from Prof. Jeff Cole lab
<i>E. coli</i> JCB5253	<i>norVW- nrfAB- nirBD- hmp- fnr- hcp-</i>	Generously gifted from Prof. Jeff Cole lab
pBAD/HisA	A vector with <i>araBAD</i> promoter, N- terminal polyhistidine tag, Enterkinase cleavage site and Ampicillin	Invitrogen Cat # V430-01

	resistance gene (β -lactamase)	
pET21a	A vector with N- terminal T7 tag and a C-terminal polyhistidine tag and Ampicillin selective marker	Invitrogen Cat # 69740-3
pJ401	A vector with T5 promoter, C-terminal polyhistidine tag, and a Kanamycin resistance marker, containing <i>cor E. coli</i> optimized gene	Generously gifted from Prof. Michel Shiloh

3.1.3 Oligos and restriction enzymes

The primers were designed manually depending on the target genes sequence obtained from <http://genolist.pasteur.fr/Colibri/index.html> or NCBI, with the proper restriction sites. All the oligos were designed as suggested in (Dieffenbach et al, 1993), and were purchased from Eurofins MWG Operons or Sigma-Aldrich, and the restriction enzymes from New England Biolab (NEB) (Table 3.2).

Table 3.2 Primers used for cloning. The table shows all the oligos with the restriction sites for *norV*, *norW* and *cor*

Primer name	Sequence
pBAD	
<i>norW</i>	
Forward primer with XhoI restriction site	GGCATCGG CTC GAG ATGAGTAACGGC
Forward primer with NcoI restriction site	GGC CCATGG GTAACGGCATTGTG
Reverse primer with HindIII restriction site	AGCGTCGCATCC AAAG CTTT AGGCACAGTA
Forward primer for fixing the 1 st mutation cons4	GGTGAATTTGCCGAGCA GTTTAATCTGCACCTG
Reverse primer for fixing the 1 st mutation cons4	CAGGTGCAGATTA AACTG CTCGGCAAATTCACC
Forward primer for fixing the 2 nd mutation cons4	CGGATGAAAGAGGCATTGGATTGTTGAAAAC

Reverse primer for fixing the 2 nd mutation cons4	GTTTTCAACAATCCAAATGCCTCTTTCATCCG
Forward primer for fixing the 1 st mutation cons2	GGAGGAATTACCATGAGTAACGGCATTGTGATC
Reverse primer for fixing the 1 st mutation cons2	GATCACAATGCCGTTACTCATGTTAATTCCTCC
<i>norV</i>	
Forward primer with NcoI restriction site	G CCATGG CTATTGTGAAAAATAAC
Reverse primer with HindIII restriction site	CCGATGATCAC AAGCTT GTTACTCATTGCC
Forward primer for fixing the 1 st mutation cons11	CAGGAGGAATTAACCATGTCTATTGTGGTG
Reverse primer for fixing the 1 st mutation cons11	CACCACAATAGACATGGTTAATCCCTCCTG
Cor	
<i>Mycobacterium smegmatis</i>	
Forward primer with XhoI restriction site	TGCGGA CTCGAG ATGGCTGAGGTTCCGGGTG
Forward primer with NcoI restriction site	CTCTCG CCATGG CTGAGGTTCCGGGTGGTC
Reverse primer with HindIII restriction site	GGTGGCA AAGCTT ATTCCGTCGGAACCC
<i>Mycobacterium tuberculosis</i>	
Forward primer with XhoI restriction site	CAGACG CTCGAG ATGGGTGAAGTTCGTGTTGTC
Forward primer with NcoI restriction site	CAGACG CCATGG ATGGGTGAAGTTCGTGTTGTC
Reverse primer with HindIII restriction site	GCCGTCCCGGCGCGCATCGTC AAGCTT
pET21a	
<i>norW</i>	
Forward primer with NdeI restriction site	GGAGGCCATATGAGTAACGGCATTGTGATC
Reverse primer with XhoI restriction site	GCATCC CTCGAG CATCGGCAATGTTTTCAACAA
Cor	
<i>Mycobacterium tuberculosis</i>	
Forward primer with NdeI restriction site	CAGACGCATATGGGTGAAGTTCGTGTTGTCCGC
Reverse primer with XhoI restriction site His	GCCAGG CTCGAG CTAGGTGGCCTTGAAATCGTC
Reverse primer with XhoI restriction site no His	GCCAGG CTCGAG GGTGGCCTTGAAATCGTC
<i>Mycobacterium smegmatis</i>	
Forward primer with NdeI restriction site	TAGGCACATATGGCTGAGGTTCCGGGTGGTC
Reverse primer with XhoI restriction site His	GCCAGG CTCGAG CTAGGTGGCCTTGAAATCGTC

Reverse primer with XhoI restriction site no His	GCCAGG CTCGAG GGTGGCCTTGAAATCGTC
<i>Cor</i>	
<i>Mycobacterium tuberculosis</i> non His in pJ401	
Forward primer with NdeI restriction site	GCTCATATGGGCGAAGTACGCGTAGTA
Reverse primer with XhoI restriction site His	TTA CTCGAG TGAGGTCGCCTTGAAGTCATC

3.1.4 Restriction enzymes

XhoI, HindIII, NcoI and NdeI restriction sites were checked by using NEB cutter website

(<http://tools.neb.com/NEBcutter2/index.php>), to ensure they didn't cut inside the target gene.

3.2 Methods

3.2.1 Primers design

The melting temperature, GC content and self-complementary features for all primers were checked by using the oligo calculator website <http://www.basic.northwestern.edu/biotools/oligocalc.html>. The primers were designed according to the guidelines in (Dieffenbach et al., 1993). The designed oligonucleotide primers were provided commercially in a lyophilized form in tube, nuclease-free water or autoclaved MilliQ water was added to resuspend the primers and the final

concentration for each primer was 100 pmol/μl or 100 μM/μl depending on the manufacturer.

3.2.2 Genomic DNA isolation

Genomic DNA was isolated from *E. coli* K12 MG1655 , by using RNeasy blood and tissue kit (QIAGEN, 2006) protocol, and from *Mycobacterium smegmatis* by using InstaGene Kit (Bio-Rad), then stored at -20 °C. Appendix 1

3.2.3 Transformation trial

All the plasmids that were used in this study were transformed to *E. coli* DH5α competent cells, using a transformation protocol

(http://www.addgene.org/plasmid_protocols/bacterial_transformation/), by using Lysogeny broth (LB) plates (Appendix 2), with 100 μg/ml ampicillin for pBAD and pET21a, and 50 μg/ml kanamycin for pET24a and pJ401. All the plates were incubated at 37 °C overnight (Appendix 3).

3.2.4 Plasmid DNA isolation

After incubation one colony was picked from each plate of transformation, cultivated in 5 ml LB broth with appropriate antibiotics. All tubes were incubated at 37 °C in a shaker incubator overnight (200 rpm). After that all cultures were spun down at 5500 rpm, for 10 min at 4 °C, the pellets were then used to isolate the DNA according to the QIA spun miniprep protocol (2004/2005) using a microcentrifuge method. All DNAs were labeled with plasmid name and stored at -20 °C.

3.2.5 Agarose gel electrophoresis

All plasmid DNA samples were run on 1% agarose gels (WebScientific), at 80 V for 45 min with 1 X TAE running buffer pH 8 (Appendix 4) and 5 X loading dye (Bioline), and 2 µl of Hyper ladder I (Bioline) was used as DNA marker to estimate the size of each fragment, and 0.1% of Gel red (Biotum) was used instead of ethidium bromide. The gels were visualized by UV light source. In addition, the DNA samples were quantified by using the Nanodrop at 260 nm with correction factor.

3.2.6 Amplification of target genes by Polymerase Chain Reaction (PCR)

PCR for cloning into pBAD/HisA, pET21, pET24a, and pJ401 was performed by using two different master mixes the Long Amp Hot start (NEB); and the Dream Taq Green polymerase (Fermentas). For pET21a, PCR was performed by using Accuzyme DNA polymerase (Bioline).

The PCR mixture was prepared as follows

25 µl master mix, 0.1 µl of forward primer, 0.1 µl of reverse primer, 1 µl genomic DNA, 23.8 µl autoclaved MilliQ water, in 1 ml Ependorff tube.

The PCR program was performed using the Techne PCR machine.

For pBAD, pET21a, the PCR program was:

30 s at 94 °C, 10-30 s at 94 °C, 15-60 s at 45-65 °C, 50 s per Kb (2.5 min) at 65 °C, 10 min at 56 °C and the final hold at 4-10 °C.

For pJ401, 5 min at 95 °C, then 35 cycles of: 30 s at 95 °C, 30 s at 55 °C, 60 s at 68 °C, then 5 min at 72 °C.

For pET21 using Techne PCR machine.

35 cycles: lid heated for 5 min at 100 °C, 15 s at 95 °C, 15 s at 55 °C, 30 s at 72 °C, 10 min at 72 °C, and the final hold at 4 °C.

After the PCR, all the products were loaded on 1% agarose gel at 80 V for 40 min, photos were taken to the gel by moving the gel to Fisher brand transilluminator and visualized it under UV light and take a photo by using iPhone 6 plus camera.

3.2.7 PCR clean up

The PCR products were purified by using QIAquick PCR purification kit (QIAGEN), according to the PCR purification spun protocol (2003/2008). After cleaning up, 3 µl of each product was loaded on a gel at 80 V for 40 min, to check the purity of the DNA.

3.2.8 Restriction digestion

All the plasmids were linearized and the inserts (PCR products) were restricted by using appropriate restriction enzymes, to create a sticky ends, after checking the potential cleavage site of the enzyme within each gene by using NEBcutter (Vincze et al., 2003). All the reaction tubes were incubated at 37 °C for 1 h and then left on the bench at room temperature overnight.

Each reaction contained 10-15 µl of plasmid/insert DNA (depending on the DNA concentration), 2 µl of cut smart or 2.1 buffer, 1 µl of each restriction enzyme, completed to 20 µl by autoclaved MilliQ water. Single digestion was performed by using one restriction enzyme, 4 µl sample of each reaction with uncut plasmids/inserts were loaded on 1% agarose gel at 90 V for 45-60 min to check the restriction results.

To isolate the pure digested plasmids, the remaining 16 µl of the restricted plasmid were loaded on 1% agarose gel, and the band that corresponded to the double digested

plasmid was extracted from gel by using QIA quick gel extraction kit as manufacturer's protocol.

3.2.9 Ligation

After the analysis of restriction results, ligation was performed for all plasmids by using T4 ligase (NEB), or Instant Sticky-end ligase master mix (NEB). Controls were tested for each reaction (cut plasmids with and without ligase), and five tubes for each plasmid were prepared with different plasmid/insert ratio according to their concentration 1:1, 1:2, 1:3, 2:1, 3:1 respectively. All the tubes were kept at 37 °C for one hour then overnight at room temperature, after which each reaction was transformed to Silver Efficiency *E. coli* for pET21a, Top10 *E. coli* for pBAD/HisA and *E. coli* BL21 for pJ401. (http://www.addgene.org/plasmid_protocols/DNA_ligation).

3.2.10 Transformation

The competent cells were transformed with the ligation reactions as recommended by Addgene protocol <https://www.addgene.org/plasmid-protocols/bacterial-transformation>

3.2.10.1 Preparation of chemically competent *E. coli* Top 10

Hanahan method was used for the preparation of chemically competent *E. coli* cells (Hanahan, 1983) (Appendix 5).

3.2.10.2 Preparation of electrocompetent *E. coli* Top 10

Top10 cells were prepared to be electrocompetent cells by using Bio-Rad protocol and electroporater <http://www.bio-rad.com/webroot/web/pdf/lsr/literature/M1652101> (Appendix 6).

3.2.10.3 Heat shock transformation

The chemically (in-house prepared and commercial) competent cells were transformed with plasmids as in (Appendix 3).

3.2.10.4 Electroporation transformation

Electrocompetent cells were transformed with plasmids (See Appendix 6).

3.2.11 Ligation results analysis

The colonies (constructs) resulting from the transformation on LB plates were selected and prepared (5 ml starter) for DNA miniprep, to analyse the ligation.

3.2.11.1 Restriction digestion of the constructs

After overnight incubation of all transformed reactions at 37 °C, the results were recorded by counting the colonies grown on LB plates. The constructs were digested that had been produced after miniprep them, by using the same restriction enzymes that were used for plasmid and insert digestion, all the restricted constructs and the undigested plasmids were loaded on a gel for 45 min at 90 V, to check which construct had the target gene.

3.2.11.2 Colony PCR for pET21a

Colony PCR was performed for 12 colonies, which were obtained from pET21a ligation, by using My Taq polymerase. The T7 forward and reverse primers (Bioline) and PCR primers for pET21a were used to check the target gene with and without the up and down stream region.

The colony PCR program was as follows: (30 cycles)

Heat lid 3 min at 95 °C

Segment 1 15 s at 94 °C

Segment 2 15 s at 52 °C

Segment 3 30 s at 72 °C

Segment 4 5 min at 72 °C

Final hold 4 °C

3.2.11.3 Sequencing

All the constructs were sent for sequencing to GATC Biotech or The University of Sheffield Medical School facility, as well as the PCR segments. 5 µl of DNA 50-100 ng/µl was sent with 5 µl of T7 (pET), T5 (pJ401) or pBAD (pBAD/HisA) primers or with PCR primers (forward or reverse).

3.2.12 Site direction mutagenesis experiment

Site direction mutagenesis was performed to fix the *norW* constructs mutations in pBAD/HisA, by using QuikChange II site-directed mutagenesis kit (Agilent) and the manufacturer's protocol (Appendix 7).

3.2.13 Protein overexpression

For **pBAD/HisA/norW** constructs with and without histidine- tag, the expression was performed in Top10 cells, by using different concentrations of arabinose, incubation temperature and time. 50 ml of LB broth in 250 ml flasks were prepared, ampicillin (100 µg/µl) and (3%) overnight cultures were added to each flask, and then all the flasks were incubated at two different temperatures (25 and 37 °C respectively) in a shaker incubator.

Samples were taken after inoculation immediately to check the optical density (OD₆₀₀) of the cultures, then every 30 min, until the OD₆₀₀ reached 0.6-0.8, then 1 ml samples were taken as pre-induction sample, and 2, 0.2, 0.02 or 0.002 % (w/v) of arabinose was used for induction. One flask was left as control without induction for each temperature. Samples of 1 ml were taken from each flask in each temperature at 1, 2,3,4,5 h and overnight after induction. All the samples were spun down and pellets were stored in -

20 °C freezer for different analysis. Final cultures after 24 h were centrifuged and the pellets stored at -20 °C.

With pJ401, the induction was performed by using 1 mM IPTG, at 37 °C in a 200-rpm shaker incubator, for 1, 2, 3 h and overnight.

3.2.14 Checking the expression

Protein expression was checked by using 1ml pellets stored at -20 °C. Samples were prepared for loading on SDS-PAGE (lab protocol) (Appendix 8), and the protein concentration was checked in each sample to know how much volume to load on the gel to get a final protein amount of 10-15 µg/µl.

3.2.15 Protein solubility

Expression of NorW with and without His-tag was analysed on SDS-PAGE. To check proteins solubility, samples were prepared by the standard Bugbuster protocol following the manufacturer's instructions. Protein concentration was measured by the Bradford method, and samples were prepared for SDS-PAGE loading as mentioned before.

3.2.16 Small scale protein purification

Batch method was used to purify the NorW His-tagged protein (Lab protocol). A 50 ml culture pellet was defrosted on ice, resuspended in 25 ml of lysis buffer and sonicated using Soniprep150 machine at 16 micron amplitude by 2x 20 s cycles. The sample then spun down in a J-25 Avanti centrifuge (Beckman), using JA 25.50 rotor at 24500 rpm (70000g) for 10 min at 4 °C, pellets were separated from the cell-free extracts (CFE), and protein concentration was checked for pellet and CFE by Bio-Rad protein assay (Bradford method). 50 µl sample of pellet and CFE was saved for SDS-PAGE analysis. Prior to purification, the Ni-NTA beads were re-activated using the standard protocol with NiCl₂ (Appendix 9).

3.2.17 Large scale protein production

Proteins large scale expression was performed at 37 °C, for 3 h for all proteins (NorW His and non-His-tagged protein, NorV non-His-tagged and Cor His-tagged protein), using 500 ml LB broth in 2 L flasks with appropriate antibiotic was used, which had been inoculated with 3% overnight culture. The OD₆₀₀ was taken until cultures reached 0.6-0.8, and 1 ml pre-induction samples were taken before induction with arabinose or IPTG, then 1 ml samples were taken every hour.

All 1 ml samples were centrifuged in a Sigma 3-16 K centrifuge at 5500 rpm for 10 min at 10 °C, pellets were then stored at -20 °C freezer, and the rest of the growth after 3 h incubation was spun down in a J-25 Avanti centrifuge (Beckman), using a JA 25.50 rotor at 24500 rpm (70000 g) for 10-20 min at 4 °C, and pellets were saved at -20 °C. The pellets were prepared for SDS-PAGE loading after measuring the protein concentration.

3.2.18 Large scale protein purification

Different columns were used to purify the proteins, via Ni-affinity, and Ion exchange and Gel filtration methods.

3.2.18.1 Ni and Ion exchange column purification

A 3 L culture of Top10 or BL21 was grown at 37 °C for and induced 3 h with 2% arabinose for Top10, and 1mM IPTG for BL21. To purify the protein, the pellets were defrosted, resuspended in 10 % lysis buffer or Tris pH 8.0. Cells were destroyed by using Soniprep150 machine at 16-micron amplitude by 2x20 s cycles. The cell suspension then was spun down in a J-25 Avanti centrifuge (Beckman), using a JA 25.50 rotor at 16-24500 rpm (70000 g) for 10-20 min at 4 °C, to separate the cell-free extract (CFE) from the pellet.

Protein concentration was measured for the CFE by method of Bradford using Bio-Rad protein assay, the His-tagged proteins were loaded onto a 5 ml HisTrap column (GE healthcare), the non-His tagged proteins were purified by ion exchange columns (DEAE FF 5 ml, Resource Q 6 ml) and then by loading onto a 1.6x60 Hi-Load Superdex 200 column at 1.5 ml/min flow rate. Fractions across the peak on the chromatogram were analyzed by SDS-PAGE.

3.2.18.2 Gel filtration (GF) purification

Gel filtration was used to purify the proteins further, using 1.6x60 Hi-Load Superdex 200 column at 1.5 ml/min flow rate in 0.5 M NaCl Tris-HCl pH 8 buffer. 2 ml fractions were collected. Protein concentration was analyzed by measuring absorbance at 280 nm and peaks were analyzed by the Bradford method and SDS-PAGE. After purification proteins was saved at 4 °C or used immediately for further studies.

3.2.19 Mass spectrometry (MS)

50-100 µl samples of each of the purified proteins were sent for analysis by MS, to confirm the right molecular weight of each protein.

3.2.20 Nuclear Magnetic Resonance (NMR) spectroscopy

NMR spectroscopy was used for some samples to confirm proteins folding, 502 µl NMR mixture was used for NMR characterization, in the MBB NMR facility, and contained 450 µl of protein mixed with 50 µl of deuterium oxide + 2 µl Trimethylsilylpropanoic acid (tsp) in the NMR tube.

3.2.21 Crystallization trial

The sitting drop vapor diffusion method of crystallization was used, and the preliminary experiment was performed by using a sparse matrix screening approach, with commercial screens (Classic, PACT, MPD, JCSG, Ammonium sulphate, Proplex, pH clear and Morpheus) on 96 well plates via a Hydra II plus 1 crystallization robot

(Matrix) was used for faster and cleaner mix of protein and chemical conditions drops. In this experiment 200 nl of protein was mixed with 200 nl of the screen precipitation in each well next to a 50 µl of precipitant reservoir, the plate was then sealed by sellotape, and incubated at a controlled temperature (7 and 17 °C).

Purified proteins were used in different concentrations to study protein crystallization. For NorW (concentration from 8.5-10 mg/ml) was used, different mixture was tried with and without NorV, with and without NADH and with and without sodium dithionite as stabilizer. Because heavy atom compounds have been seen often to bind cysteine residues and can sometimes result in more stable or better conformations for crystallization, and because NorW contains 4 cysteine, another attempt was tried to crystallize NorW by adding mercury chloride (1 mM) or 0.4 mM of potassium hexachloro palatinate before crystallization.

With NorV (10-12 mg/ml), purified with and without adding protease inhibitor (in order to obtain a full-length protein) was used with Classic, PACT, MPD, JCSG, Ammonium sulphate, Proplex, pH clear and Morpheus screens.

For Cor, a very broad range of protein concentrations were used (15-60 mg/ml), and two different incubation temperatures were used (7 and 17 °C).

The plate was labeled with protein name and concentration, date, and screen name, the plates then were routinely checked every day under microscope, and the condition that contains a crystal was labeled.

3.2.22 Optimization trial

After initial crystallization experiment, the conditions that produced crystals were optimized. The optimization was performed by using vapor diffusion hanging drop method, in this technique 1-2 µl of the protein were mixed with 1-2 µl of precipitant on a siliconised cover slip, the cover slip then convert and hanging over a reservoir contains 1-500 µl of the optimization solution (a solution with range of buffer pHs and

precipitant concentrations, that derive from the initial condition). The 24 wells plate was checked regularly, and the result was recorded.

For NorV, G4 from PACT (0.2 M potassium thiocyanate, 0.1 M bis-tris propan pH 7.5 and 20% (w/v) PEG 3350), H7 from JCSG (0.2 M Ammonium sulfate, 0.1 M bis-tris pH 5.5 and 25% (w/v) PEG 3350) and E10 from PEG (0.2 M sodium iodide and 20% (w/v) PEG 3350) were chosen to optimize by changing precipitant concentration and buffer pHs.

For Cor, PACT (G3) crystals were chosen to optimize, the initial condition was 0.2 M NaI, 0.1 M Bis-Tris propane pH 7.5, 20% (w/v) PEG 3350, rang of Bis-Tris propane pHs (6.5 – 8.5), and PEG concentration (10-24%) was used. For PACT (F2), 0.2 M Sodium bromide, 0.1M Bis-Tris propane pH 6.5, 20% (w/v) PEG 3350, different Bis-Tris propane pHs (6-7.5) and different PEG concentrations (5-30%) were used for optimization.

3.2.23 Data collection

All the crystals that obtained from initial and optimization screens were sent for X-ray diffraction at the Diamond Light Source near Oxford, after saving them in liquid nitrogen, with a suitable cryo protection solution, the cryoprotectants were prepared for each crystal condition based on the initial condition with the addition of 10, 15 or 20 % of ethylene glycol or glycerol. The crystals were mounted by using a loop match to the crystal size and shape (mostly a 0.5 mm loop was used), under a microscope, where 2 μ l of cryoprotectant solution was dispensed on the cover slip (in the optimization crystal trials), or in the S well (in the initial crystal screens), and the crystal then looped from the condition and moved to the cryoprotection solution. The crystal then was frozen in liquid nitrogen.

3.2.24 Data processing

NorV crystal data were collected, and processed by XDS in the xia2 pipeline (Winter, 2010), and analysed by the program AIMLESS from the Collaborative Computational

Project (CCP4) suite (Emsley et al., 2010). The unit cell contents were estimated on the basis of the unit cell volume and protein size with the program MATHEWS_COEF using the process proofed by Matthews (Matthews, 1968).

3.2.25 Structure determination

3.2.25.1 Phase determination

NorV crystal structure was solved in collaboration with Dr. John Rafferty by molecular replacement using the PHASER program from the CCP4 suite (McCoy et al., 2007) with the automated search mode and testing all related space groups option. *E. coli* Flavorubredoxin model (protein data bank ID 4D02) was used for molecular replacement. The cofactors and solvent were left out of the search model. The initial electron density map based on the phase estimates from the top solution in PHASER was inspected using COOT program (Emsley et al., 2010). The model of the structure fitted the map well and there was clear and easily interpreted density for the cofactor in their expected binding pockets.

3.2.25.2 Structure refinement

For refining the model, the REFMAC5 program (Murshudov et al., 2011) was used, with the coordinate file results from PHASER and the original data file processed by XDS. The cofactor (FMN) was built into the model and the water molecules were added, along with two irons added at the diiron center in the β -lactamase-like domain (C-terminal domain). The model was improved by making small changes to loop structure in the protein main and side chain positions. Cycles of inspection and model building in COOT followed by refinement in REFMAC led to a final model that was validated using the options in COOT which included checking the Ramachandran plot of the main chain phi and psi angles. The refinement was stopped once no further improvements could be made to the model and all the electron density was accounted for the R work and R free were not improved further. The refined model then was build

up by using COOT program (Emsley and Cowtan, 2004). The PyMol program (DeLano, 2002) was also used to examine the model of the structure and to produce figures.

3.2.25.3 Testing for the presence of the rubredoxin domain

Because the rubredoxin domain was not observed in our model, a sample of NorV crystals was prepared (~10 crystals grown in 0.2 M Potassium thiocyanate, 0.1 M bis Tris propane pH 8, and 25% (w/v) PEG3350), after washing the crystals in 0.5 μ l of optimization solution and a 0.5 μ l of solution with higher PEG concentration, then dissolving them in 10 μ l water, the sample was loaded onto an SDS-PAGE gel with a sample of purified NorV.

Also, a sample of NorV purified protein (filter sterilized and kept for 2 weeks in room temperature) was sent for MS, as a simple test to check if the rubredoxin domain was cleaved from the protein.

3.2.26 Biochemical studies

In this section, the methodologies that were used to study the mechanism of NorV and NorW action are detailed, and also the biochemical tests and spectrometric methods that were used with Cor protein.

3.2.26.1 NO consumption *in vitro* assay

In this assay, NO uptake by NorV and or NorW was studied under aerobic and anaerobic conditions, and under constant O₂ level. NO electrode (World Precision Instruments ISO-NO Mark II), and O₂ electrode (Rank Bros) were used to check the NO and O₂ levels, PROLI-NONOate (Santa Cruz Biotech or Cayman) was used as a NO releasing molecule.

3.2.26.1.1 NO and O₂ electrode calibration

The NO electrode was calibrated by using 20 ml of 0.1 M H₂SO₄ with 0.33 g of KI, the solution was prepared instantly and kept in a sealed glass vial (this solution is necessary to

produce NO from NO₂). The vial was put on a stirrer with low stirring and the electrode then put in the vial. Once the voltage of the electrode became stable, 50 μM NaNO₂ was added gradually (100, 200, 400, 800 μl) and the voltages increased as the NO concentration went higher.

The O₂ electrode was calibrated by adding 2 ml of 50 mM Tris pH 8 buffer to the electrode chamber, with stirrer on and water bath on to keep the temperature at 37 °C. Once the electrode was turned on the O₂ level was recorded. The value depended on the electrode lid, when the electrode was open, the buffer was saturated and the O₂ level became 100% quickly, but when the lid was on, the time for buffer to be saturated with O₂ was longer. Finally, the O₂ level reached 100%, and then a grain of sodium dithionite was added to the chamber and after a few seconds the O₂ level declined to zero.

3.2.26.1.2 Preparation of PROLI-NONOate

The PROLI-NONOate which can release NO within 1.8 s in solution in 37 °C was prepared by taking a little amount of the powder, in a fume cabinet, into a dark vial, then adding 1 ml of 0.01 M NaOH. The concentration of this solution was measured by Cary UV spectrophotometer at 252 nm, using ϵ 8,400 M⁻¹ cm⁻¹, and this solution became a stock solution, and further dilution was performed by adding MilliQ water as needed.

3.2.26.1.3 Aerobic NO consumption

Each molecule of PROLI-NONOate produces 2 molecules of NO. Purified NorV (2-5 μM) and NorW (1- 2.5 μM), NADH stock (50 mM was used to prepare 250 μM) and FAD stock (1 M) was used in this experiment. The NO released by the PROLI-NONOate at 37 °C was measured at least three times by NO electrode.

After the electrodes were calibrated, 2 ml Tris pH 8.0 buffer was added to the chamber of an O₂ electrode, the NO electrode was then put in the chamber, and (10 μl) 250 μM NADH was added. The mixture was stirred and the voltage was recorded by lab track, then (4 μl) 2 μM PROLI-NONOate was added and the electrodes voltages were recorded. The recording

was stopped once trace from the NO electrode volt became flat, and saved as a control to compare the NO consumption with and without adding the proteins.

The same measurements were repeated but with (16 μ l) 2 μ M NorV and (10 μ l) 1 μ M NorW, such that 3 editions of (4 μ l) 2 μ M PROLI-NONOate were used, then (8 μ l) 4 μ M PROLI-NONOate was added.

The measurements were repeated again as before but with NorV and with NorW separately, the measurements were repeated with NorW by adding 17 additions of (4 μ l) 2 μ M PROLI-NONOate and then another 11 additions of (4 μ l) 2 μ M PROLI-NONOate.

To check if NO uptake by NorW was dependent on NADH, (10 μ l) 1 μ M NorW was added to the buffer without NADH and with (2 μ l) 1 μ M PROLI-NONOate, then (10 μ l) 250 μ M NADH was added. Another set of measurements were done where the NADH was added without NorW, and then NorW added finally.

To check if NO uptake was occurring by the flavin adenine dinucleotide (FAD) in the NorW structure, the reaction was repeated by adding (2 μ l) 1 μ M and (10 μ l) 5 μ M of FAD without NorW, and then 300 nM of NorW was added.

3.2.26.1.4 NO consumption with gradual change in O₂ level

The measurement of anaerobic NO consumption was performed by using 2 ml of 50 mM Tris-HCl buffer pH 8.0 as a control with (10 μ l) 250 μ M NADH, then a mixture of (32 μ l) 16 mM glucose, (80 μ l) 4 unit/ml glucose oxidase, (40 μ l) 20 unit/ml *Aspergillus niger* Catalase were added to the buffer in the chamber with the lid on, to deplete it from O₂ (Thorndycroft et al., 2007). The glucose oxidase converts β -D- glucose to D-glucono-1, 5- lactone and hydrogen peroxide, then the hydrogen peroxide can be removed by the catalase. Once the O₂ electrode recorded zero, 2 μ M of PROLI-NONOate was added and the time for NO removal without NorW was recorded. The same measurements were repeated but with 2 μ M NorW final concentration, once the O₂ level started to decline as recorded by

electrode, 2 μM of PROLI-NONOate was added under the aerobic (~70-75% of O_2), microaerophilic (~20-25% of O_2) and anaerobic (~5-0% of O_2) conditions.

3.2.26.1.5 NO consumption with constant O_2 level

To determine the effect of the O_2 level on NO consumption, a reaction was set up to control the O_2 level to be steady during the experiment, by changing the stirring rate and the glucose and glucose oxidase concentration. The optimal conditions to keep the O_2 level as steady as possible were achieved. The O_2 electrode chamber was kept open, without a lid, calibrated in a volume of 2 ml 50 mM Tris buffer pH 8.0 with the stirrer at speed 3, and then a grain of sodium dithionite was added to zero the electrode. The control was measured by adding 2 ml of Tris buffer to the chamber of the O_2 electrode with 250 μM of NADH, stirring at speed 3, and then the O_2 depletion system (16 mM of glucose, 4 unit/ml of glucose oxidase and 20 unit/ml of catalase) was added. Once the O_2 level became stable, (3 μl) 6 μM of PROLI-NONOate was added. In the (test) reaction. The same components were then used with (82 μl) 4 μM of NorW, and 6, 12 and 18 μM of PROLI-NONOate final concentration was added to the chamber, the stirrer was changed from a speed of 3 to 5, the glucose/ glucose oxidase final concentrations were changed from 16 mM/ 4 unit /ml to 32 mM/ 8unit/ml. The consumption rate was recorded as mentioned before.

3.2.26.2 *in vivo* assays

3.2.26.2.1 NO consumption in intact *E. coli* cell suspension (anaerobic assay)

In this assay 5 μM of PROLI-NONOate final concentration was used as NO donor, and different electrocompetent *E. coli* mutant cells were used in this assay (Table 2.1), RKP5873 (*norR hmp*) was transformed with the *norW* expression vector, RKP5885 was RKP5873 transformed with an empty pBAD/HisA vector, and RKP5884 was RKP5873 transformed with a pPL3 *hmp* expression vector), JCB5253 (*norVW nrfAB nirBD hmp fnr hcp*) was transformed with a pBAD empty vector or with pBAD/*norW* expression vector.

100 ml overnight culture of each strain was used, cells were spun at 5500 rpm for 15 min and resuspended in 10 ml Tris-HCl pH 7.4 or 50 mM potassium phosphate buffer pH 7.6. An O₂ electrode was used to make sure that cells respired and consumed O₂. 250-500 µl of cell suspension were mixed with 1.5-1.75 ml of Tris buffer and added to the O₂ electrode chamber after checking the OD₆₀₀ for each strain, 10 mM glucose was used to keep the cells viable. Once the conditions became anaerobic, PROLI-NONOate was added to a final concentration 5 µM at 37 °C with continuous very slow stirring.

3.2.26.2.2 NO susceptibility of *E. coli* strains

In these assays, mutant strains of *E. coli* were used. RKP5873 is the *hmp norR* mutant, which means it cannot express NorW, NorV or Hmp. The electrocompetent *hmp norR* cells that were prepared, were complemented by a pBAD/HisA/*norW* expression vector, to make sure that any NO detoxification comes from NorW. RKP5885, which is *hmp norR* transformed with empty vector (pBAD/HisA) was used as a negative control. RKP5854, which is *hmp norR* complemented with a pPL341 vector containing *hmp* was used as a positive control to show the NO oxidation by Hmp. Another *E. coli* mutant was used, RKP163 with its *norVW* mutation, was also transformed with a pBAD/HisA empty vector or with a pBAD/*norW* vector (Table 3.1). The experiment was repeated three times to confirm the results. Different concentrations of DETA NONOate were prepared (0, 0.2, 0.5, 1 and 2 mM). Each tube contained 2 ml LB broth with appropriate antibiotics, arabinose, FeCl₃ and δ ALA added as needed (Table 3.3), and a 3% overnight starter of each strain was added. The tubes were incubated in a 250 rpm shaker incubator overnight, then the optical density at 600 nm was checked, the results recorded and analyzed by using Prism6 program to draw the curves.

Table 3.3 The NO susceptibility cultures. The table shows the strains that were used in the susceptibility test and the chemicals that were added to each strain with their final concentration

Strains	Chemicals				
<i>norR hmp/norW+</i>	Ampicillin 100 mg/ml	Kanamycin 50 mg/ml			Arabinose 2%
<i>norR hmp/pBAD</i>	Ampicillin 100 mg/ml	Kanamycin 50 mg/ml			
<i>norR hmp/hmp+</i>	Ampicillin 100 mg/ml	Kanamycin 50 mg/ml	δ ALA 10 mM	FeCl ₃ 0.01 mM	Arabinose 0.2%
<i>norVW/norW+</i>	Ampicillin 100 mg/ml				Arabinose 2%

3.2.26.3 Growth curve of *E. coli* mutant strains

Further assays were done to confirm the effect of NorW on NO toxicity, using 10 ml starter cultures of the *norR hmp*, *norVW* and multiple mutant strain (JCB5253) with empty vector and *norW* expression vector and they were grown overnight at 37 °C in a 250 rpm shaker incubator. 40 ml LB broth in a 250 ml flask supplemented with arabinose, FeCl₃, δ ALA and the appropriate antibiotic as mentioned in Table 2.2, 3% starter was added to each flask. Then 0, 0.5 and 1 mM final concentrations of DETA-NONOate were added to the *norVW* flasks, and 0 or 0.5 mM added to the *norR hmp*, and multiple mutant strain (JCB5253) flasks. All the flasks were incubated at 37 °C in a shaker incubator and 1 ml samples were taken every 2 h to check the OD at 600 nm. The results were recorded and then plotted by using Prism 6 program as growth curves.

3.2.26.4 Fourier transform infrared spectroscopy (FTIR) assay

In this assay cultures of *norR hmp* and a multiple mutant strain (JCB5253) were used (Table 3.1), the cultures were grown until OD_{600 nm} reached of 0.4-0.6 then induced by

addition of 2% (w/v) arabinose and the cultures left for 3 h. Samples of 1 ml were taken before and after induction. Samples were prepared and loaded on SDS-PAGE, to see if the proteins were expressed in each mutant.

N₂O release from cell suspensions, lysed cells or sterile defined or complex media was measured using gas-phase Fourier Transform Infrared (FTIR) spectroscopy. The general method used here has been previously described (Tinajero-Trejo et al., 2016) except that here an 8 m long path length multiple pass absorption cell was employed along with more sensitive liquid nitrogen cooled IR detector (EG&G Optoelectronics J15D14 MCT). At the beginning of the experiment, 20 ml of either an aerobic cell suspension in LB (the control was the mutant strain with pBAD and the test strain was the mutant strain with *norV* or *norW* expression vector), autoclaved cells in depleted LB, sterile LB or sterile minimal medium were connected to the White absorption cell via short transfer tubes. A peristaltic pump (nominal flow rate 7 l h⁻¹) and stirring of the suspension were used to rapidly bring the solution, flask headspace and absorption cell to equilibrium.

At the beginning of a measurement series, 2 mM DETA-NONOate was added to the suspension before the system was sealed and spectra recorded at 1 h or 15 min intervals for a minimum of 5 h to monitor N₂O evolution by the sample. A spectrum of the flask headspace just before NONOate addition was used as the blank for that particular series of measurements.

N₂O was quantified by integration of the N₂O ν_3 fundamental P-branch between 2172 and 2224 cm⁻¹ and comparison with the integrated area of the same band in a simulated 1 mbar N₂O spectrum with 1 bar pressure broadening using absorption coefficients obtained from the HITRAN 2012 database (Rothman et al., 2013).

3.2.26.5 ICP-MS

ICP-MS (Inductively coupled plasma mass spectrometry) was used to detect metals and several non-metals. NorW 4.8 mg/ml in 50 mM Tris-HCl pH 8, 0.5 M NaCl were sent

to the mass spectroscopy unit in the Chemistry department, University of Sheffield, to be analyzed by ICP-MS.

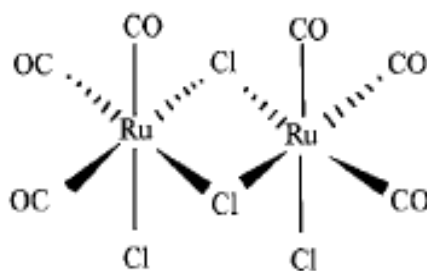
3.2.26.6 Carbon monoxide dehydrogenase (CODH) assay

An assay was performed to test if Cor can act as a CODH, to produce CO₂ from CO. 0.2% sodium dithionite was prepared in degassed 50 mM potassium phosphate buffer pH 7.0, and 1 µl was used to reduce methyl viologen (MV). The absorbance of Cor with MV as electron acceptor at 578 nm was taken for an hour, with readings at second intervals. Two controls were used in this assay; the first control was 50 mM potassium phosphate buffer with 40 mM MV degassed with N₂ for 5 min before being bubbled with CO for 5 min; the control was 4.2 mg/ml Cor in 1ml buffer degassed with N₂ for 5 min, then bubbled with CO for 5 min, A sample of 4.2 mg/ml Cor in 1 ml of 50 mM potassium phosphate buffer pH 7.0 with 40 mM MV, was first degassed by N₂ for 5 min and then bubbled with CO gas for 5 min. The values were measured by a Cary UV-visible spectrophotometer and then plotted as a graph by using the Prism6 program.

3.2.26.7 Assay of Cor protection of *E. coli* from CORM-2 toxicity

To test the hypothesis that Cor can protect *E. coli* transformed with the Cor *Mycobacterium tuberculosis* (Mtb) expression vector (pJ401) from CO toxicity (Zacharia et al., 2013), CORM-2 was used as CO donor in this assay. CORM-2 is a Tricarbonyldichlororuthenium (II) dimer (Figure 3.1). Non-transformed *E. coli* BL21 was used as a control. Both strains with and without *cor* were grown in a 130 ml of defined minimal media (Appendix 2). They both grew at 37 °C in a 200 rpm shaker incubator, until OD₆₀₀ became 0.4, then induced with 1 mM IPTG. When growth reached 0.6, the cultures were split into 30 ml aliquots, and one of the aliquots was used as a control with no CORM-2, whilst to the second one 10 µM of CORM-2 was added, and to the third one 30 µM of CORM-2 was added. The growth of all cultures was

measured by taking the OD₆₀₀ every hour, and the results plotted as graphs by using the Prism 6 program.



Tricarbonyldichloro ruthenium(II) dimer
 $[\text{Ru}(\text{CO})_3\text{Cl}_2]_2$

Figure 3.1. CORM-2: the figure shows CORM-2 structure, which contains two ruthenium at the center of the dimer (Motterlini et al., 2002)

3.2.26.8 Hematin assay

To check if Cor can work as CODH, bind heme *b* and oxidize CO according to this binding, Cor was tested by hematin assay. In this assay the hematin solution (5 mg/ml) was used as a source of heme *b*. The concentration of heme *b* in alkaline ethanol (hematin solution) was measured by using alkaline pyridine, which works as a ligand for Fe (II). The different spectrum (reduced minus oxidized form) was taken for hematin plus pyridine by adding a grain of ammonium persulfate to give the oxidized sample, and sodium dithionite to give the reduced one. To calculate the concentration of heme *b*, the different in absorbance (Δ absorbance) at 557-540 nm was calculated, and the heme *b* millimolar extinction coefficient ($\epsilon = 23.98 \text{ mM}^{-1} \text{ cm}^{-1}$) was used. Purified Cor concentration was calculated from measurement at 280 nM, then 10 μM of Cor was added to 20 μM of hematin solution and applied to a PD10 column. After gel filtration, coloured fractions (1 ml each) were taken, protein concentration was checked by the Bradford assay and two fractions were combined, then split into two 0.8 ml fraction. To one fraction sodium dithionite was added, and to the other ammonium

persulfate was added. The different spectrum (reduced minus oxidized) was taken from 400-600 nm. Albumin was used as a control protein to check if heme biniding was specific or not. It was used at the same concentration of Cor with the same concentration of hematin, and treated in the same manner. The test was repeated for 4 times to confirm the results.

3.2.26.9 Pull down assay using Cor with *E. coli* or *M. smegmatis* CFE

It was stated that Cor can protect *E. coli* from CO toxicity (Zacharia et al., 2013), thus to discover whether Cor is working independently on CO detoxification or it has a protein partner, a pull-down experiment was down, by using *E. coli* MG1655 and *M. smegmatis* cell free extracts (CFE), and *Bacillus subtilis* YloQ protein was used as a control His-tagged protein with *M. smegmatis* and *Burkholderia pseudomallei* Blf1 was used as a His-tagged protein with *E. coli*. Three buffers were used in this assay: buffer A is 50 mM Tris-HCl pH 7.5, 0.1 M NaCl; buffer B is buffer A but with 1 M NaCl; and buffer C which is 50 mM Tris-HCl pH 8.0, 0.5 M NaCl, 0.5 M Imidazole.

The first step in this assay was to prepare the cell-free extracts (CFE) of *E. coli* and *M. smegmatis*. For this, 500 ml of overnight culture was used for each species, spun down at 19000 rpm for 15 min and 4-5 mg of pellet was obtained. The pellet was frozen at -20 °C freezer for 24 h, then it was defrosted and 5 ml buffer A was added to it, before it was sonicated twice at an amplitude setting of 16 for 20 s. The lysate was spun down at 19000 rpm for 20 min, and the supernatant (CFE) was then taken to check protein concentration.

The next step was the preparation of Ni-NTA beads. 100 µl of Ni-NTA beads were taken into small column and washed with 2-3 ml of water, then 2-3 ml of buffer B. The column was closed and a 100 µl of buffer B were added.

The next step was charging Ni-NTA beads with protein. Two 1.5 ml Ependorff tubes (one for the target protein, one for the control His-tagged protein) were used, and to

each tube 1 mg of tagged protein in 0.4 ml of buffer B was added. Then 20 μ l of beads was added gently, and the tubes were left for 30 min on a rotating vertical wheel in a cold cabinet at 4 °C. After incubation, the tubes were spun down at 1000 g for 1min, the supernatants were taken carefully by gel loading tips without taking any beads, and then the beads were washed twice with buffer A with all the precautions above.

After charging the beads, the samples of CFE were loaded onto the beads in the tube. The beads were suspended carefully with the CFE and left in the cold cabinet for 2 h. Once the binding step finished, the washing step started, the tubes were spun at 1000 g for 1 min, and the supernatants were removed carefully. The beads were washed with 1.5 ml of buffer A for 3 times.

The elution step was performed by adding 50 μ l of buffer B to resuspend the beads in each tube and the tubes were then spun down as above. Supernatants were removed, and labeled as salt elution.

Elution with imidazole was the last step where 50 μ l of buffer C was added to each tube, beads resuspended and tubes spun down as above. Supernatants were moved, and labeled as Imidazole elution.

After finishing the protocol, the samples were prepared for gel loading, protein concentrations of all the samples were checked by The Bradford method, and the corresponding volumes were taken to load 15 μ g of protein in each gel well. A gradient 200-2000 NuPAGE gel was used to analyze the results, run at 200 V for 35 min, and stained with instant blue dye.

3.2.26.10 Fourier transform infrared spectroscopy (FTIR) of Cor with CO

An FTIR spectrum was taken, to check if Cor can bind CO and oxidize it to CO₂, 200 μ l of purified Cor (26 mg/ml) was diluted to 10 ml by adding 50 mM Tris-HCl pH 8 plus 0.5 M NaCl to the final concentration of 0.7 mg/ml. Throughout the experiment,

25% CO gas was circulated to the sample continuously, and the spectra were taken every 10 min for 1 hour and 40 min.

3.2.26.11 Nuclear Magnetic Resonance spectroscopy (^1H NMR) of Cor with CO

A test was performed to check Cor ability to bind CO, in which 6 mg/ml of Cor in Tris-HCl buffer pH 7.5 with and without CO was analyzed by ^1H NMR. After collecting a protein only spectrum, the same protein sample was bubbled with CO gas for 5 min in the same NMR tube, and the spectra were taken for 4 h, with one reading every hour.

3.2.26.12 ICP-MS of Cor

ICP-MS (Inductively coupled plasma mass spectrometry) was used to detect metals and several non-metals at concentrations of mg/l. A sample of Cor (26 mg/ml in 50 mM Tris-HCl pH 8, 0.5 M NaCl) was sent to the mass spectroscopy unit in the Chemistry department, University of Sheffield, to be analyzed by ICP-MS.

**Chapter 4 : Functional and structural
studies of flavorubredoxin
oxidoreductase (NorW)**

4. Introduction: NorW can consume NO without NorV

NorW is an FAD-binding protein with 377 amino acids, of approximately 41 kDa; many studies have demonstrated that NorW is the electron transporter between NADH and NorV during NO reduction (Gomes et al. 2000; Vicente et al. 2007; Vicente et al. 2009; Gardner et al. 2002; Gardner and Gardner, 2001).

In this Chapter, the details of *norW* cloning and NorW biochemical studies will be described. Functional studies on this protein were performed *in vitro* and *in vivo*, and the results that were obtained, were in contrast with other studies, and suggest that NorW has a distinct role in NO detoxification directly, in the absence of NorV.

The *in vitro* results showed that purified NorW is capable of consuming NO in both oxic and anoxic conditions. The *in vivo* assays suggested a different result.

4.1 *norW* cloning

Cloning was performed by using pBAD/HisA and pET21a plasmids, to produce a histidine-tagged untagged NorW. *E. coli* K12 strain MG1655 was used as a source of *norW*, the genomic DNA was extracted by an extraction kit, and the concentration of DNA was measured by using a Nano-Drop device. Primers were designed manually; the melting temperature and the GC content were checked as described in Chapter 3 section (3.2.1). The plasmids (pBAD/HisA and pET21a) were checked on agarose gel to confirm the right molecular sizes. (pBAD/HisA= 4102bp, pET21 =5443bp). After setting the PCR program, the target gene (*norW*) was successfully amplified, and PCR products sizes were checked by loading on a gel (*norW* = 1134bp) (Figure 4.1). PCR products were then purified by using both a clean-up kit and a gel extraction method.

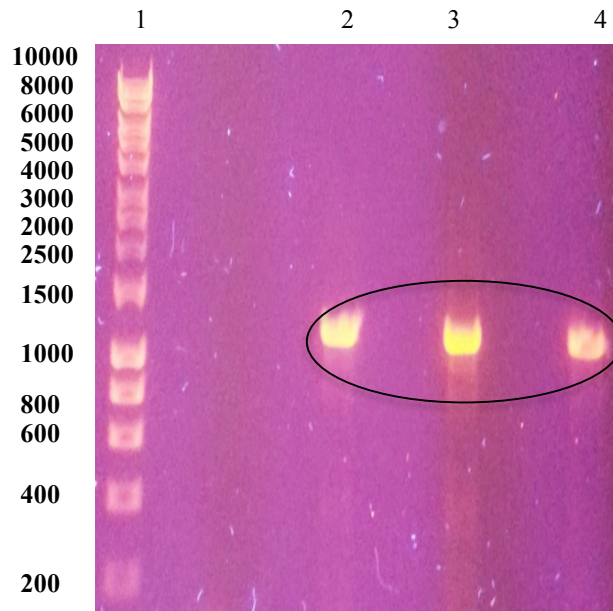


Figure 4.1 DNA gel electrophoresis of *norW* PCR products. The figure shows the PCR product bands of *norW*, lane 1 is the DNA marker (HyperLadderI), and lanes 2, 3 and 4 are the PCR products. The bands were seen at the corresponding molecular size for *norW* (1134 bp).

4.2 Restriction digestion

The PCR products, which were designed to ligate into pBAD and pET21a plasmids, to produce a His-tagged and untagged protein, were digested by using the same set of restriction enzymes (XhoI and HindIII and NcoI and HindIII for pBAD His-tagged and untagged protein respectively, and XhoI and NdeI for pET21a). Single digestion was performed as a control, to confirm the activity of the restriction enzymes, also a negative control of uncut plasmid and PCR product were included in the digestion. Restriction results showed that the linear DNA ran faster than the circular undigested one. The rest of the reaction (normally 45 μ l) then was loaded on a 1% agarose gel. The DNA then was cut and extracted from gel by using a gel extraction kit. Then the DNA concentration was measured by using a Nano-Drop. For more details see Chapter 3, section (3.2.8).

4.3 Ligation

The *norW* gene was successfully ligated into pBAD/His A, to produce an (N-terminal His-tag protein, and an untagged protein), and into pET21a, which encodes a C-terminal His-tag protein, by using the T4 ligase. The control reactions used were the cut and uncut plasmid with no PCR product with and without ligase. All the reactions were then incubated for 1 h at 37 °C as the NEB ligation protocol suggested (see Chapter 3 section 3.2.9). Then further incubation was performed at room temperature overnight.

4.4 Transformation

The ligation reactions were used to transform chemically competent *E. coli* silver efficiency cells (recommended for high efficiency transformation, efficiency CFU/ μ g pUC19 $\geq 1 \times 10^8$); transformation reactions were cultivated on LB plates with ampicillin 100 μ g/ml, or kanamycin 50 μ g/ml.

pBAD/HisA ligation was successful, 12 colonies were seen in the plate with 200 μ l, of 1: 1 plasmid to insert ligation ratio, by using Long Amp Polymerase (Figure 4.2). With Green Dream Taq polymerase 20 colonies were grew on the plate, cultivated with 200 μ l of 1:2 ligation ratio. There was no growth in the control plates (cut plasmid with and without ligase enzyme) for both ligations. However, for pET21a, the ligation was not successful. Over 200 colonies were seen in the control plates, and two colonies only in the plate cultivated with 200 μ l of the transformation mixture. Over 7 attempts to ligate pET21a with *norW* gene (Using Long Amp and Accuzyme polymerase) were done with different ligation ratios calculated with the Ligation calculator website http://www.insilico.uni-duesseldorf.de/Lig_Input.html. Some of them resulted in colonies, but when the DNA was extracted from the constructs, digested by restriction enzymes, and loaded on an agarose gel, the result showed that they were not the correct constructs.

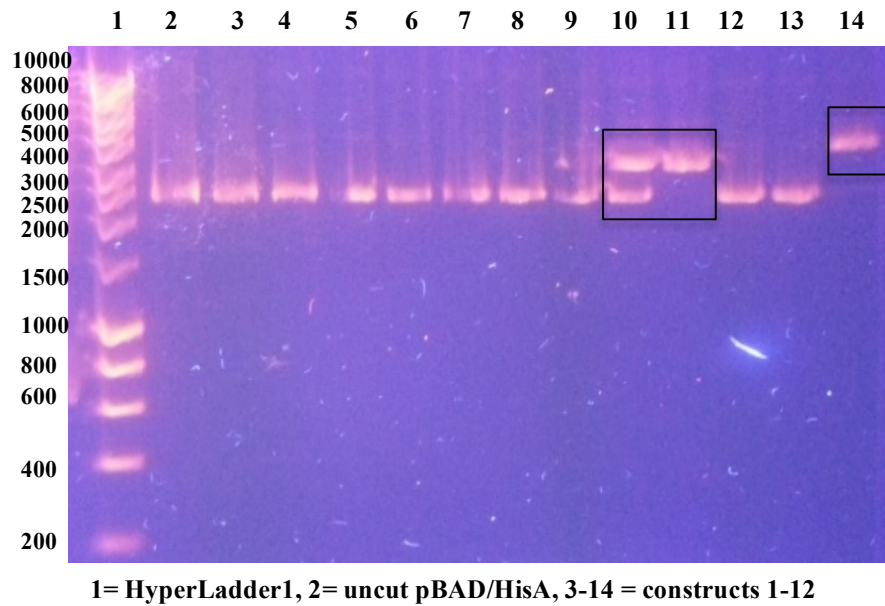


Figure 4.2 The uncut DNA extracted from pBAD/*norW* colonies. The gel shows the ligation results for pBAD/His A (12 constructs) which came from the 1st ligation using Long Amp Polymerase PCR product. It shows that the DNA of constructs in lanes 10-11-14 were ran slower than the DNA of uncut plasmid and the other constructs, and are believed to have *norW* gene. The expected size of the construct is 5236 bp

4.5 Ligation analysis by restriction digest for pBAD/ *norW* constructs

All the constructs that resulted from the ligation of pBAD/HisA plasmid with *norW* PCR products, to produce a His-tagged and untagged proteins, were digested by appropriate restriction enzymes. (Figures 4.3 A&B) show the results of restriction digestion of constructs 7 and 9 (expressing a His-tagged NorW, produced using Long Amp Polymerase in PCR).

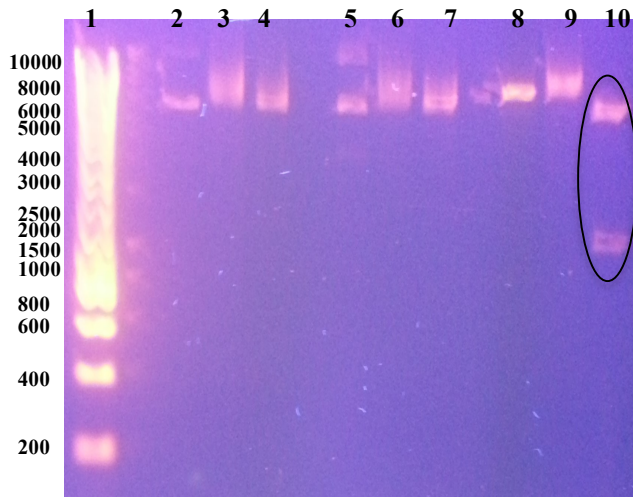


Figure 4.3 A: Restriction digestion results of the DNA of pBAD/*norW* constructs. Lane 1 is the DNA marker (HyberLadderI), lanes 2,3 and 4 corresponding to pBAD plasmid DNA digested with XhoI, HindIII, and both respectively, lanes 5, 6 and 7 are the DNA of construct 2 digested with XhoI, HindIII, and both respectively, lanes 8, 9 and 10 are the DNA of construct 7, digested with XhoI, HindIII, and both respectively. The figure shows that construct 7 contains the right band related to *norW* in the double digestion.

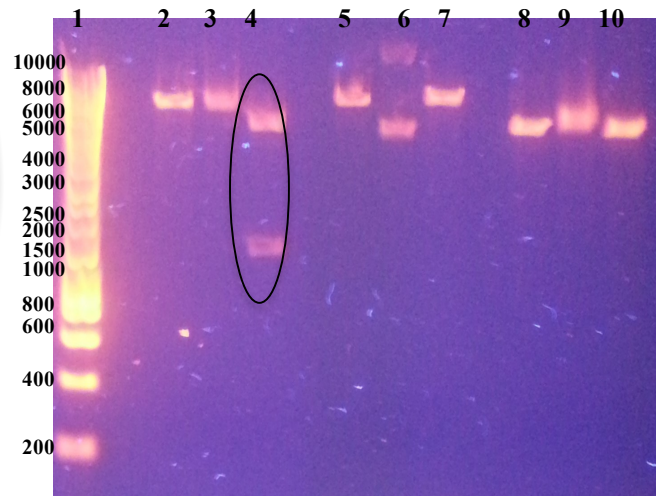


Figure 4.3 B: Restriction digestion results of the DNA of pBAD/*norW* constructs. Lane 1 is the DNA marker (HyberLadderI), lanes 2,3 and 4 corresponding to construct 9 DNA digested with XhoI, HindIII, and both respectively, lanes 5, 6 and 7 are the DNA of construct 12 digested with XhoI, HindIII, and both respectively, lanes 8, 9 and 10 are the DNA of pBAD plasmid, digested with XhoI, HindIII, and both respectively. The figure shows that construct 9 contains the right band related to *norW* in the double digestion.

The results showed that constructs 7 and 9 were the correct constructs, because they had the right molecular size of the insert, which was released after double digestion. The products were also examined that had been made with Dream Taq polymerase PCR and the DNA of the 20 colonies also were analyzed on gel (Figures 4.4).

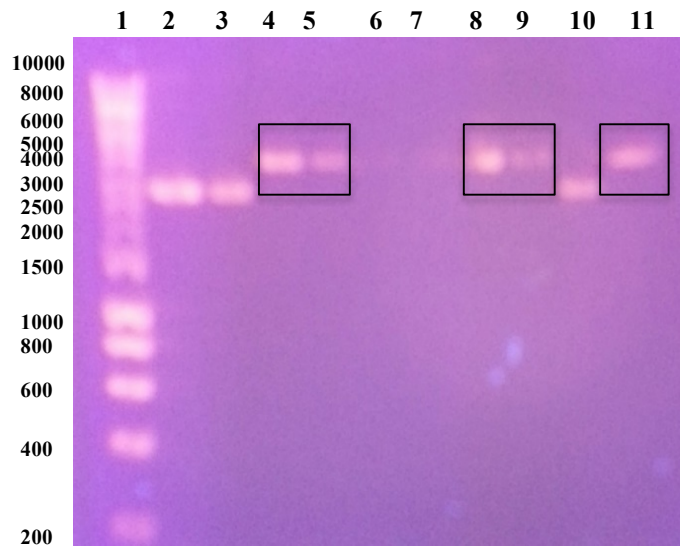


Figure 4.4: The uncut DNA extracted from pBAD/*norW* constructs. The gel shows the ligation results of pBAD/His A /*norW* constructs 2 to 18 (2-4-6-8-10-12-14-16-18) along with pBAD unligated plasmid. The gel shows that the DNA of constructs 4, 6, 12, 14 and 18 run slower than the other constructs, which suggests that they might contain the gene (the expected molecular size of the construct is 5236 bp). Lane 1 is the DNA ladder (HyperLadder I), Lane 2 is the uncut pBAD, Lanes 3-11 are constructs 2-18.

Construct 4 (expressing a His-tagged NorW) was selected to send for sequencing, after the constructs were digested and loaded on gel (Figure 4.5), and also construct 2 (expressing a non-His tagged NorW) was elected for sequencing.

For pET21a, 12 constructs were gained from the ligation with Accuzyme polymerase PCR product. Colony PCR was used to determine the correct construct, which contains *norW* gene inserted by using My Taq polymerase, with the PCR primers and T7 forward and reverse primers. Based on the results, (Figure 4.6 A&B) constructs 6, 7, 9 and 12 were chosen for sequencing.

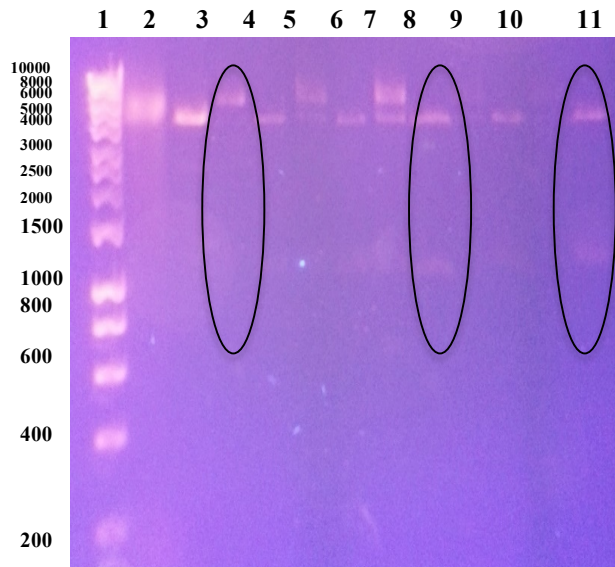


Figure 4.5: restriction digestion analysis of pBAD/*norW* constructs. The figure shows the restriction results of pBAD/His A /*norW* constructs 2 to 20 along with pBAD unligated plasmid, Lane 1 is the DNA marker (HyperLadderI), lane 2 is the pBAD unligated plasmid, lanes 3-11 are the cut pBAD/*norW* constructs. Constructs 4, 14 and 18 showed another band on the gel when digested by two enzymes (XhoI and HindIII), and the molecular size of the band was suggested that those constructs might contain the gene (1134 bp).

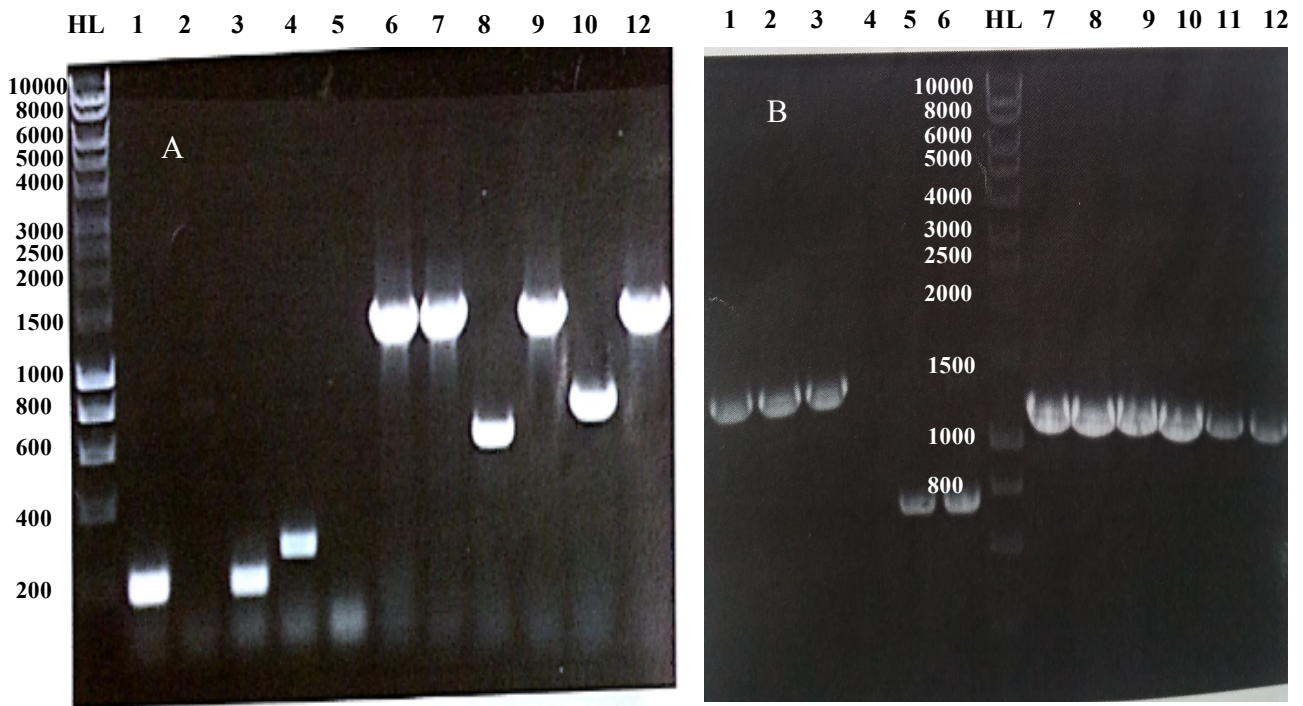


Figure 4.6: Colony PCR for pET21a/*norW* constructs. Panel A- Shows the PCR products by using the forward and reverse primers which were used in the gene amplification by PCR, the result shows that constructs 6, 7, 9 and 12 run higher than the other constructs, which suggested that they contain the gene. Panel B- Shows the bands of the PCR products by using standard T7 primers, the products obtained in constructs 1, 2, 3, 7, 8, 9, 10, 11, and 12, suggested that those constructs might contain the gene (1134 bp). HL= HyperLadderI (DNA marker).

4.6 Sequence analysis

4.6.1 pBAD/*norW* constructs.

Constructs 7, 9 and 4 (Expressing a His-tagged protein), and construct 2 (Expressing a non-His tagged protein) were selected for sequencing,

The results of the sequencing were analyzed by using a BLAST search of the National Centre for Biotechnology Information (NCBI) and the Finch TV program. The analysis revealed that pBAD construct 7 was not the correct construct; there were no matches in the construct with *norW* of *E. coli* when they were aligned together in an NCBI

nucleotide blast search. For construct 9, the sequence showed 3 mutations and an insertion (Figure 4.7 A). To know if the mutations in construct 9 came from the inset (PCR product), the PCR segment produced by the Long Amp polymerase was sent for sequencing. The results showed that the mutations came from the PCR segment. Accordingly, Long Amp polymerase was replaced by Green Dream Taq polymerase, and construct 4 produced with pBAD. Construct 4 sequence analysis showed that there were two point mutations, the first one changed glutamine to arginine; the second one changed isoleucine to arginine, and only one silent mutation (Figure 4.7 B). In the non-His tagged construct (construct 2) there was only one mutation, which was created intentionally, to make a NcoI restriction site in the second amino acid, which changed serine to glycine. The other mutation was silent (Figure 4.7 C).

A

Sequence ID: |cl|36009 Length: 1361 Number of Matches: 1

Range 1: 5 to 1351 [Graphics](#)

Next Match Previous Match

Score	Expect	Identities	Gaps	Strand
2433 bits(1317)	0.0	1340/1351(99%)	5/1351(0%)	Plus/Plus
Query 1	CTGACGCTTTTATCGCAACTCTCTACTGTTTCCATACCCGTTTTTTGGGCTAACAGG			60
Sbjct 5	CTGACGCTTTTATCGCAACTCTCTACTGTTTCCATACCCGTTTTTTGGGCTAACAGG			62
Query 61	AGGAATTAACCATGGGGGTTCTcatcatcatcatcatcatGGTATGGCTAGCATGACTG			120
Sbjct 63	AGGAATTAACCATGGGGGTTCTCATCATCATCATCATCATGGTATGGCTAGCATGACTG			122
Query 121	GTGGACAGCAAATGGGTCGGGATCTGTACGACGATGACGATAAAGGATCGATGGGGATCCG			180
Sbjct 123	GTGGACAGCAAATGGGTCGGGATCTGTACGACGATGACGATAAAGGATCGATGGGGATCCG			182
Query 181	AGCTCGAGATGATAACGGCATTGTGATCATCGGTTCCGGGCTTCGCCGCCGCCAACTGG			240
Sbjct 183	AGCTCGAGATGATAACGGCATTGTGATCATCGGTTCCGGGCTTCGCCGCCGCCAACTGG			242
Query 241	TGAAAAATATTTCGCAACAGGACGCCACTATTCATTAAACCCCTGATTGCCGCCGACAGCA			300
Sbjct 243	TGAAAAATATTTCGCAACAGGACGCCACTATTCATTAAACCCCTGATTGCCGCCGACAGCA			302
Query 301	TGGATGAGTACAACAAACCTGACCTCAACCATTTATCAGTCAGGGGCAACGTGCCGATG			360
Sbjct 303	TGGATGAGTACAACAAACCTGACCTCAACCATTTATCAGTCAGGGGCAACGTGCCGATG			362
Query 361	ACCTTACCCGCCAGACGGCGGGTGAATTTGCCGAGCAGTTAATCTGCACCTGTTTCCAC			420
Sbjct 363	ACCTTACCCGCCAGACGGCGGGTGAATTTGCCGAGCAGTTAATCTGCACCTGTTTCCAC			422
Query 421	AAACCTGGGTGACGGATATCGATGCCGAAGCCCGTGTGGTGAAAAGCCAGAATAATCAGT			480
Sbjct 423	AAACCTGGGTGACGGATATCGATGCCGAAGCCCGTGTGGTGAAAAGCCAGAATAATCAGT			482
Query 481	GGCAATACGACAAGCTAGTACTGGCAACCGGTGCCAGTGCCTTTGTCCCGCTGTGCCTG			540
Sbjct 483	GGCAATACGACAAGCTAGTACTGGCAACCGGTGCCAGTGCCTTTGTCCCGCTGTGCCTG			542
Query 541	GGCGTGAGTTAATGCTGACGTTAAATAGTCAGCAAGAGTATCGGCCCTGTGAAACGCAAC			600
Sbjct 543	GGCGTGAGTTAATGCTGACGTTAAATAGTCAGCAAGAGTATCGGCCCTGTGAAACGCAAC			602
Query 601	TGCGGGATGCCCGACGCGTGTGATTGTTGGCGGTGGTTTGGTGGTAGCGAACTGGCGA			660
Sbjct 603	TGCGGGATGCCCGACGCGTGTGATTGTTGGCGGTGGTTTGGTGGTAGCGAACTGGCGA			662
Query 661	TGGATTTTTGTCGTCAGCAAAACGGTTCACGCTAATCGACAACGCTGCCAGTATTCTGG			720
Sbjct 663	TGGATTTTTGTCGTCAGCAAAACGGTTCACGCTAATCGACAACGCTGCCAGTATTCTGG			722
Query 721	CGTCGTTAATGCCACCGGAAGTAAGCAGCCGCTTGCAGCATCGGTTGACGGAGATGGGCG			780
Sbjct 723	CGTCGTTAATGCCACCGGAAGTAAGCAGCCGCTTGCAGCATCGGTTGACGGAGATGGGCG			782
Query 781	TTCATCTGCTGTTGAATCTCAGTTACAGGGGCTGGAAAAACGGATTCTGGCATTTCAGG			840
Sbjct 783	TTCATCTGCTGTTGAATCTCAGTTACAGGGGCTGGAAAAACGGATTCTGGCATTTCAGG			842
Query 841	CAACGCTGGACCGCCAGCGCAATATCGAAGTGGATGCGGTAATTGCCGCCACCGACTGC			900
Sbjct 843	CAACGCTGGACCGCCAGCGCAATATCGAAGTGGATGCGGTAATTGCCGCCACCGACTGC			902
Query 901	GCCCGGAAACCGCCCTGGCAGCAGCGCCGGGCTGACGATTAATGCGCGGCTTTGCGTGC			960
Sbjct 903	GCCCGGAAACCGCCCTGGCAGCAGCGCCGGGCTGACGATTAATGCGCGGCTTTGCGTGC			962
Query 961	ATAGTTATCTGCAAACAGTAATACCGATATTTACGCGCTGGGCGATTGCGCGGAAATTA			1020
Sbjct 963	ATAGTTATCTGCAAACAGTAATACCGATATTTACGCGCTGGGCGATTGCGCGGAAATTA			1022
Query 1021	ACGGTCAGGTATTGCCGTTCCCTCCAGCCGATTCAACTTAGCCGATGGTGTGGCAAAA			1079
Sbjct 1023	ACGGTCAGGTATTGCCGTTCCCTCCAGCCGATTCAACTTAACCCGATGGTGTGGCAAAA			1082
Query 1080	AATCTTCTCGGCAATAACACGCGCGCTGAAACTCCCGGCTATCTGGTGAATAACAAAACG			1139
Sbjct 1083	AATCTTCTCGGCAATAACACGCGCGCTGAAACTCCCGGCTATCTGGTGAATAACAAAACG			1142
Query 1140	CCGGAATTACCGCTGCATCTGGCAGGGGAAACCCAGCGTCAGGATTTACGCTGGCAAATT			1199
Sbjct 1143	CCGGAATTACCGCTGCATCTGGCAGGGGAAACCCAGCGTCAGGATTTACGCTGGCAAATT			1202
Query 1200	AATACCGAACGCCAGGGAATGGTGGCGCGCGGCTTGACGATGCTGACCAGCTTCGCGCC			1259
Sbjct 1203	AATACCGAACGCCAGGGAATGGTGGCGCGCGGCTTGACGATGCTGACCAGCTTCGCGCC			1262
Query 1260	TTTGTGGTCAGTGAGGATCGGATGAAAGAGGCATTGGATTGTTGAAAACATTGCCGATG			1319
Sbjct 1263	TTTGTGGTCAGTGAGGATCGGATGAAAGAGGCATTGGATTGTTGAAAACATTGCCGATG			1322
Query 1320	TAGTTGGGCTACTGTGCCTAAAAAGCTTGGC 1350			
Sbjct 1323	TAGTTGGGCTACTGTGCCTAAAA-GCT-GGC 1351			

S=Serine, G= Glycine, L= Leucine

Subject = *E. coli* genome Query = construct 2 sequence

B

Sequence ID: lc|10629 Length: 1346 Number of Matches: 1

Range 1: 3 to 1344 [Graphics](#)

Next Match Previous Match

Score	Expect	Identities	Gaps	Strand
2425 bits(1313)	0.0	1331/1343(99%)	2/1343(0%)	Plus/Plus
Query 1	CTGACGC-TTTTATCGCAACTCTCTACTGTTTCTCCATACCCGTTTTTTGGGGCTAACAG	59		
Sbjct 3	CTGACGC-TTTTATCGC-ACTCTCTACTGTTTCTCCATACCCGTTTTTTGGGGCTAACAG	61		
Query 60	GAGGAATTAACCATGGGGGGTTCcatcatcatcatcatcatcatSGTATGGCTAGCATGACT	119		
Sbjct 62	GNGGAATTAACCATGGGGGGTTCcatcatcatcatcatcatcatSGTATGGCTAGCATGACT	121		
Query 120	GGTGGACAGCAAATGGGTCGGGATCTGTACGACGATGACGATAAGGATCGATGGGGATCC	179		
Sbjct 122	GGTGGACAGCAAATGGGTCGGGATCTGTACGACGATGACGATAAGGATCGATGGGGATCC	181		
Query 180	GAGCTCGAATCAGTAACGGATTCATCATCGGTTTCGGGCTTCGCCGCCGCCAACTG	237		
Sbjct 182	GAGCTCGAATCAGTAACGGATTCATCATCGGTTTCGGGCTTCGCCGCCGCCAACTG	241		
Query 240	GTGAAAAATATTCGCAAACAGGACGCCACTATTCCATTAACCCCTGATTGCCGCCGACAGC	299		
Sbjct 242	GTGAAAAATATTCGCAAACAGGACGCCACTATTCCATTAACCCCTGATTGCCGCCGACAGC	301		
Query 300	ATGGATGAGTACAACAAACCTGACCTCAGCCATGTTATCAGTCAGGGGCAACGTGCCGAT	359		
Sbjct 302	ATGGATGAGTACAACAAACCTGACCTCAGCCATGTTATCAGTCAGGGGCAACGTGCCGAT	361		
Query 360	GACCTTACCCGCCAGACGGCGGGTGAATTTGCCGAGCACTTTAATCTGCACCTGTTTCCA	419		
Sbjct 362	GACCTTACCCGCCAGACGGCGGGTGAATTTGCCGAGCGCTTTAATCTGCACCTGTTTCCA	421		
Query 420	CAAACCTGGGTGACGGATATCGATGCCGAAGCCCGTGTGGTGAAGGCCAGAATAATCAG	479		
Sbjct 422	CAAACCTGGGTGACGGATATCGATGCCGAAGCCCGTGTGGTGAAGGCCAGAATAATCAG	481		
Query 480	TGGCAATACGACAAGCTAGTACTGGCAACCGGTGCCAGTGCCTTTGTCCCGCCTGTGCCT	539		
Sbjct 482	TGGCAATACGACAAGCTAGTACTGGCAACCGGTGCCAGTGCCTTTGTCCCGCCTGTGCCT	541		
Query 540	GGCGTGAAGTTAATGCTGACGTTAAATAGTCAGCAAGAGTATCGCGCCTGTGAAACGCAA	599		
Sbjct 542	GGCGTGAAGTTAATGCTGACGTTAAATAGTCAGCAAGAGTATCGCGCCTGTGAAACGCAA	601		
Query 600	CTGCCGGATGCCCGACGCGTGTGATTGTTGGCGGTGGTTTGATTGGTAGCGAACTGGCG	659		
Sbjct 602	CTGCCGGATGCCCGACGCGTGTGATTGTTGGCGGTGGTTTGATTGGTAGCGAACTGGCG	661		
Query 660	ATGGATTTTTGTCGTGCAGGCAAAGCGGTACGCTAATCGACAACCGCTGCCAGTATCTG	719		
Sbjct 662	ATGGATTTTTGTCGTGCAGGCAAAGCGGTACGCTAATCGACAACCGCTGCCAGTATCTG	721		
Query 720	GCGTCGTTAATGCCACCGGAAGTAAGCAGCCGCTTGACAGCATCGGTTGACGGAGATGGGC	779		
Sbjct 722	GCGTCGTTAATGCCACCGGAAGTAAGCAGCCGCTTGACAGCATCGGTTGACGGAGATGGGC	781		
Query 780	GTTTCTCTGCTGTTGAAATCTCAGTTACAGGGGCTGGAAAAACCGGATTCTGGCATTTCAG	839		
Sbjct 782	GTTTCTCTGCTGTTGAAATCTCAGTTACAGGGGCTGGAAAAACCGGATTCTGGCATTTCAG	841		
Query 840	GCAACGCTGGACCGCCAGCGCAATATCGAAGTGGATGCGGTAATTCGCGCCACCGGACTG	899		
Sbjct 842	GCAACGCTGGACCGCCAGCGCAATATCGAAGTGGATGCGGTAATTCGCGCCACCGGACTG	901		
Query 900	CGCCGGAAACCGCCCTGGCACGACGCGCCGGGCTGACGATTAATTCGCGCGGTTTGGCTC	959		
Sbjct 902	CGCCGGAAACCGCCCTGGCACGACGCGCCGGGCTGACGATTAATTCGCGCGGTTTGGCTC	961		
Query 960	GATAGTTATCTGCAAACAGTAATACCGATATTTACGCGCTGGGCGATTGCGCGGAAATT	1019		
Sbjct 962	GATAGTTATCTGCAAACAGTAATACCGATATTTACGCGCTGGGCGATTGCGCGGAAATT	1021		
Query 1020	AACGSTCAGGTATTGCCGTTCCCTCCAGCCGATTCAACTTAGCGCGATGGTGTGGCAAAA	1079		
Sbjct 1022	AACGSTCAGGTATTGCCGTTCCCTCCAGCCGATTCAACTTAGCGCGATGGTGTGGCAAAA	1081		
Query 1080	AATCTTCTCGCAATAACACGCGCCTGAAACTCCCGCGATGCTGGTGAATAACAAACG	1139		
Sbjct 1082	AATCTTCTCGCAATAACACGCGCCTGAAACTCCCGCGATGCTGGTGAATAACAAACG	1141		
Query 1140	CCGGAATTACCGCTGCATCTGGCAGGCGAAACCCAGCGTCAGGATTTACGCTGGCAAAAT	1199		
Sbjct 1142	CCGGAATTACCGCTGCATCTGGCAGGCGAAACCCAGCGTCAGGATTTACGCTGGCAAAAT	1201		
Query 1200	AATACCGAACGCCAGGGAATGGTGGCGCGCGCGGCTTGACGATGCTGACCGCTTCGCGCC	1259		
Sbjct 1202	AATACCGAACGCCAGGGAATGGTGGCGCGCGCGGCTTGACGATGCTGACCGCTTCGCGCC	1261		
Query 1260	TTTGTGGTCAGTGAAGGATCGGATGAAAGAGGATTTGGATTGTTGAAAACATTGCCGATG	1319		
Sbjct 1262	TTTGTGGTCAGTGAAGGATCGGATGAAAGAGGATTTGGATTGTTGAAAACATTGCCGATG	1321		
Query 1320	TAGSTGGGCTACTGTGCCTAAAA 1342			
Sbjct 1322	TAGSTGGGCTACTGTGCCTAAAA 1344			

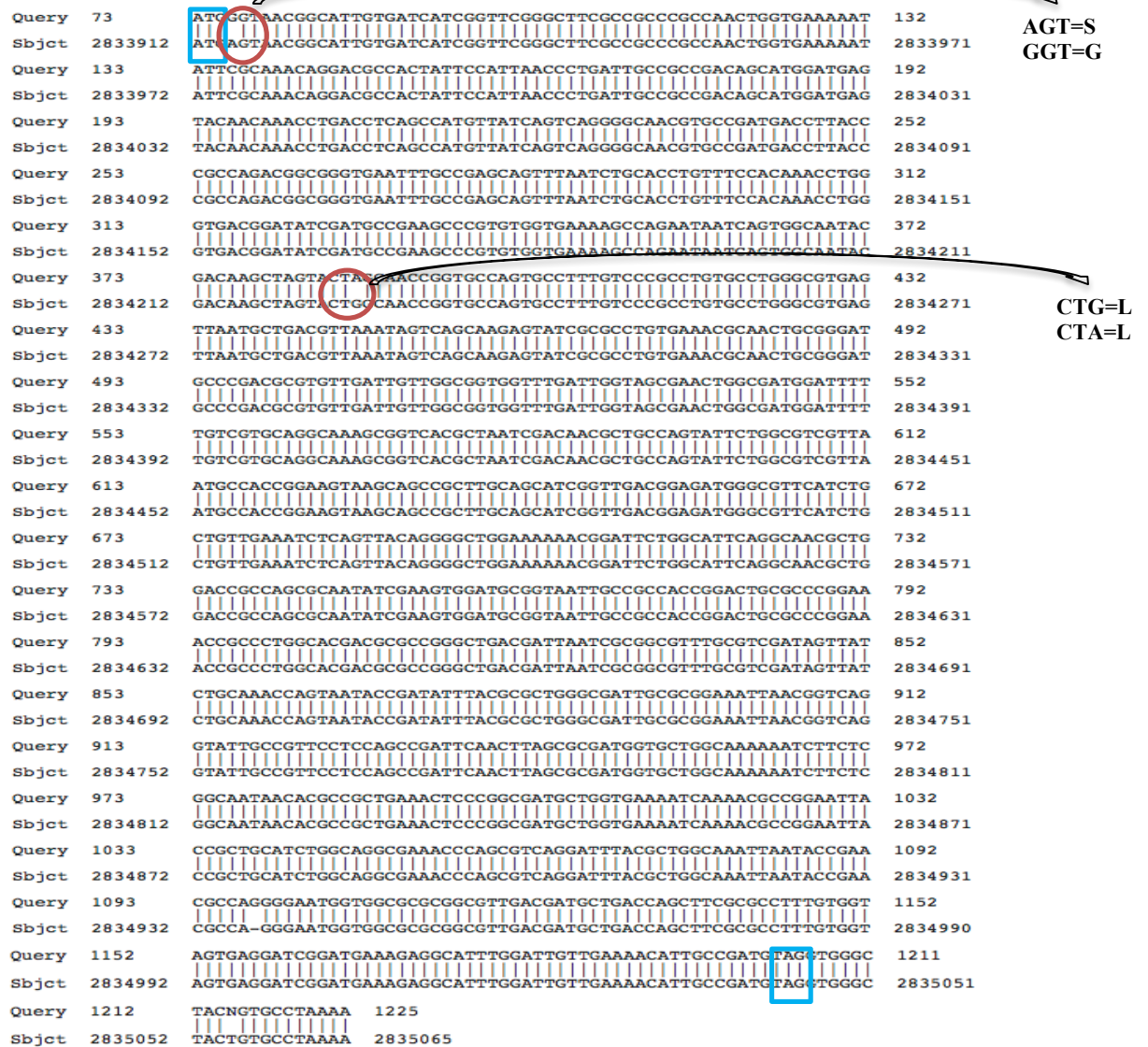
ATC=I
ATT=I

CAG=Q
CGG=R

ATT=I
AGG=R

Query= *E. coli* genome Subject= construct 4 sequence
I=Isoleucine, R=Arginine, Q= Glutamine

C



S=Serine, G= Glycine, L= Leucine
 Query= construct 2 sequence Subject= *E. coli* genome

Figure 4.7 A, B and C: DNA sequence alignment of pBAD/*norW* constructs with and without His-tag with *E. coli* MG1655 *norW* by using NCBI blast. A- Sequence alignment of construct 9 entire map and *E. coli* MG1655 *norW*. B- pBAD construct 4 aligned *E. coli* MG1655 *norW* gene. C- Sequence alignment of construct 2 and *E. coli* MG1655 *norW*. Blue box= start and stop codon, red box= 6 Histidine-tag, orange boxes= mutations

4.6.2 pET21a/ *norW* constructs sequence results

The sequencing failed for all the constructs that were obtained from pET21a, because it had either many uncharacterized nucleotides (N) in the sequence and/ or multiple mutations were found within the gene. These constructs were not used further to express NorW.

4.7 Site directed mutagenesis

Constructs 4 and 2 were chosen to express His-tagged and untagged NorW respectively all the mutations in those constructs were repaired by using the Quikchange II site directed mutagenesis kit (See Chapter 3, section 3.2.12). The repaired sequence revealed that the constructs were identical to *norW* of *E. coli* MG1655.

4.8 NorW expression

For pBAD constructs 7 and 9, NorW protein was expressed, using Top10 competent cells (See Chapter 3, section 3.2.13). Three parameters were changed in this experiment (arabinose concentration, temperature and duration of incubation). Concentrations of 2 and 0.02% (w/v) arabinose were used and the cultures were incubated at 25 and 37 °C, for 1, 2, 3 h and overnight.

The results of loading 1 ml sample taken during expression on SDS-PAGE showed that construct 9 express the protein at both 25 °C (Figure 4.8 A) and 37 °C (Figure 4.8 B) and in both arabinose concentrations (2 and 0.02% w/v). The best expression was at 37 °C in 2% (w/v) arabinose for 3 h. The band was seen between 55.4 kDa and 36.5 kDa according to the protein marker (Mark12).

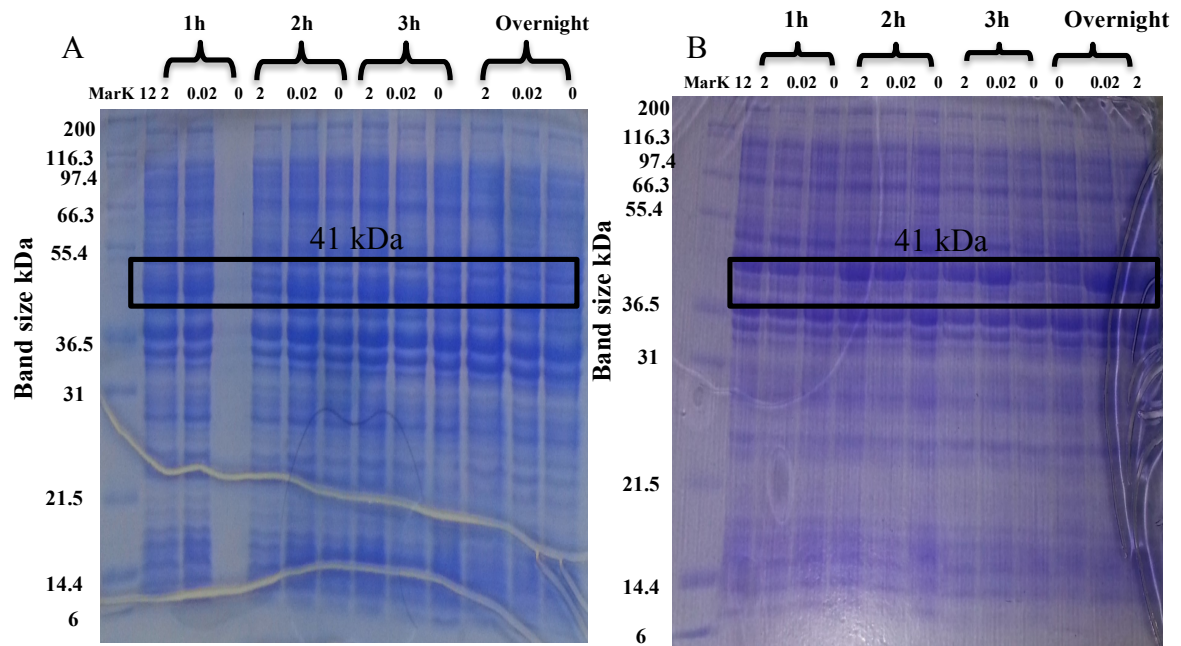


Figure 4.8: SDS-PAGE of His-tagged NorW expression from construct 9.

Panel A- the gel shows the results of loading samples of construct 9 expressed at 25 °C for 1, 2, 3 h and overnight, it shows that NorW was expressed in 0.02 and 2% (w/v) arabinose and the best expression was at 3 h and overnight.

Panel B : The SDS-PAGE of His-tagged NorW expression, shows the results of loading samples of construct 9 expressed at 37 °C for 1, 2, 3 h and overnight, it shows that NorW has been expressed in 0.02 and 2% (w/v) arabinose but the best expression was in 2% and the best incubation time was at 3 h.

The same results were gained with construct 4 (Figure 4.9 A&B).

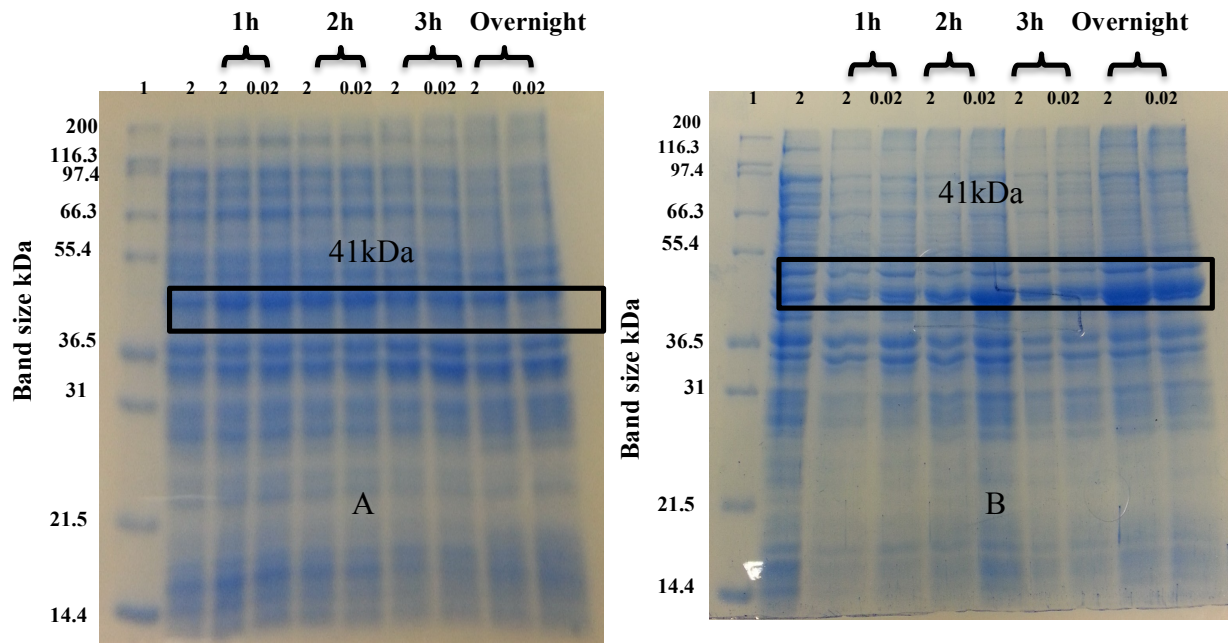


Figure 4.9: SDS-PAGE of His-tagged NorW expression in construct 4.

Panel A-the gel shows the results of construct 4 expression mutant at 25 °C for 1, 2, 3 h and overnight, with 2 and 0.02% (w/v) arabinose as inducer. It shows that there was no differences in the expression at 1, 2, 3 h, in 2 and 0.02% (w/v) arabinose, whereas it was decreased in overnight. Lane 1 is the protein marker (Mark12), lane 2 is the preinduction sample.

Panel B- The gel shows the results construct 4 mutant expression at 25 °C for 1, 2, 3 h and overnight, with 2 and 0.02% (w/v) arabinose as inducer.

After fixing the two mutations in pBAD construct 4 was expressed at only 37 °C for 3 h and overnight using 2% (w/v) arabinose to induce protein production (Figure 4.10).

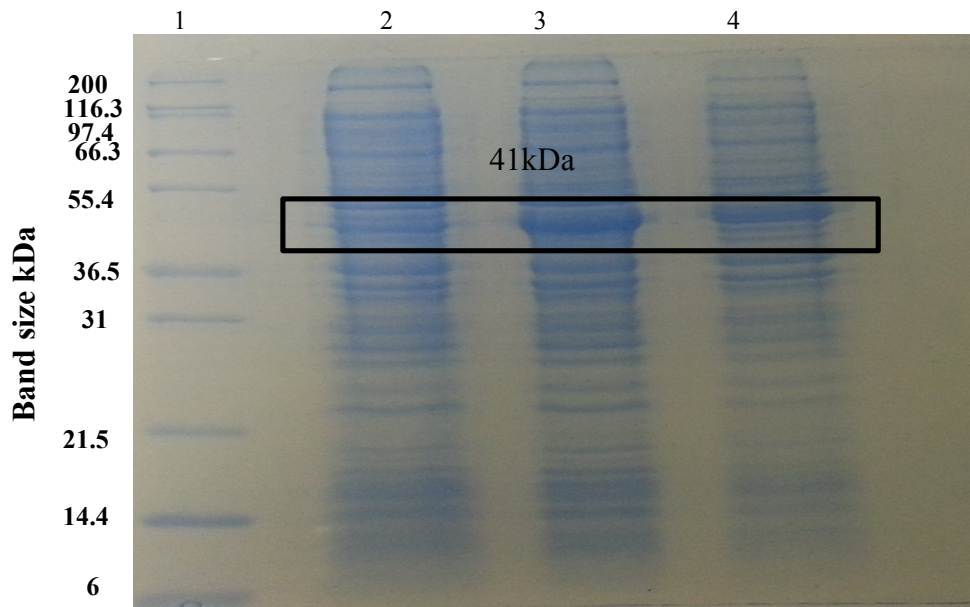


Figure 4.10: SDS-PAGE of His-tagged NorW expression in construct 4. The gel shows the results of construct 4 expression at 37 °C for 3 h and overnight, with 2% (w/v) arabinose as inducer, a strong band around 41 kDa indicates NorW expression. 1= Mark 12, 2= pre-induction, 3= 3 h induction, 4= overnight induction.

Construct 2 (non-His tagged NorW) was expressed also at 37 °C and 25 °C (Figure 4.11 A&B) by using 2 and 0.02% (w/v) arabinose at 200 rpm shaking. The SDS-PAGE of 1 ml expression samples showed that NorW was expressed well at both temperatures and both arabinose concentrations; a strong band was seen between 55 kDa and 36 kDa according to Mark 12 protein ladder.

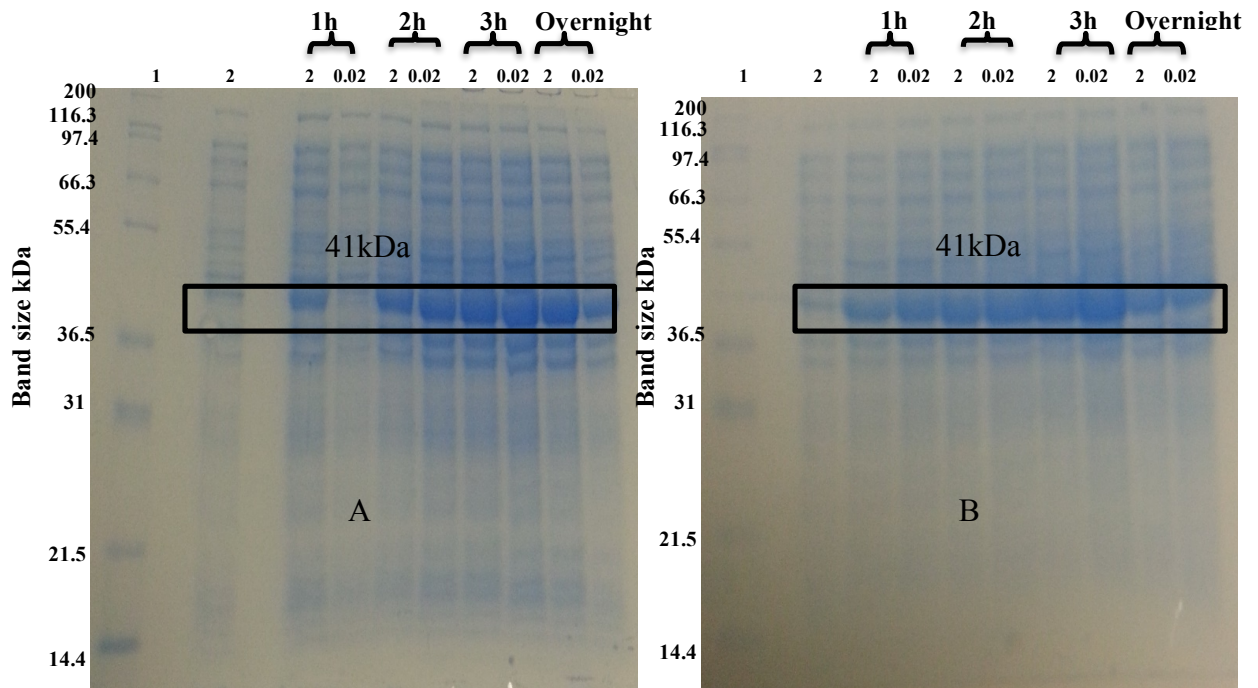


Figure 4.11 : SDS-PAGE of untagged NorW (construct 2) expression.

Panel A-shows the results of loading samples of construct 2 expressed at 25 °C for 1, 2, 3 h and overnight, it shows that NorW has been expressed in 0.02 and 2% (w/v) arabinose but the best expression was in 2% and the best incubation time was at 3 h.

Panel B- shows the results of loading samples of construct 2 expressed at 37 °C for 1, 2, 3 h and overnight, it shows that NorW has been expressed in 0.02 and 2% (w/v) arabinose but the best expression was in 2% and the best incubation time was at 3 h.

4.9 Protein solubility

The solubility test results showed that the protein was found in the soluble and non-soluble parts equally, in construct 4 (Figure 4.12 A), and approximately 40% soluble protein was obtained from construct 2 (Figure 4.12 B).

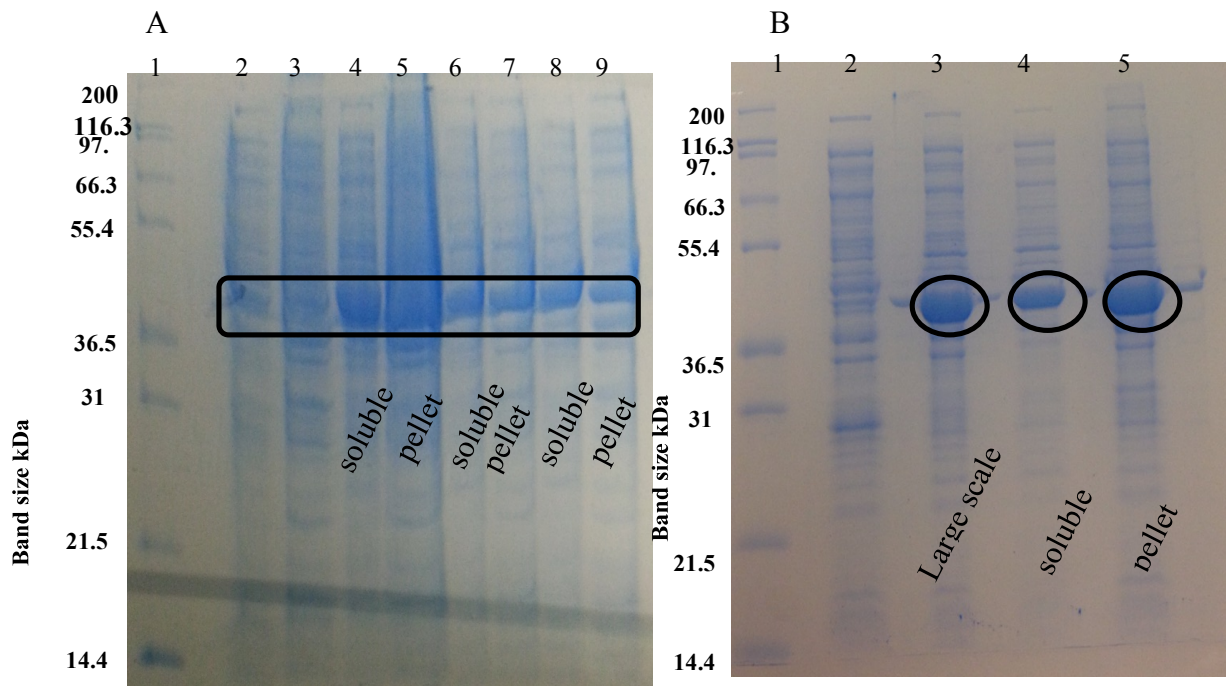


Figure 4.12: SDS-PAGE of His- tagged and untagged NorW solubility.

Panel A- shows the results of loading the samples of soluble and non soluble fractions of construct 4 expression at 37 °C, 1=Mark 12, 2 & 3 = pre-induction, 4 & 5= 1 h induction, 6 & 7= 3 h induction, and 8 & 9= overnight induction. The bands on gel showed that NorW was present in the soluble fraction at around 50%.

Panel B: shows the results of loading samples of construct 2 large scale expression at 37 °C for 3 h, and the soluble and non soluble fractions, it shows that NorW was present in the soluble fraction at around 40%. 1=Mark 12, 2 = pre-induction, 3 = large-scale protein production, 4 & 5 = post-induction for 3 h.

4.10 Large scale expression

Large scale expression results showed that the protein was well expressed in the large scale (Chapter 3, section 3.2.17). A band between 55 kDa and 36 kDa appeared, and it was bigger in the post induction than the pre-induction (Figure 4.13).

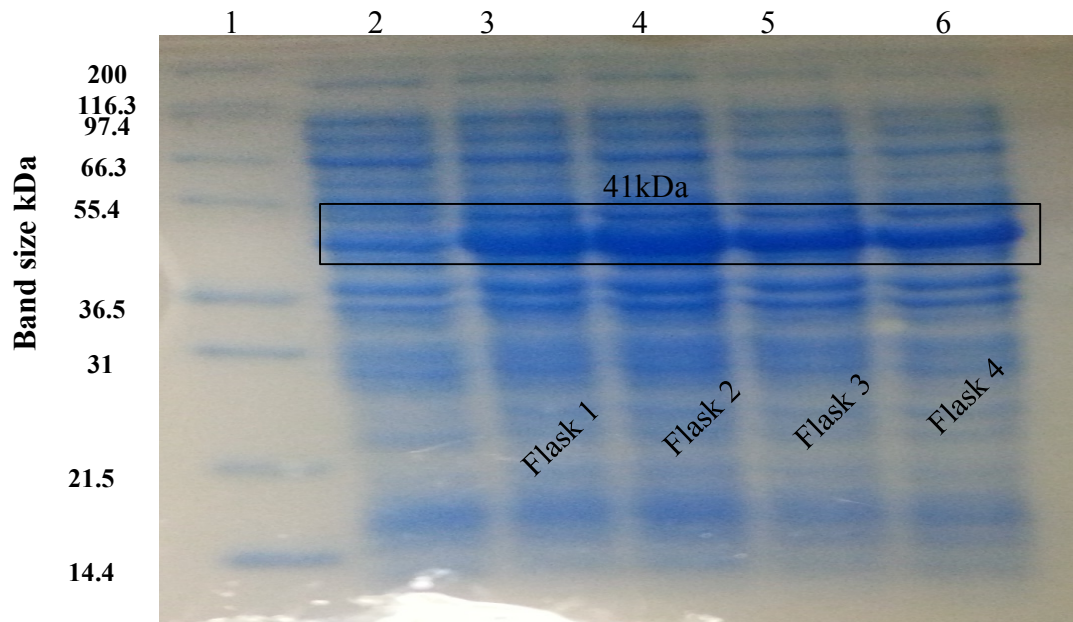


Figure 4.13: SDS-PAGE of a His-tagged NorW large scale culture expression. The gel shows the results of loading the samples from the construct 4 expression at 37 °C for 3 h with 2% (w/v) arabinose. The bands showed that NorW was over expressed in the large scale culture. 1=Mark 12, 2 = pre-induction, 3, 4, 5 &6 = post-induction for 3 h.

4.11 Protein purification

The expressed protein was purified by using the batch method (small scale purification), for further information see Chapter 3, section 3.2.16. The SDS-PAGE results confirmed that NorW eluted in buffer containing 0.5 M imidazole (Figure 4.14).

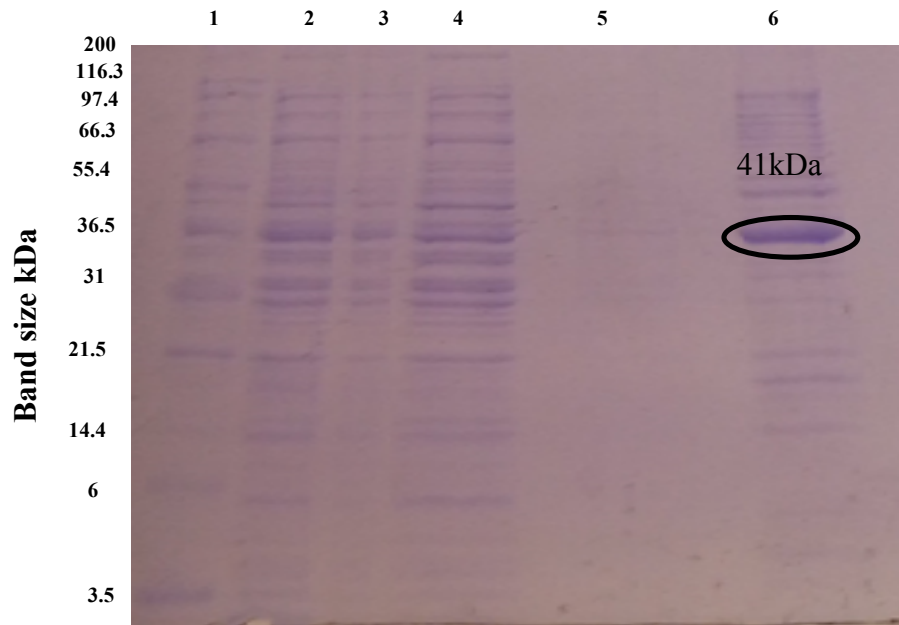


Figure 4.14: SDS-PAGE of Batch purification (Ni-NTA purification). The figure shows the fractions of His-tagged NorW, which had been expressed at 37 °C, overnight with 2% (w/v) arabinose, and eluted in buffer containing 0.5 M imidazole. 1= Mark 12, 2= cell-free extract (CFE), 3= unbound material, 4= wash 1, 5= wash 2, 6= elution.

After confirming that the tag could be used, a chromatography method was used to purify the protein via Ni-NTA (Figure 4.15 A& B), and gel filtration (Figure 4.16 A& B) columns.

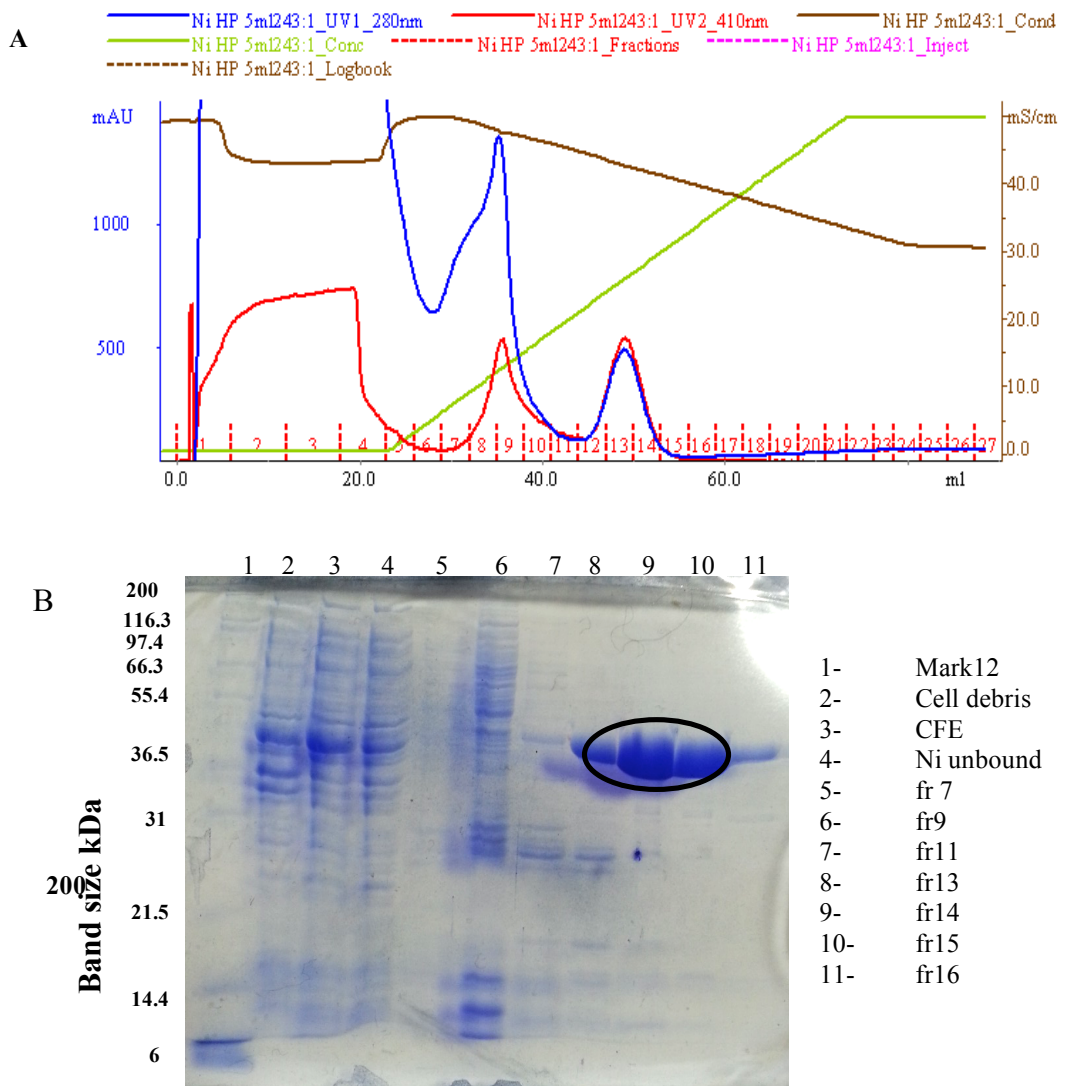


Figure 4.15: His-tagged NorW purification by Ni-NTA column. Panel A- Ni-NTA column purification chromatogram, shows a peak between fractions 12-14, which corresponded to NorW when analysed on SDS-PAGE. Panel B- The SDS-PAGE of Ni-NTA column purification, shows that fractions 12 and 16 have some NorW but fractions 14 and 15 have the majority of NorW and the purity was around 90%.

fr= fraction, CFE= cell-free extract

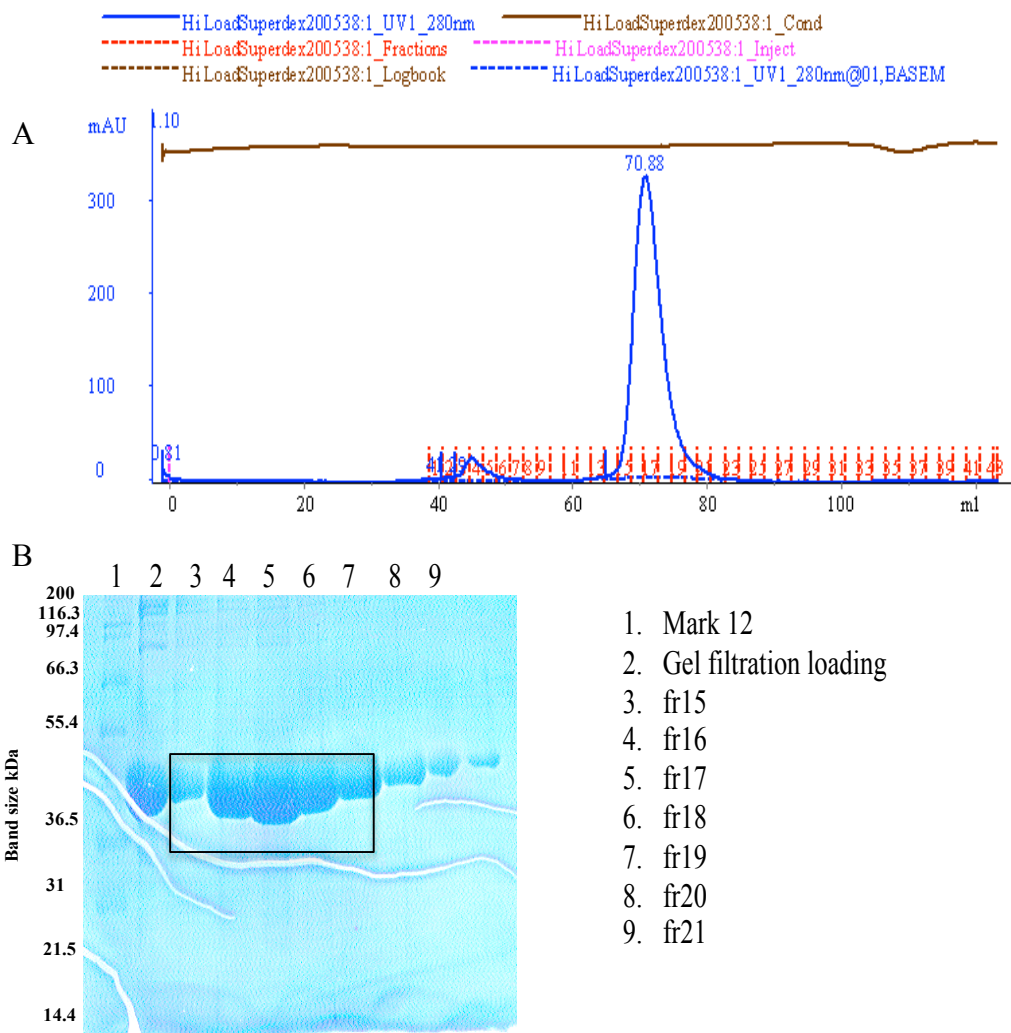


Figure 4.16: NorW purification by gel filtration. Panel A- The chromatogram of the purification, shows that the peak of NorW was eluted between fractions 15-19 at 71 ml, which was used to calculate the solution size of the protein and suggested that NorW is a dimer.

Panel B- The SDS-PAGE of the purification, shows that the fractions from the gel filtration purification of NorW have a band of the relevant size and the purity of the band is around 90%. It shows that fractions 16-18 have the majority of the protein.

The final product was a yellow protein solution, which was then concentrated to between 8.5 – 10 mg/ml (Figure 4.17).

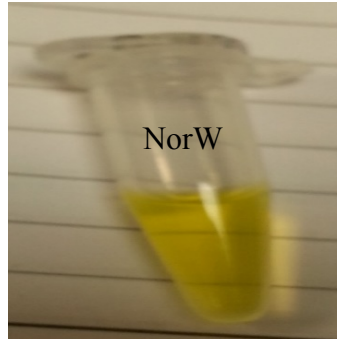


Figure 4.17: NorW purified protein. A yellow colored protein solution implied that the cofactor was bound.

A chromatography approach using ion exchange (anion DEAE), and gel filtration columns was used to purify the untagged NorW.

Two wavelengths were used, 280 nm to check the protein absorption, and 460 nm to track the flavin absorbance (Figure 4.18 A&B). The peaks across the DEAE and gel filtration chromatograms were analyzed on SDS-PAGE (Figure 4.19). The SDS-PAGE results showed that the DEAE and Superdex column combination was unable to purify the untagged protein. Resource Q columns were used for further purification of untagged NorW. The gel filtration showed that the NorW molecular weight is approximately 45 kDa, which suggests that NorW might be a dimer or a compact trimer.

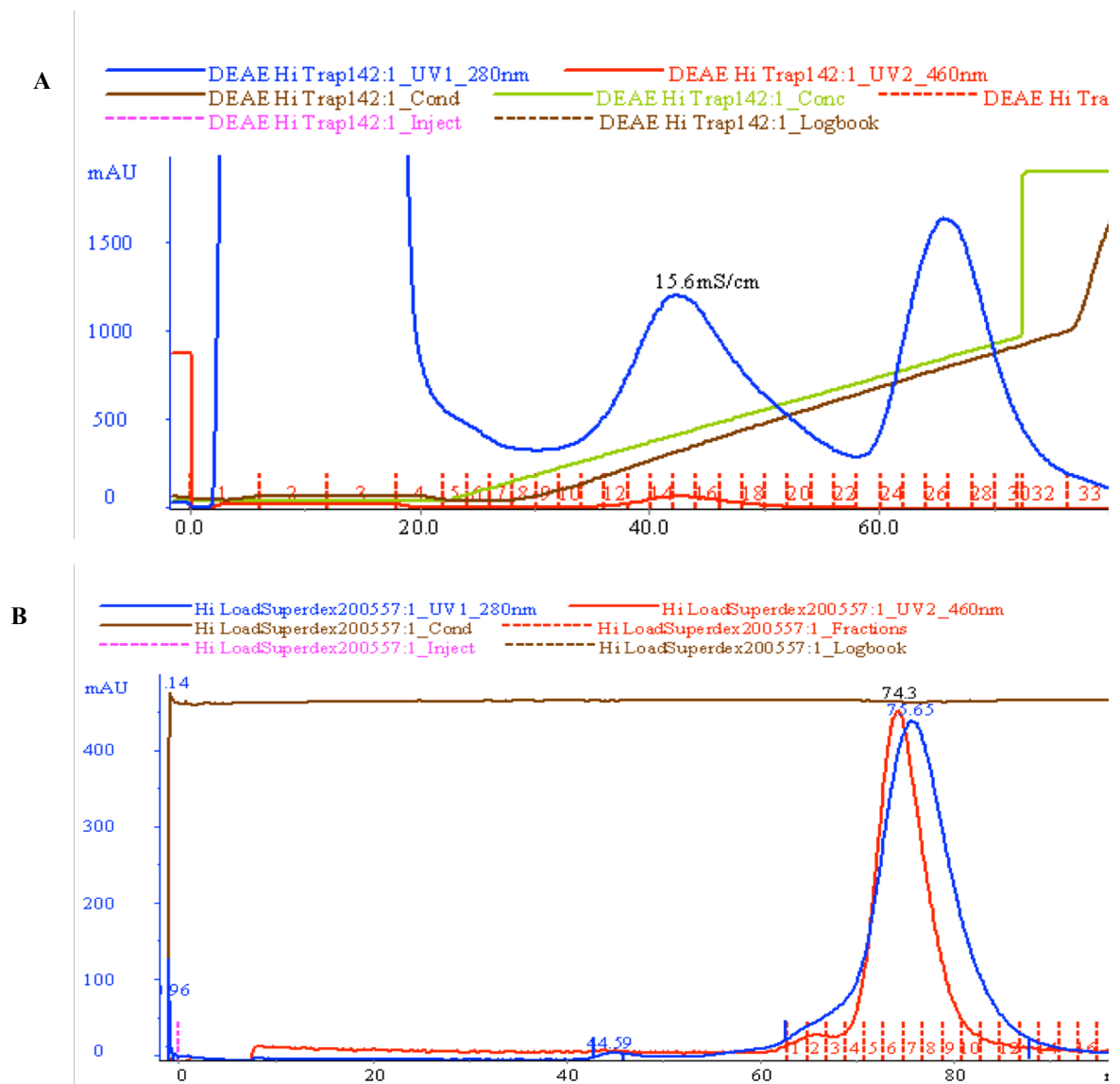


Figure 4.18 Untagged NorW purification. Panel A- The chromatogram of NorW purification using a DEAE column, shows that the untagged NorW was eluted by increasing NaCl concentration from 0-40%, the blue line is the absorption at 280 nm (protein), the red line is the absorption at 460 nm (flavin).

Panel B- The gel filtration purification chromatogram, shows that untagged NorW was eluted at 76 ml of elution buffer, corresponding to a molecular size of approx. 45 kDa.

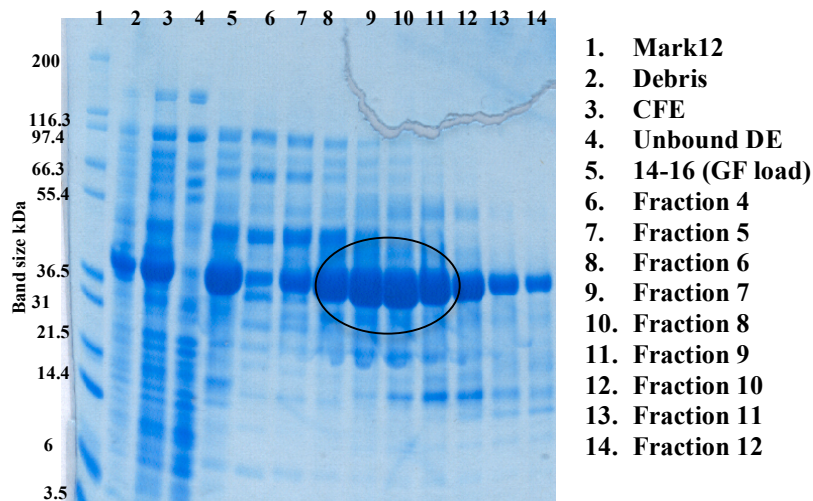


Figure 4.19 SDS-PAGE of DEAE and GF purification of untagged NorW. The figure shows that fractions 14-16 from DEAE column purification were combined and loaded on GF column (GF load) have the majority of NorW. After GF purification fractions 6-9 contained the majority of NorW, but the purity was less than 80%, so these fractions were combined and loaded on a Resource Q column.

Peaks across the chromatogram of Resource Q purification (Figure 4.20 A) were analyzed on SDS-PAGE (Figure 4.20 B). The SDS-PAGE results showed that fractions 15 and 16 contain the largest amount of the untagged NorW, and the ion-exchange chromatography was purified non-tagged NorW at 85%.

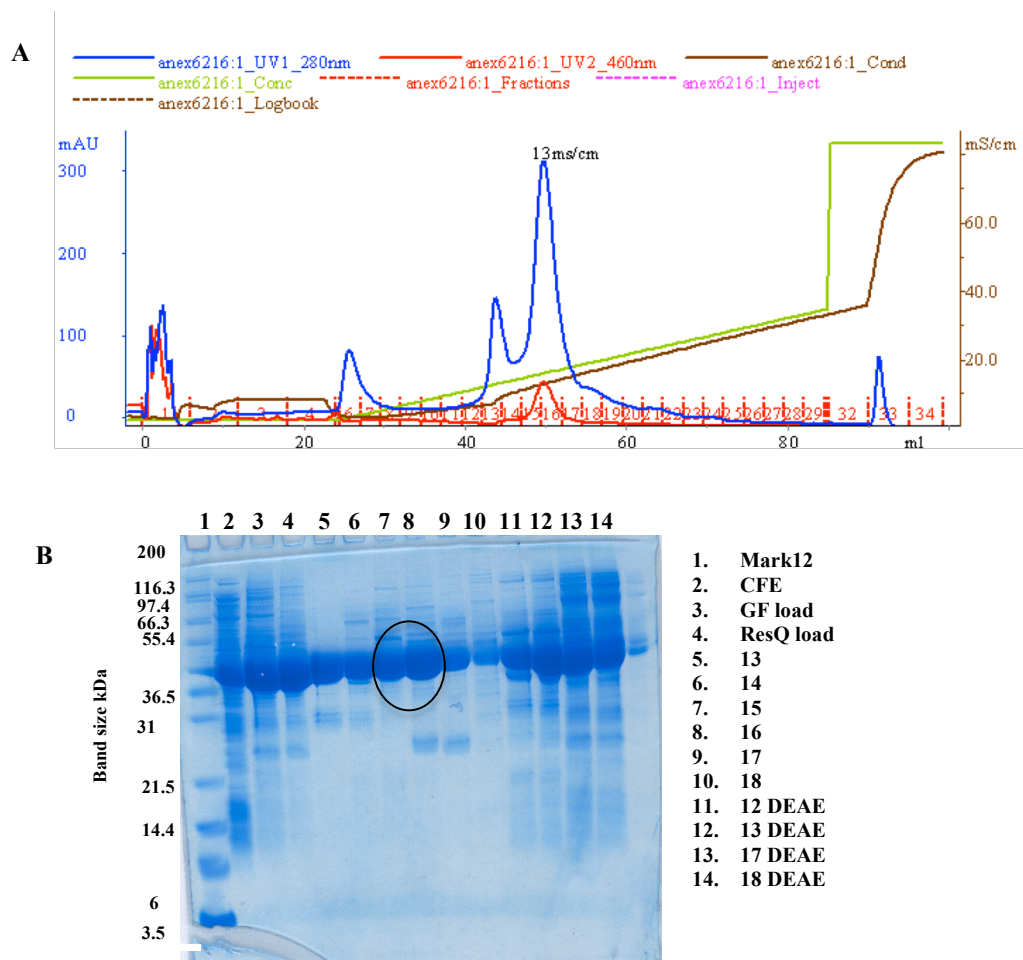


Figure 4.20 Purification of untagged NorW by Resource Q column. Panel A- The chromatogram shows that NorW was eluted by using a gradient of NaCl (0-40%) and two peaks were seen, both of which were analyzed on SDS-PAGE. Panel B- The SDS-PAGE analysis of NorW Resource Q purification, shows that fractions 15 and 16 have the majority of NorW with around 85% purity.

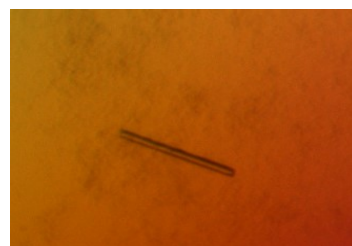
The gel filtration method was used for further purification and to confirm the protein size. It suggested that NorW is a dimer when the molecular size was calculated by using the standard curve of a Superdex 200 column. The results showed that the His-tagged protein was prepared to approx. 90% purity using Ni-NTA and gel filtration columns, and the untagged protein was prepared to around 85% purity with ion exchange and gel filtration columns.

4.12 Crystallization results

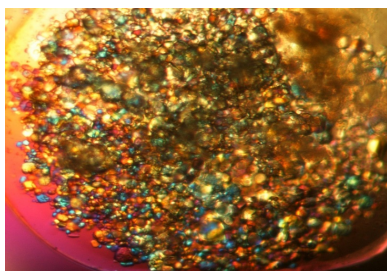
NorW was screened using different commercial crystallization screens (Chapter 3, section 3.2.21). However, only a small number of crystals were obtained (Figure 4.21). Subsequent testing by X-ray diffraction at the Diamond Light Source (DLS) showed that all the crystals tested were salt. Because heavy atom compounds have been seen often to bind cysteine residues and can sometimes result in more stable or better conformations for crystallization, mercury chloride and potassium hexachloro platinate was added to NorW solution. No crystals were obtained mercury chloride and hexachloro platinate sodium dithionite, a NorV and NADH were used in combination with NorW.



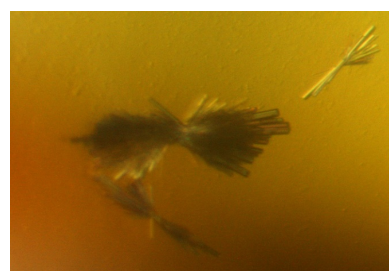
Crystals that were seen from PACT suite (0.2 M CaCl_2 , 0.1 Tris-HCl pH 8 and 20 % (w/v) PEG6000)



Crystal that grew in MPD suite (0.2 M Ammonium Sulfate and 40 % (w/v) MPD)



Crystals that grew in Ammonium sulfate suite (0.1 M citric acid pH 5 and 2.4 M Ammonium sulfate)



Crystals that appeared produced in the Classic suite (0.2 M Magnesium format)

PEG=Polyethylene glycol, MPD=2-methyl-2,4-pentandiol

Figure 4.21 Crystals observed during crystallization screening of NorW. After testing for X-ray diffraction, all of the crystals proved to be inorganic salts.

4.13 Functional studies

A series of experiments using NorV (non His-tagged), NorW (His-tagged) proteins or a combination of the two was carried out, to test the ability of NorV and/or NorW to reduce NO *in vitro*. Further *in vivo* assays have been done to test the *in vitro* finding that NorW can reduce NO without NorV.

4.13.1 NO consumption

The functional studies started with testing the NO consumption rate. There are many papers that report NO detoxification by NorV, which is the reductase enzyme for NO (Gardner et al., 2002; Gomes et al., 2002b; Helmick and Gardner, 2002). In the current study, it has been found that NorW can consume NO alone without NorV (*in vitro*). The experiments were carried under different oxygen levels, and the same results were found.

4.13.1.1 NO (*in vitro*) consumption aerobic assay

A- Assay in the presence of NorV/NorW complex

PROLI-NONOate was used as a source of NO, and an NO electrode was used to measure its depletion. NADH was added as an electron donor. The electrode was calibrated as advised by the manufacturer (Chapter 3 section 3.2.26.1.1). The control for the assay without the enzyme showed a peak in the voltage trace when NO was released from PROLI-NONOate at around 150 s, which had fallen to background levels in about 800 s (Figure 4.22).

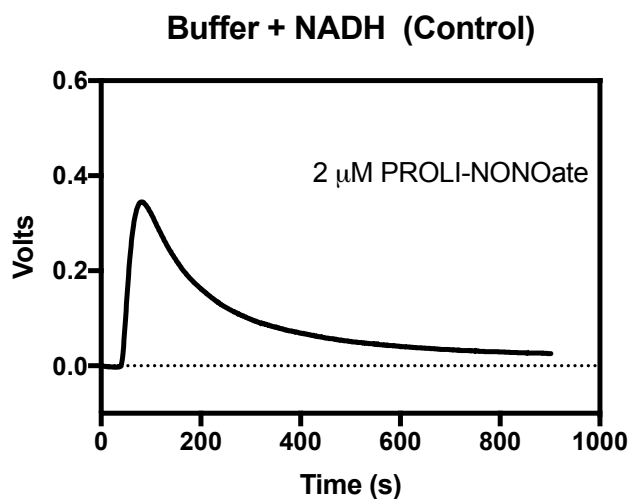


Figure 4.22: *In vitro* NO consumption (Control). The control contains 2 ml of (0.5 M NaCl, 50 mM Tris-HCl pH 8.0) buffer, (250 μ M) NADH, 2 μ M of PROLI-NONOate). A peak in the voltage trace appeared when NO was released then decreased as NO dispersed naturally to background levels, n=1.

When 1 μ M NorW and 2 μ M NorV were added to the assay conditions, no peak was seen. Repeat injection of 2 μ M PROLI-NONOate did not result in an observable peak. An increase was made in the concentration of PROLI-NONOate added (increasing to 4 μ M), and a peak was then observed (Figure 4.23 A). Thus, NorVW had a dramatic effect on NO levels compared with the control, as expected, even when 5 (Figures 4.23 B) or 7 injections (Figure 4.23 C) of NONOate (2 μ M) were added.

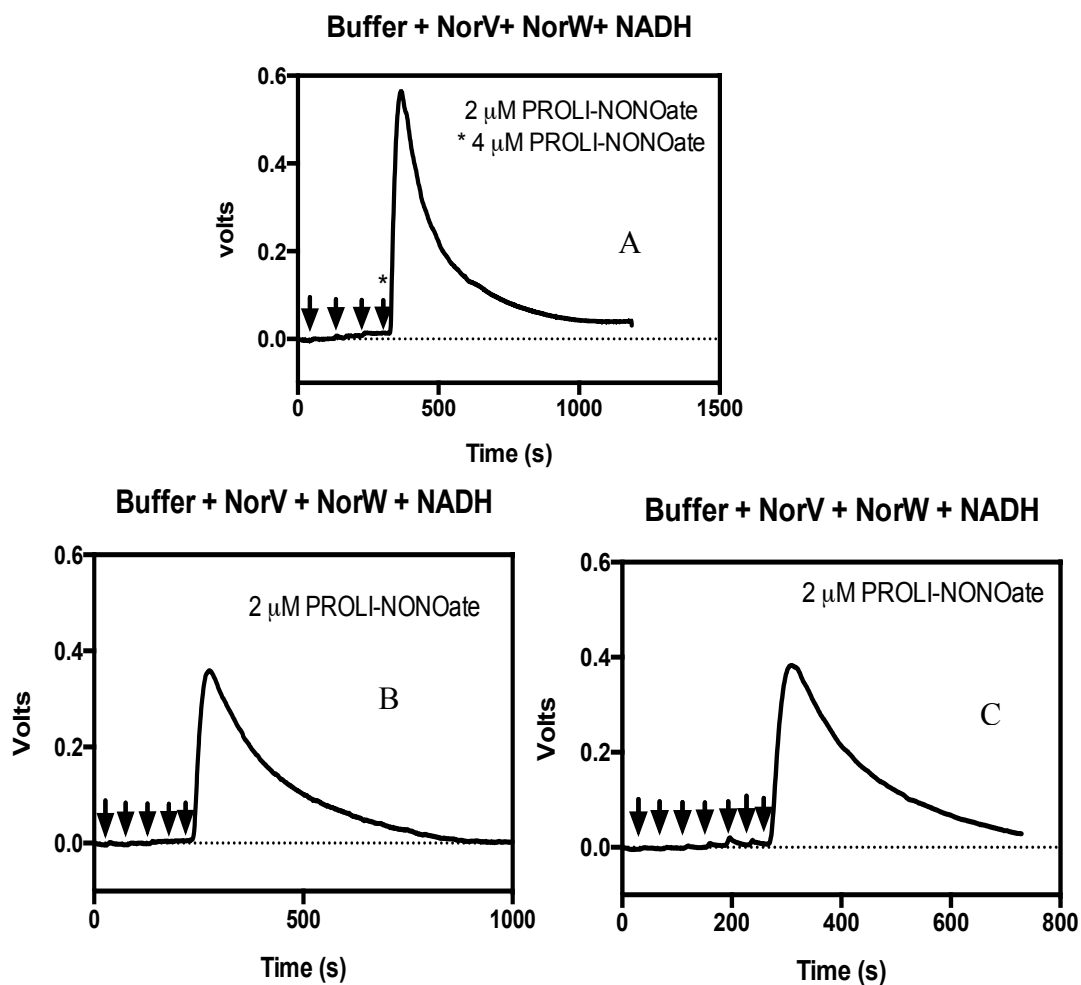


Figure 4.23. NO (*in vitro*) consumption using NorVW complex.

Panel A- In the presence of 1 μM of NorW and 2 μM of NorV, there was no peak seen when 2 μM PROLI-NONOate was repeatedly added. A peak was seen after adding 4 μM PROLI-NONOate.

Panel B- Shows the subsequent addition of 2 μM of PROLI-NONOate, 5 additions were added and no peak was seen, only a very tiny peak appeared around 200 s.

Panel C- Shows a very small peak after 5 additions of PROLI-NONOate (2 μM) at 200 s, then after around 280 s a big peak was appeared, n=1.

B- Assay in the presence of NorV alone

When NorV was added separately to the assay conditions, a peak similar to that seen with the control was noticed when 2 μM NorV was added without NorW (Figure 4.24), which means that NorV was unable to consume NO without NorW.

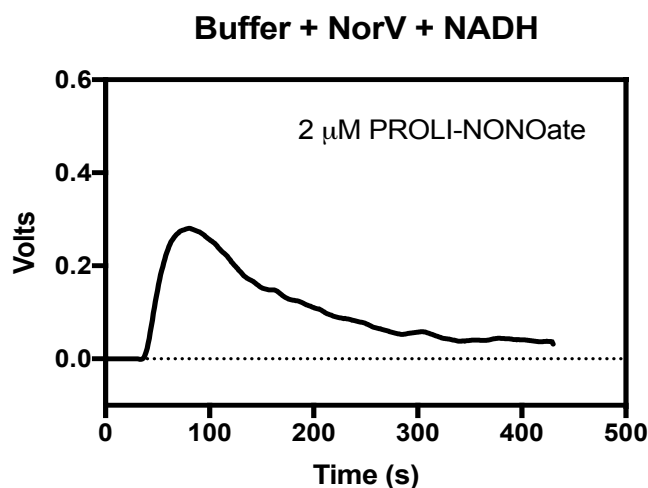


Figure 4.24: NO consumption by 2 μM NorV alone. The figure shows that a peak was seen around 90 s after 2 μM of PROLI-NONOate was added. It took more time to decline compared with the control (Figure 4.22), $n=1$.

C- Assay in the presence of NorW alone

Interestingly, when 1 μM NorW was added separately without NorV, very small peaks were noticed compared with the wide peak of the control (Figure 4.22). This suggested that NorW can consume NO directly without NorV, and the NO decomposition rate was high (Figure 4.25).

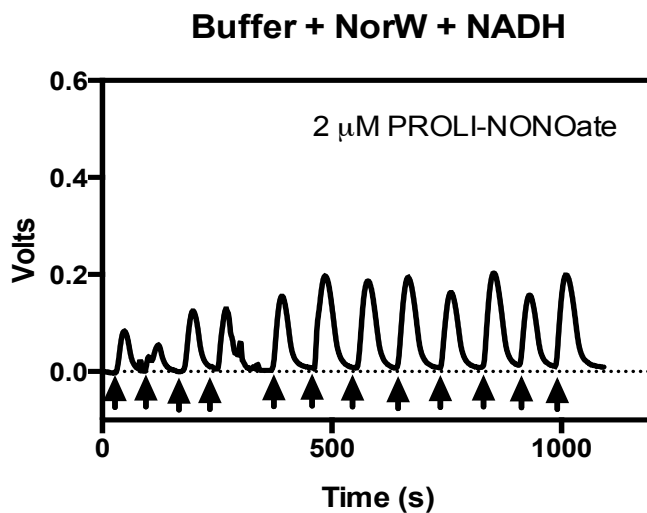


Figure 4.25: NO consumption by NorW alone. The figure shows that small peaks were seen only after 2 μM of PROLI-NONOate was added, and it declined immediately, which suggests that NorW was able to decompose NO without NorV, $n=1$.

To confirm this result, 17 additions of PROLI-NONOate were performed, and then another 1 μM NorW was added before a further 11 additions of NONOate were added. A peak was seen only when NONOate was added and it disappeared quickly on each occasion (Figure 4.26).

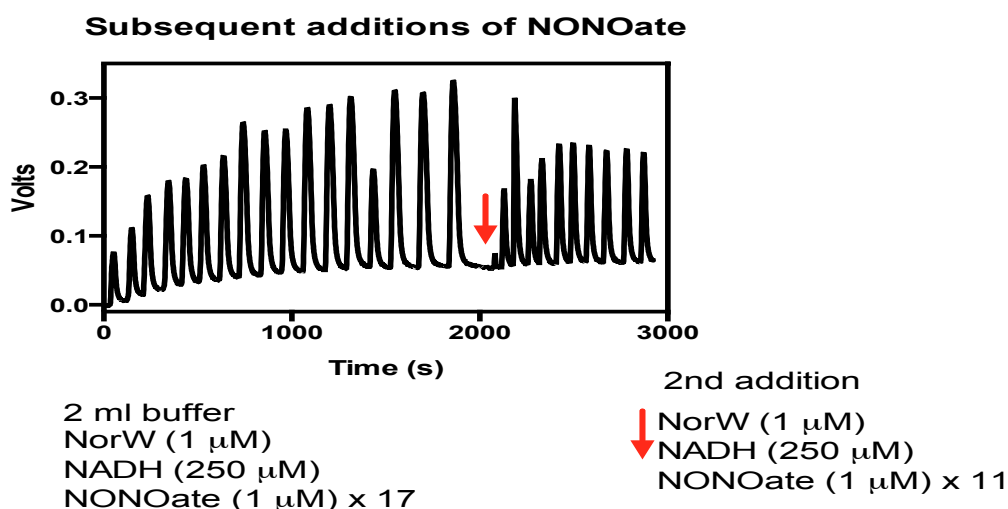


Figure 4.26: Addition of PROLI-NONOate to check NO consumption by NorW. The figure shows NorW was consuming PROLI-NONOate quickly, $n=1$.

Subsequently, the ability of NorW to consume NO with and without NADH was tested; the results showed that the consumption rate was accelerated when NADH was added with NorW, whereas the peak declined more slowly in the absence of any of the components

(NorW or NADH). These results suggest that NorW needs NADH to reduce NO (Figure 4.27 A&B).

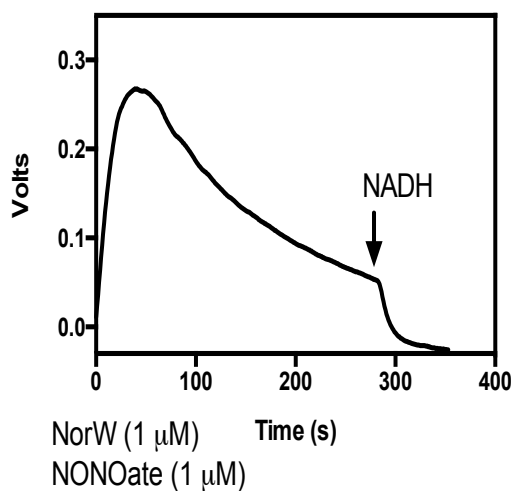


Figure 4.27 A: NO uptake by NorW without NADH. The figure shows that when NorW was added without NADH, the NO took a long time to consume, but when 250 μ M NADH was added the consumption went quickly, n=1.

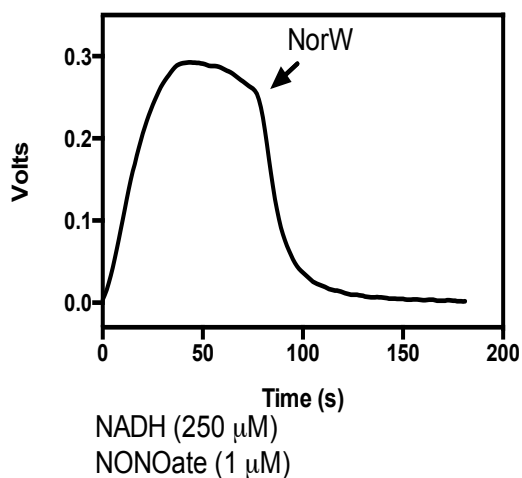


Figure 4.27 B: NO uptake by NADH without NorW. The figure shows that the NO peak was very wide when NADH was added without NorW. However, the peak declined immediately when NorW (1 μ M) was added, n=1.

Furthermore, NO depletion was tested by using different concentrations of NorW (50, 100, 200 and 300nM); it was found that the higher concentrations of NorW gave better consumption of NO (Figure 4.28).

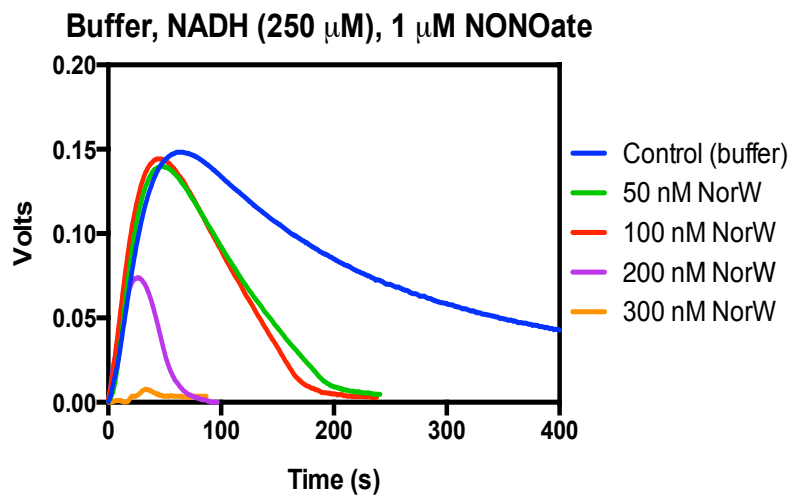


Figure 4.28: NO uptake by varying concentration of NorW. The figure shows that NorW concentration was directly proportional to NO consumption, when 50, 100, 200 and 300 nM of NorW was used. The figure shows that the time for NO consumption was reduced dramatically when NorW concentration was increased, $n=1$.

Finally, the effect of a high concentration of FAD alone was tested without NorW and no reduction could be observed (Figure 4.29). Thus, the whole protein plus cofactor were needed to reduce NO.

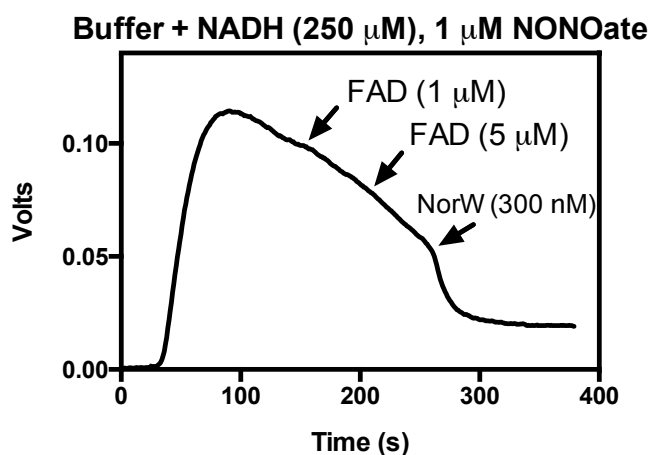


Figure 4.29: The effect of FAD on NO consumption. The figure shows that when high concentrations of FAD were added to the reaction, no NO consumption was observed, but after adding NorW, the NO peak started to decline quickly, $n=1$.

4.13.1.2 NO anaerobic consumption by NorW (*in vitro*) assay

A- Assay on the effect of O₂ level

It is well established that the NorVW system is expressed and is functional under anoxic conditions (Gardner et al., 2002). Therefore, in this experiment a glucose/ glucose oxidase / catalase system was used to deplete the O₂ from the environment. NO and O₂ electrodes were used together in this assay. An NO electrode was used to check the NO removal by NorW, and the O₂ electrode was used to check the O₂ level. The (O₂ and NO) electrodes were calibrated as described in Chapter 3, Section 3.2.26.1.1. The control reaction was checked first, and then a test reaction was performed. To the test reaction 8 μM PROLI-NONOate was added at various oxygen levels as recorded by the O₂ electrode; then 2 μM NorW was added. The PROLI-NONOate was added in aerobic conditions first of all (~70-75% of O₂), and then in microaerophilic conditions (~20-25% of O₂), and finally in anaerobic conditions (~5-0% of O₂), to compare the NO consumption by NorW in different O₂ levels.

The results showed that NorW was removing NO at high rate in the anaerobic conditions compared with the aerobic conditions, which suggests that NorW can consume NO in anaerobic conditions with no need for NorV (Figure 4.30 A&B). These results confirmed the earlier aerobic NO consumption results, which showed clearly that NO levels were affected by the presence of NorW alone.

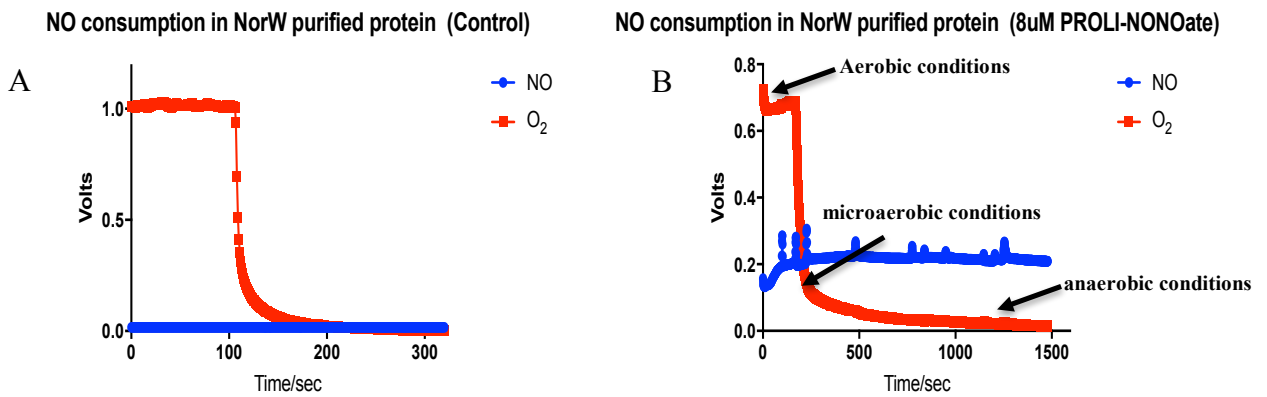


Figure 4.30: NO consumption in aerobic, microaerobic, and anaerobic conditions. Panel A shows the control reaction, The O₂ level declined to 0% once the O₂ depletion system (glucose/ glucose oxidase/ catalase) was added, as recorded by the electrode. Panel B shows the test reaction, which was performed in the same way as the control but with addition 2 µM NorW. The PROLI-NONOate was added when the O₂ level was still 100% (aerobic) then once the O₂ level started to decline (microaerobic), and finally in the anaerobic condition, the figure shows that the NO consumption was quicker while the O₂ level was declined, n=1.

B- Assay under constant O₂ level

The anaerobic NO consumption assay was repeated under steady O₂ level by using the same system, glucose/glucose oxidase/catalase at the same concentrations (See Chapter 3, Section 3.2.26.1.5). The purpose of this experiment was to measure the NO consumption rate at steady O₂ level. The oxygen level has the major effect on NO removal; therefore, changing the O₂ level would change the NO reduction rate. To allow the equilibrium between the O₂ diffuses into the solution and consumes by cells in the oxygen electrode chamber, the oxygen electrode was left open without lid, thus the measurement will not be limited by the amount of the O₂ found initially in the liquid (Degn et al., 1973). Control reaction was measured at a low stir rate (setting 3), and then the O₂ depletion system (glucose, glucose oxidase and catalase) was added. Once the O₂ level became stable, 6 µM PROLI-NONOate was added. A peak appeared once the NO was released, and declined as

NO decomposed naturally. In the test reaction, 2 μM NorW was added, a very small peak appeared when 6 or 12 μM of PROLI-NONOate was added, but upon addition of 18 μM PROLI-NONOate, a clear peak was seen which declined more quickly than the peak seen upon addition of 6 μM of PROLI-NONOate in the control (Figure 4.31 A& B)

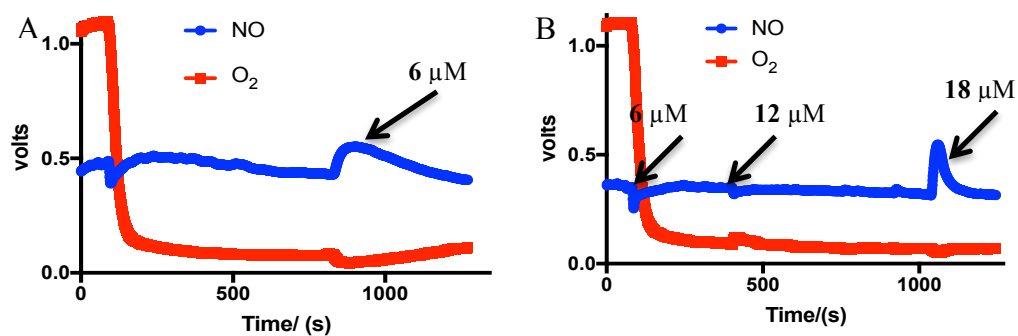


Figure 4.31: NO consumption with open O_2 electrode. Panel A- The control reaction, where the O_2 level declined from 100% to $\sim 12\%$ of its starting level, when the O_2 depletion system was added, it shows also the natural consumption of NO. Panel B- The test reaction in the presence of 2 μM NorW, which was performed as the control but with additions 6, 12 and 18 μM PROLI-NONOate. The graph shows that the NO consumption was quicker in the present of NorW, $n=1$.

The same reactions (control and test) were repeated with twice the concentration of glucose and glucose oxidase, at the same stirring speed (3), then with higher stirring speed (setting 5). A small change was noticed when the stirring speed was changed (Figure 4.32 A& B).

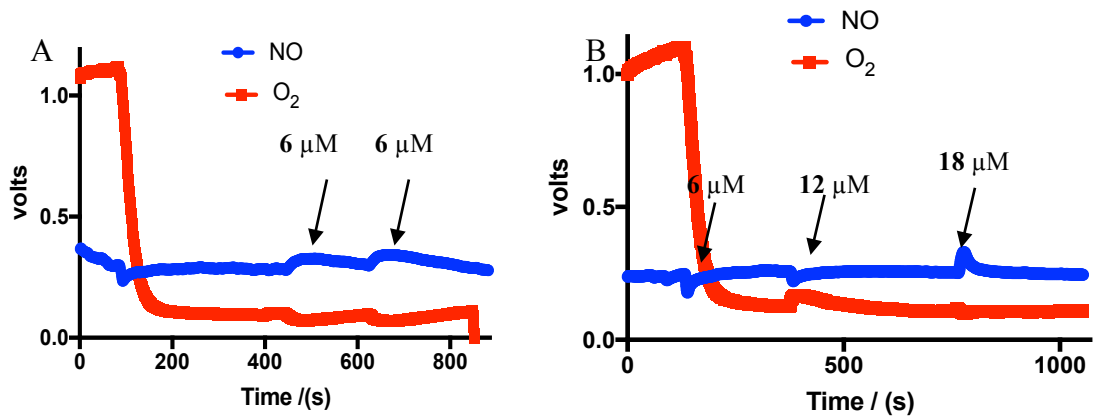


Figure 4.32: NO consumption with an open O₂ electrode under higher concentrations of the oxygen depletion system and higher stir rate. Panel A- The control reaction, where the O₂ level declined from 100% to 40-35%, by adding the O₂ depletion system. NO consumption was naturally.

Panel B- The test reaction, which was performed as the control with additions of 6, 12 and 18 μM PROLI-NONOate in the presence of 2 μM NorW. The graph shows that the NO consumption was quicker in the

However, the increase in the concentration of glucose and glucose oxidase seems to have a dramatic effect on the consumption rate (Figure 4.33 A& B).

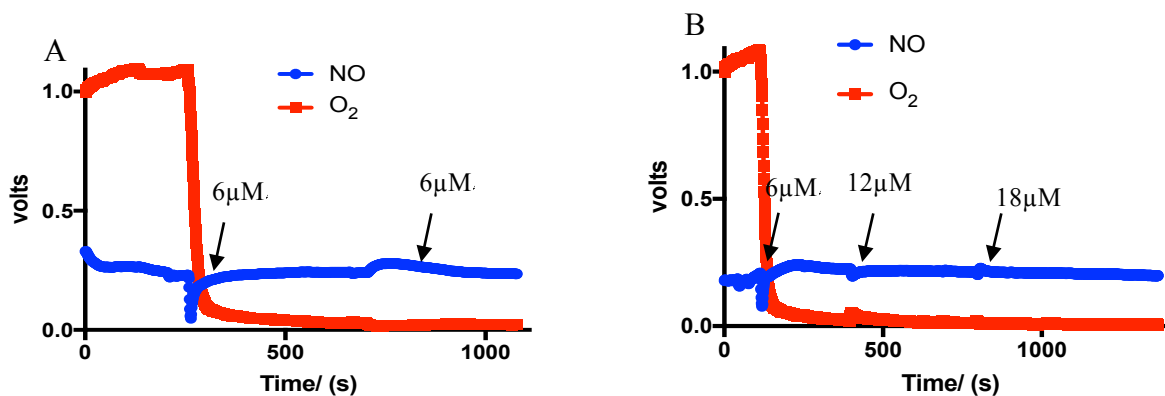


Figure 4.33: NO consumption with an open O₂ electrode. Panel A- The control reaction, stir rate at 3, where the O₂ electrode recorded 100%, until the O₂ depletion system (32 mM of glucose, 8 units/ml of glucose oxidase, and 20 units/ml of catalase) was added, the O₂ level declined to 0%. A peak was seen after NO was released upon addition of 6 μM PROLI-NONOate which declined to background in about 200 S.

Panel B- The test reaction in the presence of 2 μM NorW, which was performed as the control but with addition of 6, 12 and 18 μM PROLI-NONOate. There was little sign of any peak in the NO level following the additions of PROLI-NONOate. Thus the NO consumption appeared to be much quicker in the presence of NorW, and higher concentration of the glucose/glucose oxidase system.

4.13.2 NO consumption by NorW *in vivo* assays

To confirm the results that were obtained from NO consumption by NorW *in vitro*, two *in vivo* experiments were done. Both experiments were done at 37 °C incubation, using DETA-NONOate as NO releasing molecule unless stated otherwise. In these assays, the mutant strains of *E. coli* shown in Table 3.1 (Chapter 3, Section 3.1.2) were used.

4.13.2.1 Susceptibility test

The experiment was repeated three times to confirm the results. Different DETA-NONOate concentrations were used (as described in Chapter 3, section 3.2.26.2.2). The results showed that there was no effect of NorW in the protection from NO toxicity with an *hmp norR*/

norW⁺ strain compared with the *hmp norR*/pBAD strain, both of them were killed in all NONOate concentrations compared with the control reaction with no NONOate. A distinct effect was noticed in the *hmp norR* /*hmp*⁺ strain (Figures 4.34).

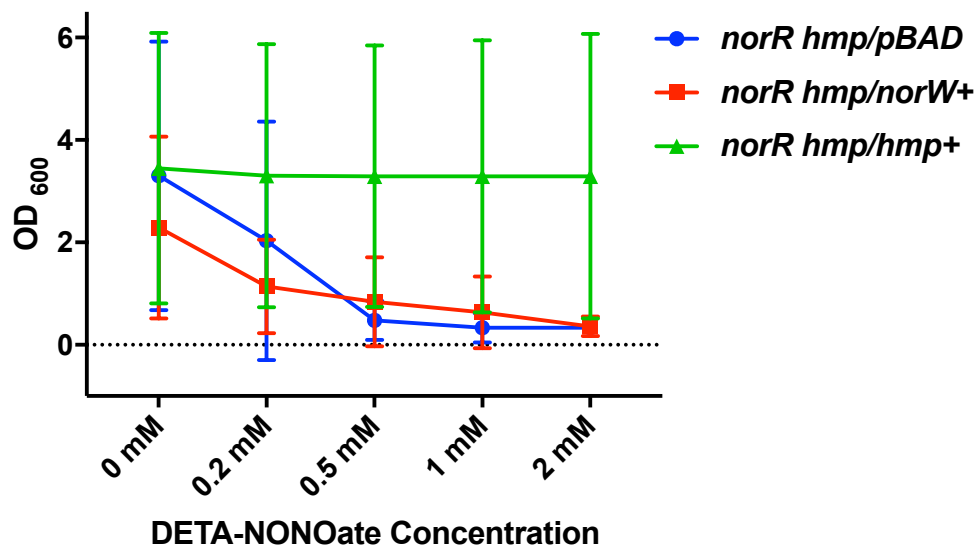


Figure 4.34: NO susceptibility test. The figure shows that there was no effect of NorW in protecting the *norR hmp* mutant from NO toxicity. The cells growth starts to decline in different concentrations of DETA-NONOate (blue trace) compared with the control with no NONOate. The same result was obtained with cells containing empty vector (red trace), but in cells expressing Hmp, the growth was unaffected by the NONOate levels (green trace). The results represent the mean of three biological repeats \pm SD.

This assay was repeated using a *norW* mutant strain complemented with pBAD expression plasmid for NorW and the same results were obtained (Figure 4.35).

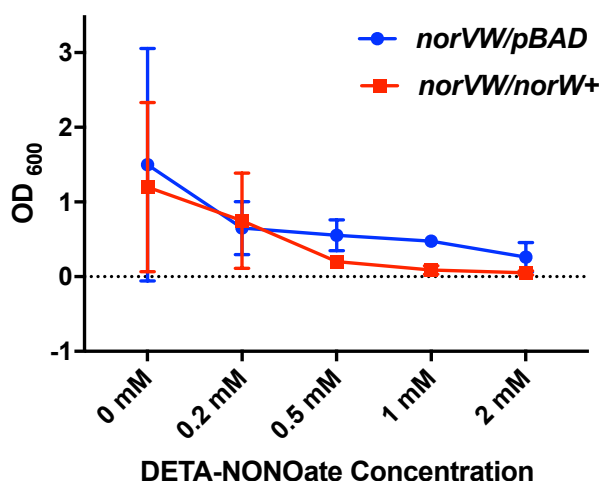


Figure 4.35: NO susceptibility test using an *E. coli norVW* mutant strain. The figure shows that there was no protective effect of NorW expression against NO toxicity (blue trace), as the strain was killed by using different concentrations of NONOate compared with the control with no NONOate. The same results were observed with cells containing empty pBAD vector (red trace). The results represent the mean of two biological repeats \pm SD.

4.13.2.2 Growth curve for *E. coli* mutants under different concentrations of NONOate

A further assay was performed to confirm the effect of NorW on NO toxicity, by measuring growth over time as plotted in the growth curve. The same mutant strains were used (*hmp norR* and *norVW*), and another more sensitive multiple mutant strain (JCB5253) from Professor Jeff Cole was used also. All the mutant strains were grown under aerobic conditions overnight, with 0-1 mM DETA-NONOate as described in Chapter 3, section 3.2.26.3. The results showed that NorW has no effect on cells protection from NO toxicity, and cells with *norW* (*hmp norR /norW⁺*, *norVW/norW⁺* and JCB5253/*norW⁺*) were killed at a similar rate to the one without *norW* (*hmp⁻ norR⁻ /pBAD* and *norVW/pBAD*, JCB5253/pBAD), whereas the strain expressing Hmp (RKP5884) showed resistance to NO. During this assay it was discovered that the strains that carried the empty vector (pBAD)

grew better than those carrying the complementary vector (pBAD/*norW*) as shown in Figure 4.36.

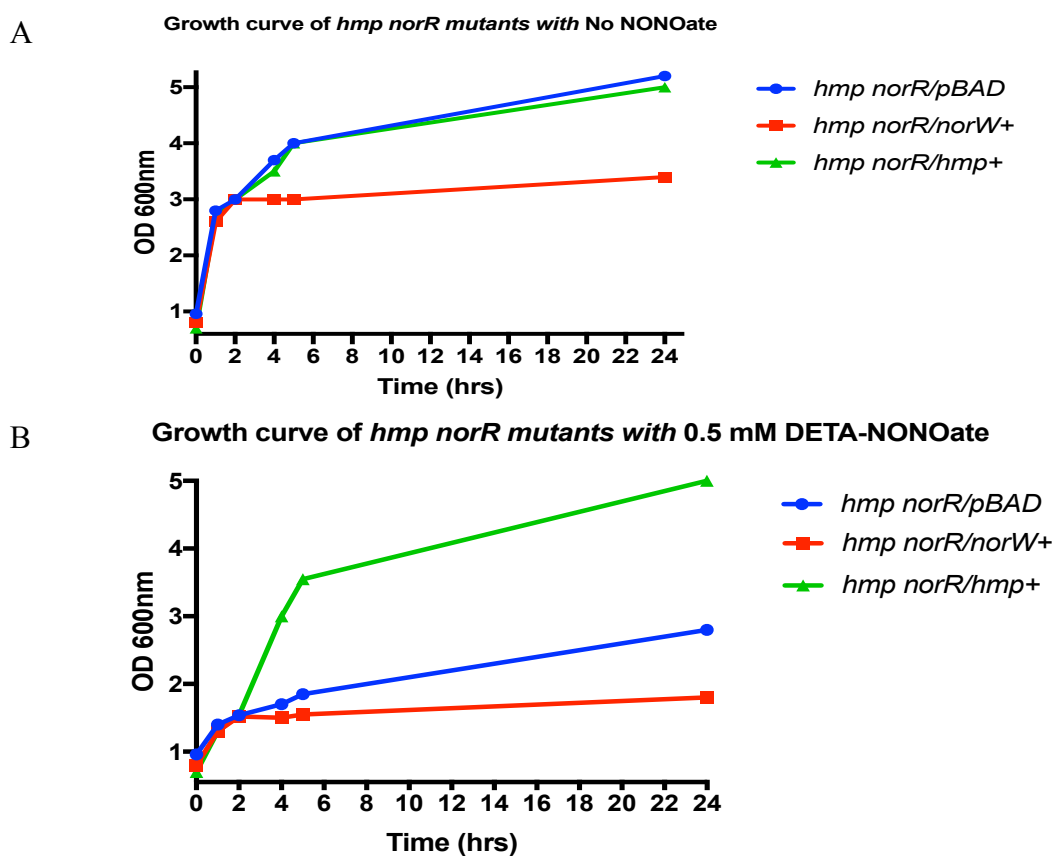


Figure 4.36: Growth curve of *E. coli norR hmp* mutant. Panel A- The control growth with no DETA-NONOate, it shows that all three mutant strains were grown exponentially. Panel B- Cultures grown under NO stress, showed that NorW did not protect the mutant strain from NO toxicity, as both cells expressing NorW (red trace) and without NorW and just empty pBAD vector (blue trace) were killed in the presence of 0.5 mM of DETA-NONOate compared with cells expressing Hmp (green trace), which grew as in the control experiment in the absence of DETA-NONOate, n=1.

With the multiple mutant (JCB5253), the growth curve was also checked with a plate reader using 200 μ l of cultures in each well with and without *norW*. The result also showed that cells expressing NorW grew less than cells with empty vector (Figure 4.37). The expression of NorW was confirmed in the *hmp⁻ norR⁻* and JCB5253 mutant strains, by analysis 1ml sample on SDS-PAGE.

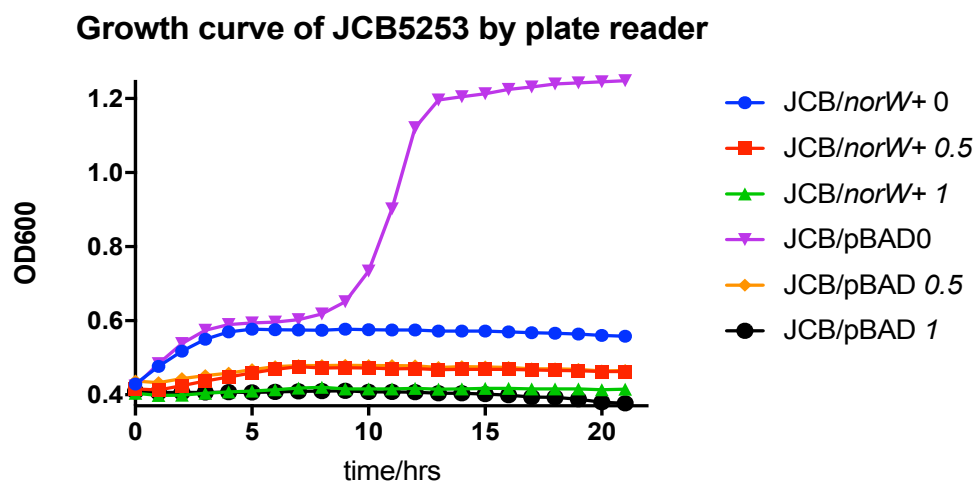


Figure 4.37: Growth curves of *E. coli* multiple mutants by plate reader. The figure shows that there was no effect of NorW in protecting the mutant strains from NO toxicity. However, in the control without NONOate, the mutant strain complemented with pBAD empty vector grew better than the one complemented with *norW* expressing vector. 0, 0.5, and 1 represent the DETA-NONOate concentrations in mM, n=1.

4.13.2.3 NO anaerobic consumption in intact cell suspension

This assay was performed as described in Chapter 3, Section 3.2.26.2.1. The results showed that NorW has no activity to protect cells from NO toxicity, both the *norR hmp/norW*+ strain and the strain with only empty vector (*norR hmp/pBAD*) showed the same NO consumption levels, whereas, the mutant strain with the *hmp* expression vector showed a rapid consumption for PROLI-NONOate (Figure 4.38).

NO consumption in intact cell suspensions

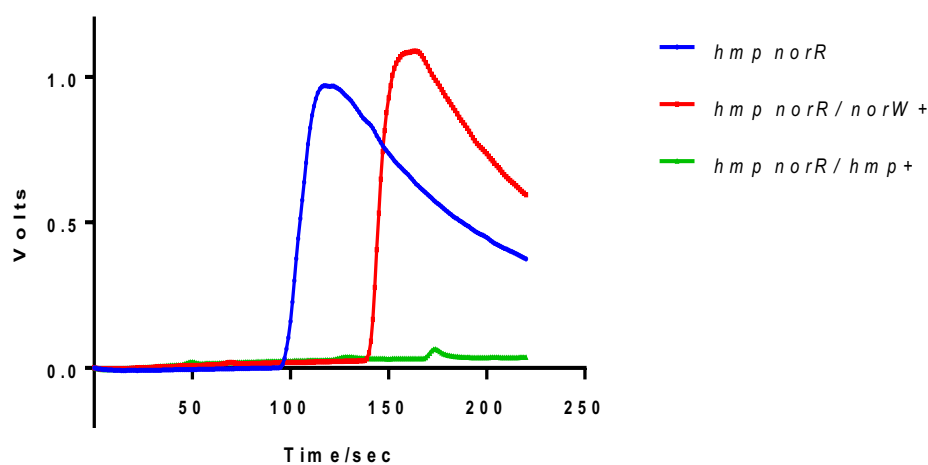


Figure 4.38: NO consumption in cell suspension. The graph shows that protection of NorW does not lead to consumption of NO when PROLI-NONOate is used as an NO donor. Once NO is released a peak appeared in both *norR hmp* strains with (red trace) and without (blue trace) expression of *norW*, and the peak decreased at a similar rate in each. In an *hmp+* strain producing Hmp from a vector (green trace) only a very small peak appears after 150 s, which decreased rapidly, corresponding to the NO consumption by Hmp, n=1.

To confirm the NO consumption in the intact cell suspension result, more sensitive *E. coli* mutant cell JCB5253 (*norVW nrfAB nirBD hmp fnr hcp*) background was used, the NO consumption was also the same in the mutant strains with and without *norW* expression, which implies that there was no effect from NorW production on NO detoxification in the intact cell (Figure 4.39).

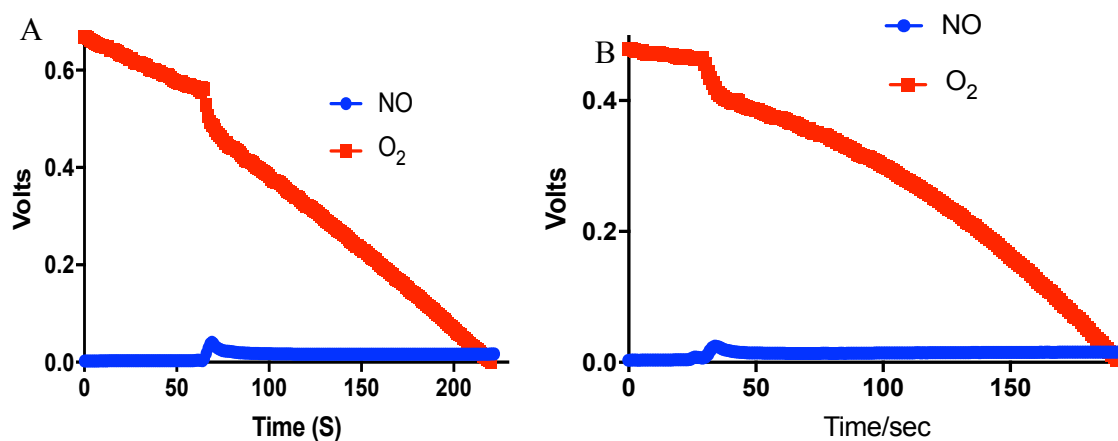


Figure 4.39: NO consumption in intact cell suspension. Panel A- shows the graph of NO consumption in anaerobic conditions, using a JCB5253 mutant strain transformed with pBAD empty vector. Panel B- shows the NO consumption using a JCB5253 mutant strain complemented with a *norW* expression vector. The figure shows that NO levels showed the same response in cells with and without NorW.

4.13.3 NO reduction to N₂O

To confirm the NO consumption *in vitro* results and to see if the NO was reduced or oxidized, FTIR (Fourier transform infrared spectroscopy) was used as described in Chapter 3, Section 3.2.24.1.3. The FTIR data showed a strong signal of N₂O in both the control and the test samples. The N₂O signal was also strong in the autoclaved culture and in media alone (LB, and defined minimal media (DMM)) (Figure 4.40). Interestingly, the results showed that the highest level of N₂O (around 19 μM) was generated from DMM. Within the first hour of the measurement, DMM medium alone, LB medium alone and the JCB5253 strain grown in LB media generated the same amount of N₂O (around 9 μM). For the JCB5253 strain transformed with either pBAD and pBAD/*norV* or *norW* expressing vectors, the measurement of N₂O was around 8-9 μM after 12 h. The lowest measurement was obtained from autoclaved *E. coli* culture (around 3.5-4 μM) in the first hour of the measurement.

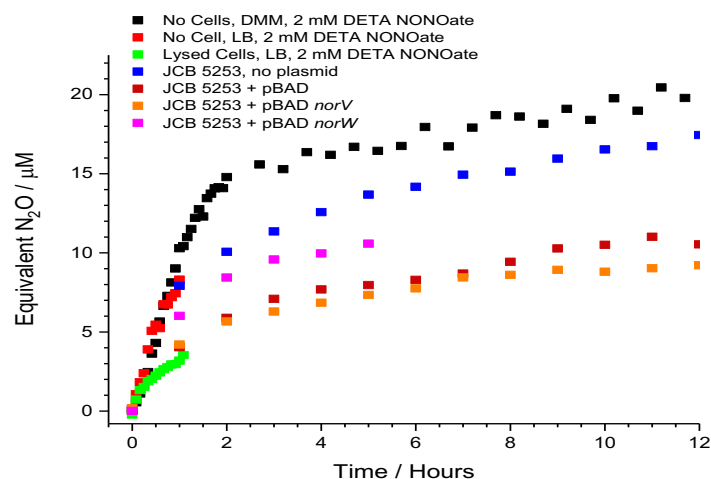


Figure 4.40. FTIR spectra of different *E. coli* cultures with and without pBAD expression vector and treated with DETA-NONOate. The figure shows the N_2O generated from the different cultures. The highest level of N_2O was recorded in DMM (defined minimal media), and the lowest level was generated from the lysed *E. coli* cells.

4.14 Chemical characterization

In this section, the chemical characterization methods that were used to identify NorW will be discussed.

4.14.1 Mass spectrometry

NorW was sent to the mass spectrometry facility in the Chemistry department, University of Sheffield, as described in Chapter 3, section 3.2.19.

The first mass spectra showed a peak of 45676.72 Da, which corresponds to the molecular weight of NorW with a six-histidine tag and 29 residue linkers between the protein and the histidine tag (Figure 4.41 A).

A mass spectrum showed a molecular mass of 41532.83Da, which corresponds to the size of NorW protein with two linker residues (leucine and glutamate) (Figure 4.40 B)

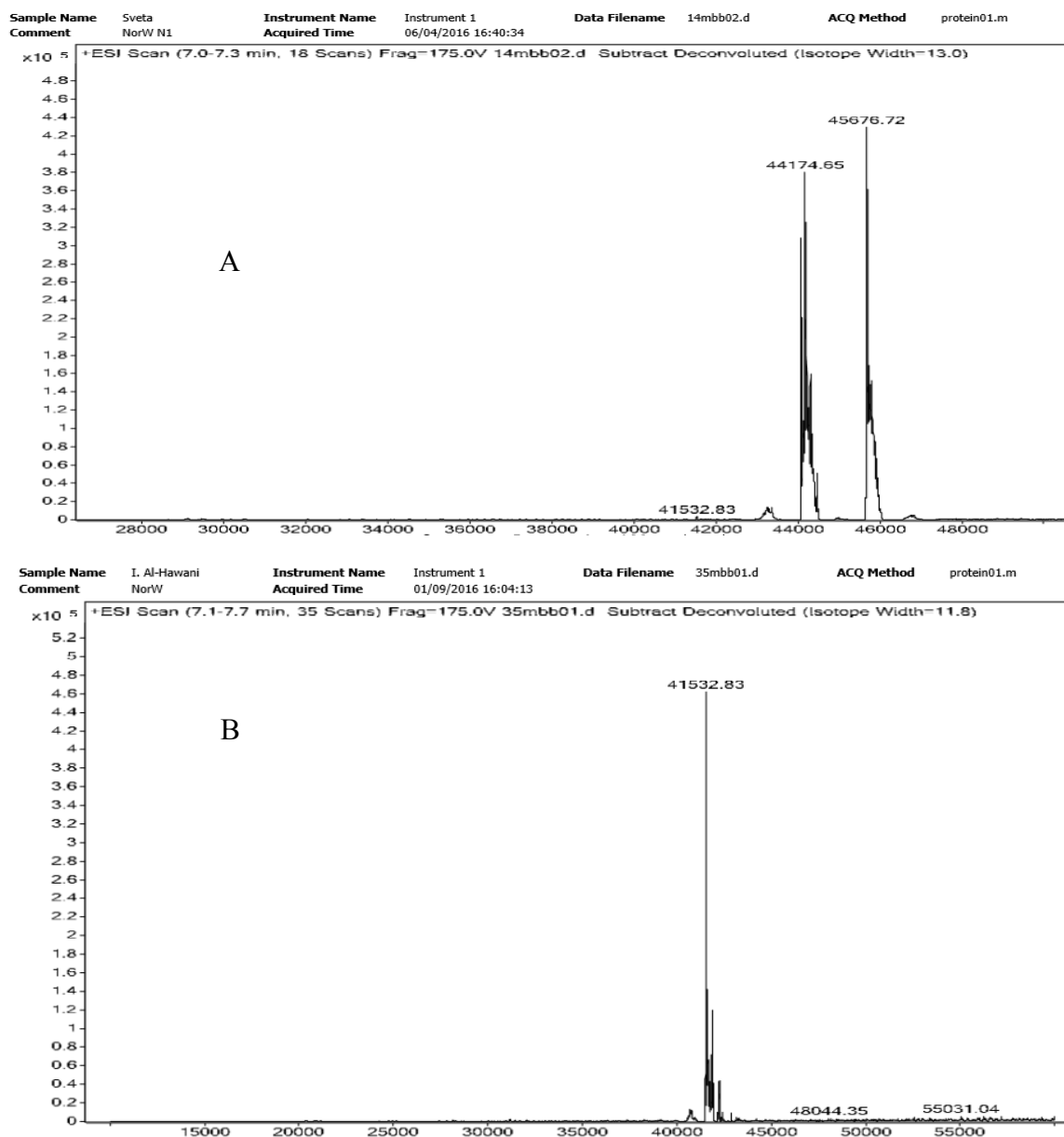


Figure 4.41: Mass spectra of NorW His-tagged protein. Panel A. the spectrum of NorW, shows that the highest peak in the spectrum was 45676.72Da, which is approximately equal the molecular weight of NorW+ 6XHis+29 residue linker.

Panel B shows the MS spectrum of NorW different prep, which gave another molecular weight 41532.83Da to NorW, this Mw corresponding to NorW Mw + leucine and glutamate

4.14.2. Inductivity Coupled Plasma- Mass Spectrometry (ICP-MS)

NorW was sent to be analyzed by ICP-MS as described in Chapter 3, Section 3.2.26.6. The ICP results showed that Sulfur, Potassium and Phosphorus were found in high amount 35.9, 22.5 and 9.72 mg/l respectively. Table 4.1 shows the results of the ICP-MS. All the results are in Mg/L after multiplying the diluted sample by the dilution factor.

Table 4.1. ICP-MS result. The table shows metals in mg/L found in NorW sample.

SAMPLE I.D.	Zn	Ni	Fe	Cu	K	Mg	P	S
PROTEIN	0.18	0.15	0.09	0.07	22.5	0.86	9.72	35.9

4.15 Discussion

4.15.1 Can NorW reduce NO to N₂O without NorV?

NorW belongs to the oxidoreductase class of enzymes and catalyzes an electron transfer from NADH through flavin adenine dinucleotide (FAD) to a partner protein (NorV in *E. coli*), which subsequently reduces NO to N₂O under anaerobic conditions (Costa et al., 2003; Gardner et al., 2003; Gardner et al., 2002; Gomes et al., 2002b; Gomes et al., 2000; Justino et al., 2003).

The ability of isolated NorW to remove NO from media or buffer was investigated in the current study. The *in vitro* assays showed that NorW was able to consume NO (provided as a product of NO releasing molecules DETA-NONOate or PROLI-NONOate) in an efficient manner. In contrast, no evidence was obtained for any NO removal by NorW *in vivo* and this disagreement between the two states is an interesting area for discussion.

4.15.2 Protein purification

The SDS-PAGE results of non-tagged NorW purification showed that NorW did not purify sufficiently even by gel filtration. Colour (yellow) fractions after gel filtration were loaded on another anion column (Resource Q); the salt (NaCl) concentration was increased gradually from 0-40% to unbind the protein from the Resource Q column matrix. The protein was prepared with purity between 80-85%, which was not highly recommended for crystallization study, but it was used for crystallization, because the protein is recorded as unstable in the protein index, so the concern was to lose the protein, if further purification were used (For further information see section 4.11).

4.15.3 NorW crystallization

Protein crystallization is the first step for solving protein structures by X-ray crystallography. The structure will reveal the overall fold and the details of regions such as the active site of the protein, which might be targeted by drugs or mutated to alter the protein structure and disrupt its function.

Different factors can influence the crystallization process: the protein size (full length or truncated); the purity and concentration of the protein; the protein surface charge; the presence or type of a purification tag; and experimental conditions such as temperature, pH of the buffer used in crystallization, and precipitant concentration (Benvenuti and Mangani, 2007; Dessau and Modis, 2011; Giege et al., 1986; Gilliland and Ladner, 1996).

Attempts were made to crystallize NorW (tagged and non-tagged versions), by using a range of chemical conditions, changing both buffer pH and precipitant concentration. However, they were unsuccessful, perhaps because of instability or flexibility in the protein. So, investigations also involved the use of an NADH coenzyme and NorV as a

protein partner in attempt to stabilise the protein. Sodium dithionite was added in order to reduce the four cysteine residues in NorW to try to obtain a crystal of a reduced form. Heavy metals (mercury and platinum) were added to NorW in order to enhance the chance of getting crystal. Heavy atoms (HAs) are used widely to solve the phasing problem but can be used simply in the crystallization because they may incorporate into the protein and give a more stable structure to the protein that can cause an ordered arrangement in a crystal.

Cysteine (Cys), methionine (Met) and histidine (His) are often the targets of metal ion binding and the ions can also bind with amino groups, chloride and ammonia ions in the buffer. A covalent bond can form between mercury ions and cysteine within the target protein (Pike et al., 2016). NorW has 4 cysteine residues, and 11 methionine that make it a good target for heavy atoms; mercury was used as mercury chloride and platinum as potassium hexachloro platinate (see Chapter 3, section 3.2.21). The protein crystallization solution can affect the binding of the protein to the heavy metals dramatically, where the pH of the buffering system can alter the side chain status and affinity for the metal ions. The salt concentration has the greatest effect on metal binding, it can block the HAs binding site on the protein by masking the sites, and it can compete with the protein on metal binding, especially if the metal affinity to bind the salt greater than to bind the protein (Pike et al., 2016). This might be the case with NorW, which purified in high salt buffer (0.5 M NaCl), The conformation of the protein might be changed, and this might explain the precipitation that happened once the metal was added to NorW. The pH of the NorW purification buffer was 8.0, which is suitable for Cys that has a pK_a 8.3 if the residue was accessible to the metal ion.

4.15.4 NorW consumes NO without NorV

The assays in sections 4.13.1.1 and 4.13.1.2 showed that NorW could apparently consume NO in different assays in different experimental conditions *in vitro*.

A- *in vitro* assays

NorW alone and in combination with NorV was tested. NorV was unable to consume NO produced from PROLI-NONOate. The presence of NorW showed very clear evidence for the removal of NO from the buffer in different experimental condition (see sections 4.13.1.1 and 4.13.1.2). In contrast with Gardner and co-workers and Gomes and co-worker's findings that NorW is an accessory protein in anaerobic NO detoxification, and that the main role is provided by NorV (Gardner et al., 2002; Gomes et al., 2002a).

My study showed that NorW detoxifies NO in both aerobic and anaerobic conditions, although the consumption was slower under aerobic conditions than in anaerobic conditions. In contrast Gardner and colleagues study showed that NO detoxification was impaired under aerobic condition (Gardner et al., 2002).

I was able to prove that NO consumption was increased under anaerobic condition comparing with aerobic and microaerobic condition (Figure 4.30 B, Chapter 4). It was observed that when the concentration of the O₂ depletion system (glucose/ glucose oxidase/ catalase) was increased, the NO consumption was increase (Figure 4.33 B, Chapter 4), which agrees with Gardner and colleagues finding (Gardner et al., 2002). The mechanism of NO consumption by NorW still under investigation.

Studies on flavin containing enzymes (flavoproteins) in *E. coli* such as NADH dehydrogenase II, fumarate and succinate dehydrogenases revealed that electron transfer can occur from the reduced FAD to oxygen to form superoxide O₂⁻ (Messner

and Imlay, 2002; Messner and Imlay, 1999; Imlay, 1995). The superoxide can then interact with nitric oxide to form peroxynitrite ONOO⁻ (Beckman et al., 1994).

NorW is flavoprotein, and after reduction of FAD by NADH electron could be transferred to form superoxide. The superoxide could then interact with nitric oxide to form peroxynitrite. In low oxygen assays for NorW activity, the system used to deplete the oxygen (Glucose/glucose oxidase/ catalase, Section 3.2.26.1.5) would generate H₂O and O₂ from the incoming air, and thus the same reaction between nitric oxide and superoxide is possible. Hence, under both NorW assay conditions tested here nitric oxide could be eliminated by reaction with superoxide. To determine whether the observed nitric oxide consumption was due to NorW activity, the reaction needs to be performed under strict anaerobic condition.

B- *in vivo* assays

No clear evidence was obtained for *in vivo* NorW detoxification of NO, in intact cell suspension, when an NO consumption assay was carried out under anaerobic condition, with *E. coli norR hmp* mutant strains (Figure 4.38, Chapter 4). Although the NO peak was very small when the cell suspension of *E. coli* multiple mutant (JCB5253) was used, but the fact that the test strain (expressing NorW) showed the same peak as the control strain (transformed with empty pBAD), reduces the probability of any NO consumption by NorW.

It is possible that this strain possesses unidentified mechanisms for removal of NO, which might obscure the low rates of NO detoxification by NorW, Recently, for example, the Hcp/Hcr system was shown to be involved in NO removal in such a background (Wang et al., 2016)

In the Gardner study (Gardner et al., 2002) they used NO gas as a stress, whereas in my study, NO releasing molecules were used as NO donor (PROLI and DETA-NONOate). Both compounds were tested and proved to release NO in the buffer (using an NO electrode).

In the susceptibility test, *E. coli hmp norR* mutant strain was used as described in Chapter 3, section 3.2.26.2.2. The results showed that, the *hmp norR* strains transformed with pBAD/ *norW* or pBAD empty vector were killed equally, which suggests that there was no effect from NorW in cell protection from NO toxicity, whereas *hmp*⁺ cells grew in the presence of NO.

Although the susceptibility experiment was carried out under aerobic condition, which as Gardner and colleagues had shown would impair NO reduction by NorV (Gardner et al., 2002), nothing was known about a NorW mechanism in NO detoxification, and the *in vitro* NO consumption under aerobic condition showed NO removal by NorW this led to the susceptibility test under aerobic conditions.

The large error bars on plots indicate that the data must be interpreted with caution. The number of repeats was small (n=3) and there was a problem with the growth of one of the cultures (*norR hmp/ hmp*⁺).

Gardner and colleagues showed NO reduction was substantially lower under aerobic condition, compared to anaerobic condition (Gardner and Gardner, 2002). Thus, if NorW provide any protection for cells expressing it, small differences should have been seen between the control (cells with empty vector) and the test strain (cells with pBAD/ *norW* vector). No differences were noticed between cells expressing NorW and with empty vector. It is possible that there is a compound (a product from the host cell), a protein or even a polypeptide that interacts with NorW and inhibits NorW function *in vivo*.

Studying the effect of NO on growth of mutant *E. coli* (*hmp norR*, *norVW*, and JCB5253) as described in Chapter 3, section 3.2.26.3, showed the same results as the susceptibility test i.e. no protection was seen against the NO toxicity effect in cells expressing NorW, and the growth of cells was declined during the protein expression (after 3 h of induction), as shown in Figure 4.36.

It was observed that cells expressing NorW often grew slower than cells with empty vector; this might be due to protein toxicity. Detrimental function of the recombinant protein in the host cell is one of the problems that faces the expression of the recombinant protein. This function might result in slower growth, lower cells density, and/or death, because it can interfere with the normal cell functions of the host cell (Doherty et al., 1993; Dong et al., 1995). Despite choosing the low copy pBAD plasmid with tightly regulated promoters to reduce the basal expression of NorW protein (Rosano and Ceccarelli, 2014). This might cause of the apparent difference.

Another reason for slower growth when protein was expressed might be because cells were manufacturing the protein and diverted cellular material into making the recombinant protein instead of making other components.

4.15.5 Checking the final product of NO removal by NorW

To check the final product of NO detoxification by NorW, and to guarantee the reduction of NO, the final product of NO removal by NorW was checked by FTIR as described in Chapter 3, section 3.2.26.4. The results showed that N₂O was produced, and there was a signal for N₂O definitely seen in LB culture (containing cells of *E. coli* mutant strains (*hmp norR*, and JCB5253)), LB medium alone, and autoclaved *E. coli* mutant strain culture. DETA-NONOate was used to produce NO, because cells were grown overnight), and DETA-NONOate is recommended for long term exposure, since

it has a longer life time (20 h at 37 °C in 0.1 M phosphate buffer, pH 7.4) than PROL-NONOate (1.8 s at 37 °C in 0.1 M phosphate buffer pH 7.4)

The FTIR results (Figure 4.40) were inconclusive, it showed that N₂O was generated in LB and minimal media alone more than in LB cultures, which might indicate that there is an abiotic reaction happening with NO. In the aerobic environment, N- containing radicals can be oxidized to NO (Bowman, 1992). In LB, the amine groups (which can be produced by peptone hydrolysis) might provide a source of NO, which then can interact with another NO to form N₂O.

The mechanisms behind this reaction, and the conversion of NO to N₂O need more investigations. However, N₂O can be produced naturally, via abiotic reaction which can occur between the redox-active metals (such as Fe and Mn), organic material, and the reactive intermediate compounds produced during the nitrogen cycle (such as NO, NO₂ and NH₂OH) (Zhu-Barker et al., 2015). Defined minimal media (DMM) contains Mn and Fe, which might interact with NO generated from DETA-NONOate, and produce N₂O.

The implication is that NO is being used by cells, but not allowed to convert to N₂O, or that cells might convert the N₂O to something else.

4.15.6 Metal content of NorW

In order to perform a reduction reaction, the enzyme in many cases has a redox active metal. To investigate the metal content of NorW, it was sent for ICP-MS testing, as described in Chapter 3, section 3.2.26.1.5. Table 4.1 in Chapter 4 shows the results of ICP-MS of NorW. According to the molecular weight of NorW (41 kDa) and the concentration of the purified NorW that was sent for ICP-MS testing, the number of atom for each ion was calculated (Table 4.2). The result shows that there are about 10

sulfur atoms. NorW has 4 cysteines, and 11 methionine which each has a sulfur. The NorW was purified in Tris-HCl and NaCl buffer and thus, the sulfur ion came from the enzyme. The disagreement between the number of sulfur atoms calculated in the sample (10) and the expected number based on the protein concentration (15) might arise from inaccuracy in the concentration which was measured by the Bradford method. Phosphorous (P) came probably from FAD, it has two phosphate groups. There was also a high amount of potassium (K), which was not found in the buffer or NorW residues and might suggest specific binding sites on the protein for this element. There was no strong signal for Fe, Ni, Cu, Mg, or Zn presence in the sample.

Table 4.2 Calculated number of atoms of selected elements per molecule of NorW. The table shows the result of the calculation for ions present in the NorW sample gained from ICP-MS. It shows that K, P and S were found in high concentration

Metal ID	Zn	Ni	Fe	Cu	K	Mg	P	S
Mg/L	0.18	0.15	0.09	0.07	22.5	0.86	9.72	35.9
Number of atom per protein molecule	0.023747	0.0220480	0.0139163	0.0095113	4.9650351	0.3053576	2.7053355	9.649526

Chapter 5 : Flavorubredoxin (NorV)
structure in E. coli

5. Introduction

NorV (flavorubredoxin oxidoreductase) is a member of the flavin diiron protein family (FDP), which catalyse the two-electron transfer from protein partner NorW to nitric oxide (NO), reducing it to nitrous oxide (N₂O), under anaerobic condition. Under aerobic condition; the activity of NorV is impaired. (Gardner et al., 2003; Gardner et al., 2002; Gomes et al., 2002a).

NorV possess three domains: N-terminal β -lactamase like domain, with a diiron center; flavin adenine dinucleotide domain with FMN; and an additional C- terminal domain which in *E. coli* NorV is a rubredoxin domain with an iron-sulfur cluster.

Under anaerobic conditions, when *E. coli* is challenged with nitrosative stress, NorR a gene regulatory protein activates *norV* transcription and NorV is produced (Gardner et al., 2003). Structural studies of many members of the FDP have been done. During the course of my investigation of the enzyme, a structure of *E. coli* NorV was published (Romao et al., 2016).

In this Chapter, the results of the investigation of NorV from gene cloning to the stage of protein structure analysis will be described.

5.1 Amplification of *norV* by polymerase chain reaction (PCR)

The target gene was amplified from *E. coli* K12 strain MG1655 ; the PCR product was loaded on a 1% agarose gel, to check the product. The result showed that the gene was successfully amplified and the PCR product size was corresponded to *norV* molecular size (1440 bp) (Figure 5.1).

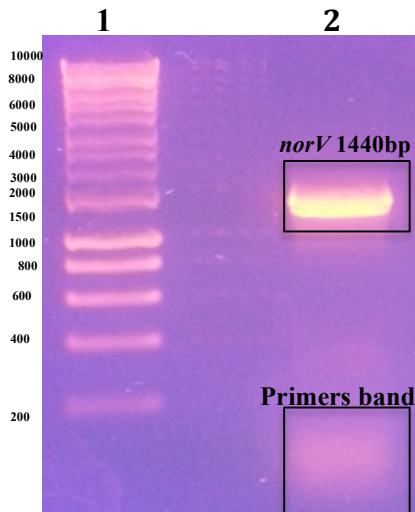


Figure 5.1: The PCR product of *norV* before cleaning up. Lane 1 is the DNA marker (Hyperladder1), lane 2 is the PCR product of *norV*. The figure shows the PCR product of *norV* a band between the 1500 and 1000 bp DNA markers.

5.2 PCR clean up

The PCR product was cleaned up as described in Chapter 3, section 3.2.7, and the cleaned product was loaded on an agarose gel, to check the purity of the product. The result showed that the primers band had disappeared and only a single band was seen corresponding to *norV* molecular size (1440 bp) (Figure 5.2)

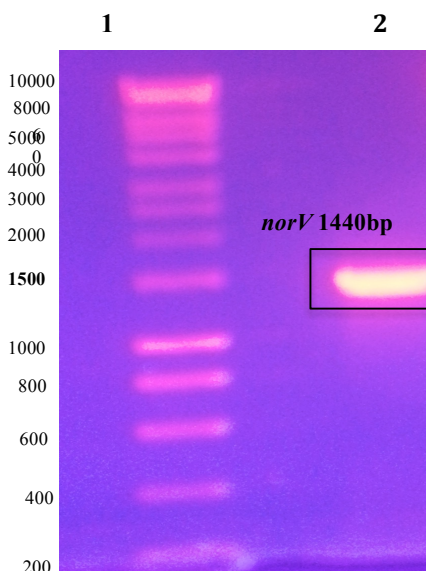


Figure 5.2: *norV* PCR product after clean up. The figure shows the band of *norV* PCR product after cleaning it up.

5.3 Restriction digestion

The plasmid (pBAD/HisA) and the PCR product were digested by NcoI and HindIII restriction enzymes (table 3.2). Both restriction reactions (plasmid & insert) were then loaded on agarose gel to check the digestion results. The result showed that the cut DNAs ran slower than the uncut (circular) DNA used as a control, which might suggest that the DNAs were cut efficiently by the restriction enzymes.

5.4 Ligation

The ligation was performed as described in Chapter 3, section 3.2.9. *norV* gene was successfully cloned into pBAD/HisA vector. The ligation mixtures were then used to transform either *E. coli* Top10 competent strain or *E. coli* Silver Efficiency chemically competent cells.

5.5 Transformation

The transformation was performed as described in Chapter 3, section 3.2.10.3. The colonies (constructs) were grown on LB plates with appropriate antibiotic and were counted and then sub-cultured to produce a single pure culture.

5.6 Ligation results analysis

The constructs were prepared for plasmid DNA extraction by miniprep kit as described in section 3.2.4. The plasmid DNA of the constructs was analyzed by restriction digestion and sequencing to confirm a successful ligation.

5.6.1 Restriction digestion of *norV* constructs

The plasmid DNAs were extracted from the construct, and loaded on a 1% agarose gel. The result showed that the DNA of the constructs ran with different size. The constructs in which the DNA ran with a size around 5000 bp were selected because the expected molecular size of the plasmid (4000 bp) plus the insert (1440 bp) should be around 5440 bp (Figure 5.3). The selected constructs then were double digested by NcoI and HindIII

restriction enzymes and loaded on gel to find the correct construct that has the correct gene size (1440 bp).

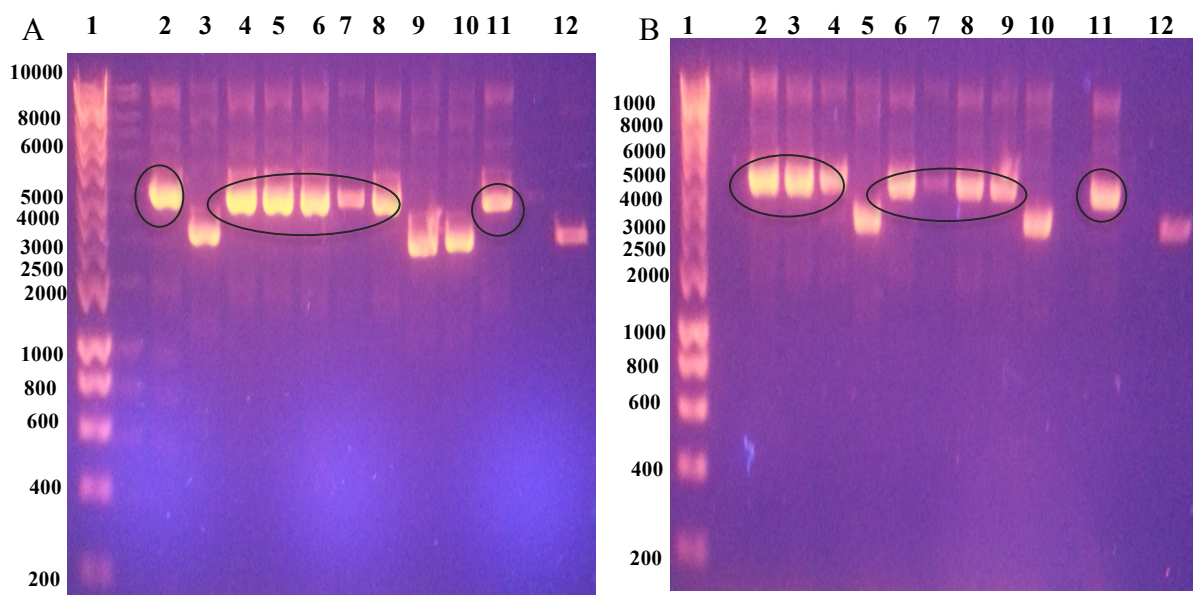


Figure 5.3: *norV* / pBAD constructs. A- lane 1 is the DNA marker (Hyperladder1), lanes 2-11 are constructs 1 to 10, and lane 12 is the pBAD vector. The figure shows that construct 1, 3, 4, 5, 6, 7, and 10 had the higher band, which could correspond to the molecular size of the construct (around 5500 bp). B- lane 1 is the DNA marker (Hyperladder1), lanes 2-11 are constructs 11 to 20, and line 12 is pBAD vector. The figure shows that the molecular size of constructs 11, 12, 13, 15, 16, 17, 18, and 20 was larger than the other constructs comparing with unligated plasmid.

5.6.2 Sequence analysis of *norV* constructs

Constructs showing the correct size on the agarose gel were sequenced. All those sequenced had some sequence mutations. Construct 11 had the smallest number of mutations which resulted in a change of Ser 2 to Ala and a replacement of Lys 478 with an additional Asn and Glu at the C-terminal end of the protein (Figure 5.4)



Figure 5.4: Sequence alignment of *norV* construct 11 (Subject) with *E. coli norV* gene from database (Query). The figure shows that there are two mutations, which are boxed in blue box, the first mutation was created during construct design to introduce an NcoI restriction site, and the second one was a deletion, which resulted in frameshift which changes Lys 478 to Asn + Glu and a new C-terminus. The red boxes represent the start and stop codons.

5.7 Site directed mutagenesis

An attempt was made to correct the point mutation by site directed mutagenesis which change serine to alanine in NorV protein (As described in Chapter 3, section 3.2.12). However, mass spectrometry result showed later that the mutation was not corrected. Thus, the mutant protein was used for further studies.

5.8 Small scale protein expression.

The expression construct was transformed into *E. coli* Top10 competent cells and a small-scale culture growth to test the expression was performed (As described in Chapter 3, section 3.2.13). Arabinose was used as an inducer. Samples were taken during the expression as described in Chapter 3, section 3.2.14. The samples were analyzed on SDS-PAGE, which showed that NorV was expressed in Top10 cells, and the best expression was seen for 3 h incubation at 37 °C following induction with 2% (w/v) arabinose (Figure 5.5).

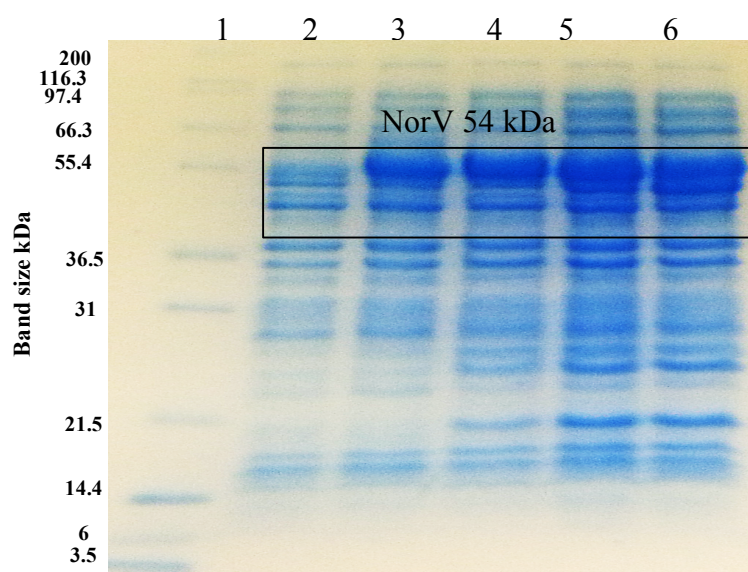


Figure 5.5: SDS-PAGE of NorV small-scale culture to test expression in Top10 cells. NorV was expressed for 1, 3, 5 h and overnight following induction with 2% (w/v) arabinose at 37 °C. The expression was similar after 5 h and overnight, and slightly better than after 3 h. The gel shows a band of 55.4 kDa according to the Mark 12

protein marker, which corresponds to NorV molecular size (54 kDa). Lane 1= Mark12, lane 2= Perinduction, lane 3, 4, 5, and 6 are 1, 3, 5 h and overnight post-induction.

5.9 NorV solubility test

To check the protein solubility, a sample of cells was lysed by sonication and centrifuged. Supernatant and the pellet fractions were analyzed on SDS-PAGE. The SDS-PAGE showed that bands (around 54 kDa) were found in soluble and non-soluble fractions, and suggested that NorV was found in the soluble fraction at approximately 40% level (Figure 5.6).

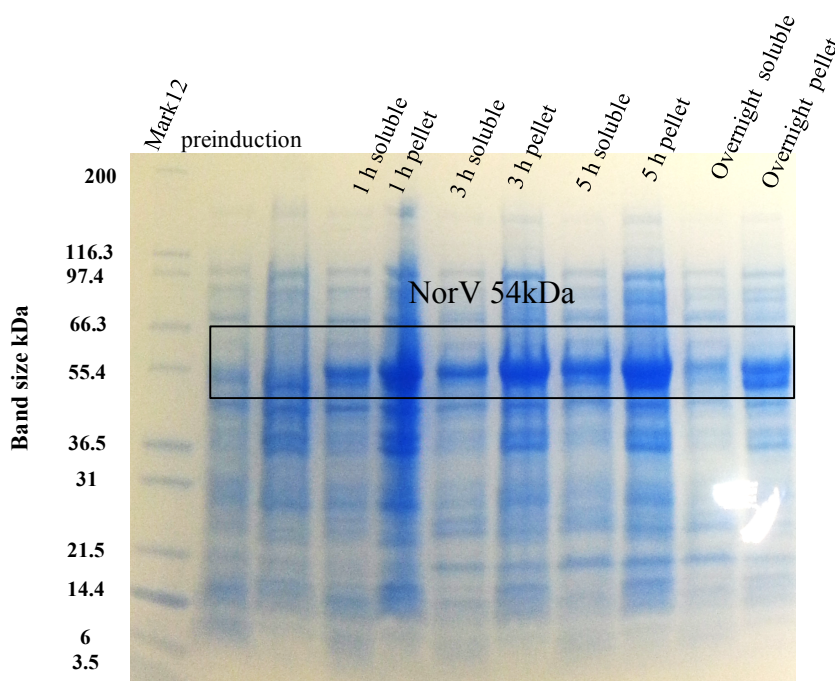


Figure 5.6: The SDS-PAGE of NorV solubility test results. The gel shows that NorV was found in the soluble fractions of all expression samples (1, 3, 5 h and overnight), and its solubility was around 40% of total NorV protein. The best results were obtained after 3 and 5 h expression.

5.10 Large-scale expression

Based on the results of the small-scale culture expression trials, a large-scale culture expression and production of NorV was performed as described in Chapter 3, section

3.2.17. An SDS-PAGE analysis of samples showed that NorV was successfully expressed in large scale, the expression was very high and the band appeared around 55 kDa according to Mark12 protein marker (Figure 5.7).

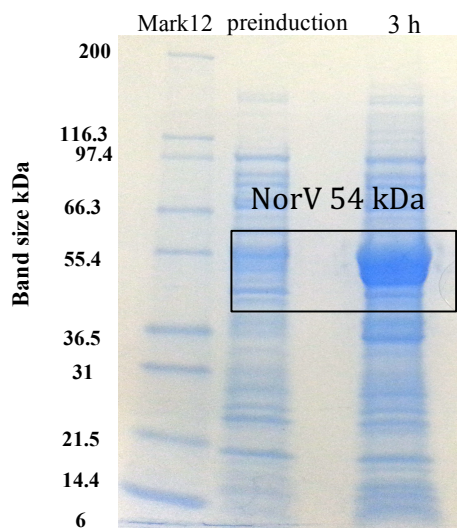


Figure 5.7: SDS-PAGE of NorV large-scale expression. The gel shows that NorV was produced at 37 °C following induction of *norV* gene with 2% (w/v) arabinose, from 500 ml culture. The expression was high and the band was found in the molecular size corresponding to NorV molecular size.

5.12 NorV purification

NorV was expressed as a non-His tagged protein and the purification was performed by using a DEAE fast flow ion exchange column followed by a Superdex 200 gel filtration (GF) column.

CFE was prepared as described in Chapter 3, section 3.2.16. CFE was applied on DEAE column. Fractions across the elution profile from DEAE purification (Figure 5.8) were analyzed on SDS-PAGE (Figure 5.8). The result showed that NorV needed further purification by gel filtration column.

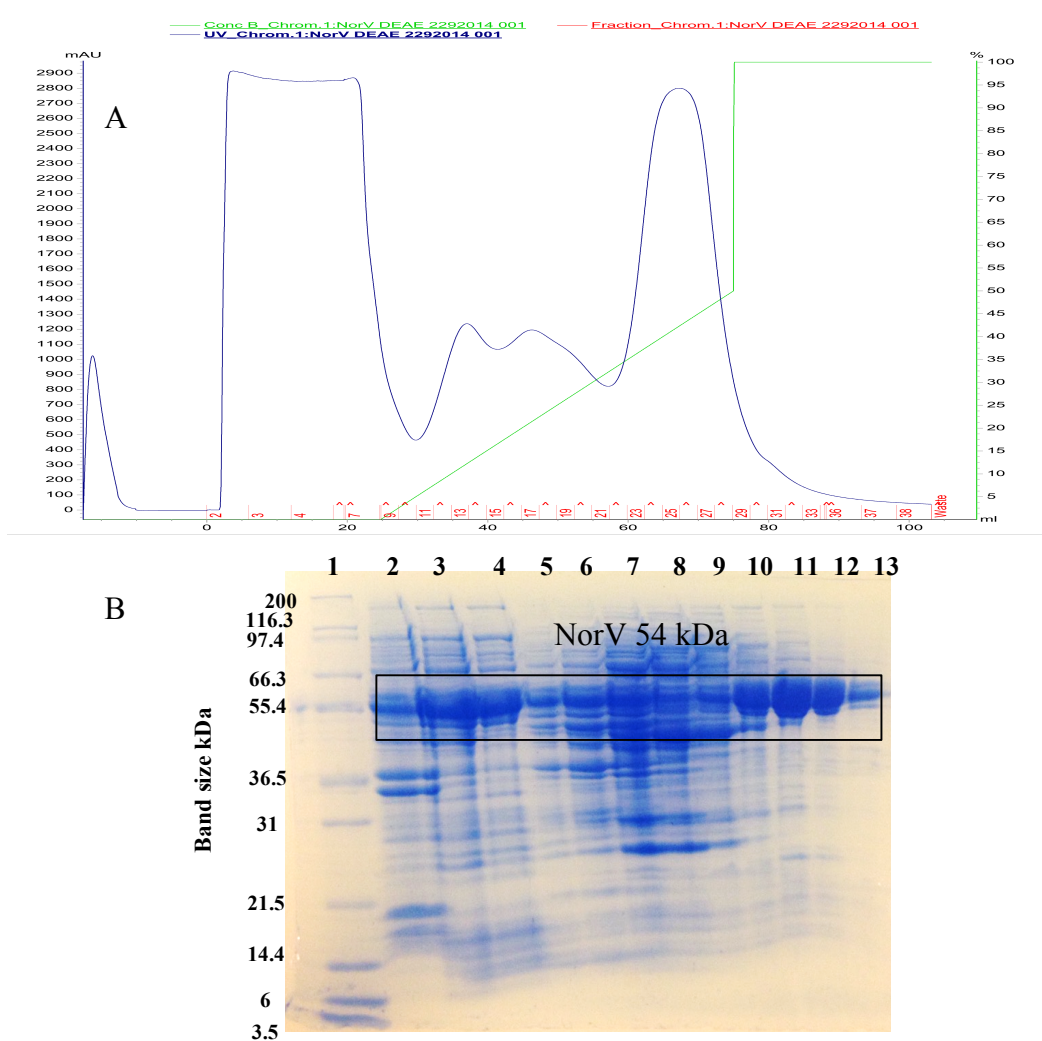


Figure 5.8: NorV purification by using DEAE column. Panel A- Chromatogram showing peaks across fractions 11-29, which were analyzed on SDS-PAGE.

Panel B- SDS-PAGE of DEAE purification of NorV. Lane 1 is mark12 protein marker, lane 2 is cell debris, lane 3 is the cell free extract (CFE), lane 4 is the unbound material, lanes 5-13 are DEAE column fractions (Fractions 13, 15, 17, 19, 21, 23, 25, 27, and 29). The gel displayed bands corresponding to the size of NorV which could be seen in fractions 25 and 27 in lanes 11 and 12.

After the DEAE column, fractions (25-27) each with 2 ml, were combined, concentrated down to 2 ml, and applied on a GF column (Described in Chapter 3, section 3.2.18.2). The results of GF column are shown in the chromatogram (Figure 5.9). The fractions (10-

17) were analyzed by SDS-PAGE (Figure 5.9) and fractions (11-13) were combined together and concentrated down to a final concentration of 12mg/ml in 130 μ l. NorV was purified with around 90% purity after gel filtration.

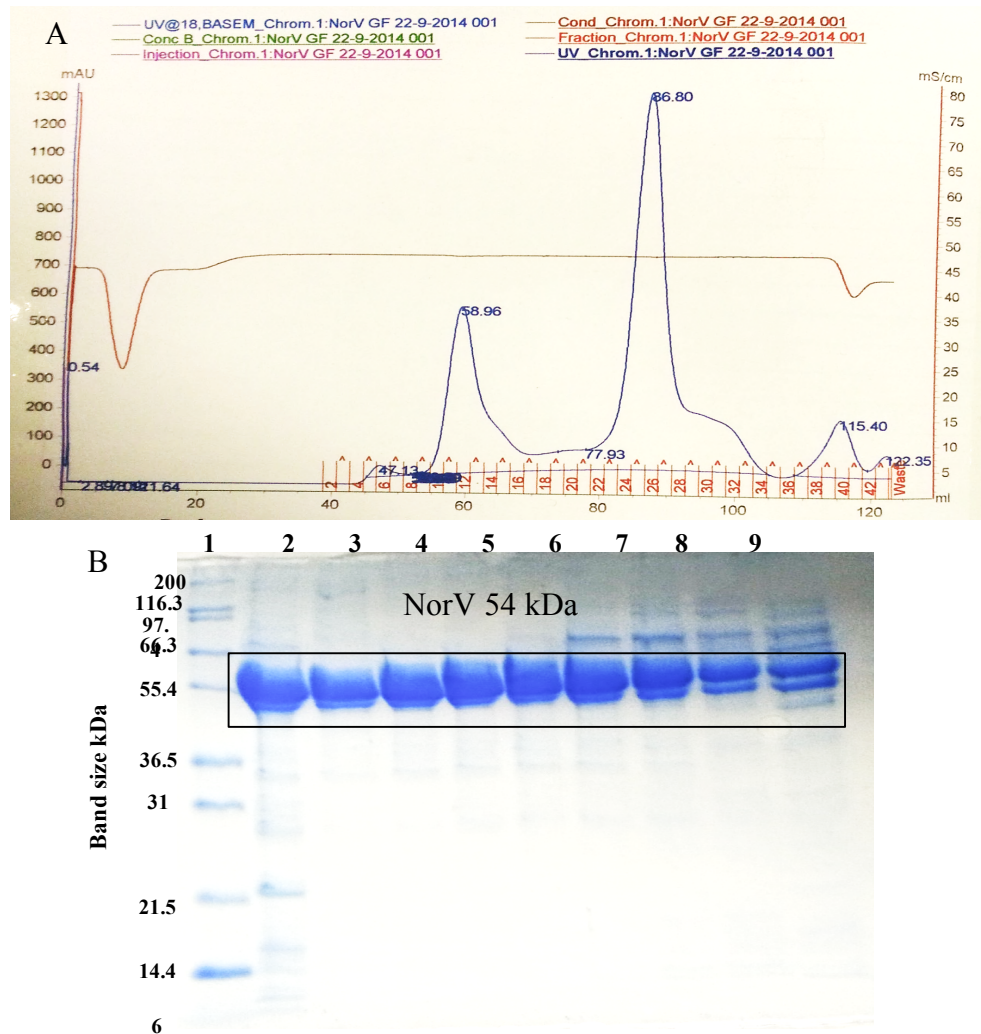


Figure 5.9: Gel Filtration purification. Panel A. Purification of NorV by using a Superdex 200 gel filtration column. The figure shows that NorV was eluted in 58.96 ml, which corresponds to 200 kDa, and suggests NorV is a tetramer.

Panel B. SDS-PAGE analysis of gel filtration purification results of NorV, lane 1 is mark 12, lane 2 is the loaded sample from DEAE purification, lane 3-10 are gel filtration fractions (10-17). The gel shows that fractions 11-13 were the purer fractions, and had the most protein, fractions 14-17 had contaminant proteins. The gel suggested that NorV was approximately 90% pure.

Finally, 130 μ l of 12 mg/ml colored NorV was obtained (Figure 5.10).

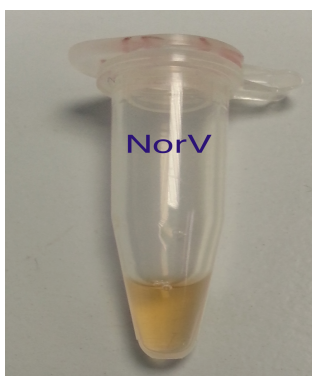


Figure 5.10 NorV purified protein. The figure shows NorV that was obtained after GF. It shows that the NorV solution was colored probably due to the presence of Flavin, which is found within the second domain of the protein (FMN domain).

5.13 NorV Mass spectrometry (MS)

A sample of purified NorV was sent for mass spectrometry as described in Chapter 3, section 3.2.19. The MS result showed that the molecular weight of NorV was 54204.80 Da (Figure 5.11), whereas the calculated molecular weight of the protein is 54234.18 Da, the difference was 29.38 Da. Taking into account that there was a sequence change of Ser 2 to Ala, and the replacement of Lys 478 with Asn and Glu, the molecular weight should be 54200.18 Da, which makes the difference between the molecular sizes 4 Da only.

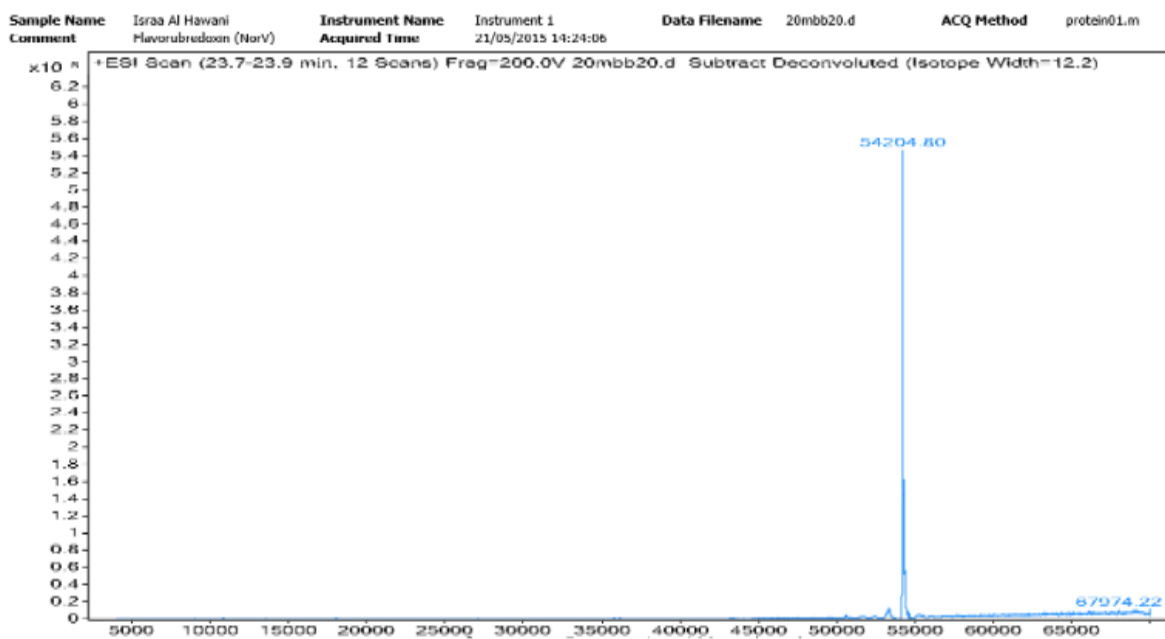


Figure 5.11 Mass spectrum for NorV. The figure shows that the molecular weight of NorV was more than the calculated molecular weight by less than 4 Da. This measurement was taken immediately after NorV was purified.

5.14 Crystallization trial

The purified protein was tested for crystallization by using a Hydra robot via the vapor diffusion (sitting drop) method and a 96 well plate as described in Chapter 3, section 3.2.21. Crystals appeared after 2 days in many conditions of the PACT, JCSG and PEG crystallization screens. Successful conditions included 0.2 M potassium thiocyanate, 0.1 M bis-tris propan pH 7.5 and 20% PEG 3350, 0.2 M Ammonium sulfate, 0.1 M bis-tris pH 5.5 and 25% PEG 3350, 0.2 M sodium iodide and 20% PEG 3350. They were chosen to be optimized by changing precipitant concentration and buffer pHs. All the crystals grew in the initial screens were small and needle shaped (Figure 5.12).

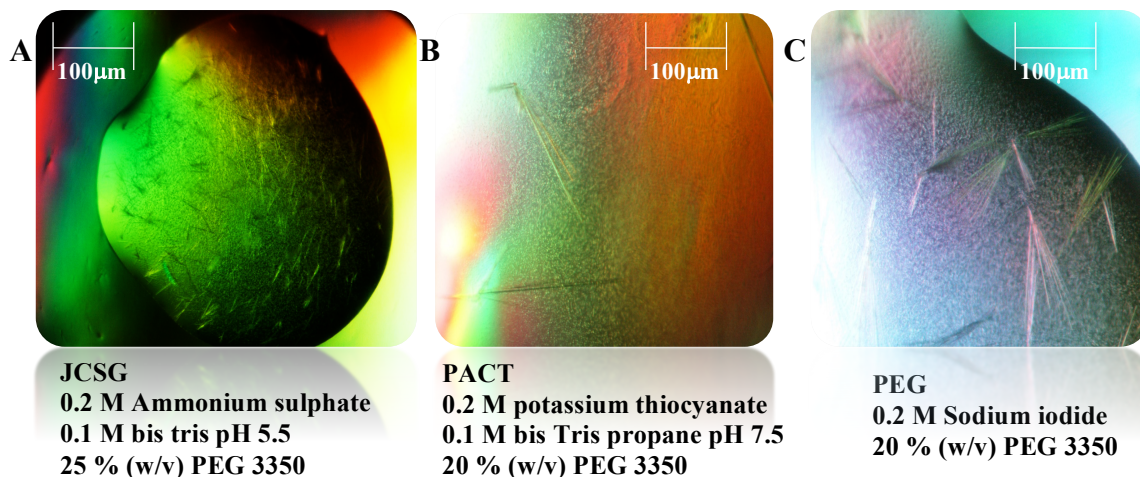


Figure 5.12: NorV crystals in the initial screens. Panel A. Crystals grew in the JCSG screen. They were very tiny needle shape crystals. Panel B. Crystals grew in the PACT screen. They were the largest crystals that grew from NorV. Panel C. Crystals grew in the PEG screen. They were longer than those in the JCSG screen, but shorter than those in the PACT screen, and very thin. Scale bar = 100 μm

Micro-seeding crystallization trial (see section 3.2.21) gave crystals in the PACT and JCSG screen. The JCSG screen crystals were all very tiny. The PACT screen crystals were also thin and needle shaped but long. A crystal grown in 0.2 M sodium sulfate and 20% PEG 3350 was chosen to be sent to the Diamond Light Source for data collection (Figure 5.13).

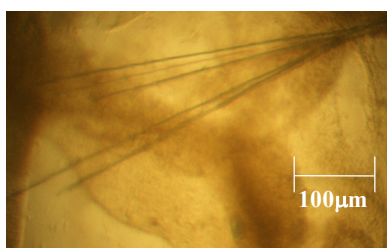


Figure 5.13: NorV crystal grown in 0.2 M sodium sulfate and 20% (w/v) PEG 3350. Scale bar = 100 μm

Further rounds of crystallization screening were carried out for NorV. Many hits appeared in the JCSG and PACT screens after 3-7 days. In the JSCG screen the crystals were in variety of forms, where some were bundled and others were single crystals. They were all

rectangular crystals. Two crystals were chosen to send to the Diamond Light Source which had grown in either 0.2 M calcium acetate hydrate, 0.1 M Sodium cacodylate pH 6.5 and 40% (w/v) PEG 300, or in 0.2 M magnesium chloride hexahydrate, 0.1 M Tris pH 7.0 and 10% (w/v) PEG 8000 (Figure 5.14).

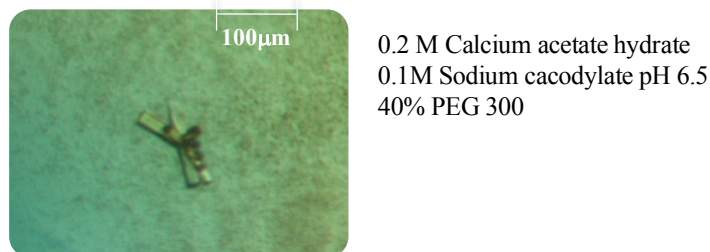


Figure 5.14 NorV crystal grown in the JCSG screen from protein purified with a protease inhibitor. Scale bar = 100 μm .

5.15 Optimization trial

NorV crystals were optimized as described in Chapter 3, section 3.2.22, by using the hanging drop method, with 24 wells plate. After 2 days crystals appeared in the plates. No crystals were grown from the PEG screen, whereas many crystals appeared in the JCSG optimization screen, but they were also very tiny crystals, and were not used for data collection. Crystals were chosen for data collection that were found from the PACT screen and which grew in 0.25 M potassium thiocyanate, 0.1 M bis-Tris propane pH 7.5 and 30% PEG 3350, and in 0.2 M potassium thiocyanate, 0.1 M bis-Tris propane pH 8 and 25% PEG 3350 (Figure 5.15).

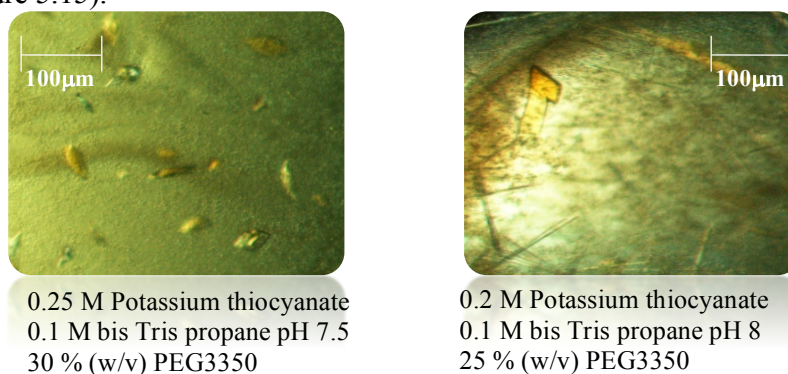


Figure 5.15: NorV optimized crystals. Crystal were identified in the PACT screens and conditions optimized to give larger, single crystals. Scale bar = 100 μm .

Optimization also gave a big rectangular crystal grown in 0.2 M Potassium thiocyanate, 0.1 M bis-Tris propane pH 7.5 and 15% (w/v) PEG 3350 which was sent to the Diamond center for data collection.

5.16 Structure determination

In order to determine the structure of NorV, crystals were sent for X-ray diffraction data collection in the Diamond Light Source (DLS) center near Oxford.

5.16.1 Data collection

All the diffraction data was processed at Diamond by using the Xia2 program, which did the autoindexing, where the unit cell dimensions and the crystal lattice type were determined; the integration, where the diffraction spots of the crystal were integrated to give their intensities; and finally scaling the data, where symmetry related measurements were scaled and merged together to give a unique set, by using the Aimless program (Bailey, 1994). Statistics on the quality of the data set are also generated by analysis of the scaled intensity values.

The first data were collected from crystal grown in 0.2 M Potassium thiocyanate, 0.1 M bis-Tris propane pH 8 and 25% (w/v) PEG3350, on beamline I04. The diffraction resolution was 2.02 Å, the data set was collected, processed by XDS and analysed by Aimless. The average unit cell was determined as 170.7 Å 64.6 Å 75.5 Å, 90.0° 102.5° 90.0° , and the space group was suggested as C 1 2 1 (Table 5.1, figure 5.16). For simplicity, this crystal will be called C2.

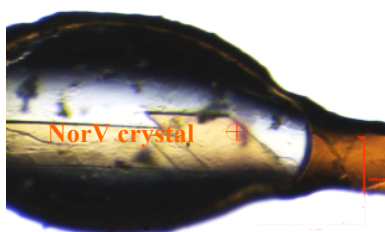


Figure 5.16 NorV C2 crystal grown in 0.2 M Potassium thiocyanate, 0.1 M bis Tris propane pH 8, and 25% (w/v) PEG3350 in the mounting loop, and used for data collection.

Another data set was collected for another crystal grown in 0.2 M Potassium thiocyanate, 0.1 M bis-Tris propane and 15% PEG 3350. The data were collected on beamline I04, the diffraction resolution was 2.05 Å, the data were processed by XDS and analysed by Aimless. The average unit cell was determined as 65.0 Å 80.0 Å 91.1 Å, 72.3° 69.1° 78.9° (Table 5.1), and the space group was suggested as P 1 (Table 5.1). This crystal will be referred to as P 1.

From the micro-seeding experiment, a crystal grown in 0.2 M sodium sulphate and 20% (w/v) PEG 3350 was chosen for X-ray data collection. The data were collected on I03 beamline, the resolution of this dataset was 2.95 Å, and the unit cell dimensions were 135.5 Å 135.5 Å 254.8 Å, 90.0° 90.0° 90.0° (Table 5.1). The space group was suggested as P 41 21 2, and the crystal will be called P4.

The last crystal of NorV sent for X-ray data collection, grown in 0.2 M calcium acetate hydrate, 0.1 M sodium cacodylate pH 6.5, and 40% (w/v) PEG 300 had a data set collected on I03 beamline. The resolution of this dataset was 2.4 Å, and the unit cell dimensions were 149.8 Å 149.8 Å 93.5 Å, 90.0° 90.0° 120.0° (Table 5.1). The space group was suggested as P 622, so the crystal will be called as P6.

Table 5.1. The processing statistics of NorV crystals. The table shows the statistics overall reflections and those in the low and high resolution shells, the unit cell dimensions, and the space group.

	Overall	Low	High
C2 crystal			
Wavelength (Å)	0.97625		
High resolution limit	2.02	9.03	2.02
Low resolution limit	41.65	41.65	2.07
Completeness	96.9	97.8	79.4
Multiplicity	3.2	3.2	2.6
I/sigma	7.7	19.3	2.0
Rmerge	0.084	0.045	0.465
Rmeas(I)	0.130	0.062	0.597
Rpim(I)	0.071	0.034	0.341
Unit cell dimensions			
a, b, c (Å)	170.7	64.6	75.5
α, β, γ (°)	90.0	102.5	90.0
Space group	C121		

	Overall	Low	High
P1 crystal			
Wavelength (Å)	0.97949		
High resolution limit	2.05	9.17	2.05
Low resolution limit	64.71	64.71	2.10
Completeness	97.4	96.2	96.2
Multiplicity	2.6	2.5	2.4
I/sigma	5.4	15.3	1.8
Rmerge	0.140	0.035	0.622
Rmeas(I)	0.203	0.064	0.744
Rpim(I)	0.123	0.039	0.446
Unit cell dimensions			
a, b, c (Å)	65.000	80.030	91.087
α , β , γ (°)	72.256	69.118	78.980
Space group	P1		
	Overall	Low	High
P4 crystal			
Wavelength (Å)	0.97625		
High resolution limit	2.95	13.19	2.95
Low resolution limit	54.73	54.73	3.03
Completeness	99.9	98.7	99.9
Multiplicity	13.3	10.1	13.5
I/sigma	5.7	20.9	0.9
Rmerge	0.533	0.065	3.218

Rmeas(I)	0.575	0.071	3.509
Rpim(I)	0.157	0.022	0.951
Unit cell dimensions			
a, b, c (Å)	135.510	135.510	254.780
α, β, γ (°)	90.000	90.000	90.000
Space group	P 4 ₁ 2 ₁ 2		
	Overall	Low	High
P6 crystal			
Wavelength (Å)	0.97626		
High resolution limit	2.4	6.51	2.40
Low resolution limit	75.84	75.88	2.44
Completeness	100	100.0	100.0
Multiplicity	20.9	17.9	20.8
I/sigma	12.4	38.7	1.7
Rmerge(I)	0.291	0.060	2.113
Rmeas(I)	0.298	0.062	2.166
Rpim(I)	0.065	0.015	0.473
Unit cell dimensions			
a, b, c (Å)	149.77	149.77	93.49
α, β, γ (°)	90	90	120
Space group	P 6 2 2		

5.16.2 Structure determination and model building

5.16.2.1 Matthews probability calculation

To estimate the number of molecules found in the asymmetric unit (AU) of the crystal, the MATTHEWS_COEF program in CCP4 (Collaborative Computational Project, Number 4) suite was used. In this program, the unit cell and the molecular weight of the molecule in the unit cell were used to calculate the Matthews coefficient (V_m), and the solvent content. (Kantardjieff and Rupp, 2003; Matthews, 1968). For C2 crystal, the Matthews calculation gave 3 possible solutions, the best solution as judged by the probability indicator P was 2 molecules in the asymmetric unit. For the P1 crystal based on the results, the Matthews calculation gave 8 solutions; the best solution with 54.58% solvent suggested 4 molecules of NorV in the AU. For P4 crystal, the best solution was 4 copies of NorV in the AU, and for P6, the best solution was one molecule in the AU (Table 5.2).

Table 5.2. Matthews coefficient. The table shows the estimated numbers of molecules in the asymmetric unit (AU) of NorV and also the solvent content in the AU based on the molecular weight (54000 Da).

Nmol/asym	Matthews Coeff	%solvent	P (2.02)	P(tot)
C2				
1	3.77	67.35	0.16	0.30
2	1.88	34.71	0.83	0.69
3	1.26	2.06	0.01	0.01

Nmol/asym	Matthews Coeff	%solvent	P (2.05)	P(tot)
P1				
1	7.77	84.18	0.00	0.00
2	3.88	68.36	0.03	0.05
3	2.59	52.53	0.65	0.69
4	1.94	36.71	0.32	0.26
5	1.55	20.89	0.00	0.00
6	1.29	5.07	0.00	0.00

Nmol/asym	Matthews Coeff	%solvent	P (2.95)	P(tot)
P4				
1	10.82	88.64	0.00	0.00
2	5.41	77.29	0.00	0.00
3	3.61	65.93	0.08	0.06
4	2.71	54.58	0.43	0.38
5	2.16	43.22	0.46	0.52
6	1.80	31.87	0.02	0.03
7	1.55	20.51	0.00	0.00
8	1.35	9.16	0.00	0.00

Nmol/asym	Matthews Coeff	%solvent	P (2.5)	P(tot)
P6				
1	2.80	56.08	0.99	0.99
2	1.40	12.15	0.01	0.01

5.16.2.2. Molecular replacement

Determination of the initial phases needed to calculate an electron density map was performed by molecular replacement using PHASER program (McCoy et al., 2007), with chain A of the recently determined *E. coli* NorV model (Protein Data Bank entry: 4D02) that was released in the Protein Data Bank (PDB) at the same time as the data on the C2 form was collected (and the data from the crystal in C2 form). *E. coli* NorV deposited in the PDB was in P 6 2 2 space group, at 1.75 Å with a monomer in the asymmetric unit. The molecular replacement gave a final solution with Translation Factor score (TFZ), Rotation Factor score (RFZ), and Long Likelihood Gain (LLG) values as RFZ=34.6 TFZ=33.2 PAK=0 LLG=2223 RF++ TFZ=88.1 PAK=0 LLG=10635 LLG=11222. The resulting map showed that the electron density was in a good agreement with the protein model except in the C and N-terminal ends. Initially FMN and Fe centre were left out of the model (Figure 5.17).

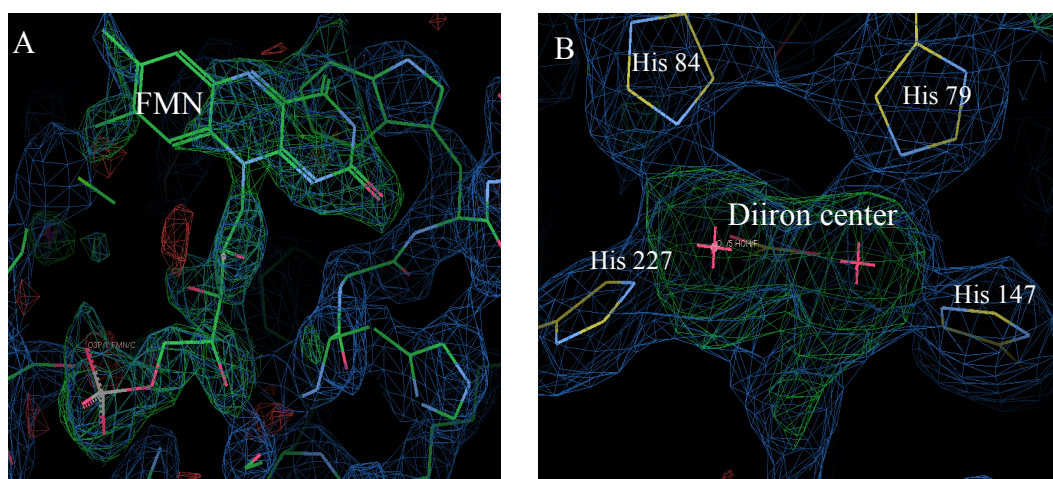


Figure 5.17: The initial density map produced from Phaser program. Panel A shows a large positive peak in the difference density maps at the expected FMN site, which was initially left out of the search model, and then built into the model using the map. Panel B shows the positive peaks at the expected diiron centre, which was left out of the model, surrounded by 4 histidine residues.

5.16.2.3 Model refinement

The model was refined by using REFMAC5 (Murshudov et al., 1997) and the uncertainty in the atomic positions was modelled by applying isotropic B-factors. Following refinement of the initial parameters of the coordinates in REFMAC5 using the first phase estimated from PHASER. Fe atoms at the diiron centre and FMN were added. The output file was examined in COOT (Emsley and Cowtan, 2004; Emsley et al., 2010), and amino acids position were changed, to improve the fit to the map. Rounds of building and refinement were carried out using COOT and REFMAC5 to improve the model. The statistics are shown in (Table 5.3) and Figure (5.19) shows how the refinement improves the electron density map around the FMN and diiron centre.

Table 5.3 The results of final refinement of NorV crystal forms judging from the R factor.

C2	Initial	Final
R factor	0.2819	0.2686
R free	0.2922	0.2862
r.m.s.d Bond Length	0.0075	0.0094
r.m.s.d Bond Angle	1.0346	1.1487
r.m.s.d Chiral Volume	0.0468	0.0585

P1	Initial	Final
R factor	0.2120	0.2093
R free	0.3040	0.3019
r.m.s.d Bond Length	0.0788	0.0716
r.m.s.d Bond Angle	5.2102	5.1759
r.m.s.d Chiral Volume	0.3554	0.3613

P4	Initial	Final
R factor	0.3179	0.2505
R free	0.3219	0.3083
r.m.s.d Bond Length	0.0099	0.0120
r.m.s.d Bond Angle	1.1429	1.6383
r.m.s.d Chiral Volume	0.0571	0.1130

P6	Initial	Final
R factor	0.1998	0.1813
R free	0.2418	0.2231
r.m.s.d Bond Length	0.0213	0.0238
r.m.s.d Bond Angle	2.1746	2.3542
r.m.s.d Chiral Volume	0.1291	0.1379

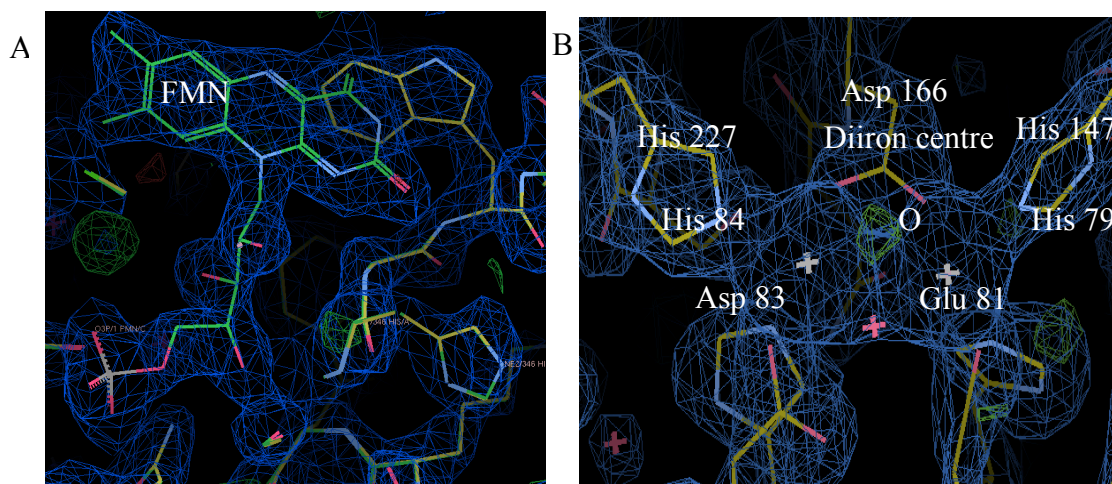


Figure 5.18: Steps of NorV structure refinement using REFMAC5. A- After refinement the FMN fitted very well into the electron density, which covers the FMN totally. B- The fit of the diiron centre with the electron density map was very good and the iron was clearly coordinated by four histidine residues and Asp 166, Glu 81 and Asp 83.

5.16.2.4 Final refined structure

The final structure of NorV was determined as a tetramer, where each subunit consists of two main domains, a β -lactamase-like domain with a diiron centre and a FMN-like domain with FMN. In the tetramer, the FMN and the Fe-centre from different monomer subunits are close to each other separated by 9.6 Å, whereas in the monomer they are well separated by 40.9 Å (Figure 5.19). There is electron transfer between the rubredoxin domain at the C-terminus of the protein to the diiron center in the β -lactamase-like domain at the N-terminus, thus the two domains should be close to each other for electron transfer purpose.

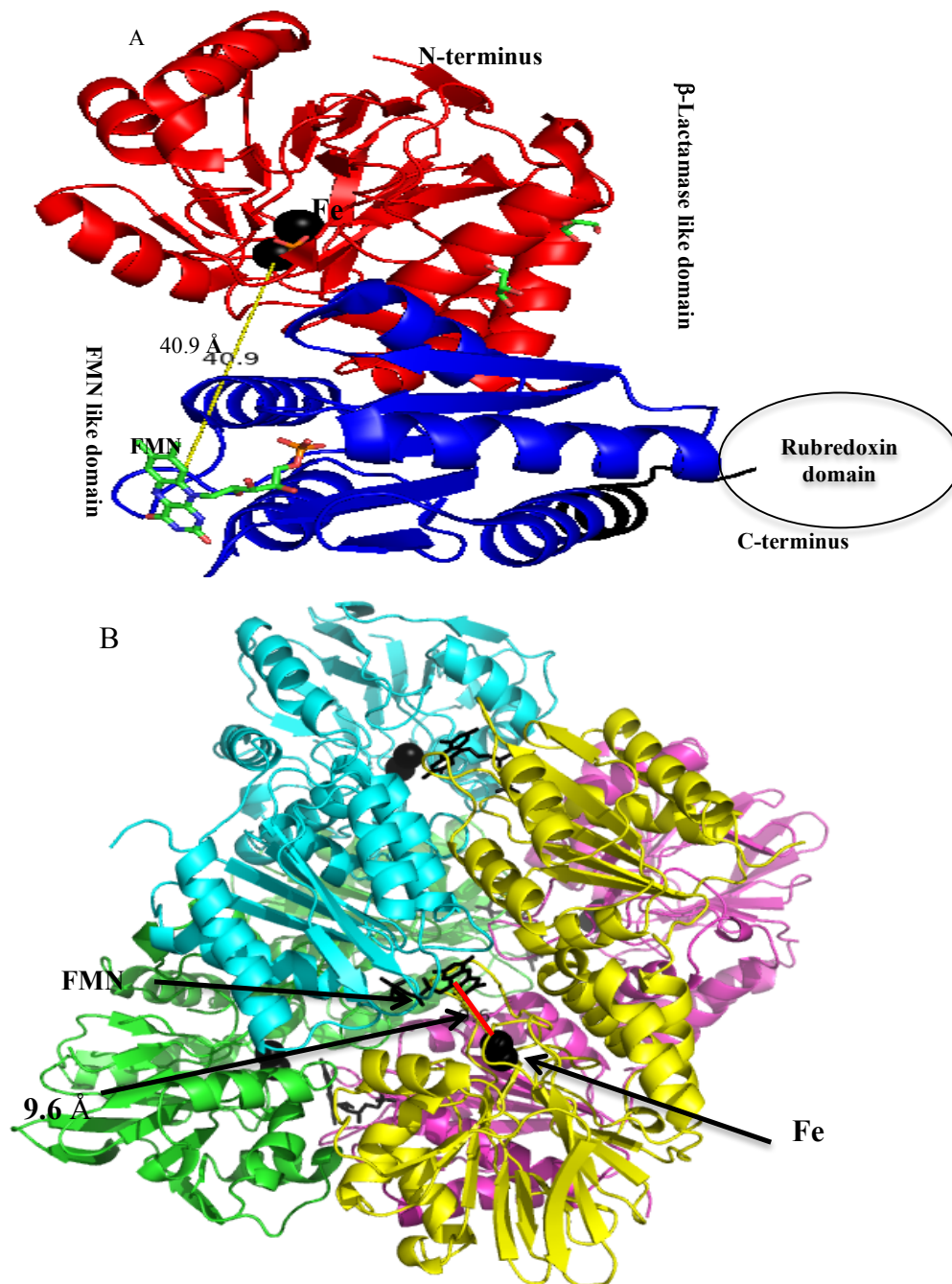


Figure 5.19: The final structure of NorV. A- shows the monomer structure which start from N-terminal β -lactamase like domain (red) consist of 250 amino acids and a diiron center, and the FMN like domain (blue) which is 132 amino acids with an FMN cofactor, and finishes with a rubredoxin domain of 59 amino acids with a 20 amino acids linker that could not observed in the map. In the monomer, the distance between the Fe and FMN is measured as 40.9 Å. B- A tetramer subunit of NorV. It shows that diiron centre (Fe) of one monomer is closed to the FMN of another monomer (9.6 Å), and thus allowing the electron transfer between them. Each monomer is colored in a different color (pink, yellow, green and blue)

The rubredoxin-like domain, was not seen in the electron density map, although there was a space within the lattice (Figure 5.20)

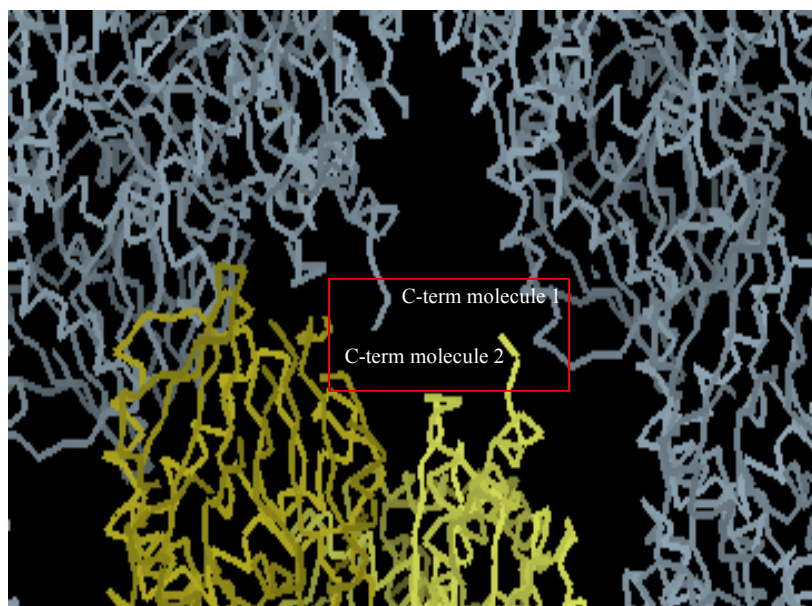


Figure 5.20: NorV crystal lattice showed that there is some space adjacent to the C-terminal end of the model (boxed in red), which might fit with the rubredoxin domain. The yellow color represents C2 model and the gray color represent the adjacent molecules in the crystal lattice.

Further investigations were carried out to discover if the rubredoxin was cleaved from the protein or it was simply not detected in the map. Simple tests were carried out as described in Chapter 3, section 3.2.25.3.

Loading NorV crystals on SDS-PAGE shows two bands. Another faint band on the gel just below the protein band was observed in both purified NorV and a solution from a dissolved crystal. The faint band in the purified protein might be the signs of a protease degradation of the fully intact protein. The band on the gel from the dissolved crystals appeared only ~6 kDa smaller than the entire molecular weight (54 kDa). This might suggest that the protein hasn't lost the entire rubredoxin domain, which is ~7 kDa (Figure 5.22). However, the small difference between the correct weight and observed band from the crystals, suggests that the intact rubredoxin domain may not have been lost, and perhaps

suggests that part of it was lost. This would be consistent with the space for some residues of a rubredoxin domain in the crystal lattice.

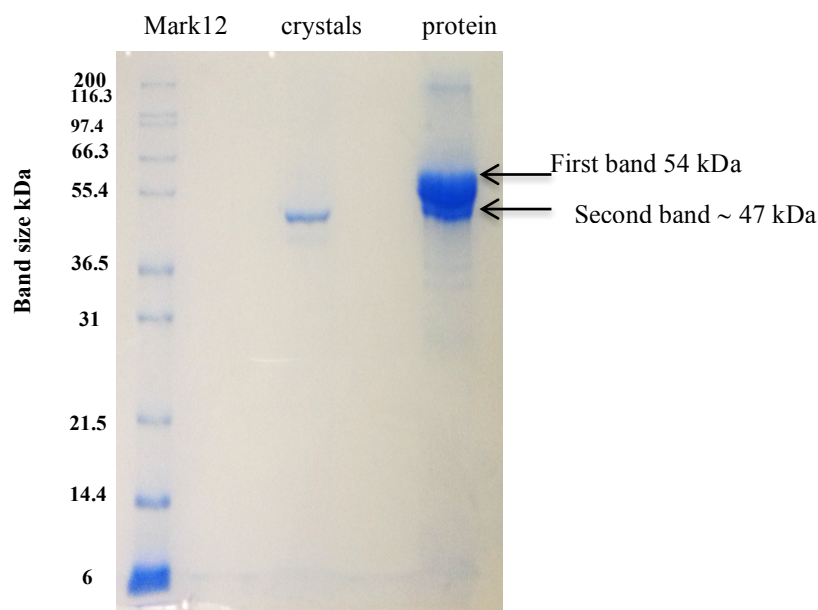


Figure 5.21: SDS-PAGE of NorV crystal solution. The figure shows that loading a solution of NorV crystals (10 crystals), with purified protein reveals that the NorV was cleaved in both crystallized and non-crystallized solution. Two bands were seen where one corresponded to full-length protein molecular weight (54 kDa), and the other band corresponded to a smaller size fragment.

Further confirmation was performed by sending the sample of the purified protein to mass spectrometry, the mass spectrum results showed that the protein molecular weight was 46.269 kDa (Figure 5.22), whereas the predicted NorV molecular weight including sequence changes is 54.200 kDa, there is a difference of 7.9 kDa which corresponds to the rubredoxin molecular (6.5 kDa) weight plus 13 residues. Although, there was a space in our crystal lattice, it is difficult to see how the rubredoxin domain can fit in it when the other molecules packed around (Figure 5.20).

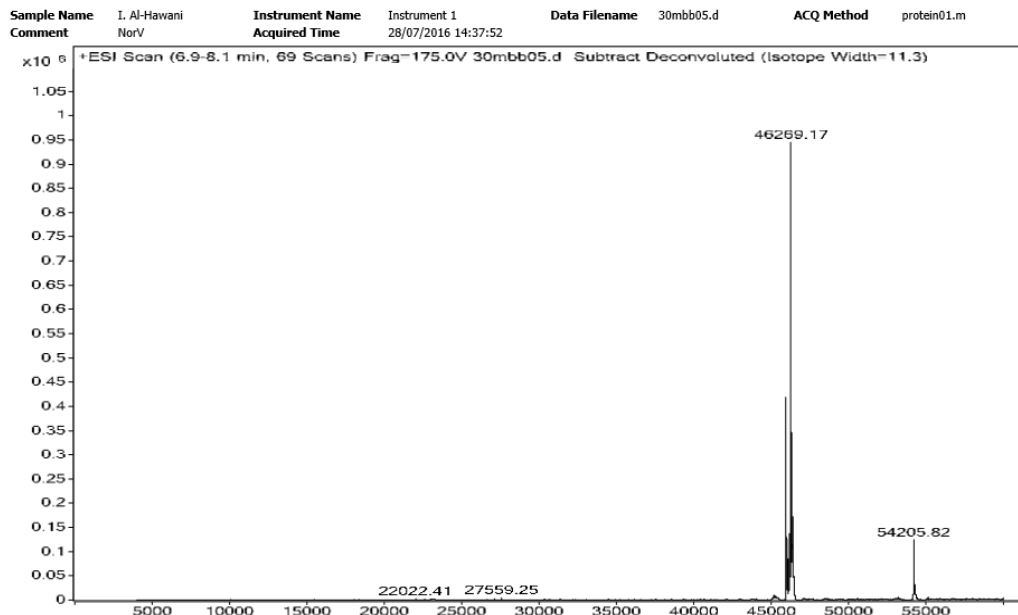


Figure 5.22: MS for NorV protein diagnosis. The figure shows the result of NorV sample kept in room temperature for 2 weeks. It shows that the major molecular weight was 46.269 kDa which corresponds to the molecular weight of NorV (54.200 kDa) minus 72 amino acids missing from the C- terminal end (including the rubredoxin domain).

5.16.3 Comparison of *E. coli* NorV structures

Different space groups were obtained from different crystals of NorV (C121, P1, P622, and P4₁ 2₁ 2). The overall structure of each model was compared with the other models, the result showed that the r.m.s.d on alpha carbon position varied between 0.0-0.4568 Å (Table 5.4). The results suggested that the overall structure of the four models was very similar.

Table 5.4 Statistics of NorV structures superposed. The table shows the r.m.s.d result from the comparison of each chain in NorV model with the other chains in the other models

		C2		P1			P4				P6
		A	B	A	B	C	A	B	C	D	A
C2	A	quality Q: 1.0000 r.m.s.d: 0.0000 (A)	quality Q: 0.9983 r.m.s.d: 0.1236 (A)	quality Q: 0.9881 r.m.s.d: 0.3293 (A)	quality Q: 0.9881 r.m.s.d: 0.2501 (A)	quality Q: 0.9810 r.m.s.d: 0.2871 (A)	quality Q: 0.9814 r.m.s.d: 0.2806 (A)	quality Q: 0.9890 r.m.s.d: 0.3169 (A)	quality Q: 0.9910 r.m.s.d: 0.2866 (A)	quality Q: 0.9904 r.m.s.d: 0.2952 (A)	quality Q: 0.9950 r.m.s.d: 0.2133 (A)
	B	quality Q: 0.9983 r.m.s.d: 0.1236 (A)	quality Q: 1.0000 r.m.s.d: 0.0000 (A)	quality Q: 0.9889 r.m.s.d: 0.3184 (A)	quality Q: 0.9888 r.m.s.d: 0.2376 (A)	quality Q: 0.9921 r.m.s.d: 0.2675 (A)	quality Q: 0.9909 r.m.s.d: 0.2873 (A)	quality Q: 0.9887 r.m.s.d: 0.3206 (A)	quality Q: 0.9904 r.m.s.d: 0.2950 (A)	quality Q: 0.9900 r.m.s.d: 0.3009 (A)	quality Q: 0.9941 r.m.s.d: 0.2314 (A)
P1	A	quality Q: 0.9881 r.m.s.d: 0.3293 (A)	quality Q: 0.9889 r.m.s.d: 0.3184 (A)	quality Q: 1.0000 r.m.s.d: 0.0000 (A)	quality Q: 0.9907 r.m.s.d: 0.1972 (A)	quality Q: 0.9810 r.m.s.d: 0.2872 (A)	quality Q: 0.9719 r.m.s.d: 0.4092 (A)	quality Q: 0.9773 r.m.s.d: 0.4568 (A)	quality Q: 0.9799 r.m.s.d: 0.4298 (A)	quality Q: 0.9805 r.m.s.d: 0.4229 (A)	quality Q: 0.9826 r.m.s.d: 0.3991 (A)
	B	quality Q: 0.9881 r.m.s.d: 0.2501 (A)	quality Q: 0.9888 r.m.s.d: 0.2376 (A)	quality Q: 0.9907 r.m.s.d: 0.1972 (A)	quality Q: 1.0000 r.m.s.d: 0.0000 (A)	quality Q: 0.9813 r.m.s.d: 0.1858 (A)	quality Q: 0.9718 r.m.s.d: 0.3499 (A)	quality Q: 0.9771 r.m.s.d: 0.4064 (A)	quality Q: 0.9797 r.m.s.d: 0.3745 (A)	quality Q: 0.9804 r.m.s.d: 0.3661 (A)	quality Q: 0.9829 r.m.s.d: 0.3331 (A)
	C	quality Q: 0.9810 r.m.s.d: 0.2871 (A)	quality Q: 0.9921 r.m.s.d: 0.2675 (A)	quality Q: 0.9810 r.m.s.d: 0.2872 (A)	quality Q: 0.9813 r.m.s.d: 0.1858 (A)	quality Q: 1.0000 r.m.s.d: 0.0000 (A)	quality Q: 0.9840 r.m.s.d: 0.3824 (A)	quality Q: 0.9644 r.m.s.d: 0.3821 (A)	quality Q: 0.9816 r.m.s.d: 0.4109 (A)	quality Q: 0.9730 r.m.s.d: 0.3965 (A)	quality Q: 0.9752 r.m.s.d: 0.3012 (A)
P4	A	quality Q: 0.9814 r.m.s.d: 0.2806 (A)	quality Q: 0.9909 r.m.s.d: 0.2873 (A)	quality Q: 0.9719 r.m.s.d: 0.4092 (A)	quality Q: 0.9718 r.m.s.d: 0.3499 (A)	quality Q: 0.9840 r.m.s.d: 0.3824 (A)	quality Q: 1.0000 r.m.s.d: 0.0000 (A)	quality Q: 0.9742 r.m.s.d: 0.3163 (A)	quality Q: 0.9921 r.m.s.d: 0.2680 (A)	quality Q: 0.9850 r.m.s.d: 0.2142 (A)	quality Q: 0.9833 r.m.s.d: 0.2473 (A)

	B	quality Q: 0.9890 r.m.s.d: 0.3169 (A)	quality Q: 0.9887 r.m.s.d: 0.3206 (A)	quality Q: 0.9773 r.m.s.d: 0.4568 (A)	quality Q: 0.9771 r.m.s.d: 0.4064 (A)	quality Q: 0.9840 r.m.s.d: 0.3824 (A)	quality Q: 0.9742 r.m.s.d: 0.3163 (A)	quality Q: 1.0000 r.m.s.d: 0.2135 (A)	quality Q: 0.9950 r.m.s.d: 0.3296 (A)	quality Q: 0.9881 r.m.s.d: 0.2822 (A)	quality Q: 0.9912 r.m.s.d: 0.2822 (A)
	C	quality Q: 0.9910 r.m.s.d: 0.2866 (A)	quality Q: 0.9904 r.m.s.d: 0.2950 (A)	quality Q: 0.9799 r.m.s.d: 0.4298 (A)	quality Q: 0.9797 r.m.s.d: 0.3745 (A)	quality Q: 0.9816 r.m.s.d: 0.4109 (A)	quality Q: 0.9921 r.m.s.d: 0.2680 (A)	quality Q: 0.9950 r.m.s.d: 0.2135 (A)	quality Q: 1.0000 r.m.s.d: 0.0000 (A)	quality Q: 0.9914 r.m.s.d: 0.2800 (A)	quality Q: 0.9932 r.m.s.d: 0.2486 (A)
	D	quality Q: 0.9904 r.m.s.d: 0.2952 (A)	quality Q: 0.9900 r.m.s.d: 0.3009 (A)	quality Q: 0.9805 r.m.s.d: 0.4229 (A)	quality Q: 0.9804 r.m.s.d: 0.3661 (A)	quality Q: 0.9730 r.m.s.d: 0.3965 (A)	quality Q: 0.9850 r.m.s.d: 0.2142 (A)	quality Q: 0.9881 r.m.s.d: 0.3296 (A)	quality Q: 0.9914 r.m.s.d: 0.2800 (A)	quality Q: 1.0000 r.m.s.d: 0.0000 (A)	quality Q: 0.9923 (A) r.m.s.d: 0.2645 (A)
P6	A	quality Q: 0.9950 r.m.s.d: 0.2133 (A)	quality Q: 0.9941 r.m.s.d: 0.2314 (A)	quality Q: 0.9826 r.m.s.d: 0.3991 (A)	quality Q: 0.9829 r.m.s.d: 0.3331 (A)	quality Q: 0.9752 r.m.s.d: 0.3012 (A)	quality Q: 0.9833 r.m.s.d: 0.2473 (A)	quality Q: 0.9912 r.m.s.d: 0.2822 (A)	quality Q: 0.9932 r.m.s.d: 0.2486 (A)	quality Q: 0.9923 r.m.s.d: 0.2645 (A)	quality Q: 1.0000 r.m.s.d: 0.0000 (A)

The crystal with C2 space group was used for model building and structure solving. The overall structure comparison between C2 chain A and 5LMC showed r.m.s.d: 0.2559 (A) and chain B with 5LMC showed r.m.s.d: 0.2597 (A) (Figure 5.23).

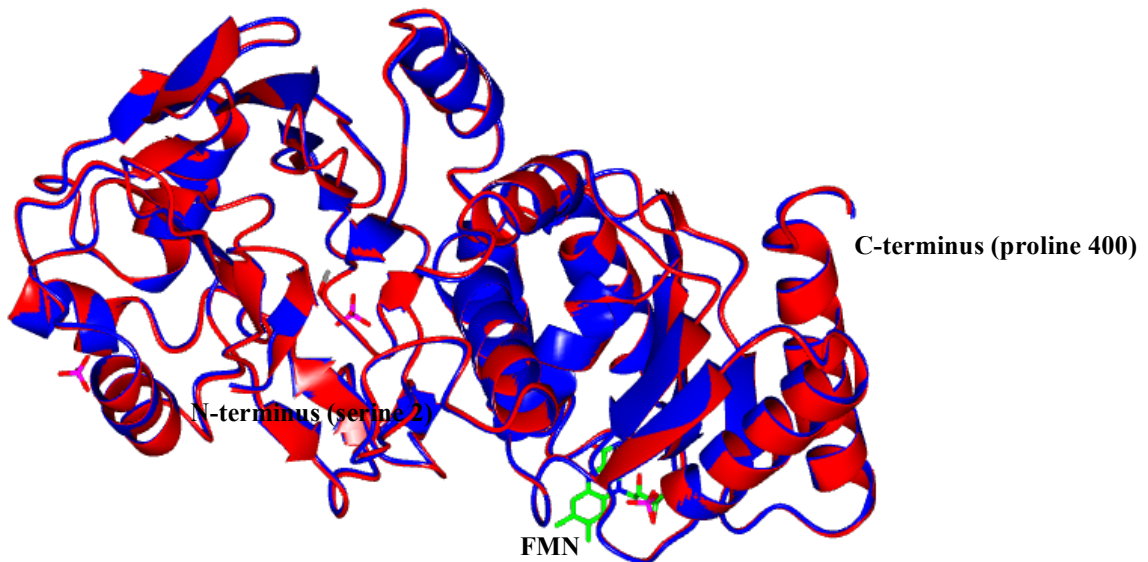


Figure 5.23: Superposition of C2 model chain A with chain A of PDB entry 5LMC. The figure shows that the overall structure of both chains superimpose very well with only a slight shift in the C-terminal residue (Pro 400), and the N-terminal residue (Ser 2). The blue cartoon structure is C2 and the red cartoon structure is 5LMC (Figure was generated by using CCP4 MG program).

The C2 structure also was compared with the homologue protein FprA from *Moorella thermoacetica* (PDB entry ID 1YCG), the superposition of chain A from C2 with chain A from 1YCG showed that there were shifts between two models especially in the loops as shown in figure 5.24. The quality value Q was 0.7690, and the r.m.s.d for alpha carbon atom was 1.5059, by align 391 alpha carbon positions. FprA contains flavin mononucleotide (FMN) and a non-heme diiron site, it shows O₂ and/or anaerobic NO consumption activity.

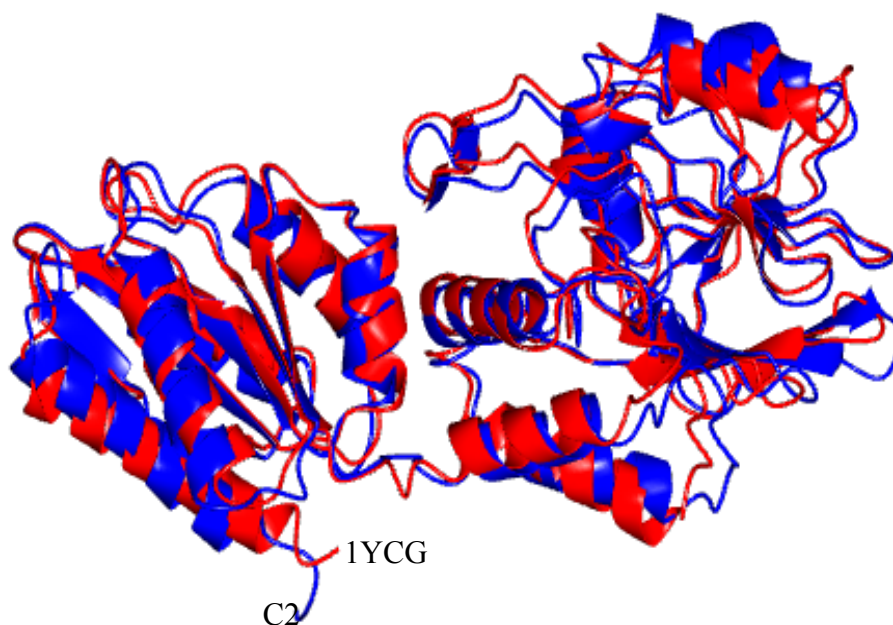


Figure 5.24: Superposition of NorV C2 crystal structure with *Moorella thermoacetica* flavoprotein A (FprA 2) NorV homologue. The red cartoon structure is 1YCG and the blue cartoon structure is C2, it shows that there are changes mainly in loops confirmation.

The C2 model had electron density between the two irons and oxygen was used to model this density and it refined well. In 5LMC structure, the same position was also occupied by a bridging oxygen. In the C2 form there was no electron density corresponding to a PO_4^- that was found in the 5LMC structure (Figure 5.25) and presumably originated from the crystallization conditions

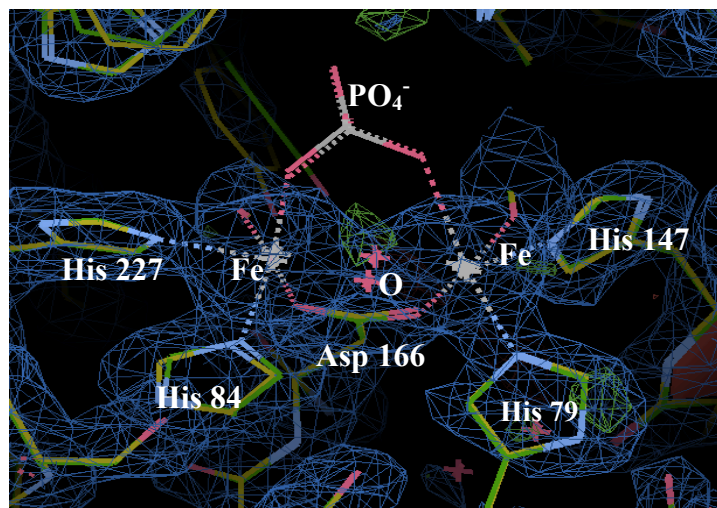


Figure 5.25: NorV (C2 and 5LMC) models superimpose. The figure shows a comparison between NorV models (C2 and 5LMC). It shows that C2 model had no electron density refer to PO_4^- group that found in 5LMC model, but it shows a density that was refined with oxygen. The carbon atom in 5LMC are green and those in the C2 model are yellow.

In contrast, an electron density possibly corresponding to a PO_4^- and oxygen between the Fe ions was found in the P1 crystal form (Figure 5.26).

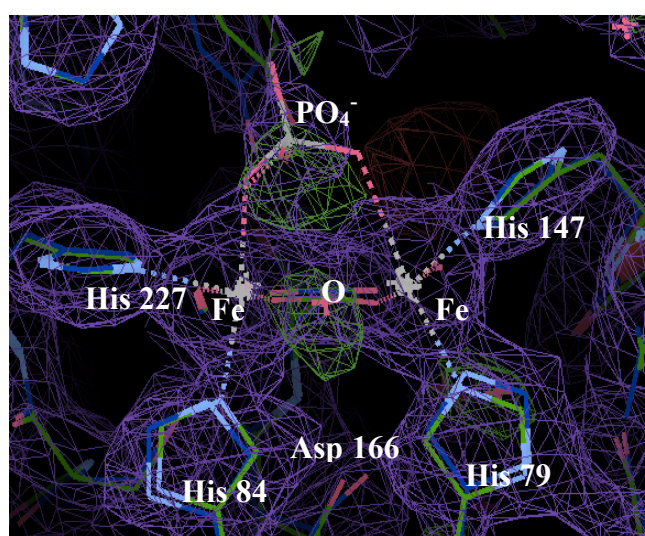


Figure 5.26: NorV P1 and 5LMC models superimpose. The figure shows a comparison between P1 and 5LMC models of NorV, an electron density refers to PO_4^- group and

oxygen between Fe ions was found in P1. Carbon atoms in the P1 model shows in blue, and in the 5LMC shows in green.

In the P4 form of NorV, when superimposed with the 5LMC model, there was also electron density that was refined as a PO_4^- , but no density was observed for the oxygen between the Fe atoms (Figure 5.27).

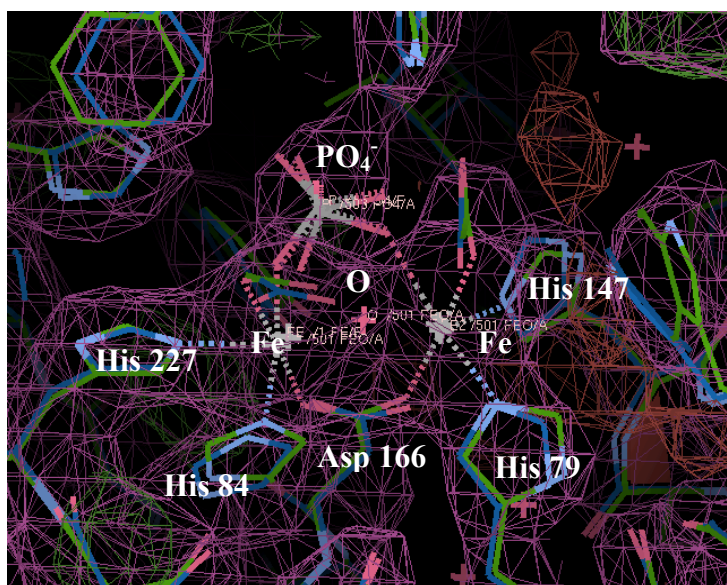


Figure 5.27: NorV 5LMC and P4 models superimpose. The figure shows a comparison between the P4 and 5LMC models of NorV. It shows that the P4 model has an electron density refer to PO_4^- group, which was refined with a PO_4^- , but no density was observed for the oxygen between the Fe ions which found in the 5LMC model. The green carbon atoms are for 5LMC and the blue carbon atoms are for the P4 model.

In the P6 crystal there was no electron density corresponding to the PO_4^- , which was found in the 5LMC structure, but an electron density was observed in the oxygen site between the Fe atoms, which refined successfully (Figure 5.28).

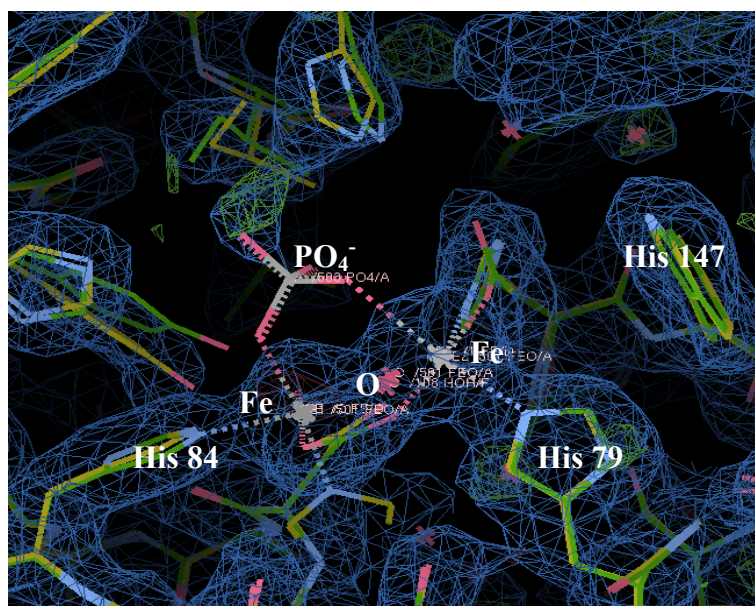


Figure 5.28: NorV 5LMC and P6 models superimpose. The P4 model has electron density corresponding to the oxygen between the Fe ions, and no density was observed for the PO_4^- that was found in the 5LMC model.

5.17 Discussion

NO is a toxic gas for bacteria and the antimicrobial action of NO has been studied intensively (Mancinelli and McKay, 1983; McMullin et al., 2005; Shank et al., 1962). NO toxicity comes mainly through interaction with the metallic center of important enzymes, such as heme and non-heme containing enzymes and enzymes with iron- sulfur clusters (Vallance and Charles, 1998).

Many bacteria including *E. coli* have developed mechanisms to disrupt the effect of NO. Among these mechanisms includes the use of flavohemoglobin, an oxygen-binding, cyanide-sensitive enzyme that oxidizes NO to NO_3^- (Gardner and Gardner, 2002; Gardner et al., 1998b; Gardner et al., 1998d). The role of flavorubredoxin (NorV) and its partner flavorubredoxin oxidoreductase (NorW) in NO detoxification has also been reviewed; NorV reduces NO to N_2O in an anoxic environment by the electron transfer from NADH via NorW to NorV (Gardner et al., 2002; Helmick and Gardner, 2002; Romao et al., 2016).

NorV contains three main domains: An N-terminal β -lactamase like domain (250 amino acids) with a diiron center, an FMN-like domain (132 amino acids), with FMN, which binds a C-terminal rubredoxin domain (59 amino acids). In the current study, the structure of *E. coli* NorV was determined, and functional assays were carried out to investigate the role of NorV in NO detoxification. The results of those studies will be discussed in this section.

5.17.1 NorV production

NorV was successfully expressed in *E. coli* Top10 cells, with 2% (w/v) arabinose. During the expression, it has been noticed that a band slightly below NorV band existed, which might suggest that NorV was degraded after expression. The degradation was less at 3 h expression but increased with time (see figure 5.5) and a compromise which gave better expression at 5 h and overnight could be used.

The protein showed approximately 40% solubility, which was enough to get sufficient material for further studies as Crystallization. The sonication methods applied to destroy cells before the supernatant was separated by centrifugation, was perhaps not very efficient, and causes bad separation of supernatant from pellets, which left the protein in the pellet more than supernatant. However, large scale of protein production was achieved in 500 ml cultures, which was used for protein purification.

5.17.2 NorV purification

NorV was expressed as a non-His tagged protein and this complicated the purification as more than one step was needed to purify NorV with sufficient purity for crystallization. The protein was purified on ion exchange (DEAE) and gel filtration (Superdex 200) columns. A band slightly below the band corresponding to NorV was observed during purification, which might indicate that NorV was degraded during purification (See Figure 5.9). After GF the protein was purified at approximately 85%, but the degradation was still occurred, adding protease inhibitor (to prevent degradation) did not make any improvement, the

protein was still shown a band of degraded version. It was not easy to notice the rubredoxin band (~7 kDa) on SDS-PAGE, but when a sample of protein was sent to MS analysis, the result showed that the protein was cleaved between residue 407 (Asn) and 408 (Thr), which might be due to the proteinase K activity which has a cleavage site between Asp and Thr.

5.17.3 NorV structure refinement and final structure

After phase determination, the models (C2, P1, P4 and P6) were refined by changing some residues side chain positions or orientation and adding water and solvent molecules. Models were validated by monitoring R-values after each refinement round; also, the refinement was evaluated by checking the Ramachandran plot. During refinement rounds the R free was decreased, which meant that the fit of the model to the map was improved (as shown in table 5.3).

The overall structure of NorV crystals (C2, P1, P4 and P6) showed the same overall structure of the 5LMC, with two domains (β -lactamase like domain and FMN-like domain). The rubredoxin was not observed in all our data. Investigations to find the missing domain showed that the rubredoxin domain was cleaved during purification. Although the full-length protein with rubredoxin domain was obtained in 5LMC model (according to MS analysis of the re-dissolved crystal) (Romao et al., 2016), the Rd domain was still not observed in the crystal structure, which suggests that the rubredoxin is a disordered domain. In the C2 form there was a small space in the crystal lattice which might fit a few residues (see Figure 5.20), and this agrees with the result of the MS which suggest that the protein contains 407 residues, 389 residues of the FDP domain (β -lactamase like domain and FMN domain) and 18 residues linker between the Rd and FMN domains.

5.17.4 Comparison between *E. coli* NorV models and homologues

During the C2 data processing a model of *E. coli* NorV was released in the PDB database (PDB ID 5LMC), this model was used for molecular replacement.

A comparison between *E. coli* NorV models from my study (C2, P1, P4 and P6) with *E. coli* NorV (PDB entry ID 5LMC) was performed. The result showed that the C2 crystal was the closest structure to 5LMC the overall structures were fitted very well, only a slight change was seen in the C and N-terminal ends. The r.m.s.d was 0.2559 when chains A from each model (C2 and 5LMC) was aligned, and 0.2597 when chain B from the C2 aligned with chain A from the 5LMC model, which indicated that the overall structure was very similar. In the 5LMC model oxygen-bridge was found between the diiron center, in the C2 and P6 models the same positive electron density was refined with water molecule, no electron density was seen in the same position in the P1 and P4 models. In the 5LMC model there was an electron density refined with phosphate group (PO_4^-) next to the diiron center (Figures 5.25, 5.26, 5.27, and 5.28) this density was only seen in the P4 model, no phosphate was found in the crystallization solution (0.2 M sodium sulphate and 20% (w/v) PEG 3350) in the P4 crystal and for the 5LMC (0.2 M magnesium acetate, 0.2 M sodium cacodylate buffer pH 6.5, 20% (w/v) PEG8000, and 0.2 μL of 0.1 M hexamine cobalt (III) chloride).

**Chapter 6 : Does Cor protect *E. coli*
from CO toxicity?**

6. Introduction

This Chapter will describe experiments that were done to examine whether mycobacterial carbon monoxide resistance protein (Cor) could protect *E. coli* from CO toxicity. It has been proposed that Cor can protect *E. coli* transformed with the expression vector from CO toxicity (Zacharia et al., 2013). The *Mycobacterium tuberculosis cor* expression vector (pJ401) was generously gifted from Dr. Michael Shiloh, University of California at San Francisco, USA. Cor was studied biologically and chemically by using different assays. Cor was characterized by using MS, NMR and ICP-MS. The ability of Cor to bind hematin also was studied to test the hypothesis that Cor works as a carbon monoxide dehydrogenase (CODH).

6.1 Carbon monoxide (CO)

Carbon monoxide is an inert, colorless and odorless gas, found naturally as one of the atmospheric gases, produced exogenously by organic material combustion (Nobre et al., 2007). For many years CO was known as an environmental hazard due to toxicity in higher concentration, reported as an air pollutant, resulting from automobile exhaust and different human activities (Nobre et al., 2007). CO can be used as a sole carbon and energy source for some bacteria (Lorite et al., 2000; Uffen, 1976), for more details see (Meyer and Schlegel, 1979). It is a paradox that the toxic hazardous gas such as CO is produced by the human body (Davidge et al., 2009; Piantadosi, 2002; Ryter et al., 2006; Wu and Wang, 2005). The “gasotransmitters” (NO, CO and H₂S) share five characteristics: 1) They are small molecules with molecular masses of 30 Da for NO, 28 Da for CO and 34 Da for H₂S. 2) Because of their small dimensions and lack of charge, they can penetrate the cell membrane freely, with no need for special receptors, although sometimes they bind to a specific molecule, such as heme (in the ferrous state) (Davidge et al., 2009). 3) They are generated endogenously and enzymatically, and their biological synthesis is regulated exquisitely. 4) The gasotransmitters have a

distinct physiological role in biological systems (NO and CO for example play an important role in vasodilation and synaptic transmission in the central nervous system).

5) Their cellular effects sometimes need secondary messengers to mediate them (Wang, 2004).

CO is produced endogenously in bacteria, plants and animals by the activity of a heme oxygenase (HO) enzyme. HO degrades the haem cofactor of hemoglobin of the erythrocytes in human to: biliverdin, CO and iron. There are two types of HO in human with 40% similarity (Rotenberg and Maines, 1991), named HO-1 and HO-2. HO-1 is a 33 kDa enzyme, found in spleen and liver (Tenhunen and Marver, 1970), and needs oxygen and NADPH (Tenhunen et al., 1969). HO-2 is a non-inducible 36 kDa enzyme, found in brain and testes (Maines, 1988). It has been reported that *Staphylococcus* and hemolytic species of *Bacillus*, generate CO when incubated aerobically with heme containing compounds, whereas the non-hemolytic bacteria failed to show any CO in the same conditions which suggests that the HO is participated in hemoglobin breakdown to produce heme and CO (Davidge et al., 2009).

6.2 Bacterial heme oxygenase

It has been found that bacteria contain enzymes that resemble HO-1. There are two types of HO in bacteria: class one HO and class two HO (Davidge et al., 2009). Class one (HmuO) was first reported in *Corynebacterium diphtheriae* the hemolytic bacterium that are the cause of diphtheria and use hemoglobin as a sole source of iron (Schmitt, 1997). *Neisseria meningitidis* and *N. gonorrhoeae* also contain a heme oxygenase named HemO, which is essential for iron utilization (Zhu et al., 2000). Further studies revealed different types of enzymes similar to HO-1 in *Pseudomonas aeruginosa* (Ratliff et al., 2001); *Campylobacter jejuni* (Ridley et al., 2006). Recently a heme oxygenase similar to that in *Campylobacter jejuni* has been discovered in *Helicobacter pylori* and named HugZ (Guo et al., 2008).

In *E. coli* K12 the search for HO homologue did not reveal any positive results, but it has been found that the enterohaemorrhagic strain of *E. coli* (O157:H7) contains an HO named ChuS (Suits et al., 2006; Suits et al., 2005).

Class two HO plays an important role in bacterial pathogenicity and was first discovered in *Staphylococcus aureus* (Skaar et al., 2004). A similar enzyme called IsdG was found in *Bacillus anthracis* (Skaar et al., 2006) and *Listeria monocytogenes* (Wu et al., 2005). This type of HO is also important in the defense against heme-mediated toxicity, caused by heme accumulation in the cell.

6.3 Effects of CO on humans and bacteria

For a hundred years CO was known as a pollutant, toxicant and waste product. It has been reported in many studies that CO created by anthropogenic activities such as engine and vehicle emissions; wood burning and tobacco, is a major cause of human toxicity, if there is exposure to it in high concentrations or for a long period (Nobre et al., 2007; Piantadosi, 2002; Wu and Wang, 2005). CO was named as a “silent killer” because of the fatal effect of it. It has been reported that CO is one of the most abundant causes of suicidal poisoning in Europe (WHO, 2000) and North America (Wu and Wang, 2005). CO deleterious effects depend on many factors: CO concentration; the pulmonary alveolar ventilation; duration of exposure; and the partial pressure of O₂ and CO (Davidge et al., 2009; Wu and Wang, 2005). CO toxicity mainly comes from its ability to bind the heme- binding or sensing proteins, such as hemoglobin. Hemoglobin is called carboxy-hemoglobin or carbonmonoxy- hemoglobin (COHb) when bound to CO. The affinity of CO to bind HbA (adult hemoglobin) is 200-250 times greater than O₂ binding to HbA. Accordingly, COHb impairs the O₂ storage and transportation by HbA (Stewart, 1975). CO can diffuse easily across membranes of the alveoli, capillary and placenta. Approximately 80-90% of the diffused gas binds to heme- binding and sensing proteins (mainly hemoglobin). With myoglobin, cytochrome *c* oxidase and

cytochrome P450, CO binding affinity is lower, with only 10-15% of CO binds to those proteins (US EPA, 1991; Stewart, 1975). In spite of all the drawbacks of CO, it has been demonstrated that CO is very important in mammalian biological systems where it has been proved that CO acts like NO in vasodilation, and muscle relaxation (Furchgott and Jothianandan, 1991; Furchgott and Zawadzki, 1980; Ignarro et al., 1987a).

The anti-inflammatory effect of CO was also proved, in a study that showed that 250 ppm of CO administered to rodents *in vivo* or supplied to murine macrophages *in vitro* was able to reduce the inflammatory response to lipopolysaccharide (Otterbein et al., 2000). More specific results were ascribed to CO as a differential and selective inhibitor of pro-inflammatory cytokines (TNF- α , IL-1 β) expression, and a cause of increases in the anti-inflammatory mediators such as IL-10 (Otterbein et al., 2000).

As a cell signaling molecule, the role of CO has been demonstrated in apoptosis in endothelial cells (Brouard et al., 2000). The role of CO in apoptosis was demonstrated in vascular smooth muscle cells (Liu et al., 2002), in hepatocytes by (Sarady et al., 2004), and in neuronal cells (Vieira et al., 2008).

The role of CO in enhancing phagocytosis has been proved in many studies. In *E. coli* infections, CO was found to improve p38- mediated surface expression of toll-like receptor 3, where this role was established in macrophages *in vitro* and *in vivo* (Otterbein et al., 2005). It has been demonstrated that endogenous CO enhances the immune defense response against microbial sepsis (Chung et al., 2008). The role of CO in macrophage sensing and killing of bacteria through inflammasome activation also has been suggested (Wegiel et al., 2014): it is proposed that CO causes ATP loss from bacteria that then acts as a signal in the inflammatory response. However, no mechanism for ATP release has been demonstrated or suggested.

The effect of CO on *E. coli*, *Staphylococcus aureus*, *Pseudomonas aeruginosa* and *Mycobacterium tuberculosis* (Mtb) the causative agent of tuberculosis has been studied extensively (Desmard et al., 2009; Nobre et al., 2009; Nobre et al., 2007). In 2008, it was demonstrated that CO derived from HO-1 was able to induce the dormancy regulon (DosR/T/S), and help in the persistence of Mtb in the macrophages (Kumar et al., 2008; Shiloh et al., 2008). It was shown that Mtb in contrast to *E. coli*, *Staphylococcus aureus* and *Pseudomonas aeruginosa* is able to resist a high concentration of CO, and this suggested a potent resistance pathway in Mtb, not found in the other microbes (Zacharia and Shiloh, 2012).

A further study in Mtb proposed a novel carbon monoxide resistance gene, essential for Mtb survival and pathogenicity. In that study, a transposon library was created by using *M. tuberculosis* Erdman strain and Φ Mycomar T7 phage, to screen for a mutant unable to grow in the presence of CO. A total of 2500 mutants were screened and only one mutant was found to be resistant to CO. In this mutant the transposon insertion was mapped to a gene with unknown function, *rv1829* which was named *cor* (carbon monoxide resistance gene), and encoded the Cor protein (Zacharia et al., 2013).

6.4 Carbon monoxide resistant protein (Cor)

The *cor* gene is widespread among bacteria, archaea and plants, and contains a domain of unknown function (DUF151). DUF151 was found in >500 sequences in the CDART database, including pathogenic mycobacteria (*M. tuberculosis*, *M. avium*, *M. kansasii*, *M. abscessus* and *M. leprae*); *Rhodococcus* sp and corynebacteriae (Figure 6.1).

```

1
50
M.tuberculosis MGEVRVVG IRVEQPQNQP VLLLREANGD RYLPIWIGQS
M.bovis MGEVRVVG IRVEQPQNQP VLLLREANGD RYLPIWIGQS
M.avium MGEVRVVG IRVEQPQNQP VLLLRETNGD RYLPIWIGQS
M.kansasii MGEVRVVG IRVEQPQNQP VLLLREADGD RYLPIWIGQS
M.smegmatis MAEVRVVG IRVEQPQNQP VLLLRESNGD RYLPIWIGQS
M.abscessus MSEVRVVG IRVEQPQNQP VLLLRESAGD RYLPIWIGQS
R.fascians MSEMVRVVG IRVEQPQNQP VLLLRESDGD RYLPIWIGQT
T.maritima MGSDKIHFFF HHXKAWVKT LALDRVSNTP VVILGIEGTN RVLPIWIGAC
Consensus ..... ..m.e.rVvg irv#qpqNqP vllLre..g# RyLPIWIGq.

51
100
M.tuberculosis EAAAIAlEQQ GVEPPRPLTH DLIRDLIAAL GHSLKEVRIV DLQEGTFYAD
M.bovis EAAAIAlEQQ GVEPPRPLTH DLIRDLIAAL GHSLKEVRIV DLQEGTFYAD
M.avium EAAAIAlEQQ GVEPPRPLTH DLIRDVIAAL GHSLKEVRIV DLQEGTFYAD
M.kansasii EAAAIAlEQQ GVEPPRPLTH DLIRDVIAAL GHSLKEVRIV DLHEGTFYAD
M.smegmatis EAAAIAlEQQ GVEPARPLTH DLIRDLIAAL GHSLKEVRIV DLQEGTFYAD
M.abscessus EAAAIAlEQQ GVEPARPLTH DLIRDLIAAL GHSLKEVRIV DLQEGTFYAD
R.fascians EAAAIAlEQQ GVQPARPLTH DLVKNLISAL GHELKEVRIV DLQEGTFYAD
T.maritima EGHAlAlAXE KXEFPRPLTH DLLLSVLESL EARVDKVIH SLKDNFTFYAT
Consensus EaaAialEq# gv#ppRPLTH DL...vi.aL gh.lkevriv dLq#gTFYAD

101
150
M.tuberculosis LIFDRNIKVS ARPSDSVAIA LRVGVPIYVE EAVLAQAGLL IPDESDEEAT
M.bovis LIFDRNIKVS ARPSDSVAIA LRVGVPIYVE EAVLAQAGLL IPDESDEEAT
M.avium LVFDRNITVS ARPSDSVAIA LRVGVPIYVE EAVLAQAGLL IPDESDEEGG
M.kansasii LIFDRDIKVS ARPSDSVAIA LRVGVPIYVE EAVLAQAGLL IPDESDEEAS
M.smegmatis LIFDRDIKVS ARPSDSVAIA LRVGVPIYVE EAVLAEAGLL IPDENDEEES
M.abscessus LIFDSIRVS ARPSDSVAIA LRVGVPIYVE EAVLAEAGLI IPDEDDEDSG
R.fascians LVFDKDIRVS ARPSDSVAIA LRAGVPIYAE EPVLAEAGLL MPDE-----
T.maritima LVIRDLYTID EEDEEAALID IDSRPSDAII LAVKTGAPIF VSDNLVEKHS
Consensus L!fd..i.vs arps#svaIa lr.gvpiy.e eaVla.Agll .pD#...e.s

151
179
M.tuberculosis TAVREDEVEK FKEFLDSVSP DDFKAT
M.bovis TAVREDEVEK FKEFLDSVSP DDFKAT
M.avium TAVREDEVEK FKEFLDSVSP DDFKAT
M.kansasii SAVREDEVEK FKEFLDSVSP DDFKAT
M.smegmatis GTVREDEVEK FKEFLDSVSP DDFKAT
M.abscessus GALREDEVEK FKEFLDSVSP DDFKATEGP
R.fascians ---REDEVEK FKEFLESVSP DDFKATDG
T.maritima IELEVNERDL INSR
Consensus ...re#Ev#k fkefl.svsp ddfkat..

```

Figure 6.1: Alignment of *cor* gene in pathogenic *Mycobacteria*, *Rodococcus facians* and *Thermotoga martima*. The figure shows the highly conservative residues in *cor* sequence in different organisms that might have role in Cor protein function.

Although Cor contains a DUF151 domain, which is also found in the OmBBB protein from rice *Oryza minuta* where it exhibits a nuclease activity (You et al., 2010), the crystal structure of a Cor homologue from *Thermotoga martima* (PDB entry 1VJL) (Figure 6.2) is novel and has no structural homologue. So the function of Cor was still unrevealed.

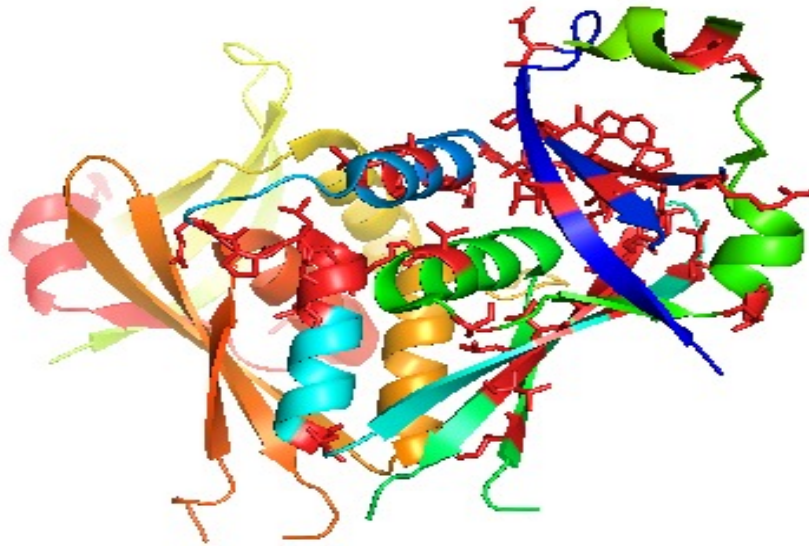


Figure 6.2: The crystal structure of a Cor homologue from *Thermotoga maritima* (PDB entry 1VJL). Starting from the blue (N-terminal end), to the red (C-terminal end), the conserved residues were presented as red sticks. The figure shows that the conserved residues are clustered at the N-terminal end and form a potential binding pocket.

In the studies on the *cor* gene the metabolite pool in the mutant and wild strains was screened to find any metabolite differences. It was observed that an Mtb *cor* mutant develops an unregulated redox environment, accumulates different reducing equivalents and elevated levels of the unsaturated and saturated long-chain fatty acids (Zacharia et al., 2013).

Results

6.5 Cor Mtb expression

In order to find the best condition for *cor* gene expression, *E. coli* BL21 strain complemented with pJ401 *cor* expression vector was grown at 37 °C for 1, 2, 3 h and overnight, with 200 rpm shaking, followed by induction via addition of 1 mM IPTG. No band was seen in the preinduction prep corresponding to Cor molecular weight, whereas after adding IPTG (post-induction), bands were seen at 1, 2, 3, h and overnight. Expression improved after 2 to 3 h incubation but was not better overnight. A band was

seen in SDS-PAGE analysis slightly higher than the expected molecular size of Cor (18 kDa) (Figure 6.3).

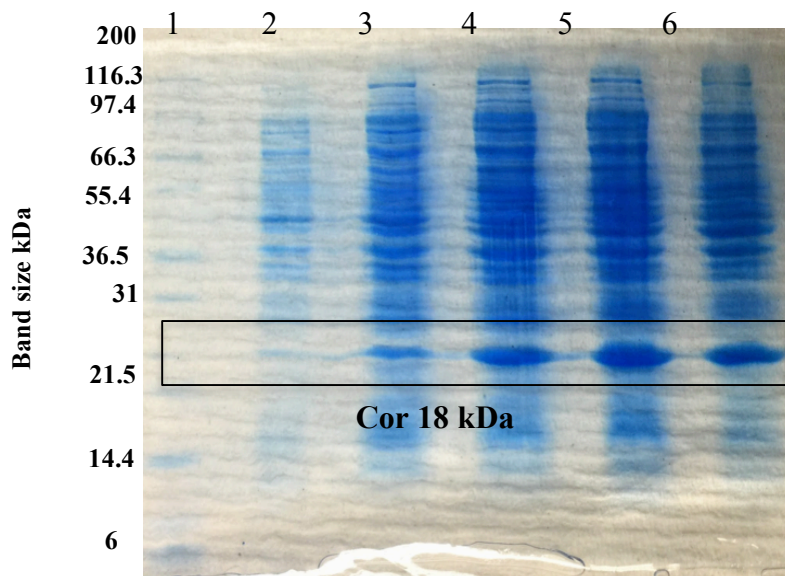


Figure 6.3: 12% SDS-PAGE of Cor small-scale expression. The figure shows that Cor was expressed after 1,2,3 hours and overnight incubation following induction, but the best expression was in 3 hours. Lane 1 is Mark12, lane 2 is the Preinduction, lanes 3, 4, 5 and 6 are 1, 2, 3 h induction and overnight respectively.

6.6 Solubility test

Cor solubility was checked as described in Chapter 3, section 3.2.15. and samples were checked on SDS-PAGE as described in Chapter 3, section 3.2.14. The SDS-PAGE results showed that Cor was highly soluble and the band in the soluble fractions was around 90% of total protein (Figure 6.4).

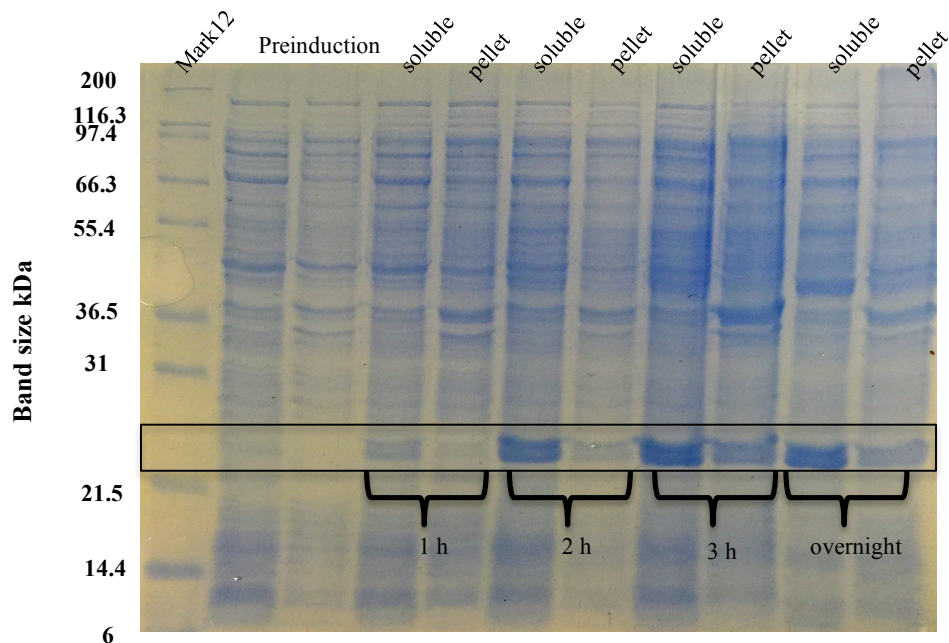


Figure 6.4: 12% SDS-PAGE of Cor solubility test. The figure shows that Cor was found in the soluble fractions as approximately 90% of total protein

6.7 Large scale protein expression

In order to obtain a large amount of Cor protein, *cor* was expressed in large scale by using 500 ml cultures as described in section 3.2.17. 1 ml pre and post induction samples were taken. Samples were prepared and loaded on SDS-PAGE gel as described in section 3.2.14. The SDS-PAGE results showed that *cor* was expressed well in the large-scale volumes after 3 h by using 1 mM IPTG at 37 °C (Figure 6.5).

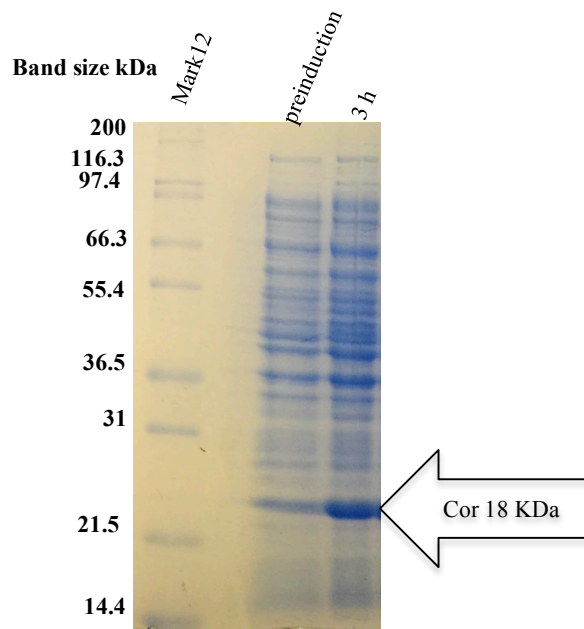


Figure 6.5: 12% SDS-PAGE of *cor* large-scale expression. The figure shows that Cor was expressed well after 3 h incubation, by using 500 ml culture at 37 °C following incubation with 1 mM IPTG

6.8 Protein purification

Purification was performed using a 5 ml His-Trap column (GE healthcare) as described in Chapter 3, section 3.2.18.1. The chromatogram of the elution steps of the Ni column purification (Figure 6.6 A) showed two peaks whose content were analyzed by SDS-PAGE (Figure 6.6 B). The SDS-PAGE results showed that Cor was eluted in fractions 13 & 14, which were combined together and concentrated. The purity of Cor protein was around 85-90%.

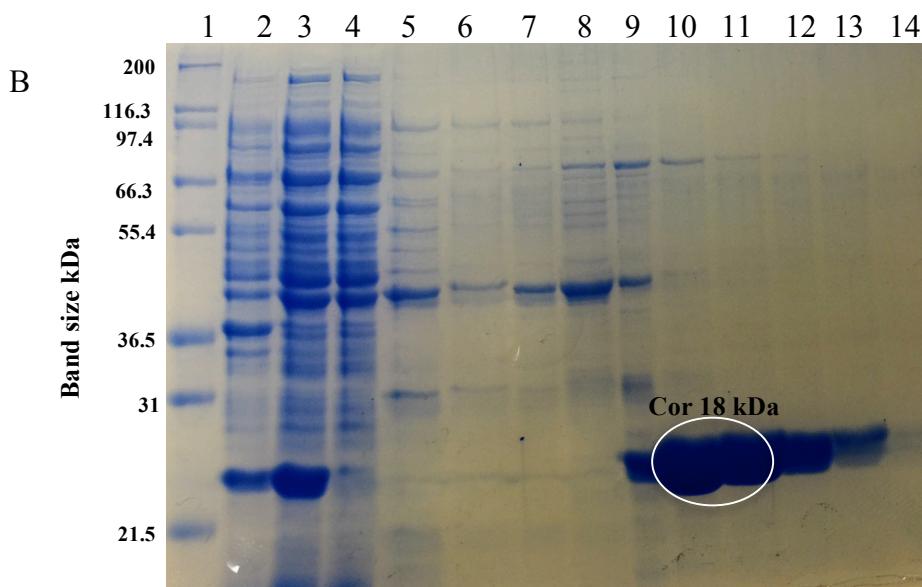
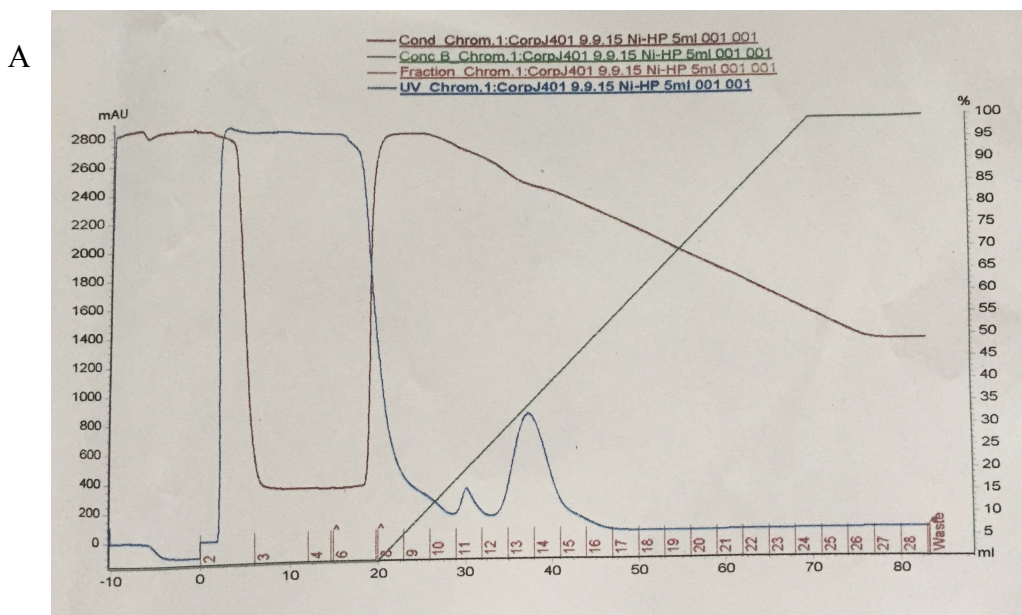


Figure 6.6: Cor purification by Ni column. Panel A- shows the chromatogram of Ni column purification of Cor. It shows that Cor was eluted by buffer containing imidazole in fractions 13 and 14. Panel B- 12% SDS-PAGE of His-tagged Cor purification. The figure shows that Cor was eluted in 0.5 M Imidazole, the purity was around 85-90%, bands were seen higher than the expected molecular size of Cor. Lane 1 is Mark12, lane 2 is cell debris, lane 3 is the cell free extract (CFE), lane 4 is the unbound material (Fraction 3), lanes 5-14 are fractions 8-17.

Because it has been reported that a Cor homologue has a DUF151 domain, which in the OmBB1 protein act as a nuclease, the ability of Cor to bind DNA was checked by loading on a Heparin HP 5 ml column (GE healthcare) as a simple test to check Cor binding affinity to DNA. The results showed that no peak was seen following elution of the column with 2 M NaCl and the Cor protein was found in the flow through which suggested that Cor did not bind the heparin (Figure 6.7 A).

In order to check the molecular size of the protein, the flow through from Heparin column was concentrated down to 2 ml and loaded on a 1.6x 60 Hi-Load Superdex 200 column at 1.5 ml/min flow rate as described in section 3.2.18.2. After gel filtration, the chromatogram showed that Cor was eluted at 73.91 ml (Figure 6.7 B), which revealed that the solution molecular size of Cor was 50 kDa and suggested a trimeric structure in contrast to the published finding, which suggested that Cor was dimeric based on a native PAGE gel (Zacharia et al., 2013). The protein was 99% pure as the SDS-PAGE gel showed. (Figure 6.7 C).

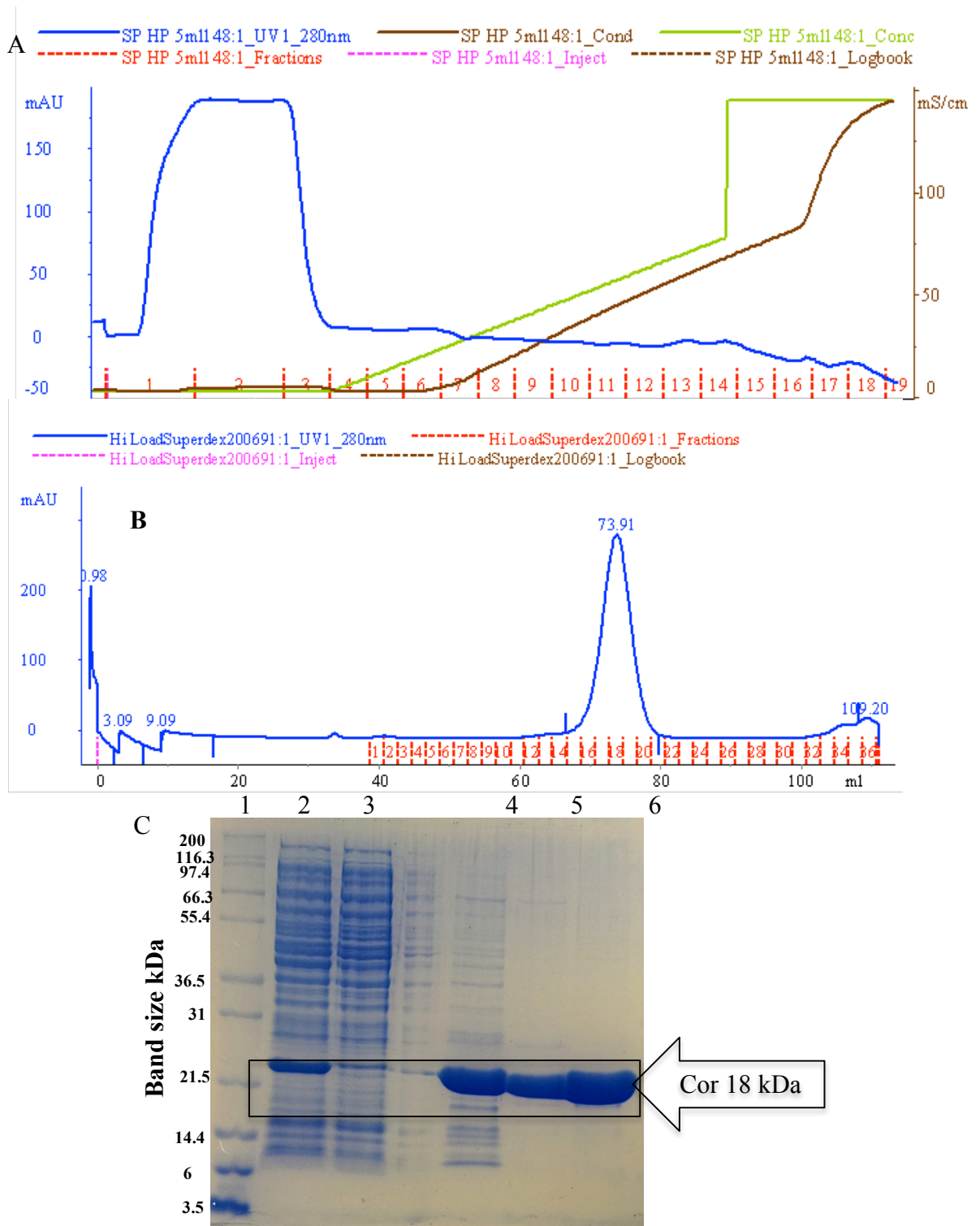


Figure 6.7: Cor purification. Panel A- Heparin column purification chromatogram, shows that Cor was not eluted with the NaCl gradient and gel showed it in the unbound material (data not shown); Cor was not bind to heparin. Panel B- Cor elution profile from a Superdex 200 gel filtration column shows that Cor was eluted in one peak at 73.91 ml, corresponding to 50 kDa, which suggests that Cor is trimeric. Panel C- 12% SDS-PAGE trace of Cor purification, shows that Cor was purified to around 99% purity by using additional gel filtration. Lane 1 is Mark12, lane 2 is the CFE, lane 3 is the Ni

unbound material, lane 4 is the Ni column product, lane 5 is the Gel-filtration load, and lane 6 is the final product of gel-filtration purification.

6.9 Chemical characterization of Cor

Cor was characterized by using different chemical methods. It was sent to mass spectrometry, NMR and ICP-MS.

6.9.1 Mass spectrometry

In order to check the molecular weight of Cor, it was sent for mass spectrometry analysis as described in section 3.2.19. The result showed that Cor molecular weight was 18806.25 Da. The calculation of the expected molecular weight with 6X His-tag is 18824.6 Da (Figure 6.8).

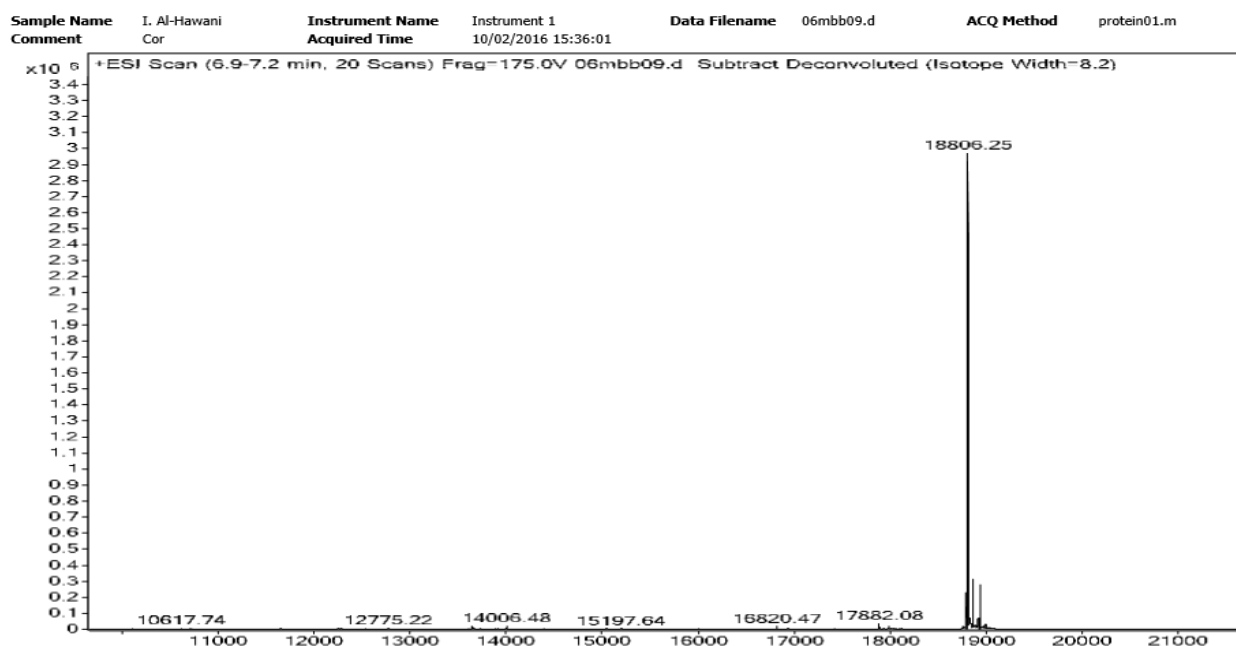


Figure 6.8: Mass spectrometry of Cor. The figure shows that the molecular weight of Cor + 6xhistidine was 18.806 kDa, which is less than the calculated molecular weight by 18 Da.

6.9.2 Nuclear magnetic resonance NMR

To check if Cor was folded properly, a sample of purified protein was sent to the NMR facility in MBB department in the University of Sheffield, as described in section 3.2.20. The one dimension ^1H NMR result showed that Cor was fully folded, according to the chemical shifts of the amino acids in HN; aromatic; HA and aliphatic regions (Figure 6.9)

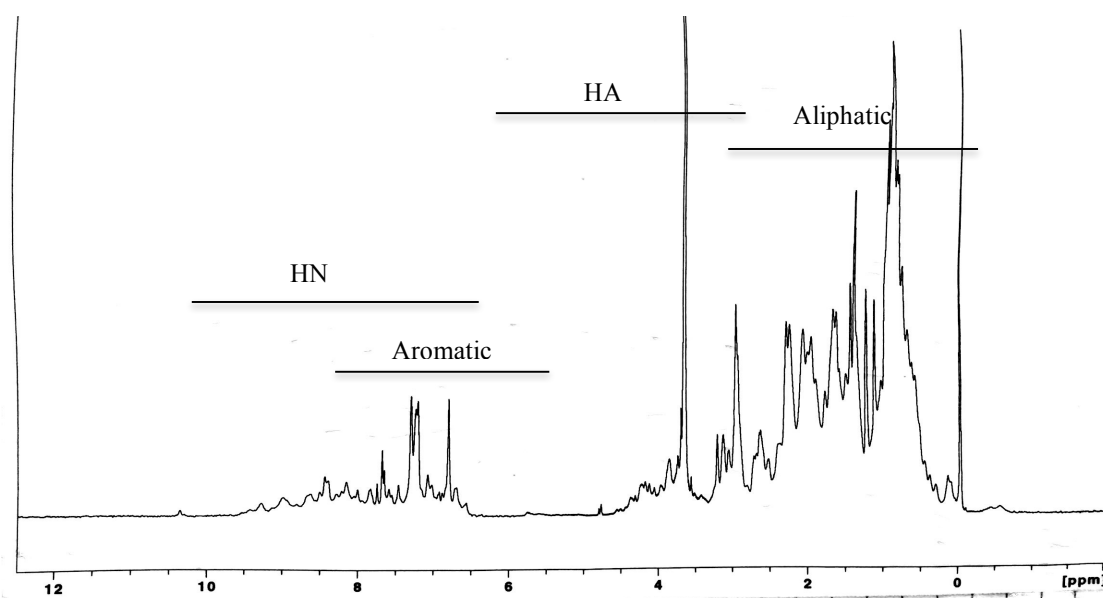


Figure 6.9: ^1H NMR one dimension spectrum of Cor. It shows that Cor was fully folded according to the chemical shift of the proton in the HN, aromatic, HA and aliphatic regions

6.9.3 ICP-MS

To probe the Cor mechanism of action, we sought potential ligands to the protein. To determine whether Cor has any metal ligand that binds to it, a sample of Cor was sent to the mass spectrometry faculty in Chemistry department University of Sheffield, to be analyzed by ICP-MS, as described in section 3.2.26.12.

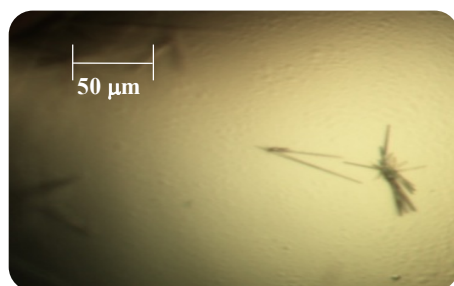
The ICP-MS result showed that Cor has no strong signal for any metal, which suggested that there is no tightly bound metal to Cor in the sample tested (Table 5.1).

Table 6.1. Cor ICP-MS results. The table shows that there was no high concentration value for any metals, which indicates that there was no metal bind to Cor in the sample

Metal	Al	Na	Ca	P	S	Fe	Si	K	Mg	Zn
Mg/L	0.26	9200	0.44	4.48	5.64	0.08	0.36	0.64	1.72	0.27

6.10 Initial crystallization and optimization trials

Different ranges of protein concentration were used in crystallization trials (15-60 mg/ml), and two different incubation temperatures were used (7 and 17 °C), as described in section 3.2.21. After 5 days of crystallization, a bundle of very tiny needle shape crystals were seen in a PACT screen (0.2 M Sodium bromide, 0.1 M Bis Tris propane pH 6.5, 20% (w/v) PEG 3350) (Figure 6.10).



PACT
0.2 M Sodium bromide
0.1 M Bis-Tris propan pH6.5
20% (w/v) PEG 3350

Figure 6.10; Result from the initial crystal screening of Cor. Cor crystals grown at 17 °C after 5 days. Scale bar = 50 μm

The condition then was optimized for crystal growth, by changing buffer pHs (6 - 7.5) and PEG concentrations (5 – 30% w/v). A bundle of slightly bigger crystals were grown when the buffer pH changed from 6.5 to 6 and PEG concentration from 20 to 25% (w/v). Other tiny crystals where grown in the same conditions as the initial crystal. A bundle of very tiny crystals also was appeared when the PEG concentration was changed from 20 to 25% (w/v), and the buffer pH was changed from 6.5 to 7 (Table 5.2).

Another single rectangular crystal was grown in the PACT screen (0.2 M calcium chloride, 0.1 M Tris pH 8.0, and 20% (w/v) PEG 6000), when 23 mg/ml of Cor protein was used (Figure 6.11).

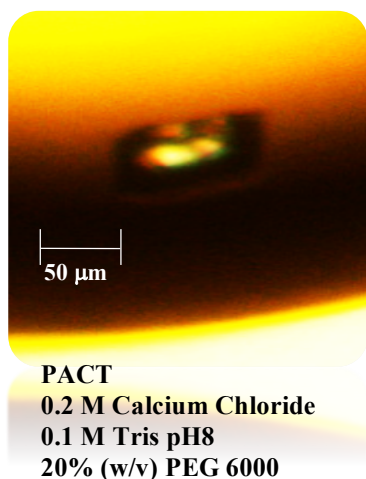


Figure 6.11: Crystal of Cor grown at 17 °C in higher Cor concentration (23 mg/ml). Scale bar = 50 μm

Other crystallization hits were obtained when Cor was used at a concentration of 26 mg/ml in screens incubated at 7 °C. Very tiny needle-shaped crystals appeared in the PACT initial screen (0.2 M sodium iodide, 0.1 M Bis Tris propane pH 7.5, 20 % (w/v) PEG3350) (Figure 6.12).

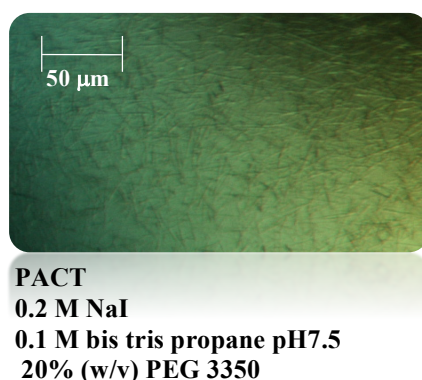


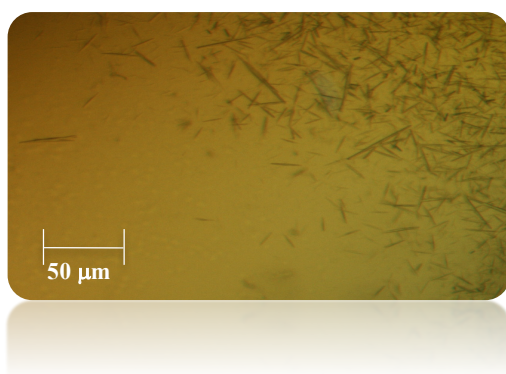
Figure 6.12: Cor crystal screen results. Crystals were obtained using protein at concentration of 26-27 mg/ml at 7 °C. Scale bar = 50 μm

This condition was then optimized by using different buffer pH values ranging from 6.5 to 8.5, and different PEG concentrations between 10 to 24% (w/v). Crystals were grown when buffer pH was changed from 7.5 to 8.0, and the PEG concentration was changed from 20 to 15% (w/v). Another bundle of needle-shape crystals were grown when the

buffer pH was 6.5 and PEG3350 concentration was 15% (w/v). Very tiny crystals were obtained in buffer pH 7.0 and 24% (w/v) PEG, pH 7.0 and 10% PEG, pH 7.5 and 24% (w/v) PEG, and pH 6.5 and 20% (w/v) PEG (Table 5.2).

Another needle shaped tiny crystal was obtained when Cor at 26 mg/ml was used, in the PACT screen. The initial condition was 0.2 M potassium thiocyanate, 0.1 M Bis Tris propane pH 6.5 and 20% (w/v) PEG3350 (Figure 6.13).

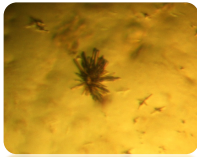

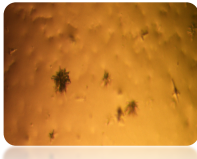
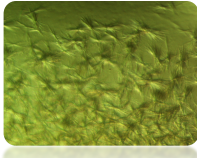
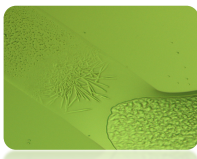
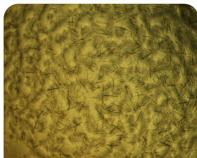
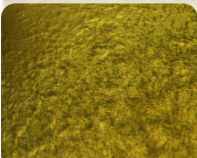
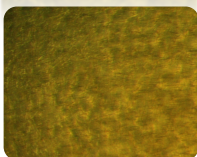
This condition was optimized by changing the pH of Bis Tris propane buffer and the concentration of PEG, one hit was obtained after optimization, which was in buffer pH 7.5 and 10% (w/v) PEG (Table 6.2)

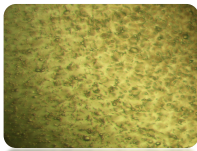
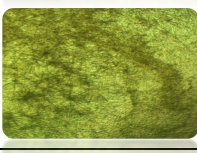


PACT F4 Initial crystals
0.2M potassium thiocyanate
0.1M Bis tris propane pH 6.5
20% (W/V) PEG 3350

Figure 6.13: Cor crystals grown at 7 °C using 26 mg/ml protein. Scale bar = 50 μm

Table 6.2. Cor crystals optimization. The table shows the optimization conditions for Cor initial crystals, the salt, buffer and precipitant values and a photo of the crystals grown in each optimization condition

Salt	Buffer	Precipitant	Photo
0.2 M Sodium bromide	0.1 M Bis-Tris propan pH 6	25% (w/v) PEG 3350	
0.2 M Sodium bromide	0.1 M Bis-Tris propan pH 7	25% (w/v) PEG 3350	
0.2 M NaI	0.1 M bis tris propane pH 8	15% (w/v) PEG 3350	
0.2 M NaI	0.1 M bis tris propane pH 8	15% (w/v) PEG 3350	
0.2M NaI	0.1M bis tris propane pH6.5	15% (w/v) PEG 3350	
0.2 M NaI	0.1 M Bis Tris propane pH 7.0	24% (w/v) PEG 3350	
0.2 M NaI	0.1 M Bis Tris propane pH 7	10% (w/v) PEG 3350	
0.2 M NaI	0.1 M Bis Tris propane pH 7.5	24% (w/v) PEG 3350	

0.2 M NaI	0.1 M Bis Tris propane pH 6.5	20% (w/v) PEG 3350	
0.2 M potassium thiocyanate	0.1 M Bis tris propane pH 7.5	10% (w/v) PEG 3350	

6.11 X-ray Data collection

Many crystals were sent to the Diamond Light Source center near Oxford, for testing their X-ray diffraction on a number of different beam lines. No diffraction was obtained from any of the crystals. This can be interpreted as the result of poor handling of the crystals but could also be the result of extremely weak or no diffraction from very small crystals of a protein. Inorganic salt crystals would have been expected to show diffraction, even at this very small size if handled moderately well. To determine if the crystals were salt or protein crystals, 0.5 μ l of Izit dye was added to a 2 μ l drop of potential protein crystals and crystallization solution. Unfortunately, the crystals dissolved once the dye was added. Attempts to optimize the condition for dye addition where the dye was diluted twice with mother liquor solution, still resulted in dissolved crystals when the dye was added.

6.12 Studies to reveal Cor mechanism of action

A series of assays were done using His-tagged Cor purified protein to test CO detoxification by Cor. To test if Cor has a mechanism similar to CODH for detoxifying CO, the ability of Cor to reduce methyl viologen was tested. The ability cells were to protect *E. coli* from CO toxicity when overexpressing Cor protein was tested. The ability of Cor to bind heme was tested on the basis that CO binding and sensing proteins contain heme. To discover if Cor worked alone on CO detoxification or with protein partner, a simple pull down assay was carried out.

6.12.1 Carbon monoxide dehydrogenase (CODH) assay

An assay was performed in order to see if Cor could act as a CODH in oxidizing CO to CO₂.



An absorbance measurement of Cor with Methyl viologen (MV) as electron acceptor at 578 nm was taken for 1 h following bubbling with CO gas (the assay was carried out as described in section 3.2.26.6). The readings were taken every minute and the results showed that there were no differences between the time course of the reaction of the sample (Cor + MV) and the control (MV only) (Figure 6.14).

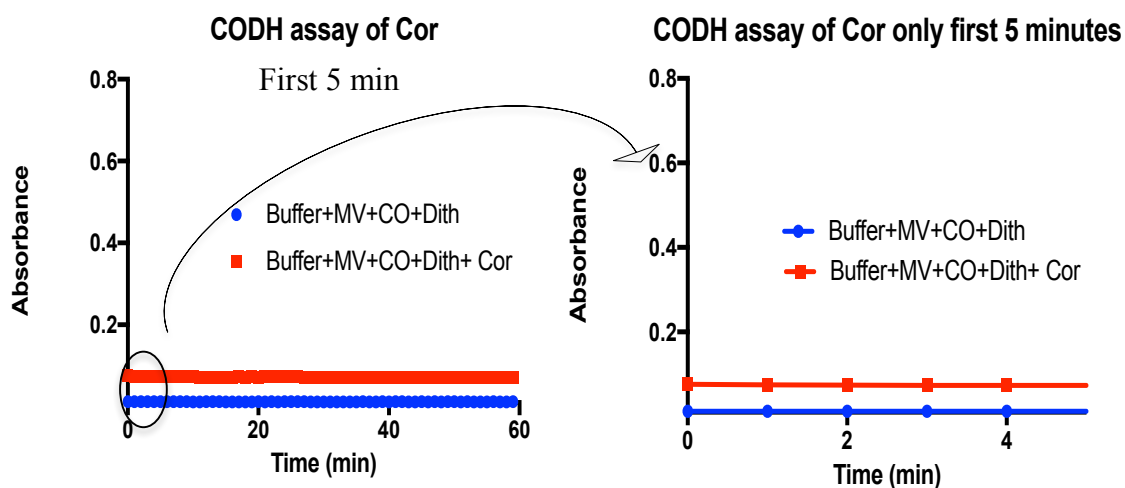


Figure 6.14: CODH assay. The blue line represents the background signal of the control reading at 578 nm. The red line represents the sample signal, which involved addition of 2.2 mg of Cor. The figure shows that there was no increase signal with time in the sample and suggests that no CO₂ was formed.

6.12.2 The ability of Cor to protect *E. coli* from CORM-2

To test the published assertion that Cor can protect the *E. coli* transformed with the expression vector from CO toxicity, a carbon monoxide releasing molecule (CORM-2) was used as CO donor an assay as described in section 3.2.26.7. In this assay *E. coli* BL21 was used as a control and the same strain transformed with pJ401 vector harboring the *cor* gene used as the test strain. The results showed that there was no

differences between the control (BL21 without *cor*) and the test strain (BL21 with *cor*) in 30 μM concentration of CORM-2 where they were both killed in the same rate, which suggested that Cor is not protecting *E. coli* from CO toxicity. At a sublethal dose of CORM-2 (10 μM), the test strain grew slightly better than the control strain. The same result was seen without any CORM-2 present, where the strain expressing Cor grew better (Figure 6.15).

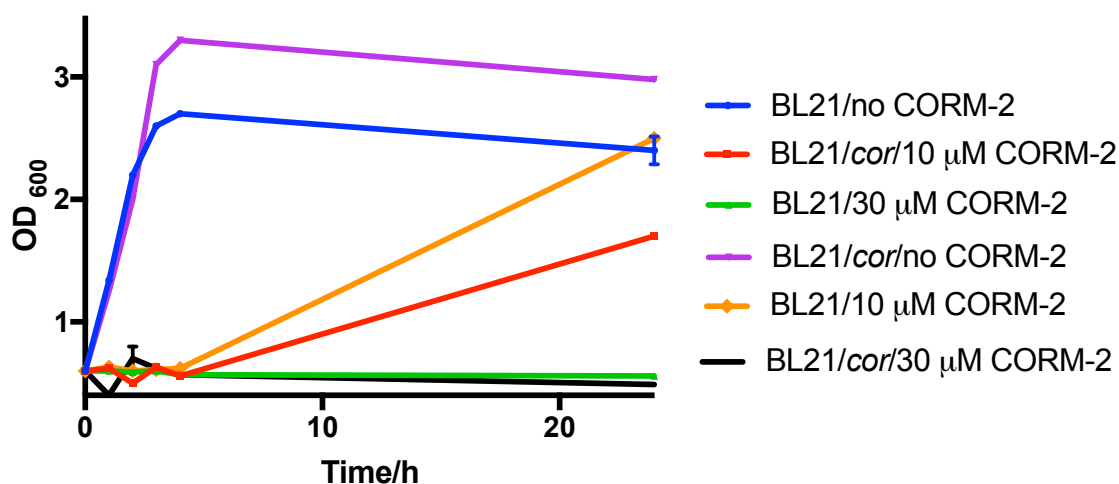


Figure 6.15: Cor protein protection of *E. coli* cells from the toxic effects of CO. Growth was from the optical density at 600nm, and was assessed in the presence of varying levels of CO, generated by addition of CORM-2. The cells expressing the *cor* gene (the purple lines) can be compared with control, not expressing the *cor* gene (the blue lines). The purple and blue lines are cells grown in minimal media without any CORM-2, the red and orange lines indicate cells grown with 10 μM CORM-2, and the black and green lines represent cultures supplemented with 30 μM CORM-2. A small advantage is seen for the cultures that express *cor* but this did not correlate with CO presence. The results represent the mean of three biological repeats \pm SD.

6.12.3 Hematin assay

In order to know if Cor has the ability to bind heme, which in turn can react with CO and detoxify it, Cor was tested by a hematin assay. The test was carried out as described

in section 3.2.26.8. Bovin serum albumin (BSA) was used as a control protein to see if the binding is specific to Cor. The results showed no peaks at 540 and 557 nm indicative of heme binding and thus Cor does not appear to bind heme *b*. Clear peaks were observed as expected for control BSA sample (Figure 6.16 A and B).

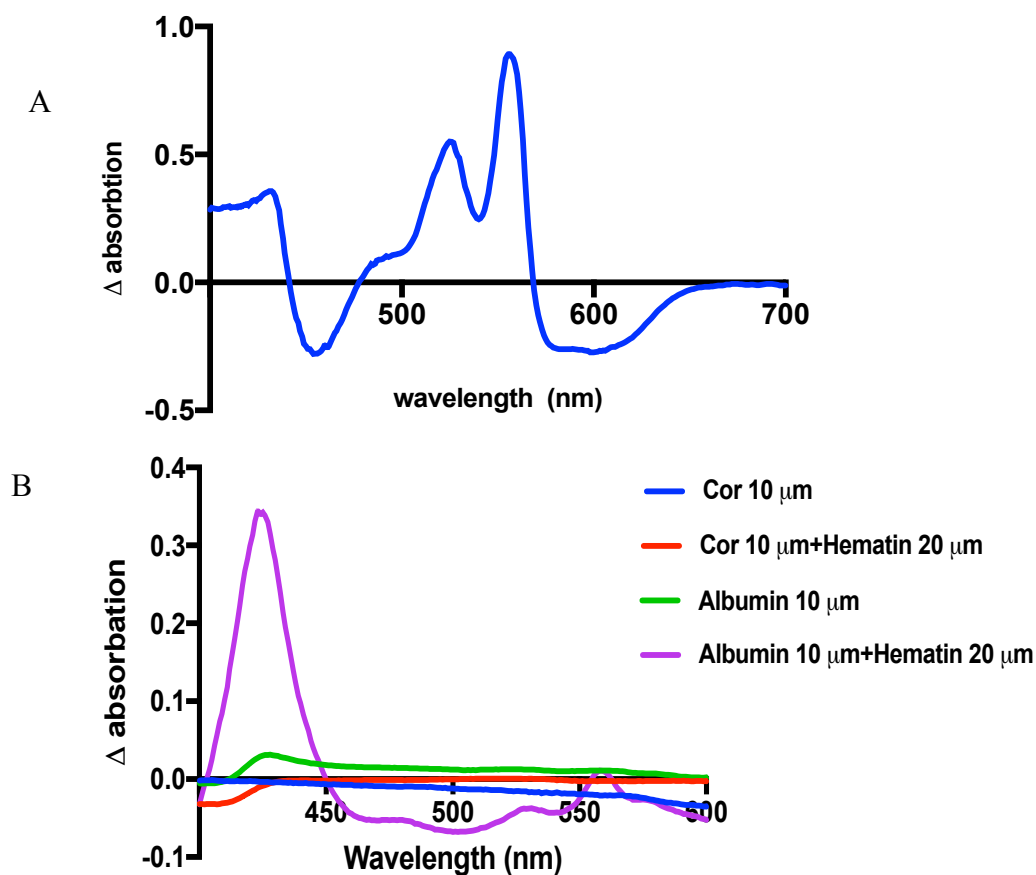


Figure 6.16: Hematin assay. Panel A- Spectrum of hematin+pyridine. It shows two peaks of heme *b* at 557 and 540 nm. Panel B- Spectra of Cor and BSA: the blue line is 10μM of Cor; the red line is 10 μM Cor + 20 μM Hematin; the green line is 10 μM BSA; the purple line is 10 μM BSA+ 20 μM hematin. The spectra showed that Cor does not appear to bind to heme *b*, whereas BSA does. BSA has a peak at 557 nm corresponding to the heme *b* peak.

6.12.4 Pull down assay

This assay was performed to test if Cor has a protein partner that might assist in CO detoxification. The experiment was carried out by using *E. coli* MG165 and *M. smegmatis* cell free extracts (CFE) because it had been published that Cor protein expression conferred resistance to CO in both *E. coli* and Mycobacterial species. YloQ was used as a control His-tagged protein with *M. smegmatis* and Blf1 as a His-tagged protein with *E. coli* as described in section 3.2.26.9. The SDS-PAGE showed no clear additional band following imidazole elution of His-tagged Cor from a Ni-HP column that had been loaded with either *M. smegmatis* or *E. coli* CFE. (Figure 6.17 A and B)

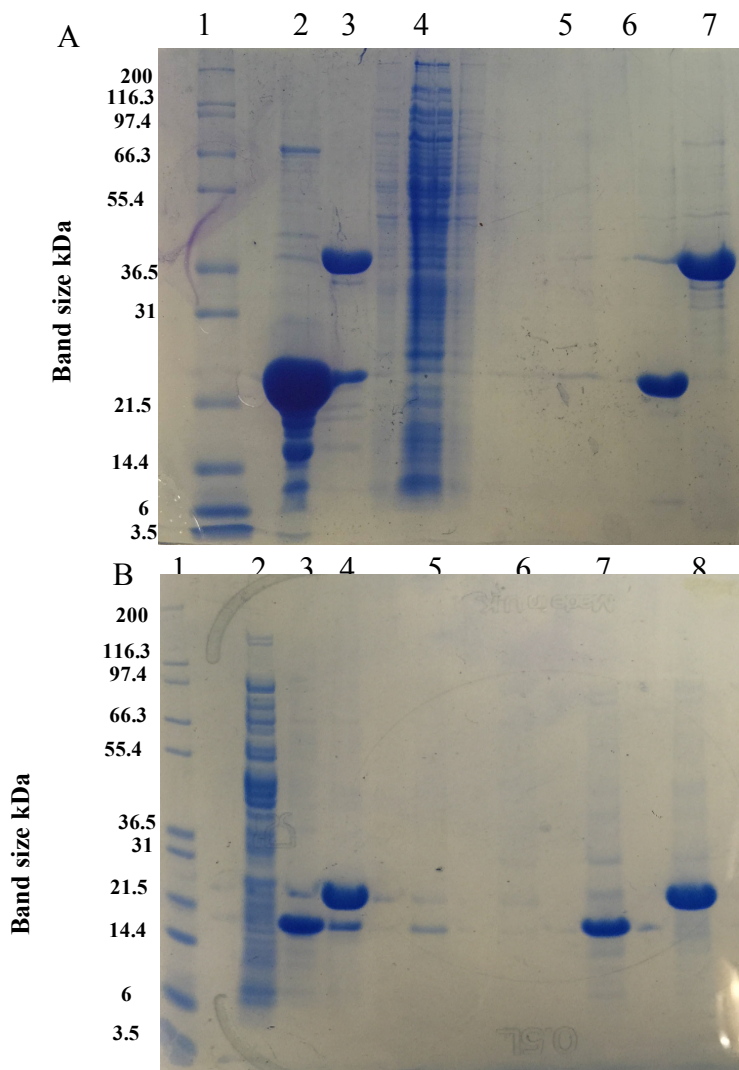


Figure 6.17: Pull down assay.

A- 12% SDS-PAGE of Cor with *M. smegmatis* CFE. Lane 1 is a protein ladder Mark12, lane 2 is 2 μ g of Cor, lane 3 is 2 μ g of YloQ, lane 4 is salt elution of Cor to reduce the non-specific binding to the Ni beads, lane 5 is salt elution of YloQ, lane 6 is the imidazole elution of Cor and lane 7 is the imidazole elution of YloQ. The gel shows that there was no clear band found in Cor imidazole suggests that no interaction was found between Cor and any *M. smegmatis* proteins.

B- SDS-PAGE of Cor with *E. coli* CFE. Lane 1 is a protein ladder Mark12, lane 2 is CFE of *E. coli*, lane 3 is 2 μ g of Cor, lane 4 is 2 μ g of BIF1, lane 5 is salt elution of Cor, lane 6 is salt elution of BIF1, lane 7 is the imidazole elution of Cor and lane 8 is the imidazole elution of BIF1. The gel results showed that there was no clear band to indicate any interaction, between a protein in the CFE of *E. coli* and Cor protein.

6.12.5 FTIR (Fourier transform infrared spectroscopy)

To check if the final product of CO detoxification by Cor was CO₂, an FTIR spectra were taken for purified Cor, flashed with CO, as described in Chapter 3, section 3.2.26.2.10. The spectra were taken every 10 min for 1 h and 37 min following the addition of CO to the sample. They showed that there was no signal for CO₂ production and the CO signal did not decline, indicating that the CO was not consumed (Figure

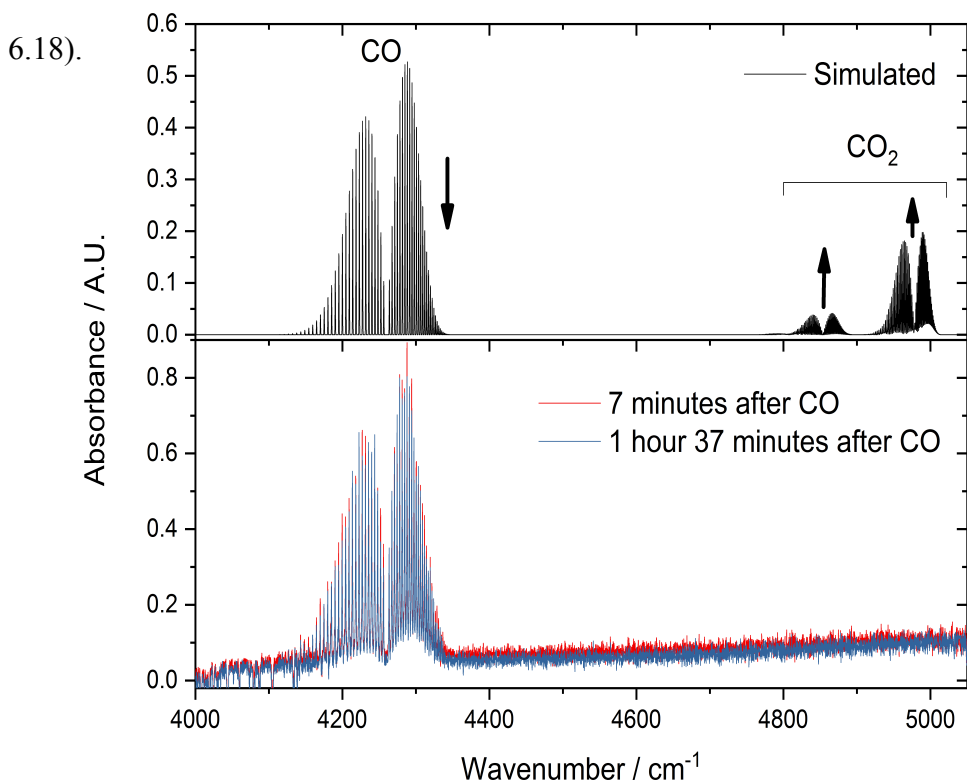


Figure 6.18: FTIR spectrum of Cor solution circulated with CO gas. Comparison of simulated (top) and experimental (bottom) FTIR spectra of headspace above Cor suspension measuring using an 8 m path length multiple pass cell. The simulated spectrum shows CO and CO₂ absorption band strengths assuming a 50:50 mixture of the two components; CO reductase activity would lead to the simulations disappearance of the CO band and appearance of the CO₂ bands. In the experiment, essentially no change is observed in the CO band and no CO₂ is observed, indicating that Cor has little or no reductase activity under these conditions. Simulated spectra were generated using absorption cross-sections from the HITRAN 2012 database and convoluted with 0.6 cm⁻¹ Gaussian profile to simulate the instrument resolution.

6.12.6 NMR for Cor with and without CO gas

If Cor can detoxify CO directly as proposed by Zacharia et al., 2003, it should bind CO. NMR spectra were taken of a Cor solution before and after it was bubbled with CO gas, as described in section 3.2.26.11. The NMR spectra showed that there was a slight shift in the indole region, but the results showed that there was no notable change in Cor spectra with and without CO over time (Figure 6.19 A and B).

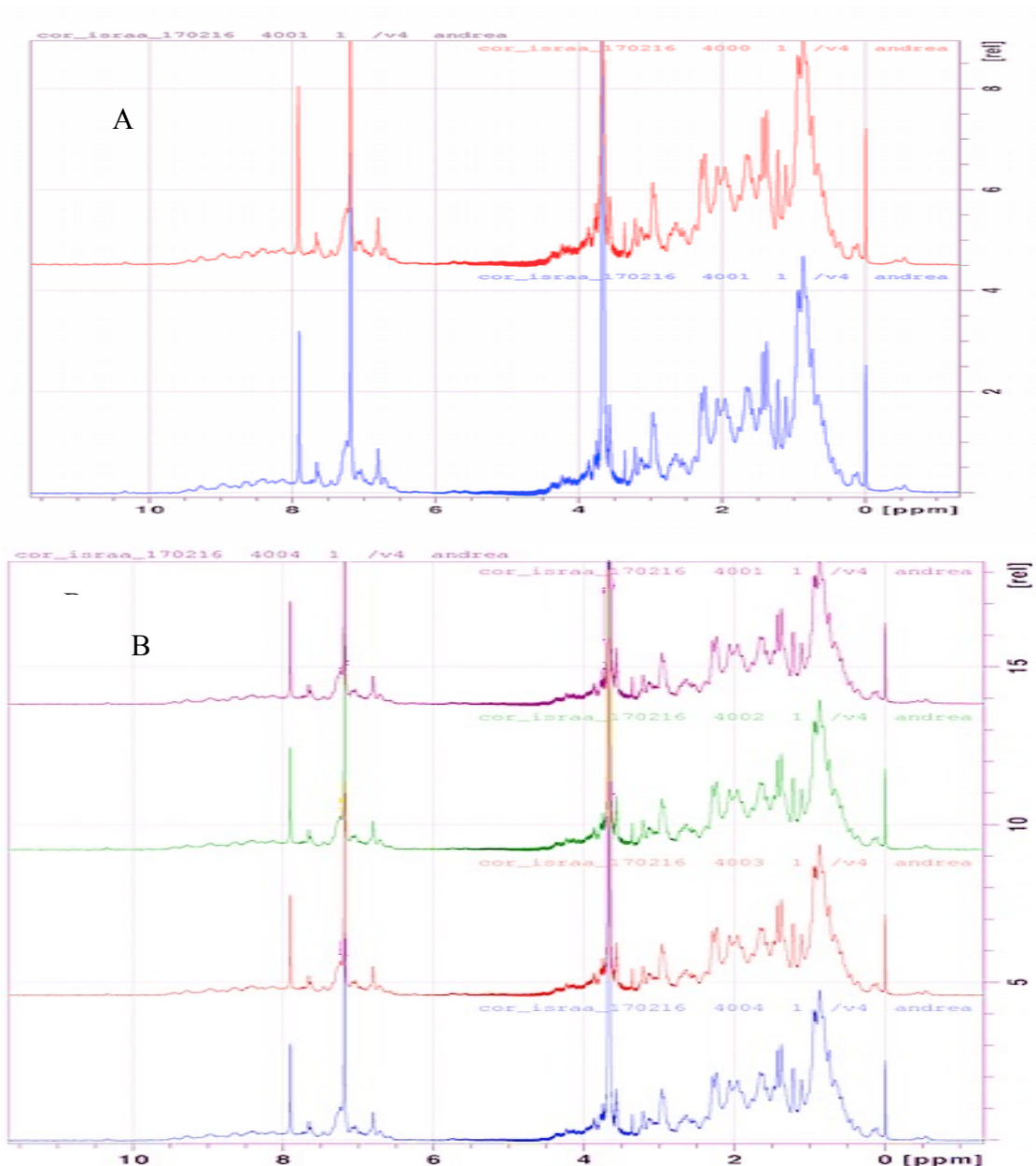


Figure 6.19: Cor ^1H NMR spectra with and without bubbling with CO gas.

A- The red spectrum is the control (6 mg/ml Cor in 10 mM Tris pH 7.5 +0.1 M NaCl). The blue spectrum is the same sample after bubbling with CO gas for 5 min. There were no differences between the Cor spectrum before and after CO bubbling.

B- The spectra of Cor bubbled with CO gas for over 4 h. It shows that over prolonged time there was no change in the spectra, which suggests no clear evidence for Cor binding to CO.

6.13 Discussion

Carbon Monoxide Resistance protein (Cor)

Cor is a protein with unknown function, comprised of 164 amino acids, with 18 kDa molecular weight (Zacharia et al., 2013). It has been shown that when *Mtb cor* was expressed in *E. coli*, it was able to protect the later from CO toxicity, when exposed to CORM-2 (a CO-releasing molecule contain ruthenium).

In the multidisciplinary approach described here, no evidence was obtained to show a Cor protection effect on *E. coli*. Assays were performed to investigate the functional activity of Cor and provide material for structural studies (as described in Chapter 3) but the results showed that there was no clear evidence about Cor function.

6.13.1 Cor purification

Cor was expressed as a His-tagged protein, the purification was performed by Ni column as described in Chapter 6, section 6.8. The results of the purification showed that Cor was 85-90% pure by using Ni-column, this purity level is not ideal for successful crystallization, but the protein sample was tested for crystallization. Further purification was carried out by using both Ni and gel-filtration columns, which resulted in purity around 99%. Thus, gel filtration was needed for further purification, and was used to calculate the molecular weight of Cor in solution, and hence determine the likely stoichiometry. Accordingly, after calculation of the molecular weight by using the standard curve of Superdex 200 column, it was suggested that Cor might exist as a trimer. This result was in contrast with Zacharia and colleagues study, where they run Cor on native gel and according to the molecular marker the molecular mass of Cor was 36 kDa, which suggested that Cor is a dimer (Zacharia et al., 2013).

Cor contains a DUF151 domain, which in the OmBBD protein in rice was proposed to have a nuclease activity (You et al., 2010). A simple assay was performed to test for DNA binding by Cor. DNA-binding proteins have often been seen to bind heparin

columns during purification because heparin is a structural analogue of the backbone of (Raman et al., 2003). So, a heparin column was used as a simple initial test of the ability of Cor to bind DNA. The result shows that Cor did not bind to the column, which suggest that Cor might be unable to bind the DNA, and thus might not has a nuclease activity. This result was agreed with the Zacharia et al. study, which showed no DNase or RNase activity of Cor when tested as a maltose-binding protein, compared with His-MBP alone (Zacharia et al., 2013).

6.13.2 Chemical characterization of Cor

The metal composition of Cor was determined by using ICP-MS (Chapter 6, section 6.9.3), according to the concentration of the protein sample that was sent to the ICP-MS test, the amino acids composition of Cor, and the atomic number of each ion, the number of ions per protein molecule was calculated, as shown in table 6.3. No metal binding by Cor was revealed by an ICP-MS analysis.

Table 6.3. ICP-MS results for Cor. The table shows the metallic composition of Cor revealed by ICP-MS, it shows the measured atomic mass of each ion in mg/l and the number of ionic atoms in Cor sample.

Ion	Al	Ca	P	S	Fe	Si	K	Mg	Zn
Measured mg/l	0.26	0.44	4.48	5.64	0.08	0.36	0.64	1.72	0.27
Number of atoms/ protein molecule	0.0067	0.00765	0.1007	0.1224	0.001	0.0089	0.0114	0.0493	0.0029

6.13.3 Crystallization and data collection

Crystallization is a very complicated process, and needs control of different parameters, such as protein concentration, purity of protein, homogeneity, temperature, pH of the crystallization buffer and precipitant concentration. For this reason, a set of experiment

should be carried out before deciding which condition is the best for crystal forming and growing.

The purity is the most important factor that can affect crystal forming, since a minute contamination might cause a protein instability, or it can disturb the structural determination (Lorber et al., 1993).

Cor is a highly soluble protein, which expresses very well, and purified Cor can be very highly concentrated (60 mg/ml). Thus, the concentration was not a problem with Cor, since a set of concentrations (60-15 mg/ml) was used in different crystallization experiments. Although the purity might be an issue in some protein samples, 99% purity was achieved, which was enough for crystallization purposes. Sample heterogeneity is an issue in protein crystallization, since more than one version of the protein might be found, such as tetramer with trimer or dimer and monomer in the same preparation, which might corrupt the ordered arrangement of protein crystal. The aggregation of full length and truncated protein might be also a problem in crystallization, since a minute contamination in the protein preparation can cause instability and interfere with protein molecules ordered in the crystal. Purified Cor showed no contamination of full length and truncated version as shown by MS, which showed only one peak corresponding to the molecular weight of the full length protein. However, a combination of trimer and dimer might be found after Cor purification, this could potentially affect Cor crystallization. Crystals were obtained, although most of the crystals were tiny and needle-shaped (see Chapter 6, section 6.10). Some of them were successfully sent for X-ray diffraction testing.

The data showed no diffraction for all the crystals tested (see Chapter 6, section 6.11). There are many factors that can affect X-ray diffraction (Rohrbaugh and Wu, 1989), such as the molecular packing pattern, or the small size of the crystal which leads to diffraction so weak that it cannot be measured.

Cryoprotection is an important step in X-ray diffraction testing, since the crystal is grown in a solution containing water, which under the cryogen temperature necessary in crystal flash cooling during data collection forms an ice crystals. The consequence is that the ice water crystals can interact with protein diffraction or disrupt the crystal lattice (Shah et al., 2011). For example, during crystal mounting it was noted that crystals grown in 0.2 M potassium thiocyanate, 0.1 M bis-Tris propane pH 6.5 and 20% (w/v) PEG3350, dissolved in the cryoprotection solution, which contained the mother liquor with 15% ethylene glycol (EG), but when the crystal was mounted with a higher concentration of polyethylene glycol (40% w/v) it was survive. Thus, Cor crystal might have been very sensitive to the correct cryoprotection conditions.

The X-ray diffraction images that were collected did not show any evidence of salt crystal diffraction, which suggested that the crystal was a protein crystal. Also, the crystals were all fragile and many of them may have suffered mechanical damage during mounting. Further test was carried out, to check if the crystals were a protein crystal, by adding a blue Izit dye to the crystals, the Izit dye is a small molecule dye, uses to distinguish protein from salt crystal. It can penetrate the protein crystal (bind loosely) and bind to the amino acids and color the protein. Test with Izit dye was inconclusive, the crystals were dissolved once the dye was added.

6.13.4 Biochemical studies for Cor

After many crystallization screens and attempts to solve the crystal structure of Cor, which might give some insight for Cor function, a series of biochemical tests were performed, in attempt to find the mechanism behind Cor function as described in Chapter 6, section 6.12. It was suggested that Cor might act as a Carbon Monoxide Dehydrogenase (CODH), to oxidize CO to CO₂, and for this reason, Cor was tested by using methyl viologen (MV) as an electron acceptor. The reaction is oxygen and light sensitive, so all the solutions were degased by nitrogen gas, and the MV solution was

kept in the dark. The spectrum was taken at 578 nm, CO gas was used as CO source. No difference in the spectrum was seen when Cor was added, which suggest that Cor was not oxidizing CO.

A further test was performed to check the ability of Cor to protect *E. coli* cells against CO toxicity. Based on the published paper assertion that Cor can protect *E. coli* cells from CO toxicity (Zacharia et al., 2013), a test was carried out by using CORM-2 as a CO source. CO is an antimicrobial gas, which penetrates the cell membranes easily (Li and Moore, 2007). A controlled release for this gas was achieved by using different metal carbonyl compounds, such as CORM-2, which has used in the therapeutic field (Garcia-Gallego and Bernardes, 2014). The ruthenium carbonyl compound CORM-2 can produce CO even in dark, in compare with magnesium and iron carbonyl which need light to liberate CO (Motterlini et al., 2002).

In this study, no effect was observed for Cor in *E. coli* protection against CO released from CORM-2. Both control *E. coli* BL21, and the same cells transformed with pJ401 containing *Mtb cor* were killed by using 30 μ M of CORM-2 in defined minimal media (DMM). Cor expression was checked on SDS-PAGE, and the gel showed that the protein was expressed. This finding was in contrast to the findings of Zacharia and colleagues, which suggest Cor protection against CO toxicity in *E. coli*. The differences between the method here and the published method are the concentrations of CORM-2, which were (10 and 30 μ M) in this study, whereas higher concentration of 25 and 250 μ M were in published study. Although the concentration in the published study was higher, the exposure time in this study was longer, (30 min versus overnight). The question is whether 30 min is enough to give a clear picture of the CORM-2 effect on *E. coli*. Longer exposure might be preferable, since it can reduce the error because the number of sample points is more.

Cor has no metal bound to it, in the crystal structure of the Cor homologue (PDB entry 1VJL), and as demonstrated here by ICP-MS analysis. For a protein to react in an oxidation or reduction process, metals are often needed, for example iron, manganese, cobalt, and molybdenum. To detoxify CO, there should be a metal that can act as a redox center. It was proposed that CO might bind to heme, which is in turn bound to Cor, and thus the CO binds to Cor indirectly. This assumption was tested by investigating the ability of Cor to bind heme. A simple test was carried out by using hematin as heme *b* source. Albumin was used as a control protein, since albumin is available and it is known to bind a variety of molecules, as described in Chapter 3, section 3.2.26.8. The ability of human serum albumin to bind heme has been intensively studied by using techniques as steady-state fluorescence and the binding between heme and human serum albumin proved (Kamal and Behere, 2005). Thus, in this study the albumin was used as a positive control. The result showed that the albumin bound hematin, whereas Cor did not bind. No peaks were seen in 540 and 557 nm when Cor was added to the hematin solution, whereas two peaks were observed when the same concentration of bovine serum albumin was added. This result suggests that Cor is unable to bind to heme.

Many proteins need a partner protein, to be able to catalyse a certain reaction. The interaction of Cor with a partner protein was tested, by using a pull-down assay (As described in Chapter 3, section 3.2.26.9). The difficulty in getting a cell free extract of Mtb prevented the use of a pull-down Cor with Mtb CFE, thus the CFE of *M. smegmatis* (which has a Cor homologue with 96% similarity to Mtb Cor protein), was used. The *E. coli* K12 CFE was used also, based on the published work suggesting that Cor can protect *E. coli* from CO toxicity, it was hypothesized that there might be a protein partner for Cor within the *E. coli* proteins. Two His-tagged protein were used as positive His-tagged protein controls, YloQ and BLF1. The result showed that there was

no clear band in the SDS-PAGE, suggesting no interaction between Cor and another protein in *E. coli* or *M. smegmatis* CFEs.

To check if purified Cor is able to interact directly with CO and detoxify it, a number of tests were carried out. Firstly, an FTIR spectrum was taken for Cor in the presence of CO gas, as described in Chapter 3, section 3.2.26.5. The result was inconclusive showed that the CO was not consumed in the presence of Cor, and no signal was observed corresponding to CO₂. It might be that the concentrations of Cor or CO needed to be optimized or that the exposure time was not enough (1 h and 37 min).

NMR spectra were taken for Cor with and without CO gas as described in Chapter 3, section 3.2.26.6. to investigate if there was any shift in the NMR signal, which might give an initial indication of any interaction between Cor and CO. The result showed that there were no differences in spectra taken over 4 h in the presence and absence of CO gas. There was a slight shift in the aromatic region, but this might be due to the buffer pH changing from 8 to 7.5 (see Chapter 6, section 6.12.5).

Chapter 7 : Conclusion and future plan

Conclusion

The *in vitro* studies of NorW revealed a new aspect in NO detoxification, it showed that NorW can reduce NO in different oxygen levels directly without NorV. However, *in vivo*, the *norW* gene did not confer resistance toward NO. Thus, the activity of the NorW enzyme in the *in vitro* assays could be an artefact of the experimental approach. In contrast, it might suggest that *in vivo* there is an inhibitory factor bound to NorW which normally blocks or regulates its activity if NorV is absent but that is lost during the purification of NorW. The presence of an additional NO detoxification activity in the cell provided by NorW alone could offer an advantage under certain conditions when perhaps supplies of cofactors like iron are low.

The crystallization results of NorV showed two main domains the N- terminal β -lactamase like domain and the FMN like domain and the C-terminal rubredoxin like domain was missing in the data. The mass spectrum of the protein in solution revealed that the rubredoxin domain was cleaved during the purification, because there was a signal corresponding to the molecular weight of the protein without the rubredoxin domain. The dissolved crystal SDS-PAGE also revealed a band corresponding to the cleaved protein around 47 kDa, which was agree with the mass spectrometry analysis.

The results from the assays and analyses with Cor gave no evidence for a CO binding or detoxification activity. Thus, it is possible that the published data

have mistakenly suggested that the observed CO resistance is because of a direct role of the Cor protein. It was suggested that a Cor-like domain might have a DNA binding function based on some nuclease activity and it is possible that Cor maybe a DNA-binding regulatory protein whose function is indirectly linked to CO resistance. It is not clear why this could not be seen in the *E. coli* growth assays in this study but perhaps it is dependent on factors in the growth conditions or even the strain tested.

Ideas for future experiments

A structure of NorW alone or a NorV-NorW complex has proved impossible with the intact proteins and therefore a truncated version of NorV could be employed which consists of just the rubredoxin domain. Purified His-tagged NorW from *E. coli* could be combined with the rubredoxin domain from *E. coli* NorV, in order to co-crystallize a more stable complex, in attempts to get a protein crystal structure of NorW. The structure will help to understand the mechanism behind NorW function, and electron transfer by cofactor, details on metal binding and important motifs which could be a target for drugs.

The FTIR assay for NorW should be repeated using other NO releasing molecules, such as PROLI-NONOate, which was used in the *in vitro* assays, in order to confirm that NO is released and is effecting cells, because it was argued that DETA-NONOate might not release NO in that assay. Changing the solution from bacterial growth media to a buffer system should be performed to check if any of the media components interacted with NO and converted it to N₂O independent of the NorW in an abiotic reaction. This will eliminate any possibility of an abiotic reaction that could have happened because of the media components.

Future work on a structure of NorV could include attempts to get a stable version of the full length NorV by using additional protease inhibitors to those already tested or mutation of amino acids in the protease sensitive cleavage site. This protein might then be used for crystallization, and determination of the structure at high resolution, in order to see the structure of the rubredoxin domain. A stable NorV construct might also be used to investigate the stoichiometry of a NorV-NorW complex. As part of an examination of the effect of structure on enzyme catalytic rates, the interface residues in the NorV tetramer might also be probed by mutagenesis to examine their relative importance in stabilizing the interface between FAD and Fe centres in adjacent

subunits. Simple structure and bioinformatics sequence analysis could be used to identify key residues such as tryptophan residues W148, W348 and W375. Differences in enzyme catalyzed reaction rates could then be correlated with the changes in the residues at the interface and possible differences in the electron transfer distance.

The experiments with Cor did not show any signs of resistance to CO. However, they might be repeated to test the ability of Cor to protect *E. coli* from the effect of CO, by using CORM-401 (a manganese containing CORM) instead of CORM-2 in order to confirm that the toxicity was not caused by ruthenium (contained in CORM-2). Viability based on cell counts could be employed, which gives a more accurate indication than measurement of simple optical density of cultures. The actual functional role of Cor remains unclear and a structure might help to clarify its possible mode of activity by comparisons with other proteins already studied. Further efforts could be made to obtain a construct for a non His-tagged Cor that could be used for crystallization, because it has been known that the His-tag might cause a disorder or instability for some proteins, which can reduce the chance to get protein crystals. Attempts to crystallize Cor might be tried by expressing Cor in *M. smegmatis*, which might provide cofactors or mechanisms of loading not available in normal *E. coli* cells. Alternatively, *in vitro* reconstitution of Cor with possible cofactors could be tested by adding molecules such as heme, NADH, FADH or NADPH, which might be part of the Cor mechanism of action. Finally, the FTIR experiment could be repeated with increased Cor concentration and reduced CO gas concentration, which might give some signs of low level CO consumption.

References

Akihito Yamano (2012). Introduction to single crystal X-ray analysis. The Rigaku journal 28 (2).

Attwood, D. (2002). Soft x-ray microscopy and extreme ultraviolet lithography: Imaging in the 20–50 nm regime (abstract) (invited). Review of Scientific Instruments 73, 1637-1637.

Babcock, G.T., and Wikstrom, M. (1992). oxygen activation and the conservation of energy in cell respiration. nature 356, 301-309.

Bailey, S. (1994). the ccp4 suite - programs for protein crystallography. acta crystallographica section d-biological crystallography 50, 760-763.

Baptista, J.M., Justino, M.C., Melo, A.M.P., Teixeira, M., and Saraiva, L.M. (2012). Oxidative stress modulates the nitric oxide defense promoted by *Escherichia coli* flavorubredoxin. J Bacteriol 194, 3611-3617.

Benjamini, E. (1991). Immunology a short course second edition. immunology.

Benjamini, E., and Leskowitz, S. (1991). Immunology a short course second edition. Benjamini, E and S Leskowitz Immunology: a short course, second edition Xxvi+459p John Wiley and Sons, Inc: New York, New York, USA; Chichester, England, Uk Illus Paper, XXVI+459P.

Benvenuti, M., and Mangani, S. (2007). Crystallization of soluble proteins in vapor diffusion for x-ray crystallography. Nature Protocols 2, 1633-1651.

Bergfors TM. (1999). Protein crystallization: techniques, strategies, and tips: a laboratory manual. La Jolla, Calif: International University Line.

Bogdan, C. (2001). Nitric oxide and the immune response. *Nat Immunol* 2, 907-916.

Bonamore, A., and Boffi, A. (2008). Flavohemoglobin: structure and reactivity. *IUBMB LIFE* 60, 19-28.

Bradford, M.M. (1976). A rapid and sensitive method for the quantitation of microgram quantities of protein utilizing the principle of protein-dye binding. *Analytical Biochemistry* 72, 248-254.

Bragg, W.L. (1913). The structure of some crystals as indicated by their diffraction of x-rays. *Proceedings of the Royal Society of London Series a-Containing Papers of a Mathematical and Physical Character* 89, 248-277.

Brouard, S., Otterbein, L.E., Anrather, J., Tobiasch, E., Bach, F.H., Choi, A.M.K., and Soares, M.P. (2000). Carbon monoxide generated by heme oxygenase 1 suppresses endothelial cell apoptosis. *Journal of Experimental Medicine* 192, 1015-1025.

Brown, K., Tegoni, M., Prudêncio, M., Pereira, A.S., Besson, S., Moura, J.J., Moura, I., and Cambillau, C. (2000). A novel type of catalytic copper cluster in nitrous oxide reductase. *NAT STRUCT BIOL* 7, 191-195.

Bueno, R., Pahel, G., and Magasanik, B. (1985). Role of *glnB* and *glnD* gene-products in regulation of the *glnALG* operon of *Escherichia coli*. *Journal of Bacteriology* *164*, 816-822.

Busch, A., Pohlmann, A., Friedrich, B., and Cramm, R. (2004). A DNA region recognized by the nitric oxide-responsive transcriptional activator NorR is conserved in beta- and gamma-proteobacteria. *Journal of Bacteriology* *186*, 7980-7987.

Cheesman, M.R., Zumft, W.G., and Thomson, A.J. (1998). The MCD and EPR of the heme centers of nitric oxide reductase from *Pseudomonas stutzeri*: Evidence that the enzyme is structurally related to the heme-copper oxidases. *Biochemistry* *37*, 3994-4000.

Chen, L., Liu, M.Y., Legall, J., Fareleira, P., Santos, H., and Xavier, A.V. (1993a). Purification and characterization of an *nadh*-rubredoxin oxidoreductase involved in the utilization of oxygen by *Desulfovibrio gigas*. *European Journal of Biochemistry* *216*, 443-448.

Chen, L., Liu, M.Y., Legall, J., Fareleira, P., Santos, H., and Xavier, A.V. (1993b). Rubredoxin oxidase, a new flavo-hemo-protein, is the site of oxygen reduction to water by the strict anaerobe *Desulfovibrio gigas*. *Biochemical and Biophysical Research Communications* *193*, 100-105.

Chen, L., Pereira, M.M., Teixeira, M., Xavier, A.V., and Legall, J. (1994). Isolation and characterization of a high-molecular-weight cytochrome from the sulfate-reducing bacterium *Desulfovibrio gigas*. *Febs Letters* *347*, 295-299.

Chen, Z.Q., Foster, M.W., Zhang, J., Mao, L., Rockman, H.A., Kawamoto, T., Kitagawa, K., Nakayama, K.I., Hess, D.T., and Stamler, J.S. (2005). An essential role for mitochondrial aldehyde dehydrogenase in nitroglycerin bioactivation. *Proceedings of the National Academy of Sciences of the United States of America* *102*, 12159-12164.

Chung, S.W., Liu, X., Macias, A.A., Baron, R.M., and Perrella, M.A. (2008). Heme oxygenase-1-derived carbon monoxide enhances the host defense response to microbial sepsis in mice. *Journal of Clinical Investigation* *118*, 239-247.

Collman, J.P., Yang, Y., Dey, A., Decréau, R.A., Ghosh, S., Ohta, T., and Solomon, E.I. (2008). A functional nitric oxide reductase model. *P Natl Acad Sci. USA* *105*, 15660-15665.

Corker, H., and Poole, R.K. (2003). Nitric oxide formation by *Escherichia coli* - Dependence on nitrite reductase, the NO-sensing regulator FNR, and flavohemoglobin Hmp. *Journal of Biological Chemistry* *278*, 31584-31592.

Costa, P.N., Vicente, J.B., Teixeira, M., and Saraiva, L.M. (2003). *E. coli* flavorubredoxin, a novel type of nitric oxide reductase. *Free Radical Bio Med* *35*, S175-S175.

Cramm, R., Pohlmann, A., and Friedrich, B. (1999). Purification and characterization of the single-component nitric oxide reductase from *Ralstonia eutropha* H16. *Febs Letters* *460*, 6-10.

Cramm, R., Siddiqui, R.A., and Friedrich, B. (1994). Primary sequence and evidence for a physiological-function of the flavohemoprotein of *Alcaligenes eutrophus*. *Journal of Biological Chemistry* 269, 7349-7354.

Cramm, R., Siddiqui, R.A., and Friedrich, B. (1997). Two isofunctional nitric oxide reductases in *Alcaligenes eutrophus* H16. *J Bacter* 179, 6769-6777.

Cutruzzolà, F. (1999). Bacterial nitric oxide synthesis. *BBA-Bioenergetics* 1411, 231-249.

D'Autreaux, B.D., Tucker, N.P., Dixon, R., and Spiro, S. (2005). A non-haem iron centre in the transcription factor NorR senses nitric oxide. *Nature*, 437, 769-772.

Davidge, K.S., Motterlini, R., Mann, B.E., Wilson, J.L., and Poole, R.K. (2009). Carbon Monoxide in Biology and Microbiology: Surprising Roles for the "Detroit Perfume". *Advances in Microbial Physiology*, 56, 85-167.

Degn H, Lilleor M, Iversen JLL. (1973). The occurrence of a stepwise-decreasing respiration rate during oxidative assimilation of different substrates by resting *Klebsiella aerogenes* in a system open to oxygen. *Biochem J.* 136,1097-1104.

de Vries, S., Strampraad, M.J.F., Lu, S., Moenne-Loccoz, P., and Schroder, I. (2003). Purification and characterization of the MQH(2): NO oxidoreductase from the hyperthermophilic archaeon *Pyrobaculum aerophilum*. *Journal of Biological Chemistry* 278, 35861-35868.

Desmard, M., Davidge, K., Bouvet, O., Morin, D., Roux, D., Ricard, J.D., Foresti, R., Denamur, E., Poole, R.K., Montravers, P., *et al.* (2009). A Carbon Monoxide-Releasing Molecule (CORM-3) Exerts Bactericidal Activity Against *Pseudomonas aeruginosa*. *American Journal of Respiratory and Critical Care Medicine* 179.

Dessau, M.A., and Modis, Y. (2011). Protein Crystallization for X-ray Crystallography. *Jove-Journal of Visualized Experiments*.

Di Matteo, A., Scandurra, F.M., Testa, F., Forte, E., Sarti, P., Brunori, M., and Giuffrè, A. (2008). The O₂-scavenging flavodiiron protein in the human parasite *Giardia intestinalis*. *J Biol Chem* 283, 4061-4068.

Dieffenbach, C.W., Lowe, T.M.J., and Dveksler, G.S. (1993). General concepts for PCR primer design. *Genome Research* 3, S30-S37.

Doherty, A.J., Connolly, B.A., and Worrall, A.F. (1993). Overproduction of the toxic protein, bovine pancreatic dnase in *Escherichia coli* using a tightly controlled T7-promoter-based vector. *Gene* 136, 337-340.

Dong, H.J., Nilsson, L., and Kurland, C.G. (1995). gratuitous overexpression of genes in *Escherichia coli* leads to growth-inhibition and ribosome destruction. *J. Bacterio* 177, 1497-1504.

Eckert, M. (2012). Max von Laue and the discovery of X-ray diffraction in 1912. *Annalen Der Physik* 524, A83-A85.

Emsley, P., and Cowtan, K. (2004). Coot: model-building tools for molecular graphics. *Acta Crystallographica Section D-Biological Crystallography* 60, 2126-2132.

Emsley, P., Lohkamp, B., Scott, W.G., and Cowtan, K. (2010). Features and development of Coot. *Acta Crystallographica Section D-Biological Crystallography* 66, 486-501.

Fang, F.C. (1997). Perspectives series: host/pathogen interactions. Mechanisms of nitric oxide-related antimicrobial activity. *J CLIN INVEST* 99, 2818-2825.

Favey, S., Labesse, G., Vouille, V., and Boccarda, M. (1995). Flavohaemoglobin hmpX - a new pathogenicity determinant in *Erwinia chrysanthemi* strain-3937. *Microbiology-Uk* 141, 863-871.

Fearon, D.T., and Locksley, R.M. (1996). Elements of immunity - The instructive role of innate immunity in the acquired immune response. *Science* 272, 50-54.

Flatley, J., Barrett, J., Pullan, S.T., Hughes, M.N., Green, J., and Poole, R.K. (2005). Transcriptional responses of *Escherichia coli* to S-nitrosoglutathione under defined chemostat conditions reveal major changes in methionine biosynthesis. *Journal of Biological Chemistry* 280, 10065-10072.

Frazao, C., Silva, G., Gomes, C.M., Matias, P., Coelho, R., Sieker, L., Macedo, S., Liu, M.Y., Oliveira, S., Teixeira, M., *et al.* (2000). Structure of a dioxygen reduction enzyme from *Desulfovibrio gigas*. *Nature Structural Biology* 7, 1041-1045.

Frey, A.D., Farrés, J., Bollinger, C.J.T., and Kallio, P.T. (2002). Bacterial hemoglobins and flavohemoglobins for alleviation of nitrosative stress in *Escherichia coli*. *Appl Environ Microb* 68, 4835-4840.

Furchgott, R.F., and Jothianandan, D. (1991). Endothelium-dependent and endothelium-independent vasodilation involving cyclic-gmp - relaxation induced by nitric-oxide, carbon-monoxide and light. *Blood Vessels* 28, 52-61.

Furchgott, R.F., and Zawadski, J. (1980). The obligatory role of the endothelium in the relaxation of arterial smooth-muscle by acetylcholine. *Blood Vessels* 17, 151-151.

Garcia-Gallego, S., and Bernardes, G.J.L. (2014). Carbon-Monoxide-Releasing Molecules for the Delivery of Therapeutic CO *In vivo*. *Angewandte Chemie-International Edition* 53, 9712-9721.

Gardner, A.M., and Gardner, P.R. (2002). Flavohemoglobin detoxifies nitric oxide in aerobic, but not anaerobic, *Escherichia coli*. Evidence for a novel inducible anaerobic nitric oxide-scavenging activity. *J BIOL CHEM* 277, 8166-8171.

Gardner, A.M., Gessner, C.R., and Gardner, P.R. (2003). Regulation of the nitric oxide reduction operon (norRVW) in *Escherichia coli*. Role of NorR and sigma54 in the nitric oxide stress response. *J Biol Chem* 278, 10081-10086.

Gardner, A.M., Helmick, R.A., and Gardner, P.R. (2002). Flavorubredoxin, an inducible catalyst for nitric oxide reduction and detoxification in *Escherichia coli*. *J Biol Chem* 277, 8172-8177.

Gardner, A.M., Martin, L.A., Gardner, P.R., Dou, Y., and Olson, J.S. (2000a). Steady-state and transient kinetics of *Escherichia coli* nitric-oxide dioxygenase (flavo-hemoglobin) - The B10 tyrosine hydroxyl is essential for dioxygen binding and catalysis. *Journal of Biological Chemistry* 275, 12581-12589.

Gardner, A.M., Martin, L.A., Salzman, A.L., Gardner, P.R., Gardner, A.M., Martin, L.A., and Salzman, A.L. (1998a). Nitric oxide dioxygenase: An enzymic function for flavo-hemoglobin. *Free Radical Bio Med* 25, S59-S59.

Gardner, P.R. (2002). Aconitase: Sensitive target and measure of superoxide. *Superoxide Dismutase* 349, 9-23.

Gardner, P.R., Costantino, G., and Salzman, A.L. (1998b). Constitutive and adaptive detoxification of nitric oxide in *Escherichia coli* - Role of nitric-oxide dioxygenase in the protection of aconitase. *Journal of Biological Chemistry* 273, 26528-26533.

Gardner, P.R., Costantino, G., Szabo, C., and Salzman, A.L. (1997). Nitric oxide sensitivity of the aconitases. *Journal of Biological Chemistry* 272, 25071-25076.

Gardner, P.R., Gardner, A.M., Martin, L.A., Dou, Y., Li, T.S., Olson, J.S., Zhu, H., and Riggs, A.F. (2000b). Nitric-oxide dioxygenase activity and function of

flavo-hemoglobins - Sensitivity to nitric oxide and carbon monoxide inhibition. *Journal of Biological Chemistry* 275, 31581-31587.

Gardner, P.R., Gardner, A.M., Martin, L.A., and Salzman, A.L. (1998c). Nitric oxide dioxygenase: an enzymic function for flavo-hemoglobin. *PNAS USA* 95, 10378-10383.

Gardner, P.R., Gardner, A.M., Martin, L.A., and Salzman, A.L. (1998d). Nitric oxide dioxygenase: An enzymic function for flavo-hemoglobin. *Proceedings of the National Academy of Sciences of the United States of America* 95, 10378-10383.

Gardner, P.R., Martin, L.A., Hall, D., and Gardner, A.M. (2001). Dioxygen-dependent metabolism of nitric oxide in mammalian cells. *Free Radical Biology and Medicine* 31, 191-204.

Giege, R., Dock, A.C., Kern, D., Lorber, B., Thierry, J.C., and Moras, D. (1986). The role of purification in the crystallization of proteins and nucleic-acids. *Journal of Crystal Growth* 76, 554-561.

Gilliland, G.L. (1988). A biological macromolecule crystallization database: A basis for a crystallization strategy. *Journal of Crystal Growth* 90, 51-59.

Gilliland, G.L., and Ladner, J.E. (1996). Crystallization of biological macromolecules for X-ray diffraction studies. *Current Opinion in Structural Biology* 6, 595-603.

Gilliland, G.L., Tung, M., Blakeslee, D.M., and Ladner, J.E. (1994). Biological Macromolecule Crystallization Database, Version 3.0: new features, data and the NASA archive for protein crystal growth data. *Acta Crystallographica Section D* 50, 408-413.

Gomes, C.M., Giuffrè, A., Forte, E., Vicente, J.B., Saraiva, L.M., Brunori, M., and Teixeira, M. (2002a). A novel type of nitric-oxide reductase - *Escherichia coli* flavorubredoxin. *Journal of Biological Chemistry* 277, 25273-25276.

Gomes, C.M., Giuffrè, A., Forte, E., Vicente, J.B., Saraiva, L.M., Brunori, M., and Teixeira, M. (2002b). A novel type of nitric-oxide reductase. *Escherichia coli* flavorubredoxin. *Journal of Biological Chemistry* 277, 25273-25276.

Gomes, C.M., Silva, G., Oliveira, S., LeGall, J., Liu, M.Y., Xavier, A.V., Rodrigues-Pousada, C., and Teixeira, M. (1997). Studies on the redox centers of the terminal oxidase from *Desulfovibrio gigas* and evidence for its interaction with rubredoxin. *Journal of Biological Chemistry* 272, 22502-22508.

Gomes, C.M., Vicente, J.B., Wasserfallen, A., and Teixeira, M. (2000). Spectroscopic studies and characterization of a novel electron-transfer chain from *Escherichia coli* involving a flavorubredoxin and its flavoprotein reductase partner. *Biochemistry. US* 39, 16230-16237.

Guo, G., Mao, X., Zhang, W., and Xiao, J. (2008). Functional identification of HugZ, a heme oxygenase from *Helicobacter pylori*. *BMC Microbiol* 8.

Hagelueken, G., Wiehlmann, L., Adams, T.M., Kolmar, H., Heinz, D.W., Tuemmler, B., and Schubert, W.-D. (2007a). Crystal structure of the electron transfer complex rubredoxin-rubredoxin reductase of *Pseudomonas aeruginosa*. Proceedings of the National Academy of Sciences of the United States of America *104*, 12276-12281.

Hagelueken, G., Wiehlmann, L., Adams, T.M., Kolmar, H., Heinz, D.W., Tuemmler, B., and Schubert, W.D. (2007b). 2V3A: Crystal Structure Of Rubredoxin Reductase From *Pseudomonas Aeruginosa*. Worldwide Protein Data Bank.

Hanahan, D. (1983). Studies on transformation of *Escherichia coli* with plasmids. Journal of Molecular Biology *166*, 557-580.

Haskin, C.J., Ravi, N., Lynch, J.B., Münck, E., and Jr, LQ. (1995). Reaction of NO with the Reduced R2 Protein of Ribonucleotide Reductase from *Escherichia coli*. Biochemistry, *34*, 11090-11098.

Hauptman, H.A. (1990). History of X-Ray Crystallography. Structural Chemistry *1*, 617-620.

Hausladen, A., Gow, A.J., and Stamler, J.S. (1998). Nitrosative stress: Metabolic pathway involving the flavohemoglobin. Proceedings of the National Academy of Sciences of the United States of America *95*, 14100-14105.

Haveman, S.A., Greene, E.A., Stilwell, C.P., Voordouw, J.K., and Voordouw, G. (2004). Physiological and gene expression analysis of inhibition of *Desulfovibrio vulgaris* Hildenborough by nitrite. *Journal of Bacteriology* 186, 7944-7950.

Heiss, B., Frunzke, K., and Zumft, W.G. (1989). Formation of the n-n-bond from nitric-oxide by a membrane-bound cytochrome *bc* complex of nitrate-respiring (denitrifying) *Pseudomonas stutzeri*. *Journal of Bacteriology* 171, 3288-3297.

Helliwell, J.R., Blake, A.J., Blunden-Ellis, J., Moore, M., and Schwalbe, C.H. (2012). Some historical extracts relevant to the discovery and application of the diffraction of X-rays by crystals to contribute to the Centennial celebration and the International Year of Crystallography (Taylor & Francis Group), pp. 3-19.

Helmick, R.A., and Gardner, P.R. (2002). Flavorubredoxin: A critical nitrosative stress response enzyme for NO reduction and detoxification in anaerobic *Escherichia coli*. Abstracts of the General Meeting of the American Society for Microbiology 102, 284.

Hendriks, J., Oubrie, A., Castresana, J., Urbani, A., Gemeinhardt, S., and Saraste, M. (2000). Nitric oxide reductases in bacteria. *BBA Bioenergetics* 1459, 266-273.

Hendriks, J., Warne, A., Gohlke, U., Haltia, T., Ludovici, C., Lubben, M., and Saraste, M. (1998). The active site of the bacterial nitric oxide reductase is a dinuclear iron center. *Biochemistry* 37, 13102-13109.

Hino, T., Matsumoto, Y., Nagano, S., Sugimoto, H., Fukumori, Y., Murata, T., Iwata, S., and Shiro, Y. (2010). Structural Basis of Biological N₂O Generation by Bacterial Nitric Oxide Reductase. *Science* *330*, 1666-1670.

Ho, Y.S.J., Burden, L.M., and Hurley, J.H. (2000). Structure of the GAF domain, a ubiquitous signaling motif and a new class of cyclic GMP receptor. *Embo Journal* *19*, 5288-5299.

Hughes, M.N. (1999). Relationships between nitric oxide, nitroxyl ion, nitrosonium cation and peroxyxynitrite. *Biochimica Et Biophysica Acta-Bioenergetics* *1411*, 263-272.

Hutchings, M.I., Mandhana, N., and Spiro, S. (2002a). The NorR protein of *Escherichia coli* activates expression of the flavorubredoxin gene *norV* in response to reactive nitrogen species. *Journal of Bacteriology* *184*, 4640-4643.

Hutchings, M.I., Mandhana, N., and Spiro, S. (2002b). The NorR protein of *Escherichia coli* activates expression of the flavorubredoxin gene *norV* in response to reactive nitrogen species. *Journal of Bacteriology* *184*, 4640-4643.

Ignarro, L.J., Buga, G.M., Wood, K.S., Byrns, R.E., and Chaudhuri, G. (1987a). Endothelium-derived relaxing factor produced and released from artery and vein is nitric-oxide. *Proceedings of the National Academy of Sciences of the United States of America* *84*, 9265-9269.

Ignarro, L.J., Byrns, R.E., Buga, G.M., and Wood, K.S. (1987b). Endothelium-derived relaxing factor from pulmonary-artery and vein possesses pharmacological and

chemical-properties identical to those of nitric-oxide radical. *Circulation Research* 61, 866-879.

Imlay J. A. (1995). A Metabolic Enzyme That Rapidly Produces Superoxide, Fumarate Reductase of *Escherichia coli*. *Journal of Biological Chemistry*. 270, 19767–19777.

Ji, X.B., and Hollocher, T.C. (1988). Reduction of nitrite to nitric-oxide by enteric bacteria. *Biochemical and Biophysical Research Communications* 157, 106-108.

Justino, M.C., Almeida, C.C., Teixeira, M., and Saraiva, L.M. (2007). *Escherichia coli* di-iron YtfE protein is necessary for the repair of stress-damaged iron-sulfur clusters. *Journal of Biological Chemistry* 282, 10352-10359.

Justino, M.C., Costa, P.N., Vicente, J.B., Teixeira, M., and Saraiva, L.M. (2003). *E coli* flavorubredoxin, a novel type of nitric oxide reductase. *Free Radical Biology and Medicine* 35, S175-S175.

Justino, M.C., Vicente, J.B., Teixeira, M., and Saraiva, L.M. (2005). New genes implicated in the protection of anaerobically grown *Escherichia coli* against nitric oxide. *Journal of Biological Chemistry* 280, 2636-2643.

Kamal, J.K.A., and Behere, D.V. (2005). Binding of heme to human serum albumin: Steady-state fluorescence, circular dichroism and optical difference spectroscopic studies. *Indian Journal of Biochemistry & Biophysics* 42, 7-12.

Kantardjieff, K.A., and Rupp, B. (2003). Matthews coefficient probabilities: Improved estimates for unit cell contents of proteins, DNA, and protein-nucleic acid complex crystals. *Protein Science* 12, 1865-1871.

Kendrew, J.C., Bodo, G., Dintzis, H.M., Parrish, R.G., Wyckoff, H., and Phillips, D.C. (1958). 3-dimensional model of the myoglobin molecule obtained by x-ray analysis. *Nature* 181, 662-666.

Kim, S.O., Oori, Y., Lloyd, D., Hughes, M.N., and Poole, R.K. (1999). Anoxic function for the *Escherichia coli* flavohaemoglobin (Hmp): reversible binding of nitric oxide and reduction to nitrous oxide. *Febs Letters* 445, 389-394.

Kleywegt, G.J. (2007). Separating model optimization and model validation in statistical cross-validation as applied to crystallography. *Acta Crystallographica Section D-Biological Crystallography* 63, 939-940.

Kumar, A., Deshane, J.S., Crossman, D.K., Bolisetty, S., Yan, B.S., Kramnik, I., Agarwal, A., and Steyn, A.J.C. (2008). Heme oxygenase-1-derived carbon monoxide induces the *Mycobacterium tuberculosis* dormancy regulon. *Journal of Biological Chemistry* 283, 18032-18039.

Laver, J.R., Stevanin, T.M., Messenger, S.L., Lunn, A.D., Lee, M.E., Moir, J.W.B., Poole, R.K., and Read, R.C. (2010). Bacterial nitric oxide detoxification prevents host cell S-nitrosothiol formation: a novel mechanism of bacterial pathogenesis. *FASEB Journal* 24, 286-295.

Lee, H.J., Basran, J., and Scrutton, N.S. (1998). Electron transfer from flavin to iron in the *Pseudomonas oleovorans* rubredoxin reductase-rubredoxin electron transfer complex. *Biochemistry*. US 37, 15513-15522.

Li, L., and Moore, P.K. (2007). An overview of the biological significance of endogenous gases: new roles for old molecules. *Biochemical Society Transactions* 35, 1138-1141.

Liu, X.M., Chapman, G.B., Peyton, K.J., Schafer, A.I., and Durante, W. (2002). Carbon monoxide inhibits apoptosis in vascular smooth muscle cells. *Cardiovascular Research* 55, 396-405.

Lorber, B., Skouri, M., Munch, J.P., and Giege, R. (1993). The influence of impurities on protein crystallization - the case of lysozyme. *Journal of Crystal Growth* 128, 1203-1211.

Lorite, M.J., Tachil, J., Sanjuan, J., Meyer, O., and Bedmar, E.J. (2000). Carbon monoxide dehydrogenase activity in *Bradyrhizobium japonicum*. *Applied and Environmental Microbiology* 66, 1871-1876.

Ma, K., and Adams, M.W. (1999). A hyperactive NAD(P)H:Rubredoxin oxidoreductase from the hyperthermophilic archaeon *Pyrococcus furiosus*. *Journal of Bacteriology* 181, 5530-5533.

Ma, K., and Adams, M.W. (2001). Ferredoxin:NADP oxidoreductase from *Pyrococcus furiosus*. *Method Enzymol* 334, 40-45.

Maines, M.D. (1988). Heme oxygenase - function, multiplicity, regulatory mechanisms, and clinical-applications. *Faseb Journal* 2, 2557-2568.

Mancinelli, R.L., and McKay, C.P. (1983). Effects of nitric-oxide and nitrogen-dioxide on bacterial growth. *Applied and Environmental Microbiology* 46, 198-202.

Massey, V. (1995). Introduction: flavoprotein structure and mechanism. *FASEB J* 9, 473-475.

Massey, V., and Hemmerich, P. (1980). Active-site probes of flavoproteins. *Biochemical Society Transactions* 8, 246-257.

Matthews, B.W. (1968). Solvent content of protein crystals. *Journal of Molecular Biology* 33, 491.

McCord, J.M., and Fridovic, I. (1969). superoxide dismutase an enzymic function for erythrocyte hemocuprein (hemocuprein). *Journal of Biological Chemistry* 244, 6049.

McCoy, A.J., Grosse-Kunstleve, R.W., Adams, P.D., Winn, M.D., Storoni, L.C., and Read, R.J. (2007). Phaser crystallographic software. *Journal of Applied Crystallography* 40, 658-674.

McLean, S., Bowman, L.A.H., Sanguinetti, G., Read, R.C., and Poole, R.K. (2010). Peroxynitrite Toxicity in *Escherichia coli* K12 Elicits Expression of Oxidative Stress

Responses and Protein Nitration and Nitrosylation. *Journal of Biological Chemistry* 285, 20724-20731.

McMullin, B.B., Chittock, D.R., Roscoe, D.L., Garcha, H., Wang, L., and Miller, C.C. (2005). The antimicrobial effect of nitric oxide on the bacteria that cause nosocomial pneumonia in mechanically ventilated patients in the intensive care unit. *Respiratory care* 50, 1451-1456.

McPherson A. Crystallization of biological macromolecules. Cold Spring Harbor, NY: Cold Spring Harbor Laboratory Press; 1999.

McPherson, A., and Gavira, J.A. (2014). Introduction to protein crystallization. *Acta Crystallographica Section F. Structural Biology Communications* 70, 2-20.

Messner K. R., Imlay J. A. (1999). The Identification of Primary Sites of Superoxide and Hydrogen Peroxide Formation in the Aerobic Respiratory Chain and Sulfite Reductase Complex of *Escherichia coli*. *Journal of Biological Chemistry* 274, 10119–10128.

Messner K. R., Imlay J. A. (2002). Mechanism of Superoxide and Hydrogen Peroxide Formation by Fumarate Reductase, Succinate Dehydrogenase, and Aspartate Oxidase. *Journal of Biological Chemistry* 277, 42563-42571.

Meyer, O., and Schlegel, H.G. (1979). Oxidation of carbon monoxide in cell extracts of *Pseudomonas carboxydovorans*. *Journal of Bacteriology* 137, 811-817.

Moenne-Loccoz, P., Richter, O.M.H., Huang, H.W., Wasser, I.M., Ghiladi, R.A., Karlin, K.D., and de Vries, S. (2000). Nitric oxide reductase from *Paracoccus denitrificans* contains an oxo-bridged heme/non-heme diiron center. *Journal of the American Chemical Society* *122*, 9344-9345.

Moncada, S., and Higgs, A. (1993). The L-arginine-nitric oxide pathway. *New Engl J Med* *329*, 2002-2012.

Morita, H., Yoshikawa, H., Sakata, R., Nagata, Y., and Tanaka, H. (1997). Synthesis of nitric oxide from the two equivalent guanidino nitrogens of L-arginine by *Lactobacillus fermentum*. *Journal of Bacteriology* *179*, 7812-7815.

Motterlini, R., Clark, J.E., Foresti, R., Sarathchandra, P., Mann, B.E., and Green, C.J. (2002). Carbon monoxide-releasing molecules - Characterization of biochemical and vascular activities. *Circulation Research* *90*, E17-E24.

Mukhopadhyay, P., Zheng, M., Bedzyk, L.A., LaRossa, R.A., and Storz, G. (2004). Prominent roles of the NorR and Fur regulators in the *Escherichia coli* transcriptional response to reactive nitrogen species. *Proceedings of the National Academy of Sciences of the United States of America* *101*, 745-750.

Murshudov, G.N., Skubak, P., Lebedev, A.A., Pannu, N.S., Steiner, R.A., Nicholls, R.A., Winn, M.D., Long, F., and Vagin, A.A. (2011). REFMAC5 for the refinement of macromolecular crystal structures. *Acta Crystallographica Section D. Biological Crystallography* *67*, 355-367.

Murshudov, G.N., Vagin, A.A., and Dodson, E.J. (1997). Refinement of macromolecular structures by the maximum-likelihood method. *Acta Crystallographica Section D. Biological Crystallography* 53, 240-255.

Nathan, C. (1992). Nitric-oxide as a secretory product of mammalian cells. *Faseb Journal* 6, 3051-3064.

Nathan, C. (1997). Inducible nitric oxide synthase: what difference does it make? *J Clin Invest* 100, 2417-2423.

Nobre, L.S., Al-Shahrour, F., Dopazo, J., and Saraiva, L.M. (2009). Exploring the antimicrobial action of a carbon monoxide-releasing compound through whole-genome transcription profiling of *Escherichia coli*. *Microbiol-SGM* 155, 813-824.

Nobre, L.S., Seixas, J.D., Romão, C.C., and Saraiva, L.M. (2007). Antimicrobial action of carbon monoxide-releasing compounds. *Antimicrob Agents CH* 51, 4303-4307.

Otterbein, L.E., Bach, F.H., Alam, J., Soares, M., Lu, H.T., Wysk, M., Davis, R.J., Flavell, R.A., and Choi, A.M.K. (2000). Carbon monoxide has anti-inflammatory effects involving the mitogen-activated protein kinase pathway. *Nature Medicine* 6, 422-428.

Otterbein, L.E., May, A., and Chin, B.Y. (2005). Carbon monoxide increases macrophage bacterial clearance through toll-like receptor (TLR)4 expression. *Cellular and Molecular Biology* 51, 433-440.

Pacher, P., Beckman, J.S., and Liaudet, L. (2007). Nitric oxide and peroxynitrite in health and disease. *Physiological Reviews* 87, 315-424.

Payne, W.J., Liu, M.Y., Bursakov, S.A., and Le Gall, J. (1997). Microbial and plant metabolism of NO. *Biofactors* 6, 47-52.

Petitdemange, H., Blusson, H., and Gay, R. (1981). Detection of NAD(P)H--rubredoxin oxidoreductases in Clostridia. *Anal Biochem* 116, 564-570.

Petoukhov, M.V., Vicente, J.B., Crowley, P.B., Carrondo, M.A., Teixeira, M., and Svergun, D.I. (2008). Quaternary structure of flavorubredoxin as revealed by synchrotron radiation small-angle X-ray scattering. *Structure* 16, 1428-1436.

Piantadosi, C.A. (2002). Biological chemistry of carbon monoxide. *ANTIOXID REDOX SIGN* 4, 259-270.

Pike, A.C.W., Garman, E.F., Krojer, T., von Delft, F., and Carpenter, E.P. (2016). An overview of heavy-atom derivatization of protein crystals. *Acta Crystallographica Section D. Structural Biology* 72, 303-318.

Plamann, M.D., and Stauffer, G.V. (1983). Characterization of the *Escherichia coli* gene for serine hydroxymethyltransferase. *Gene* 22, 9-18.

Pohlmann, A., Cramm, R., Schmelz, K., and Friedrich, B. (2000). A novel NO-responding regulator controls the reduction of nitric oxide in *Ralstonia eutropha*. *Molecular Microbiology* 38, 626-638.

Poock, S.R., Leach, E.R., Moir, J.W.B., Cole, J.A., and Richardson, D.J. (2002). Respiratory detoxification of nitric oxide by the cytochrome *c* nitrite reductase of *Escherichia coli*. *Journal of Biological Chemistry* 277, 23664-23669.

Poole, R.K., and Hughes, M.N. (2000). New functions for the ancient globin family: bacterial responses to nitric oxide and nitrosative stress. *Molecular Microbiology* 36, 775-783.

Ramachandran, G.N., Ramakrishnan, C., and Sasisekharan, V. (1963). Stereochemistry of polypeptide chain configurations. *Journal of Molecular Biology* 7, 95.

Raman, R., Venkataraman, G., Ernst, S., Sasisekharan, V., and Sasisekharan, R. (2003). Structural specificity of heparin binding in the fibroblast growth factor family of proteins. *Proceedings of the National Academy of Sciences of the United States of America* 100, 2357-2362.

Ratliff, M., Zhu, W., Deshmukh, R., Wilks, A., and Stojiljkovic, I. (2001). Homologues of neisserial heme oxygenase in gram-negative bacteria: degradation of heme by the product of the *pigA* gene of *Pseudomonas aeruginosa*. *Journal of Bacteriology* 183, 6394-6403.

Rhodes, G. (2006). *Crystallography made crystal clear*. London: Academic Press.

Richardson, D., Felgate, H., Watmough, N., Thomson, A., and Baggs, E. (2009). Mitigating release of the potent greenhouse gas N₂O from the nitrogen cycle - could enzymic regulation hold the key? *Trends in Biotechnology* 27, 388-397.

Ridley, K.A., Rock, J.D., Li, Y., and Ketley, J.M. (2006). Heme utilization in *Campylobacter jejuni*. *J BACTERIOL* 188, 7862-7875.

Rohrbaugh, W.J., and Wu, E.L. (1989). Factors affecting x-ray-diffraction characteristics of catalysts materials. *Acs Symposium Series* 411, 279-302.

Romao, C.V., Vicente, J.B., Borges, P.T., Victor, B.L., Lamosa, P., Silva, E., Pereira, L., Bandejas, T.M., Soares, C.M., Carrondo, M.A., *et al.* (2016). Structure of *Escherichia coli* Flavodiiron Nitric Oxide Reductase. *Journal of Molecular Biology* 428, 4686-4707.

Rosano, G.L., and Ceccarelli, E.A. (2014). Recombinant protein expression in *Escherichia coli*: advances and challenges. *Frontiers in Microbiology* 5.

Rossmann, M.G. (2001). Molecular replacement - historical background. *Acta Crystallographica Section D-Biological Crystallography* 57, 1360-1366.

Rotenberg, M.O., and Maines, M.D. (1991). Characterization of a cDNA-encoding rabbit brain heme oxygenase-2 and identification of a conserved domain among mammalian heme oxygenase isozymes - possible heme-binding site. *Archives of Biochemistry and Biophysics* 290, 336-344.

Rothman, L.S., Gordon, I.E., Babikov, Y., Barbe, A., Benner, D.C., Bernath, P.F., Birk, M., Bizzocchi, L., Boudon, V., Brown, L.R., *et al.* (2013). The HITRAN2012 molecular spectroscopic database. *Journal of Quantitative Spectroscopy & Radiative Transfer* *130*, 4-50.

Ruettinger, R.T., Griffith, G.R., and Coon, M.J. (1977). Characterization of omega-hydroxylase of *Pseudomonas oleovorans* as a nonheme iron protein. *Archives of Biochemistry and Biophysics* *183*, 528-537.

Ryter, S.W., Alam, J., and Choi, A.M.K. (2006). Heme oxygenase-1/carbon monoxide: from basic science to therapeutic applications. *Physiol Rev* *86*, 583-650.

Sakurai, T., Sakurai, N., Matsumoto, H., Hirota, S., and Yamauchi, O. (1998). Roles of four iron centers in *Paracoccus halodenitrificans* nitric oxide reductase. *Biochem Biophys Res Commun* *251*, 248-251.

Sarady, J.K., Zuckerbraun, B.S., Bilban, M., Wagner, O., Usheva, A., Liu, F., Ifedigbo, E., Zamora, R., Choi, A.M.K., and Otterbein, L.E. (2004). Carbon monoxide protection against endotoxic shock involves reciprocal effects on iNOS in the lung and liver. *FASEB Journal* *18*, 854-+.

Saraiva, L.M., Vicente, J.B., and Teixeira, M. (2004). The role of the flavodiiron proteins in microbial nitric oxide detoxification. *Advances in Microbial Physiology*, Vol *49*, 77-129.

Saraste, M., and Castresana, J. (1994). Cytochrome-oxidase evolved by tinkering with denitrification enzymes. *Febs Letters* 341, 1-4.

Schmitt, M.P. (1997). Utilization of host iron sources by *Corynebacterium diphtheriae*: identification of a gene whose product is homologous to eukaryotic heme oxygenases and is required for acquisition of iron from heme and hemoglobin. *Journal of Bacteriology* 179, 838-845.

Shah, B.N., Chinte, U., Tomanicek, S.J., Hanson, B.L., and Schall, C.A. (2011). Flash Cooling Protein Crystals: Estimate of Cryoprotectant Concentration Using Thermal Properties. *Crystal Growth & Design* 11, 1493-1501.

Shank, J.L., Silliker, J.H., and Harper, R.H. (1962). The effect of nitric oxide on bacteria. *Appl Microbiol* 10, 185-189.

Shiloh, M.U., Manzanillo, P., and Cox, J.S. (2008). *Mycobacterium tuberculosis* senses host-derived carbon monoxide during macrophage infection. *Cell Host & Microbe* 3, 323-330.

Shingler, V. (1996). Signal sensing by sigma(54)-dependent regulators: Derepression as a control mechanism. *Molecular Microbiology* 19, 409-416.

Silaghi-Dumitrescu, R., Coulter, E.D., Das, A., Ljungdahl, L.G., Jameson, G.N.L., Huynh, B.H., and Kurtz, D.M. (2003). A flavodiiron protein and high molecular weight rubredoxin from *Moorella thermoacetica* with nitric oxide reductase activity. *Biochemistry*. US 42, 2806-2815.

Silaghi-Dumitrescu, R., Kurtz, D.M., Ljungdahl, L.G., and Lanzilotta, W.N. (2005a). X-ray crystal structures of *Moorella thermoacetica* FprA. Novel diiron site structure and mechanistic insights into a scavenging nitric oxide reductase. *Biochemistry*. US *44*, 6492-6501.

Silaghi-Dumitrescu, R., Ng, K.Y., Viswanathan, R., and Kurtz, D.M. (2005b). A flavo-diiron protein from *Desulfovibrio vulgaris* with oxidase and nitric oxide reductase activities. Evidence for an *in vivo* nitric oxide scavenging function. *Biochemistry*. US *44*, 3572-3579.

Skaar, E.P., Gaspar, A.H., and Schneewind, O. (2004). IsdG and IsdI, heme-degrading enzymes in the cytoplasm of *Staphylococcus aureus*. *J Biol Chem* *279*, 436-443.

Skaar, E.P., Gaspar, A.H., and Schneewind, O. (2006). *Bacillus anthracis* IsdG, a heme-degrading monooxygenase. *Journal of Bacteriology* *188*, 1071-1080.

Smith, M.S. (1983). Nitrous-oxide production by *Escherichia coli* IS correlated with nitrate reductase-activity. *Applied and Environmental Microbiology* *45*, 1545-1547.

Spiro, S. (2012). Nitrous oxide production and consumption: regulation of gene expression by gas-sensitive transcription factors. *Philosophical Transactions of the Royal Society B-Biological Sciences* *367*, 1213-1225.

Stamler, J.S., Simon, D.I., Osborne, J.A., Mullins, M.E., Jaraki, O., Michel, T., Singel, D.J., and Loscalzo, J. (1992). S-Nitrosylation of proteins with nitric-oxide - synthesis

and characterization of biologically-active compounds. Proceedings of the National Academy of Sciences of the United States of America 89, 444-448.

Stewart, R.D. (1975). The effect of carbon monoxide on humans. Annu Rev Pharmacol 15, 409-423.

Strube, K., de Vries, S., and Cramm, R. (2007). Formation of a dinitrosyl iron complex by NorA, a nitric oxide-binding Di-iron protein from *Ralstonia eutropha* H16. Journal of Biological Chemistry 282, 20292-20300.

Suharti, Heering, H.A., and de Vries, S. (2004). NO reductase from *Bacillus azotoformans* is a bifunctional enzyme accepting electrons from menaquinol and a specific endogenous membrane-bound cytochrome *c* (551). Biochemistry 43, 13487-13495.

Suharti, Strampraad, M.J.F., Schroder, I., and de Vries, S. (2001). A novel copper A containing menaquinol NO reductase from *Bacillus azotoformans*. Biochemistry 40, 2632-2639.

Suits, M.D.L., Jaffer, N., and Jia, Z.C. (2006). Structure of the *Escherichia coli* O157 : H7 heme oxygenase ChuS in complex with heme and enzymatic inactivation by mutation of the heme coordinating residue His-193. Journal of Biological Chemistry 281, 36776-36782.

Suits, M.D.L., Pal, G.P., Nakatsu, K., Matte, A., Cygler, M., and Jia, Z.C. (2005). Identification of an *Escherichia coli* O157 : H7 heme oxygenase with tandem functional

repeats. Proceedings of the National Academy of Sciences of the United States of America *102*, 16955-16960.

Tenhunen, R., and Marver, H.S. (1970). Enzymatic catabolism of hemoglobin - stimulation of microsomal heme oxygenase by hemin. Journal of Laboratory and Clinical Medicine *75*, 410.

Tenhunen, R., Marver, H.S., and Schmid, R. (1969). Microsomal heme oxygenase. Characterization of the enzyme. J Biol Chem *244*, 6388-6394.

Thorndycroft, F.H., Butland, G., Richardson, D.J., and Watmough, N.J. (2007). A new assay for nitric oxide reductase reveals two conserved glutamate residues form the entrance to a proton-conducting channel in the bacterial enzyme. Biochemical Journal *401*, 111-119.

Tinajero-Trejo, M., Rana, N., Nagel, C., Jesse, H.E., Smith, T.W., Wareham, L.K., Hippler, M., Schatzschneider, U., and Poole, R.K. (2016). Antimicrobial Activity of the Manganese Photoactivated Carbon Monoxide-Releasing Molecule Mn(CO)(3)(tpa-kappa N-3) (+) Against a Pathogenic *Escherichia coli* that Causes Urinary Infections. Antioxidants & Redox Signaling *24*, 765-780.

Uffen, R.L. (1976). Anaerobic growth of a *Rhodopseudomonas* species in dark with carbon-monoxide as sole carbon and energy substrate. Proceedings of the National Academy of Sciences of the United States of America *73*, 3298-3302.

United States Environmental Protection Agency (1991). Air quality criteria for carbon monoxide. Office of Research and Development, EPA-600/B-90/045F.

Vallance, P., and Charles, J. (1998). Nitric oxide as an antimicrobial agent: does NO always mean NO? *Gut* 42, 313-314.

van den Berg, W.A.M., Hagen, W.R., and van Dongen, W. (2000). The hybrid-cluster protein ('prismane protein') from *Escherichia coli* - Characterization of the hybrid-cluster protein, redox properties of the 2Fe-2S and 4Fe-2S-20 clusters and identification of an associated NADH oxidoreductase containing FAD and 2Fe-2S. *European Journal of Biochemistry* 267, 666-676.

Vicente, J.B., Scandurra, F.M., Rodrigues, J.V., Brunori, M., Sarti, P., Teixeira, M., and Giuffrè, A. (2007). Kinetics of electron transfer from NADH to the *Escherichia coli* nitric oxide reductase flavorubredoxin. *FEBS J* 274, 677-686.

Vicente, J.B., and Teixeira, M. (2005). Redox and spectroscopic properties of the *Escherichia coli* nitric oxide-detoxifying system involving flavorubredoxin and its NADH-oxidizing redox partner. *J Biol Chem* 280, 34599-34608.

Vicente, J.B., Tran, V., Pinto, L., Teixeira, M., and Singh, U. (2012). A Detoxifying Oxygen Reductase in the Anaerobic Protozoan *Entamoeba histolytica*. *Eukaryotic Cell* 11, 1112-1118.

Vieira, H.L.A., Queiroga, C.S.F., and Alves, P.M. (2008). Pre-conditioning induced by carbon monoxide provides neuronal protection against apoptosis. *Journal of Neurochemistry* *107*, 375-384.

Vincze, T., Posfai, J., and Roberts, R.J. (2003). NEBcutter: a program to cleave DNA with restriction enzymes. *Nucleic Acids Research* *31*, 3688-3691.

Wang, J., Vine, C.E., Balasiny, B.K., Rizk, J., Bradley, C.L., Tinajero-Trejo, M., Poole, R.K., Bergaust, L.L., Bakken, L.R., and Cole, J.A. (2016). The roles of the hybrid cluster protein, Hcp and its reductase, Hcr, in high affinity nitric oxide reduction that protects anaerobic cultures of *Escherichia coli* against nitrosative stress. *Molecular Microbiology* *100*, 877-892.

Wasser, I.M., de Vries, S., Moëgne-Loccoz, P., Schröder, I., and Karlin, K.D. (2002). Nitric oxide in biological denitrification: Fe/Cu metalloenzyme and metal complex NO(x) redox chemistry. *Chem Rev* *102*, 1201-1234.

Wasserfallen, A., Ragettli, S., Jouanneau, Y., and Leisinger, T. (1998). A family of flavoproteins in the domains Archaea and Bacteria. *Eur J Biochem* *254*, 325-332.

Wastl, J., Duin, E.C., Iuzzolino, L., Dörner, W., Link, T., Hoffmann, S., Sticht, H., Dau, H., Lingelbach, K., and Maier, U.G. (2000a). Eukaryotically encoded and chloroplast-located rubredoxin is associated with photosystem II. *J Biol Chem* *275*, 30058-30063.

Wastl, J., Sticht, H., Maier, U.G., Rösch, P., and Hoffmann, S. (2000b). Identification and characterization of a eukaryotically encoded rubredoxin in a cryptomonad alga. *FEBS LETT* 471, 191-196.

Watmough, N.J., Butland, G., Cheesman, M.R., Moir, J.W.B., Richardson, D.J., and Spiro, S. (1999). Nitric oxide in bacteria: synthesis and consumption. *Biochimica Et Biophysica Acta-Bioenergetics* 1411, 456-474.

Wegiel, B., Larsen, R., Gallo, D., Chin, B.Y., Harris, C., Mannam, P., Kaczmarek, E., Lee, P.J., Zuckerbraun, B.S., Flavell, R., *et al.* (2014). Macrophages sense and kill bacteria through carbon monoxide-dependent inflammasome activation. *Journal of Clinical Investigation* 124, 4926-4940.

WHO (2000). Carbon monoxide. In: WHO regional office for Europe, Air Quality Guidelines, pp. Chapter 5.5. Copenhagen.

Winter, G. (2010). xia2: an expert system for macromolecular crystallography data reduction. *Journal of Applied Crystallography* 43, 186-190.

Wlodawer, A., Minor, W., Dauter, Z., and Jaskolski, M. (2008). Protein crystallography for non-crystallographers, or how to get the best (but not more) from published macromolecular structures. *Febs Journal* 275, 1-21.

Wu, L., and Wang, R. (2005). Carbon monoxide: endogenous production, physiological functions, and pharmacological applications. *Pharmacol Rev* 57, 585-630.

Wu, R., Skaar, E.P., Zhang, R., Joachimiak, G., Gornicki, P., Schneewind, O., and Joachimiak, A. (2005). Staphylococcus aureus IsdG and IsdI, heme-degrading enzymes with structural similarity to monooxygenases. *J Biol Chem* 280, 2840-2846.

Ying, L., and Hofseth, L.J. (2007). An emerging role for endothelial nitric oxide synthase in chronic inflammation and cancer. *Cancer Research* 67, 1407-1410.

You, M.K., Shin, H.Y., Kim, Y.J., Ok, S.H., Cho, S.K., Jeung, J.U., Yoo, S.D., Kim, J.K., and Shin, J.S. (2010). Novel Bifunctional Nucleases, OmBBD and AtBBD1, Are Involved in Abscisic Acid-Mediated Callose Deposition in Arabidopsis. *Plant Physiology* 152, 1015-1029.

Zacharia, V.M., Manzanillo, P.S., Nair, V.R., Marciano, D.K., Kinch, L.N., Grishin, N.V., Cox, J.S., and Shiloh, M.U. (2013). *cor*, a novel carbon monoxide resistance gene, is essential for *Mycobacterium tuberculosis* pathogenesis. *M Bio* 4, e00721-e00713.

Zacharia, V.M., and Shiloh, M.U. (2012). Effect of carbon monoxide on *Mycobacterium tuberculosis* pathogenesis. *Med Gas Res* 2, 30-30.

Zhu, W.M., Hunt, D.J., Richardson, A.R., and Stojiljkovic, I. (2000). Use of heme compounds as iron sources by pathogenic *Neisseria* requires the product of the *hemO* gene. *Journal of Bacteriology* 182, 439-447.

Zhu-Barker, X., Cavazos, A.R., Ostrom, N.E., Horwath, W.R., and Glass, J.B. (2015). The importance of abiotic reactions for nitrous oxide production. *Biogeochemistry* 126, 251-267.

Zumft, W.G. (1997). Cell biology and molecular basis of denitrification. *Microbiology and Molecular Biology Reviews* 61, 533.

Zumft, W.G. (2002). Nitric oxide signaling and NO dependent transcriptional control in bacterial denitrification by members of the FNR-CRP regulator family. *J Mol Microb Biotech* 4, 277-286.

Appendices

Appendix 1: Genomic DNA isolation protocol

Procedure

1. Cells were harvested in a microcentrifuge tube by centrifuging for 10 min at 5000 g (7500 rpm). The supernatant was then discarded.
2. Pellet was resuspended in 180 μ l buffer ATL.
3. 20 μ l of proteinase K was added, sample mixed thoroughly by vortexing, and incubated at 56 °C until the tissue was completely lysed. During incubation, the mixture was vortexed occasionally to disperse the sample, or placed in a thermomixer, shaking water bath, or on a rocking platform. Lysis time varied depending on the type of tissue processed.
5. The mixture then was vortexed for 15 s. 200 μ l buffer AL was added to the sample, and mixed thoroughly by vortexing. Then 200 μ l ethanol (96–100%) was added, and the sample mixed again thoroughly by vortexing.

Appendix 2: Media

LB: 10 g Trypton (Oxoid), 5 g Yeast extract (Oxoid), 10 g NaCl (Fisher), 15 g Agar (Oxoid) / 1L

Defined minimal media (DMM): To 250 ml of distilled water, 4 g of K_2HPO_4 , 1 g of KH_2PO_4 , 1 g of NH_4Cl , 10 mg of $CaCl_2$, and 2.6 g of K_2SO_4 were added, then 10 ml of (0.5 g $FeCl_3 \cdot 6H_2O$, 50 mg ZnO , 10 mg $CuCl_2 \cdot 2H_2O$, 10 mg $CoNO_3 \cdot 6H_2O$, 10 mg H_3BO_3 , 0.12 mg ammonium molybdate, 17 mg Sodium selenite) were added, then the pH was adjusted to 7.4, the volume of the media then completed to 1L and the media autoclaved After autoclaving 1 ml/L of 1 M $MgCl_2$ was added

Appendix 3: Transformation protocol (Chemotransformation)

1. The competent cells were taken out of -80 °C and thawed on ice (approximately 20-30 min).
2. Agar plates were taken (containing the appropriate antibiotic) out of 4 °C to warm up to room temperature or placed in 37 °C incubator.
3. 1 to 5 µl of DNA (usually 10 pg to 100 ng) was mixed into 20-50 µl of competent cells in a microcentrifuge or falcon tube. Mixed by flicking the bottom of the tube with fingers a few times.
4. The mixture of the competent cell and DNA was placed on ice for 20-30 min.
5. Each transformation tube was placed in a 42 °C water bath for 30-60 s.
6. Transformation tubes were then put back on ice for 2 min.
7. 250-500 µl LB or SOC media (without antibiotic) was added and tubes placed in 37 °C shaking incubator for 45 min.
8. 20 or 200 µl of the transformation mixture then was plated onto LB agar plate containing the appropriate antibiotic.

Appendix 4: Buffers and solutions that were used in this study

Solution	Chemical composition
1X TAE buffer	40 mM Tris-acetate+1 mM EDTA pH 8.0
1X SDS-PAGE running buffer	1 g SDS+3 g Tris-Cl+ 14.4 g Glycine pH 8.8
0.1% Coomassie blue stain	0.1% Coomassie blue+1 volume methanol+1 volume acetic acid +1 volume dH ₂ O

De-stain solution	300 ml methanol+ 100 ml acetic acid+ 600 ml dH ₂ O
Buffer A (lysis buffer)	0.5 M NaCl Tris-HCl pH 8.0
Buffer B	Buffer A + 0.5 M Imidazole
12% Resolving SDS-PAGE	30% acrylamide (Severn Biotech Ltd) 2.5 ml + 1 M Tris (Fisher) pH 8.8 (2.35 ml) + 1.28 ml MilliQ+10% SDS (Sigma) 62.5µl + 6.25 µl TEMED (Sigma)+ 62.5 µl of 10% APS (1g of Ammonium persulfate (Sigma) in 10 ml MilliQ)
6% Stacking gel	30 % acrylamide (Severn Biotech Ltd) (0.75 ml) + 1 M Tris (Fisher) pH 8.8 (0.47 ml) + 2.46 ml MilliQ+ 10% SDS (Sigma) (37.5 µl) + 3.75 µl TEMED (Sigma)+ 37.5 µl of 10% APS (1 gm of Ammonium persulfate (Sigma) in 10 ml MilliQ)

Appendix 5: Hannah method for chemocompetent cell preparation

Solutions required were stored at 4 °C, all the concentrations mentioned here are the final concentrations.

RF1 solution was prepared from 100 mM KCl, 50 mM MnCl₂.4H₂O, 30 mM potassium acetate, 10 mM CaCl₂.2H₂O, 15% (w/v) glycerol, made up to 200 ml with dH₂O and pH adjusted to 5.8 with diluted acetic acid then filter sterilized

RF2 solution was prepared from 10 mM MOPS, 10 mM KCl, 75 mM CaCl₂.2H₂O, 15% (w/v) glycerol, made up to 100 ml with dH₂O then pH adjusted to 6.8 with NaOH, and filter sterilized

Method:

1. Cultures of *E. coli* DH5 α 100 ml were grown to OD₆₀₀ 0.6.
2. Cultures were then split into 2x50 ml and incubated on ice for 15 min.
3. Cultures were spun down at 10000 rpm for 15 min at 4 °C.
4. Pellets were resuspended in 50 ml ice cold RF1.
5. Pellets were then incubated on ice for 15 min and centrifuged as in step 3.
6. Pellets were resuspended again in 8 ml ice cold RF2, and then they incubated on ice for 20 min.
7. The pellets were divided into 1 ml aliquots and stored at -80 °C.

Appendix 6: electrocompetent cell preparation and electroporation

1. 500 ml of L-broth were inoculated with 1/100 volume of a fresh overnight *E. coli* culture.
2. Cultures were grown at 37 °C shaking at 300 rpm to an OD₆₀₀ of approximately 0.5–0.7.
3. Cells were chilled on ice for ~20 min. For all subsequent steps, the cells were kept as close to 0 °C as possible (in an ice) and all containers were chilled on ice before adding cells. To harvest, the cells were transferred to a cold centrifuge bottle and spun at 4000 x g for 15 min at 4 °C.
4. The supernatant was then discarded. It was better to sacrifice the yield by pouring off a few cells than to leave any supernatant behind.
5. The pellet was resuspended gently in 500 ml of ice-cold 10% glycerol. The sample was centrifuged at 4000 g for 15 min at 4 °C and the supernatant was carefully poured off and discarded.

6. The pellet was resuspended again, in 250 ml of ice-cold 10% glycerol and centrifuged as in step 5.
7. The pellet was resuspended again in ~20 ml of ice-cold 10% glycerol. Transferred to a 50 ml sterile Falcon tube and centrifuged as in step 5.
8. The cell pellet was resuspended in a final volume of 1–2 ml of ice-cold 10% glycerol. Then dispensed into a 50 μ l aliquots on dry ice and stored at -80 °C.

Electroporation

1. Cells were gently thawed at room temperature and then immediately placed on ice. The sterile 0.2 cm cuvette was removed from the pouch and placed on ice with the white chamber slide.
2. 40 μ l of the cell suspension was mixed with 1 to 2 μ l of DNA in a cold, 1.5 ml polypropylene tube, mixed well and put on ice ~ 1 min.
3. The MicroPulser was set to Ec2 because a 0.2 cm cuvette was used
4. The mixture of cells and DNA was transferred to a cold electroporation cuvette and tapped down the suspension to the bottom. The cuvette was placed in the chamber slide and the slide was pushed into the chamber until the cuvette was seated between the contacts in the base of the chamber. It was pulsed once.
5. The cuvette was then removed from the chamber and immediately 1 ml of LB medium was added to the cuvette. Quickly but gently the cells were suspended with a Pasteur pipette
6. The cell suspension was transferred to a 17 x 100 mm polypropylene tube and incubated at 37 °C for 1 h, at 250 rpm
7. The cell culture was then plated on LB plates with appropriate antibiotics.

Appendix 7 Site directed mutagenesis

Calculations for the primers and plasmid DNA were done manually by using the equation

$$\text{Xpmoles of oligo} = \frac{125 \text{ ng of oligo}}{330 \text{ oligo base pairs}} \times 1000$$

DNA concentration in construct 4 miniprep was measured by a Nanodrop, using 2 μl of the sample, with lid No.10.

Procedure

Two reactions were done, one with template DNA concentration 50 ng and one with 20 ng DNA concentration.

5 μl of 10 \times reaction buffer

0.6 μl (50 ng) of dsDNA template according to the DNA concentration

0.114 μl (125 ng) of oligonucleotide forward primer (equation)

0.114 μl (125 ng) of oligonucleotide reverse primer

1 μl of dNTP mix

Autoclaved MilliQ water was added to a final volume of 50 μl (43.17 μl)

Then 1 μl of *Pfu Ultra HF* DNA polymerase (2.5 U/ μl) was added.

20 ng reaction was same but the dsDNA that has been taken was 0.24 μl and the MilliQ that added was (43.57 μl).

Mutation No.2 has been done by the same protocol, using 0.118 μl of each primer and 0.2 μl of dsDNA for (50 ng concentration) and 0.08 μl for 20 ng.

A PCR program was run for 12 cycles according to the following protocol:

Temperature	Time
95 °C	30 s
55 °C	1 min
68 °C	1 min/Kilobase of plasmid

After finishing the PCR 1 μ l of *Dpn I* restriction was added to each tube. Afterward 5 μ l of each reaction were loaded on a 1% agarose gel and run them for 30 min at 110V. Tubes were flicked gently and the mixture pipetted up and down several times, then were spun down for 1 min at 13000 rpm, finally they were incubated for 1-2 h at 37 °C water bath.

Transformation to XL1-Blue competent cells.

1. XL1-Blue super-competent cells were gently thawed on ice. For each control and sample reaction to be transformed, 50 μ l aliquot of the super-competent cells was placed into a pre-chilled 14 ml BD Falcon polypropylene round-bottom tube.
2. 1 μ l of the *Dpn I*-treated DNA was transferred from each control and sample reaction to separate aliquots of the super-competent cells.
3. The transformation reactions were heat pulsed for 45 s at 42 °C and then the reactions were placed on ice for 2 min.
4. 0.5 ml of LB broth was preheated to 42 °C and added, before the transformation reactions were incubated at 37 °C for 1 h with shaking at 225–250 rpm.
5. 250 μ l sample of the culture and 1:10 dilution of it for each transformation reaction was plated on LB plates with appropriate antibiotic, along with control (XL1 competent cell only). All the plates were incubated at 37 °C overnight and then colonies select.

Appendix 8: protein expression

All pellets were defrosted on ice, and resuspended by adding 100 μ l buffer A (50 mM Tris pH 8.0 + 0.5 M NaCl) for the His-tagged proteins and 50 mM Tris pH 8.0 for the non-tagged proteins.

Sonication was performed to lyse bacterial cells by using the Soniprep150 machine at 16 micron amplitude by 2x 20 s cycles. All the Ependorff tubes were kept on ice during the sonication.

Protein concentration was measured by the Bradford method (Bradford, 1976), where 1-10 μ l of suspension was mixed with 800 μ l Milli Q water and 200 μ l Bradford reagent in 1 ml cuvette and the absorbance at 595 nm measured. Total protein concentration was calculated by using the equation:

$$\text{Concentration of protein mg/ml} = \frac{OD_{595} \times 15}{\text{Volume of protein } (\mu\text{l})}$$

After measuring the total protein concentration for all samples, an SDS-PAGE gel was prepared to check the expression with a 12% resolving gel and a 6% stacking gel. Standard 1X SDS running buffer (see Appendix 4) was used, and Marker 12 as protein marker (Bioline).

Samples were prepared by taking specific volumes of each sample, to reach 10-15 μ g of protein, and mixed with 5 μ l SDS loading buffer (Novex) and 2 μ l reducing agent (Novex), and completed to 20 μ l by adding MilliQ water. During samples preparation, a heating block was used to boil the samples, samples were boiled for 2 min, and they were loaded onto an SDS-PAGE gel along with Mark12 protein ladder, run at 80 V for 10 min and then at 200 V for 30-50 min in 1X SDS loading buffer (Appendix 4). Gels were then stained by using Instant blue (Expedeon), or 0.1% Coomassie blue stain (Appendix 4) for 2 h, and de-stained by using de-stain solution (Appendix 4) overnight. Next day photos were taken, gels were dried in frames. The rest of the samples were stored again at -20 °C for further studies.

Appendix 9 Batch method for protein purification

1. 0.1 ml of NTA beads were added to a 2 ml Falcon tube, with 100 μ l buffer A.
2. The tube contents were spun down at 10444 rpm for 1 min.
3. The buffer was removed and 2 ml of dH₂O added.

4. The sample was spun down repeated again.
5. The pellet was resuspended with a few ml of dH₂O, and the mixture was placed into the column.
6. The column was drained for few m and the end was closed later.
7. The column then was charged with Ni, by adding 1 ml of 1 M NiCl₂, mixed gently for 2 min then drained again.
8. The beads were then washed by dH₂O, then with 1 ml of buffer A.

At this point the column became ready to use, after that the beads were placed in a 2 ml Falcon tube, spun down in a Sigma 1-14 centrifuge at 10444 rpm for 1 min, buffer removed, and CFE added then. The beads and CFE were incubated for 40 min in the cold cabinet, then the tube was centrifuged at 10444 rpm for 1 min, supernatant removed, stored and labeled as unbound material. Then 2 ml of buffer A were added to the beads, which were spun down, and the supernatant removed and stored as wash1. The process was repeated to give wash 2. Finally, an elution of His-tagged protein was achieved by adding 100 µl of buffer B (Appendix 4), to the beads, which were then mixed gently, spun down at 10444 rpm for 1 min, and the supernatant was collected and labeled as elution. Protein concentration were taken for all samples by the Bradford method, and samples prepared for loading and analysis by SDS-PAGE.